Extending a dynamic mathematical model of metabolism in *Trypanosoma brucei*

Eduard Johannes Kerkhoven, BSc MSc

Submitted in fulfilment of the requirements for the degree of Doctor in Philosophy

School of Life Sciences
College of Medical, Veterinary and Life Sciences
University of Glasgow

December 2012

Abstract

There is an urgent need for new chemotherapies against human African trypanosomiasis (HAT), caused by the protozoan parasite *Trypanosoma brucei*. It is anticipated that the parasites' divergent biochemistry will enable development of novel therapies. To study the behaviour of a complex network as metabolism, one can employ mathematical models.

In this thesis, metabolism of bloodstream form *T. brucei* was investigated. Cellular metabolism consists as a complex system connecting enzymes with metabolites, and to study such a network one can construct mathematical models that describe the connections within the biological system. A previously published, and well-curated model of glycolysis in bloodstream form *T. brucei* (Bakker BM, *et al.* (1997) J Biol Chem 272:3207−15), was extended here with the pentose phosphate pathway (PPP), the second major pathway in glucose metabolism in most life forms. Several hypotheses were derived during the model building process and these were tested experimentally.

It became apparent that the glycosomal bound-phosphate balance is essential for the parasite. Extension of the glycolytic model with the PPP introduced the risk of a so-called 'phosphate leak', where bound-phosphates are depleted in the glycosome. Two hypotheses were investigated *in silico*, while one hypothesis could also be tested experimentally; (i) a glycosomal ATP:ADP antiporter was proposed, but *in silico* analysis indicated that the activity of such an antiporter requires tight regulation. (ii) A glycosomal ribokinase was investigated both *in silico* and experimentally. Genetic mutants indicated that ribokinase is essential to bloodstream form *T. brucei*, albeit at low levels.

Additional analysis of the generated models indicated that ablation of 6-phosphogluconate dehydrogenase (6PGDH) in *T. brucei* is lethal by a different mechanism as seen in other

organisms. Overall, extension of the glycolytic model with the PPP demonstrated the fragility of the model regarding the bound-phosphate balance and indicated that future analysis on glycosomal metabolism should be focused on this.

Important in the use of mathematical models of metabolism is that the underlying stoichiometry of the model reflects (albeit with simplification) the *in vivo* system. It is therefore paramount to know what enzyme activities are present in the organism of interest. In this thesis a metabolomics approach was used to elucidate the function of three *T. brucei* genes. These genes were putatively annotated as arginase (ARG), *N*-acetylornithine deacetylase (NAO) and nicotinamidase (NAM). The results suggested that ARG has catalytic activity as tryptophan monooxygenase (EC 1.3.12.3), while substrate promiscuity was indicated for NAO and NAM.

The work presented in this thesis has provided us with new insights on trypanosomal metabolism. The extended model now allows us to research a larger part of *T. brucei* metabolism with mathematical modelling, and will thereby aid in the identification and further investigation of (proposed) drug targets.

Contents

Abstract i

List of Tables vii

List of Figures ix

Acknowledgements xi

Author's declaration xii

Abbreviations xiii

1. Introduction 1

1.1. Human African trypanosomiasis 2
1.1.1. Chemotherapy 3
1.2. *Trypanosoma brucei* 5
1.2.1. A unique life cycle 5
1.3. Trypanosomal glycolysis 6
1.3.1. Compartmentalisation of glycolysis 7
1.4. A unique organelle: the glycosome 10
1.4.1. Glycosomal targeting of enzymes 10
1.4.2. Transport of metabolites over the membrane 11
1.5. Pentose phosphate pathway 12
1.5.1. Oxidative PPP 13
1.5.2. Non-oxidative PPP 13
1.5.3. Functions of PPP 14
1.6. Redox metabolism 14
1.6.1. Ornithine biosynthesis 15
1.7. Metabolomics 16
1.8. Systems biology of metabolism 17

1.8.1. Why modelling metabolism? . . . 18
1.8.1.1. Metabolic control analysis . . . 18
1.8.2. Top-down versus bottom-up . . . 19
1.8.3. Generation of a dynamic model . . . 21
1.8.4. Applications of dynamic models . . . 23
1.8.4.1. Dynamic models of glycolysis . . . 24
1.8.4.2. Dynamic models of PPP . . . 25
1.8.5. Dynamic model of trypanosomal glycolysis . . . 26
1.8.5.1. Stoichiometric analysis of trypanosomal glycolysis . . . 26
1.8.5.2. Metabolic control analysis of trypanosomal glycolysis . . . 28
1.9. Aim: extension of the dynamic model of trypanosomal metabolism . . . 29

2. Methods 31
2.1. Trypanosome growth . . . 31
2.1.1. Culturing *T. brucei* . . . 31
2.1.2. Transformation of parasites . . . 32
2.1.3. AlamarBlue assays . . . 32
2.1.4. Cell extracts . . . 32
2.2. Molecular biology . . . 33
2.2.1. PCR . . . 33
2.2.2. Plasmid generation . . . 33
2.2.2.1. Plasmids for recombinant protein overexpression . . . 38
2.2.2.2. RNA interference constructs . . . 39
2.2.2.3. Gene knockout constructs . . . 39
2.2.3. Northern blot . . . 40
2.3. Protein expression . . . 40
2.3.1. Overexpression . . . 40
2.3.2. Purification . . . 40
2.4. Enzyme assays . . . 41
2.4.1. Ribokinase . . . 41
2.4.2. Hexokinase . . . 42
2.4.3. Glucose-6-phosphatase assay . . . 42
2.5. Western blotting . . . 43
2.5.1. Ribokinase polyclonal antibody . . . 44
2.6. Metabolomics . . . 45
2.6.1. Metabolomics enzyme assay sampling . . . 45
2.6.2. Parasite metabolite extraction . . . 46
2.6.3. Internal and authentic standards . . . 46
2.6.4. Liquid chromatography-mass spectrometry . . . 46
2.6.5. Data analysis . . . 47

2.7. Computational methods . . . 48
2.7.1. Model description . . . 48
2.7.1.1. Generic rate equations . . . 49
2.7.1.2. Modified glycolysis equations . . . 49
2.7.1.3. Rate equations of PPP extension . . . 50
2.7.1.4. Rate equation of fructose extension . . . 51
2.7.1.5. Kinetic parameters . . . 51
2.7.1.6. Metabolite concentrations . . . 52
2.7.2. Simulations . . . 52

3. Extensions of the model of trypanosomal metabolism 54
3.1. Introduction . . . 55
3.1.1. Towards an *in silico* trypanosome . . . 55
3.1.2. Trypanosomal PPP . . . 56
3.1.3. Aim . . . 56
3.2. Results . . . 58
3.2.1. Modelling glycolysis including uncertainty of the parameters . . . 58
3.2.2. Stepwise extension with the PPP . . . 60
3.2.2.1. Cytosolic PPP . . . 67
3.2.2.2. Prevention of cytosolic Glc-6-P accumulation . . . 70
3.2.2.3. Oxidative stress regulates flux through PPP . . . 71
3.2.3. Further extension with the glycosomal PPP . . . 74
3.2.3.1. Glycosomal ATP:ADP antiporter requires tight regulation . . . 77
3.2.3.2. Glycosomal RK in reverse . . . 79
3.2.3.3. Conserved moieties in model 6 . . . 81
3.2.3.4. Glycosomal RK is potentially essential . . . 81
3.2.3.5. Increased ribose levels are lethal *in silico*, but not *in vivo* . . . 83
3.3. Discussion . . . 85

4. The role of a putative *T. brucei* ribokinase 88
4.1. Introduction . . . 89
4.2. Results . . . 91
4.2.1. Putative *T. brucei* RK gene has a typical RK sequence . . . 91
4.2.2. Kinetic characterization of recombinant *T. brucei* RK . . . 93
4.2.3. Ablation of *T. brucei* RK by RNA interference . . . 95
4.2.4. Limited changes in metabolome of RK^{RNAi} . . . 96
4.2.5. RK mainly produces Rib-5-P . . . 98
4.2.6. *T. brucei* produces octulose 8-phosphate from Rib-5-P . . . 98
4.2.7. Unable to knockout RK . . . 99
4.3. Discussion . . . 103

4.3.1. *T. brucei* RK can work both ways . . . 103
4.3.2. RK is potentially essential, but low levels suffice . . . 103
4.3.3. The importance of uncommon metabolites . . . 104
4.3.4. RK alone is unlikely to prevent the glycosomal phosphate leak . . . 105

5. Studying enzyme function with metabolomics 107
5.1. Introduction . . . 108
5.1.1. Metabolomics for elucidation of enzyme function . . . 109
5.2. Results . . . 113
5.2.1. A putative *T. brucei* arginase without arginase activity . . . 113
5.2.1.1. Recombinant ARG binds to an *E. coli* chaperone . . . 113
5.2.1.2. ARG is a potential tryptophan oxygenase . . . 114
5.2.1.3. ARG null mutant is less susceptible to trypanocidals . . . 118
5.2.1.4. ARG null mutant affects phosphocholines, PPP and methionine metabolism 120
5.2.1.5. Different functions suggested for ARG . . . 124
5.2.2. Putative *N*-acetylornithine deacetylase . . . 125
5.2.2.1. Metabolomics assay confirms deacetylase function . . . 125
5.2.2.2. Metabolome of NAO null mutant shows limited changes . . . 127
5.2.2.3. NAO does not affect eflornithine sensitivity . . . 129
5.2.3. Putative nicotinamidase . . . 130
5.2.3.1. Nicotinamidase function confirmed by metabolomics enzyme assay . . . 130
5.2.3.2. Attempt to ablate NAM by RNA interference . . . 131
5.3. Discussion . . . 136
5.3.1. Complicated metabolite changes observed in *T. brucei* ARG elucidation . 136
5.3.2. Should NAO be annotated as N-acetylornithine deacetylase? . . . 137
5.3.3. NAM also seems to have a broader substrate range than predicted . . . 138
5.3.4. Improvements on metabolomics enzyme function elucidation . . . 138

6. Why does the loss of 6PGDH kill trypanosomes? 141
6.1. Introduction . . . 142
6.2. Results . . . 145
6.2.1. 6PGDH loss in *T. brucei* does not inhibit PGI . . . 145
6.2.2. Fructose is unable to rescue 6PGDH loss *in silico* . . . 147
6.2.3. Preliminary experimental results on ablation of 6PGDH . . . 149
6.3. Discussion . . . 151

7. General discussion and future work 153
7.1. Unravelling glycosomal metabolism . . . 153
7.2. How essential is the glycosomal PPP? . . . 156
7.3. Enzymes, the forgotten workhorses? . . . 157

References **159**

A. Creek's minimal medium (CMM) **187**

B. Elementary mode analysis of glycosomal proteome **188**

C. Parameter distributions **191**
C.1. Methods: sampling the parameters 191
C.2. Distributions 193

D. Metabolomics **204**
D.1. Standards 204
D.2. Metabolomics data 209
D.3. ARG metabolomics assay 209
D.4. ARG null mutant metabolic profiling 213
D.5. NAO metabolomics enzyme assay 217
D.6. NAO null mutant metabolic profiling 220
D.7. NAM metabolomics enzyme assay 222

E. Publications **225**

List of Tables

1.1. Conserved moieties in the glycolysis model 27
1.2. Elementary modes of glycolysis model 27

2.1. Oligonucleotides used in this thesis 34
2.2. Plasmids produced in this study 36
2.3. SilicoTryp assay buffer 41
2.4. Cofactor mixtures used in metabolomics enzyme assays 45
2.5. Main principle of rank product analysis 48

3.1. Model stoichiometry 62
3.2. Kinetic parameters of the reactions related to the PPP 63
3.3. Elementary mode analysis of model 2. 68
3.4. Conserved moieties in the glycolysis model 69
3.5. Conserved moieties in the glycolysis model 81

4.1. Phosphorylation of different substrates by RK 93
4.2. Activity of recombinant *T. brucei* RK 94
4.3. Affinity constants of RK 94
4.4. AlamarBlue assays of 7-days induced RK^{RNAi} 96
4.5. Changes in metabolite concentrations in RK^{RNAi} 97

5.1. Contents of cofactor mixtures 115
5.2. Changes in indoles and quinolines in ARG assay 116
5.3. Toxicity of various trypanocidals in Δarg and wild-type parasites 120
5.4. Significantly changed metabolites in NAO assay 126
5.5. Metabolic changes in Δnao 128
5.6. Eflornithine sensitivity of Δnao 129
5.7. Significantly changed metabolites in NAM assay 132
5.8. Metabolic changes in NAM^{RNAi} 135

6.1. Parameter values of fructose extension 148

A.1. Creek's minimal medium (CMM) 187

B.1. Additional glycosomal enzymes 189
B.2. Elementary modes of glycosomal proteome 190

D.2. ARG metabolomics enzyme assay, cofactor mixture 1 209
D.3. ARG metabolomics enzyme assay, cofactor mixture 2 212
D.4. Δ*arg* metabolic profiling, pHILIC 213
D.5. Δ*arg* metabolic profiling, HILIC 215
D.6. NAO metabolomics enzyme assay, cofactor mixture 1 217
D.7. NAO metabolomics enzyme assay, cofactor mixture 2 219
D.8. Δ*nao* metabolic profiling, pHILIC 220
D.9. Δ*nao* metabolic profiling, HILIC 221
D.10. NAM metabolomics enzyme assay, cofactor mixture 1 222
D.11. NAM metabolomics enzyme assay, cofactor mixture 2 223

List of Figures

1.1. Distribution of human African trypanosomiasis 2
1.2. Reported cases of sleeping sickness and population screened, 1939–2004 4
1.3. Life-cycle stages of *Trypanosoma brucei* 6
1.4. The autocatalytic design of glycolysis 8
1.5. Glycolysis in the glycosomes of bloodstream form *T. brucei* 9
1.6. The PPP in *T. brucei* 12
1.7. The trypanothione biosynthetic pathway 16
1.8. Ornithine biosynthetic pathway from glutamate 16
1.9. Top-down versus bottom-up systems biology 20
1.10. Four-step construction of a dynamic model of metabolism 21
1.11. Example of output from a time-course simulation 23

2.1. Plasmid maps as generated in this study (1) 37
2.2. Plasmid maps as generated in this study (2) 38
2.3. Coupled enzyme assays 43

3.1. Overview of modelling with uncertainty 59
3.2. Overview of different versions of models described in this Chapter . . . 60
3.3. Overview of metabolic pathways modelled in this Chapter 61
3.4. Scans of parameter values related to the cytosolic PPP 69
3.5. Steady-state fluxes of the various model versions 72
3.6. Simulations of oxidative stress 73
3.7. A 'phosphate leak' introduced by the glycosomal PPP 75
3.8. ATP:ADP antiporter mimics turbo-state 78
3.9. Scan of RK activity 82
3.10. Ribose sensitivity in the extended model 83
3.11. Sensitivity to extracellular ribose 84

4.1. Structural alignment of *T. brucei* to *E. coli* RK 91

4.2. Protein sequence alignment of ribokinases 92
4.3. Protein gel of recombinant RK purification 93
4.4. Growth curve of RK^{RNAi} 95
4.5. Northern and western blot of RK^{RNAi} 96
4.6. PCR confirming targeted replacement of RK gene 100
4.7. PCR confirmation of $\Delta rk::HYG/PAC::RK^{i}$ 101
4.8. Western blot of RK in RK re-expressor 101

5.1. The use metabolomics in functional elucidation of enzymes 110
5.2. Purification of recombinant ARG 114
5.3. Peptide changes in ARG metabolomics assay 117
5.4. Chemical structure of quinoline, indole and tryptophan 117
5.5. Potential substrate-product pairs from ARG metabolomics assay 118
5.6. Confirmation of genetic mutants by PCR 119
5.7. Growth curves of various genetic mutants 120
5.8. Correlation of metabolomes of different genetic mutants 121
5.9. Changes in lipid concentrations of Δarg 122
5.10. Biosynthetic pathway of phosphatidylcholines 122
5.11. Schematic map of metabolite changes in Δarg 123
5.12. Possible connection of observed changes in Δarg 125
5.13. Potential connection between changes in *N*-acetylmethionine and MTA 127
5.14. Changes in metabolites upon eflornithine treatment 129
5.15. Reaction catalysed by nicotinamidase 130
5.16. Nicotinamidase gene within the *T. brucei* strain 427 genome 130
5.17. Northern blot of NAM^{RNAi} 133

6.1. Schematic overview of positive feedback loop of 6PGDH inhibition . . 143
6.2. Schematic overview of model versions considered 145
6.3. Effects of ablation of 6PGDH 146
6.4. Simulations of the fructose model 149
6.5. Growth curve of $6PGDH^{RNAi}$ on glucose and fructose 150

Acknowledgements

Foremost I would like say thanks to Mike Barrett. Mike, you've been an outstanding supervisor, allowing me to pursuit my own ideas, but also reeling me in and steering me in the right direction when needed. I hope we will stay in contact for years to come, perhaps you will find another art-house film that you were about to throw out?

I would like to thank Rainer Breitling and Barbara Bakker for all the fruitful discussions and for their patience with the many revisions of papers. Barbara, you introduced me to trypanosomes, systems biology, and even Mike; nothing in this thesis would have happened without you. There are a number of people that have been particularly involved with this thesis, thank you so much for all your help: Fiona, Brunda, Darren and Felicity. Thanks to Dave, Rusty, Hyun and Fiona for proofreading. And thanks also to the members of Breitling-group, offering me a second home in the Joseph Black building.

My family might not be too happy with me not living in the Netherlands (you tell me often enough!), but they still support me and visit me multiple times per year (or is that just for the shopping?).

There is a huge list of people who made my four years in Glasgow an unforgettable experience. Thank you all for the great times, you know who you are. There are three names that stand out: Emilie, David & Paul, I can not imagine the last four years without you. Finally, but arguable the most, I would like to thank past and present members of Team Barrett (and other L5 groups). It was because of you that I came to work with a smile every day, it is because of you that I feel sad for finishing this thesis. Hopefully I won't forget anybody: Brunda, Darren, Dave, Fede, Gordon, Hyun, Isabel, Jana, Jane, Kat, Kate, Mike, Noushin, Pieter, Pui Ee, Roy and Susan. Thank you all :-)

> *Everybody needs his memories. They keep the wolf of insignificance from the door.* ~ Saul Bellow

Author's declaration

I declare that, except where explicit reference is made to the contribution of others, this dissertation is the result of my own work and has not been submitted for any other degree at The University of Glasgow or any other institution.

Eduard Kerkhoven

Abbreviations

$_c$	cytosolic
$_g$	glycosomal
1,3-BPGA	1,3-bisphosphoglycerate
2-PGA	2-phosphoglycerate
2,3-BPG	2,3-bisphosphoglycerate
3-PGA	3-phosphoglycerate
3PGAT	3-phosphoglycerate transport
6-PG	6-phosphogluconate
6-PGL	6-phosphogluconolactonase
6PGDH	6-phosphogluconate dehydrogenase
AK	adenylate kinase
ALD	aldolase
ARG	putative arginase (gene Tb427.08.2020)
ATPu	ATP utilisation
CMM	Creek's minimal medium (see appendix A)
C_v^J	flux control coefficient
DHAP	dihydroxyacetone phosphate
E-4-P	erythrose 4-phosphate
ENO	enolase
FBS	fetal bovine serum
FDR	false discovery rate
Fru	fructose
Fru-1,6-BP	fructose 1,6-bisphophate
Fru-6-P	fructose 6-phosphate
FruT	fructose transport
G3PDH	glycerol-3-phosphate dehydrogenase
G6PDH	glucose-6-phosphate dehydrogenase
GA-3-P	glyceraldehyde 3-phosphate
GAPDH	glyceraldehyde-3-phosphate dehydrogenase
GC	gas chromatography
GDA	Gly-3-P:DHAP antiporter

GK	glycerol kinase
Glc	glucose
Glc-6-P	glucose 6-phosphate
GlcT	glucose transport
Gly-3-P	glycerol 3-phosphate
GSpdSH	glutathionylspermidine
HAT	human African trypanosomiasis
HXK	hexokinase
IMAC	immobilised metal ion affinity chromatrography
J	flux
LC	liquid chromatography
MS	mass spectrometry
NAM	putative nicotinamidase (gene Tb427tmp.160.2540/2600)
NAO	putative N-acetylornithine deactylase (gene Tb427.08.1910)
NECT	nifurtimox-eflornithine combination therapy
pAB	polyclonal antibody
PEP	phosphoenolpyruvate
PFK	phosphofructokinase
PGI	phosphoglucose isomerase
PGK	phosphoglycerate kinase
PGL	phosphogluconolactonase
PGAM	phosphoglycerate mutase
PPE	pentose phosphate epimerase
PPI	pentose phosphate isomerase
PPP	pentose phosphate pathway
PTS	peroxisomal targetting sequence
PYK	pyruvate kinase
PyrT	pyruvate transport
Rib-5-P	ribose 5-phosphate
RK	ribokinase (gene Tb427tmp.03.0090)
RNAi	RNA interference
Rul-5-P	ribulose 5-phosphate
S-7-P	sedoheptulose 7-phosphate
TAL	transaldolase
TKT	transketolase
TOX	oxidative stress reaction in dynamic models
TPI	triose phosphate isomerase
TR	trypanothione reductase
TS_2	trypanothione (oxidised)
$T(SH)_2$	trypanothione (reduced)
VSG	variable surface glycoprotein
WHO	World Health Organisation
X-5-P	xylulose 5-phosphate

Chapter 1

Introduction

Human African trypanosomiasis is a neglected tropical disease caused by subspecies of the parasite *Trypanosoma brucei.* The unique metabolic characteristics of *T. brucei* might provide potential targets for rational drug design. This project was conceived to further the understanding of trypanosomal metabolism by studying its dynamics both *in silico* and with wet-lab experimentation.

1.1. Human African trypanosomiasis

Human African trypanosomiasis (HAT) is a deadly parasitic disease also known by the misleadingly name of "sleeping sickness". HAT is caused by an infection with subspecies of the protozoan parasite *Trypanosoma brucei* which is transmitted via the tsetse fly vector. The distribution of tsetse flies (Cecchi *et al.*, 2008) restricts the spread of the disease to sub-Saharan Africa (Figure 1.1).

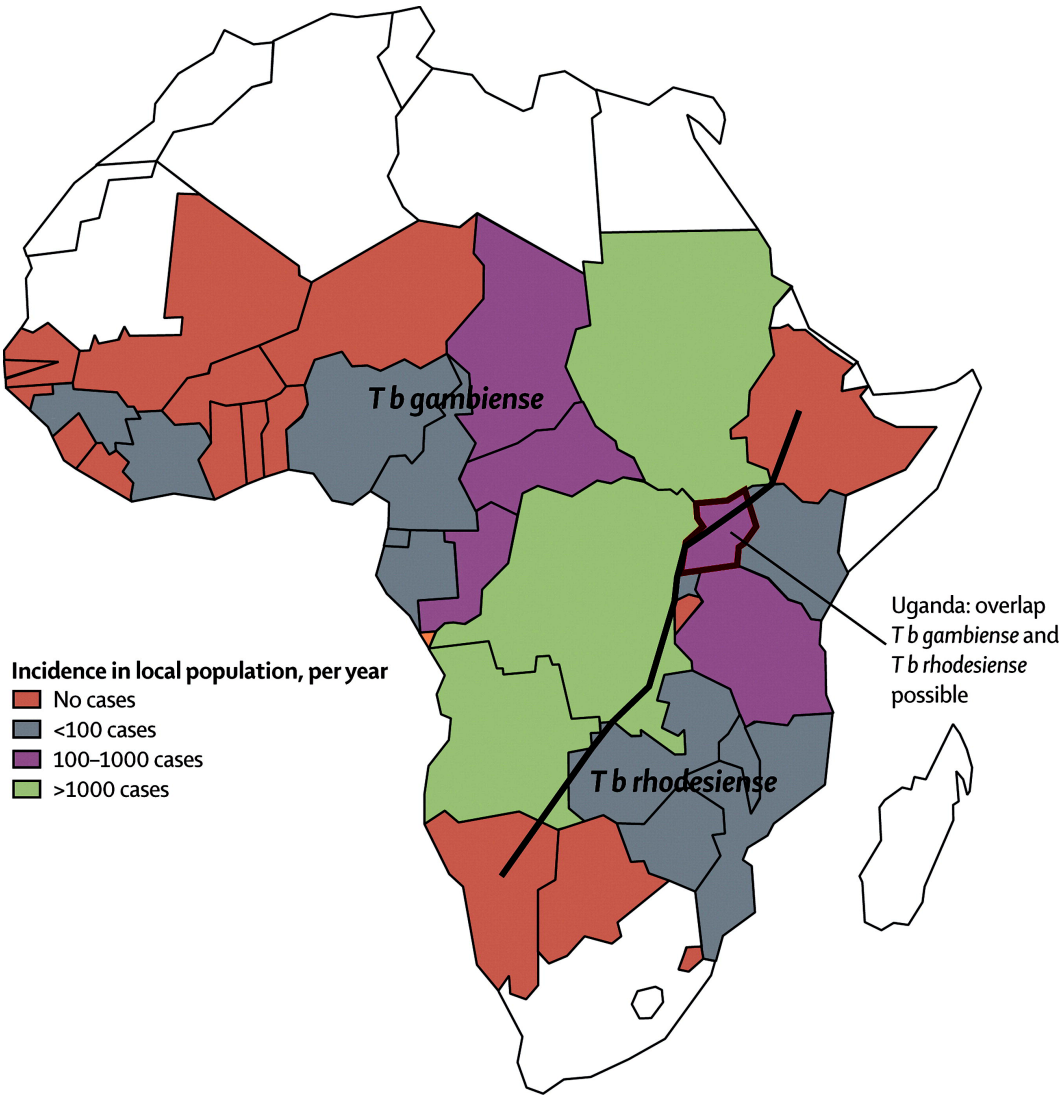

Figure 1.1.: Distribution of human African trypanosomiasis. The black line divides the areas in which either of the two subspecies predominates. Adapted from Brun *et al.* (2010), permission to reproduce this image has been granted by Elsevier.

HAT is a disease with two stages, defined by the presence of the parasites at different locations within the mammalian host. In the first stage of the disease, parasites reside in the blood plasma and lymph and symptoms vary from general malaise, headache and fever, to pulmonary oedema and pancarditis. The parasites evade the host's immune response by a combination of a dense glycoprotein coat and the remarkable ability to modulate its structure through a process of antigenic variation (Cross, 1975). The duration of the first stage of disease depends on the subspecies of *T. brucei* involved, and varies from a few weeks to months for *T. b. rhodesiense*, to several months to years for *T. b. gambiense*. Patients eventually progress into the second stage of the disease, when the parasites have entered the cerebral spinal fluid and eventually the brain. The second stage of HAT often leads to the characteristic symptoms of sleeping sickness: nocturnal insomnia and diurnal somnolence. It is in the second stage of the disease when patients usually present themselves at health clinics. Untreated infection leads invariably to coma and death.

The number of new cases of HAT have declined significantly in the last decade; in 2009, for the first time in 50 years, less than 10,000 cases were reported (Simarro *et al.*, 2008). However, the statistics on sleeping sickness incidence suffer from gross errors due to under-reporting of new cases and deaths (Odiit *et al.*, 2005). Many of the people affected do not present themselves at health clinics, which are often located beyond their reach or infected patients are not diagnosed correctly. In 2010, 7,139 new cases of HAT were reported to the World Health Organisation (WHO), while the predicted total number of cases was almost 5-fold higher (WHO, 2012). Although the recent decline in new cases of HAT is promising, a similar decline in the prevalence of HAT in the last century did not result in the eradication of the disease (Figure 1.2). Particularly, political instability and war are important factors increasing the risk of reemergence of HAT in countries including the Democratic Republic of the Congo and South Sudan (Berrang-Ford *et al.*, 2011; Tong *et al.*, 2011; Ruiz-Postigo *et al.*, 2012).

1.1.1. Chemotherapy

There are currently four licensed treatment regimes for HAT: pentamidine, suramin, melarsoprol, eflonithine and an additional nifurtimox-eflornithine combination therapy (NECT, Simarro *et al.*, 2012) which is used off-license having been placed on the WHO list of essential medicines. While many of these drugs have been around for decades,

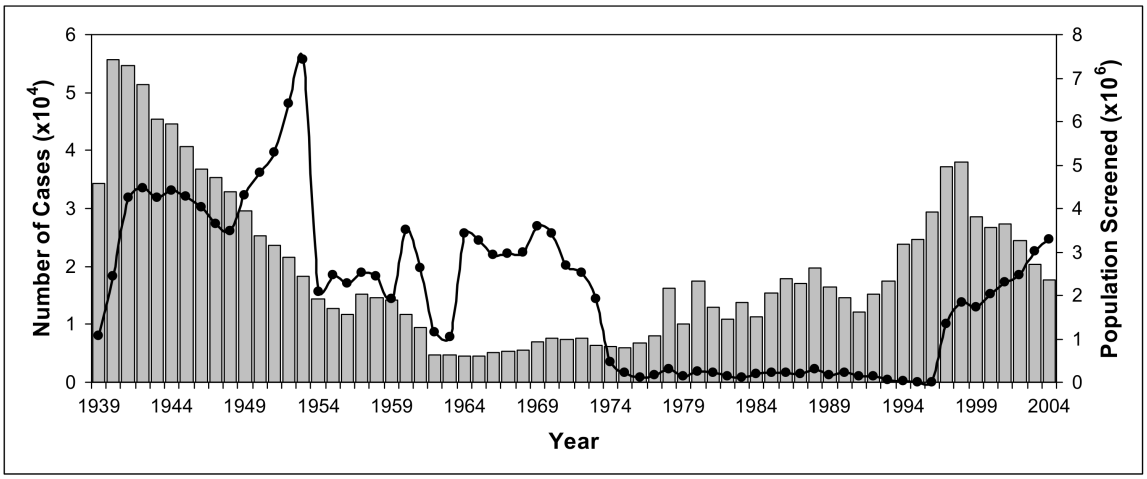

Figure 1.2.: Reported cases of sleeping sickness and population screened, 1939–2004. Grey columns, number of reported cases; black circles, population screened. From Steverding (2008), reproduced under the Creative Commons Attribution License.

only the mode of action of eflornithine is understood, as a suicide inhibitor of the enzyme ornithine decarboxylase (Poulin *et al.*, 1992).

The current available chemotherapies against HAT are unsatisfactory for a number of reasons: the drugs require parenteral administration, show severe side-effects and are relatively expensive when considering the impoverished state of most of HAT's victims (Barrett *et al.*, 2007). In 2010, the average cost to treat a stage II HAT patient was €336 (Simarro *et al.*, 2012). Pentamidine is only used against *T. b. gambiense*, while melarsoprol and eflornithine are the only effective drugs against stage II disease and melarsoprol may cause drug induced encephalopathy in 5−10 % of the patients. Additionally, resistance against the current drugs is of concern: resistant parasites to all the drugs have been selected in the laboratory (Phillips and Wang, 1987; Scott *et al.*, 1996; Bridges *et al.*, 2007; Vincent *et al.*, 2010), and treatment failures to all of the drugs have been noted in the field (Barrett *et al.*, 2011).

There is a renewed optimism that in the post-genomic era (Berriman *et al.*, 2005), our knowledge of the parasite's divergent biochemistry will enable development of novel therapies for the disease. The Kinetoplastida diverged early in evolution from other eukaryotes (Hannaert *et al.*, 2003b) and is replete with peculiar biochemical features that have encouraged those interested in drug development (Verlinde *et al.*, 2001; Stuart *et al.*, 2008). The development of genetic tools in trypanosomes, such as gene knock out and RNA interference allow the study of these potential drug targets in more detail (Barrett *et al.*, 1999; Clayton, 1999).

1.2. *Trypanosoma brucei*

Trypanosoma brucei is a flagellated protozoan parasite, a member of the order Kinetoplastida and the family Trypanosomatida. There are three subspecies of *T. brucei*, of which two are human infective. *T. b. gambiense* causes >90 % of the reported cases of HAT and can be found in West and Central sub-Saharan Africa, while *T. b. rhodesiense* is found in East sub-Saharan African and causes the remaining 10 % of HAT (Simarro *et al.*, 2008). The third subspecies, *T. b. brucei*, is non-infective for humans, and is therefore routinely used in laboratories. Other members of the Trypanosomatida include *T. congolense* and *T. vivax*, causing n'gana in cattle in Africa; *Trypanosoma cruzi*, the causative agent of Chagas' disease in South-America; and members of the genus *Leishmania*, causative agents of a range of diseases in the tropics and subtropics (Barrett *et al.*, 2003).

1.2.1. A unique life cycle

T. brucei has a complex life cycle during which they encounter vastly differing environments (Figure 1.3). Upon injection into the bloodstream, *T. brucei* is fully adapted to the glucose-rich environment of mammalian blood. Bloodstream form parasites express a coat of variable surface glycoproteins (VSG), in an attempt to evade the host's immune system. Metacyclic trypomastigotes transform into the rapidly dividing bloodstream form trypomastigotes, which can be readily cultured in the laboratory (Hirumi and Hirumi, 1989). When parasitaemia in the host increases, the long-slender bloodstream form trypomastigotes differentiate into the non-dividing short-stumpy trypomastigote forms via a quorum-sensing type mechanism that has not been fully elucidated (Fenn and Matthews, 2007).

Stumpy form parasites are primed to differentiate upon uptake into the tsetse fly vector to the procyclic form trypomastigtes (Figure 1.3). During differentiation in the tsetse midgut, the surface coat switches from VSGs to the expression of the non-variable GPEET and EP procyclins (Vassella *et al.*, 2001). While migrating towards the salivary glands, the parasites differentiate into the metacyclic trypomastigotes that are ready to be injected into a new mammalian host. While residing in the tsetse fly, *T. brucei* relies on the use of amino acids, particularly proline, for energy metabolism (Bursell, 1981; Bringaud *et al.*, 2006).

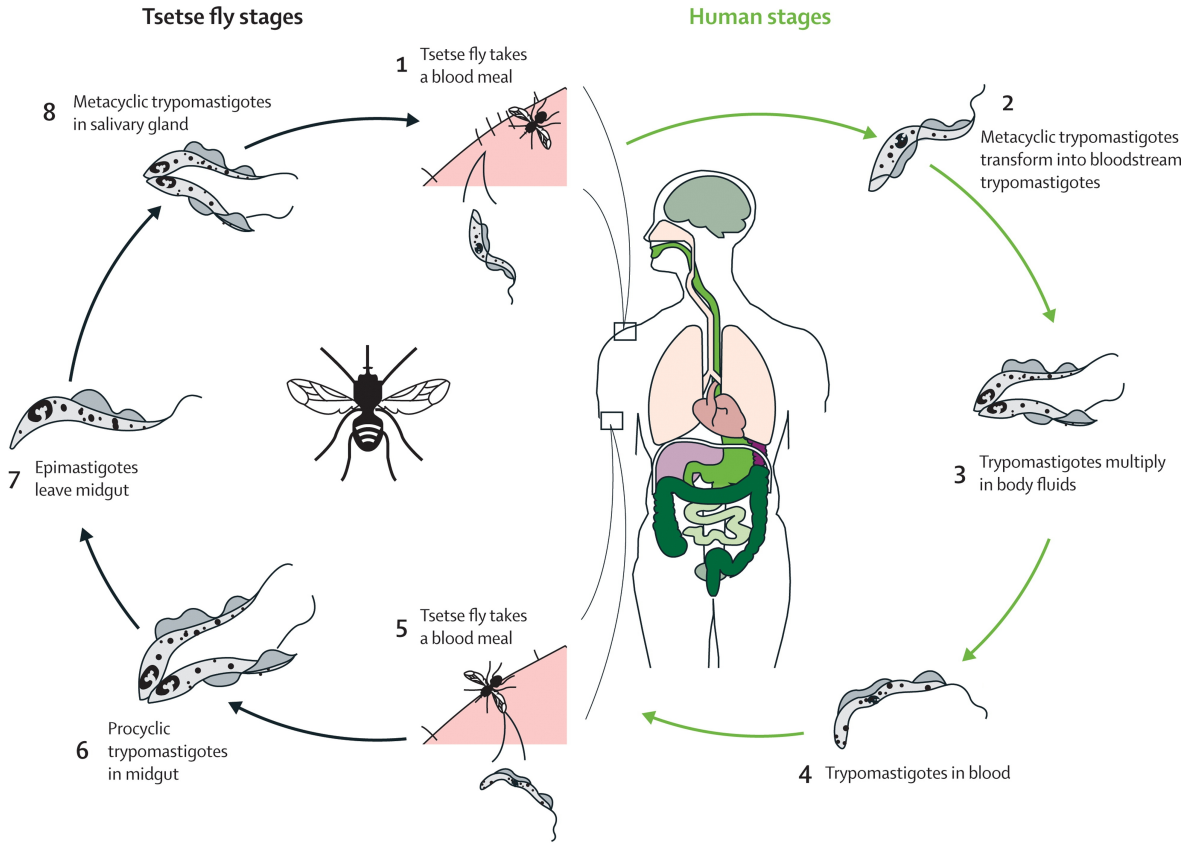

Figure 1.3.: Life-cycle stages of *Trypanosoma brucei*. Adapted from Blum *et al.* (2008), permission to reproduce this image has been granted by Elsevier.

1.3. Trypanosomal glycolysis

In the mammalian host, where glucose is available in high (5 mM) and constant levels, glucose is the sole energy source for *T. brucei*, that has no functional citric acid cycle in the bloodstream form stage (Ryley, 1956; Durieux *et al.*, 1991). The bloodstream form of *T. brucei* has a streamlined energy metabolism, where glucose is only catabolised in glycolysis to pyruvate and glycerol (Grant and Fulton, 1957), with negligible amounts used in biosynthetic processes (Haanstra *et al.*, 2012). Recent tracking of ^{13}C-labelled glucose through untargeted metabolomics challenges this view, with glucose-derived carbons ending up in various tricarboxylic acids, although labelling patterns indicate these are glycosomal derived following fixation of CO_2 onto phosphoenolpyruvate rather than products of a citric acid cycle (unpublished data; Dr Darren Creek, University of Glasgow).

1.3.1. Compartmentalisation of glycolysis

A major part of trypanosomal glycolysis is compartmentalised in peroxisome-related microbodies called glycosomes, which were first described by Opperdoes and Borst (1977), described in detail in Section 1.4. The compartmentalisation of glycolysis is thought to have a selective advantage by providing a greater metabolic flexibility to the vastly differing environments *T. brucei* encounters during its life-cycle (Herman *et al.*, 2008; Gualdrón-López *et al.*, 2012a). Over 90 % of the total protein content of the glycosomes in bloodstream form *T. brucei* is comprised of glycolytic enzymes (Aman *et al.*, 1985; Misset *et al.*, 1986), while the same enzymes in the procyclic form only make up 40–50 % of the total glycosomal protein (Hart *et al.*, 1984).

In the glycosome, glucose is converted to 3-phosphoglycerate, that is subsequently catabolised further to pyruvate in the cytosol (Figure 1.5). Pyruvate is the end product of glycolysis in bloodstream form *T. brucei* due to the absence of lactate dehydrogenase (Dixon, 1966; Ormerod *et al.*, 1970) or a functional tricarboxylic acid cycle (Ryley, 1956; Durieux *et al.*, 1991). The glycosome has been described as a permeability barrier for sugar-phosphates, ATP/ADP and NADH/NAD^+—although this has recently been challenged, as discussed in Section 1.4.

The partial glycosomal compartmentalisation compels the flux through glycolysis to adhere to the strict stoichiometry of the pathway. Any reduction of NAD^+ by glyceraldehyde-3-phosphate dehydrogenase needs to be balanced by the oxidation of NADH by glycerol-3-phosphate dehydrogenase, reducing dihydroxyacetone phosphate (DHAP) to glycerol 3-phosphate (Gly-3-P). Under aerobic conditions, a Gly-3-P:DHAP shuttle subsequently reoxidises glycerol 3-phosphate to DHAP via a mitochondrial glycerol-3-phosphate oxidase (Clarkson *et al.*, 1989). DHAP can subsequently be directed towards pyruvate production via triosephosphate isomerase (TIM). Under anoxic conditions, glycerol 3-phosphate cannot be oxidised in the mitochondrion, and is converted to glycerol by the reverse action of glycerol kinase. While aerobic glycolysis yields two ATP molecules by pyruvate kinase per glucose molecule consumed, anaerobic glycolysis only yields one molecule and equimolar amounts of pyruvate and glycerol (Ryley, 1956; Haanstra *et al.*, 2012).

With part of glycolysis localised to the glycosome, trypanosomal glycolysis has lost some of the regulation seen in other organisms. Glycolysis is an example of an autocatalytic pathway, as the surplus ATP production of glycolysis can fuel its early steps in a positive feedback loop (Figure 1.4). This has been called the “turbo” principle and contains a inherent risk (Teusink *et al.*, 1998). The surplus of ATP produced

could boost the flux through the early reactions of glycolysis above the capacity of the enzymes downstream, resulting in extreme accumulation of the intermediates, hexose-phosphates. Most organisms prevent this "turbo design" of glycolysis by additional negative feedback to hexokinase and phosphofructokinase (Teusink *et al.*, 1998), e.g., inhibition of hexokinase by glucose 6-phosphate (Weil-Malherbe and Bone, 1951) or phosphofructokinase by phosphoenolpyruvate (Blangy *et al.*, 1968).

T. brucei lacks feedback regulation through hexokinase and phosphofructokinase (Nwagwu and Opperdoes, 1982). Bakker *et al.* (2000) predicted from mathematical modelling of trypanosomal metabolism (discussed in 1.8.5) that the loss of glycosomal localisation of the glycolytic enzymes in *T. brucei* would result in a "turbo explosion". And indeed, later experimentation confirmed that parasites deficient in glycosomal protein localisation accumulate hexose-phosphates (Haanstra *et al.*, 2008). Additionally, other groups have confirmed that high glucose concentrations are lethal for glycosome-deficient bloodstream forms, while procyclic forms could be rescued by the removal of sugars from the medium (Furuya *et al.*, 2002), or by the ablation of hexokinase (Kessler and Parsons, 2005). The essentiality of the glycosome for the prevention of a turbo effect is likely a consequence of the glycosomal compartmentalisation, rather than the cause (Gualdrón-López *et al.*, 2012b).

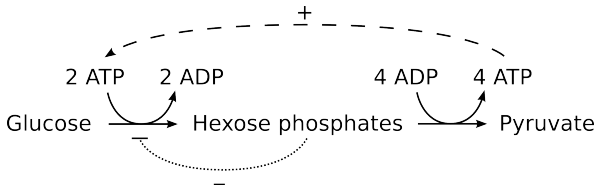

Figure 1.4.: The autocatalytic design of glycolysis. The conversion of glucose to pyruvate through glycolysis, with the intrinsic positive feedback (dashed arrow). Most organisms have some sort of negative feedback from the hexose phosphates to the early steps of glycolysis (dotted arrow).

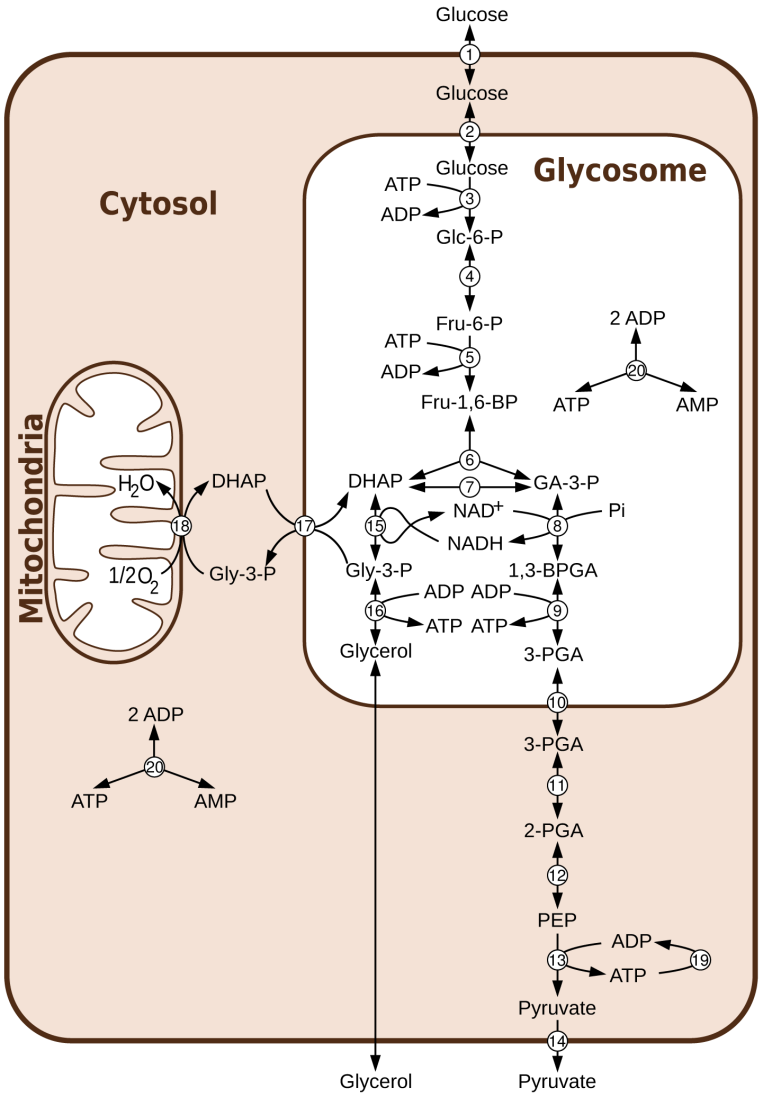

Figure 1.5.: Glycolysis in the glycosomes of bloodstream form *T. brucei*. Abbreviations used are as follows: *Glc-6-P*, glucose 6-phosphate; *Fru-6-P*, fructose 6-phosphate; *Fru-1,6-BP*, fructose 1,6-bisphosphate; *DHAP*, dihydroxyacetone phosphate; *GA-3-P*, glyceraldehyde 3-phosphate; *Gly-3-P*, glycerol 3-phosphate; *1,3-BPGA*, *Pi*, inorganic phosphate; 1,3-bisphosphoglycerate; *3-PGA*, 3-phosphoglycerate; *2-PGA*, 2-phosphoglycerate; *PEP*, phosphoenolpyruvate. Reactions shown are as follows: step *1*, transport of glucose across the cytosolic membrane ($GlcT_c$); *2*, transport of glucose across the glycosomal membrane ($GlcT_g$); *3,* hexokinase (HXK); *4*, phosphoglucose isomerase (PGI); *5*, phosphofructokinase (PFK); *6,* aldolase (ALD); *7*, triosephosphate isomerase (TIM); *8*, glyceraldehyde-3-phosphate dehydrogenase (GAPDH); *9*, phosphoglycerate kinase (PGK); *10*, transport of 3-PGA across the glycosomal membrane (3PGAT); *11*, phosphoglycerate mutase (PGM); *12*, enolase (ENO); *13*, pyruvate kinase (PYK); *14*, transport of pyruvate across the cytosolic membrane (PYRT); *15*, glycerol 3-phosphate dehydrogenase (G3PDH); *16*, glycerol kinase (GK); *17*, Gly-3-P:DHAP antiporter (GDA); *18*, glycerol-3-phosphate oxidation (AOX); *19*, ATP utilisation (ATPu); *20*, adenylate kinase (AK). From Achcar *et al.* (2012), reproduced under the Creative Commons Attribution License.

1.4. A unique organelle: the glycosome

Glycosomes are globular microbodies, related to peroxisomes and glyoxysomes (Opperdoes, 1988). Glycosomes have a diameter of around 0.27 μm, while bloodstream form trypanosomes contain 240 glycosomes on average, representing 4.3 % of the total cell volume (Opperdoes *et al.*, 1984). Several early reports show evidence of particle-bound glycolytic enzymes in trypanosomes, such as hexokinase (HXK) (Risby and Seed, 1969), phosphoglucose isomerase (PGI) (Risby *et al.*, 1969) and glycerol-3-phosphate dehydrogenase (G3PDH) (Reynolds, 1975), but this was poorly understood at the time. Opperdoes and Borst (1977) purified microbodies from bloodstream form *T. brucei* and showed that nine glycolytic enzymes are predominantly localised to these microbodies. The term glycosome was coined for the high glycolytic content.

1.4.1. Glycosomal targeting of enzymes

Glycosomal proteins are encoded by nuclear genes (microbodies, including glycosomes, do not contain DNA, Opperdoes, 1984), and therefore need to be transported into the glycosome. It has been demonstrated that import of proteins in peroxisomes is dependent upon three amino acids (serine-lysine-leucine, or related motifs) at the very end of the C-terminus (Gould *et al.*, 1988). This peroxisomal targeting signal (PTS-1) was first noted with the observation that firefly luciferase, containing a C-terminal serine-lysine-leucine sequence, was transported into mammalian peroxisomes (Keller *et al.*, 1987). Similar transport of luciferase into glycosomes indicates that the PTS-1 sequence can also target proteins to glycosomes (Sommer *et al.*, 1992).

Substitutions of amino acids in the PTS-1 have demonstrated that the exact amino acid sequence of PTS-1 is less strict for transport into glycosomes when compared to mammalian peroxisomes (Sommer and Wang, 1994). PTS-1 is present in many glycosomal enzymes, but absent in others, such as hexokinase, aldolase and triosephosphate isomerase (Colasante *et al.*, 2006). However, an additional peroxisomal targeting signal has been identified at the N-terminal of peroxisomal proteins (Swinkels *et al.*, 1991). This signal, PTS-2, has also been demonstrated to function in trypanosomes (Blattner *et al.*, 1995), and identified to be present in various proteins, including aldolase (Chudzik *et al.*, 2000). An internal peroxisomal targeting signal (I-PTS) has also been reported for peroxisomal targeting in *Saccharomyces cerevisiae* (Klein *et al.*, 2002), which is present in trypanosomal triosephosphate isomerase (Galland *et al.*, 2007).

Importing proteins into peroxisomes and glycosomes involves a protein complex, including PEX2 (Guerra-Giraldez *et al.*, 2002), PEX5 (de Walque *et al.*, 1999) and PEX14 (Moyersoen *et al.*, 2003). PEX5 is the cytosolic receptor recognising the PTS-1 sequence, while PEX14 is a membrane bound protein that acts as a docking station for PEX5, and PEX2 is involved in the actual translocation of the protein across the glycosomal membrane (Schliebs, 2006). Conditional knock-out of various PEX proteins showed that the glycosome is an essential organelle for trypanosomes (Fry *et al.*, 1993; Guerra-Giraldez *et al.*, 2002; Moyersoen *et al.*, 2003; Krazy and Michels, 2006; Verplaetse *et al.*, 2009) .

1.4.2. Transport of metabolites over the membrane

It has been suggested that the glycosome acts as a permeability barrier preventing the glycolytic intermediates, ATP/ADP and NADH/NAD^+ from freely moving between the glycosome and cytosol (Opperdoes and Borst, 1977; Opperdoes, 1987; Clayton and Michels, 1996). This separation of cytosolic and glycosomal pools of metabolites has been particularly important to prevent the aforementioned turbo effect (Bakker *et al.*, 2000; Haanstra *et al.*, 2008). It is noteworthy that while most metabolites were assumed to not cross the glycosomal membrane, glucose, 3-phosphoglycerate, glycerol and the combination of DHAP and glycerol 3-phosphate were assumed to cross the glycosomal membrane by unknown mechanisms (Bakker *et al.*, 1997).

Recently, this hypothesis of non-permeable glycosomes has been challenged by the discovery of two types of pores in glycosomes, similar to pores in peroxisomes (Grunau *et al.*, 2009; Rokka *et al.*, 2009). An investigation by Gualdrón-López *et al.* (2012c) defined channel-forming proteins in the glycosomal membrane that would allow the free flow of small molecules across the glycosomal membrane. This poses a problem with the previously observed importance of glycosomal compartmentalisation of glycolysis. In an additional paper, Gualdrón-López *et al.* (2012a) argue that, even though the non-specific channels are present, glycolytic intermediates are retained within the glycosome. This could be accomplished by; (i) the glycolytic enzymes forming a multi-enzyme complex, where there is limiting availability of free intermediates; (ii) a Donnan equilibrium, where the glycosomal enzymes have a higher pI than cytosolic enzymes and therefore attract the intermediates; (iii) a regulatory mechanism involving regulatory enzymes or proteins that are currently unknown.

1.5. Pentose phosphate pathway

Although the glycosome is named after the presence of glycolytic enzymes, it also houses other metabolic pathways. One of those is the pentose phosphate pathway (PPP, Figure 1.6). Early reports show that the release of CO_2 from a trypanosome culture accounted for less than 1 % of the glucose consumed, from which it was concluded that the PPP was not very active (Grant and Fulton, 1957). This was supported by the observation that no activity for 6-phosphogluconate dehydrogenase (6PGDH) could be detected (Ryley, 1962). However, a later report demonstrated that the activity of 6PGDH can be detected in trypanosomes and is dependent on Mg^{2+}, which was absent in earlier experiments (Cronin *et al.*, 1989). This report also showed the activity of other enzymes from the PPP.

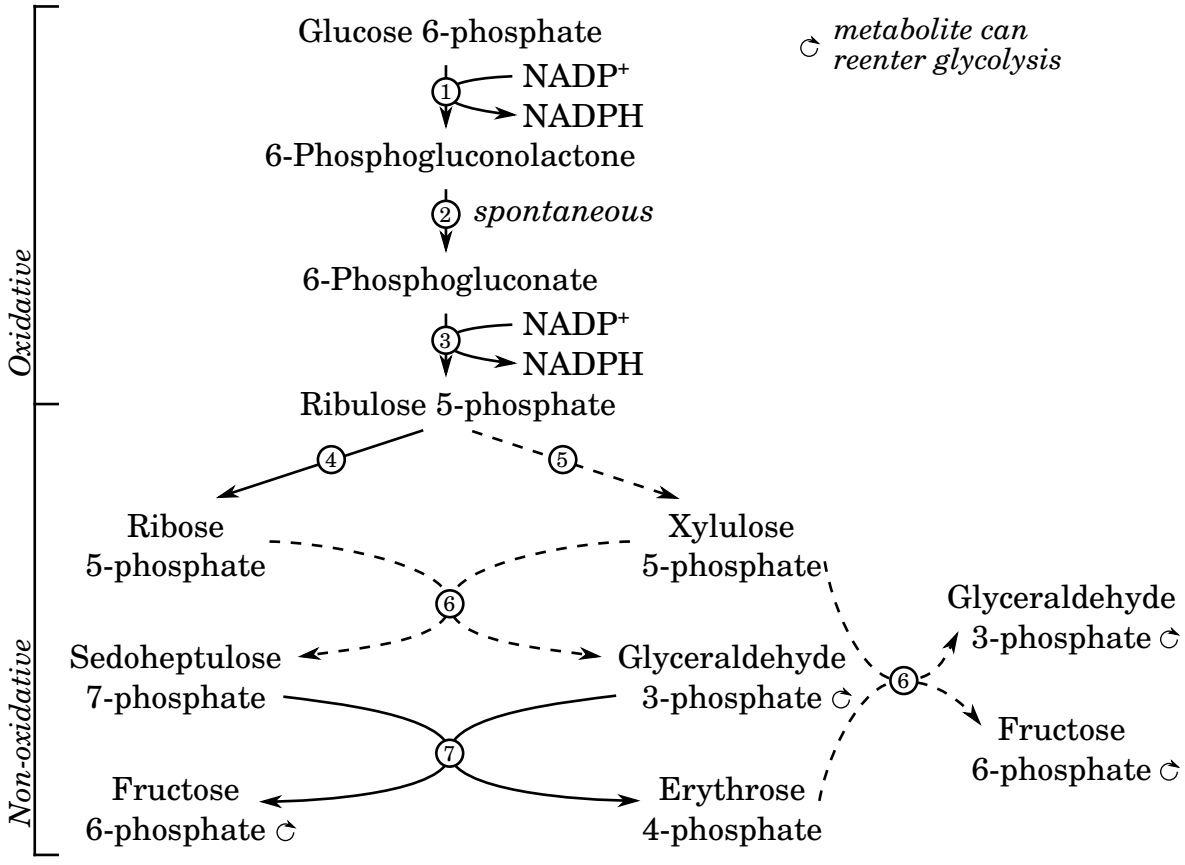

Figure 1.6.: The PPP in *T. brucei*. Solid arrows indicate reactions present in all life-stages, dashed arrows indicate reactions that are not present in the bloodstream form stage. *1:* glucose-6-phosphate dehydrogenase (G6PDH); *2:* 6-phosphogluconolactonase (PGL, reactions also occurs spontaneously); *3:* 6-phosphogluconate dehydrogenase (6PGDH); *4:* pentose phosphate isomerase (PPI); *5:* pentose phosphate epimerase (PPE); *6:* transketolase (TKT, catalyses two reactions); *7:* transaldolase (TAL).

1.5.1. Oxidative PPP

In the oxidative part of the PPP (or hexose monophosphate shunt) glucose 6-phosphate is oxidised to 6-phospogluconolactone (6-PGL) by glucose-6-phosphate dehydrogenase (G6PDH), while $NADP^+$ is reduced to NADPH. 6-PGL is hydrolysed to 6-phosphogluconate (6-PG) by both a spontaneous reaction (Kupor and Fraenkel, 1972) and catalysed by the enzyme 6-phosphogluconolactonase (PGL). The dedication of an enzyme to the catalysis of an already spontaneously occurring reaction probably has the function to keep the concentration of 6-PGL as low as possible, as this strong electrophile can have toxic effects (Rakitzis and Papandreou, 1998). NMR analysis has also shown that the 6-PGL that is produced by G6PDH is of the so called δ-form, which can lead to the γ-form by intramolecular rearrangement (Miclet *et al.*, 2001). However, only the δ-form undergoes spontaneous hydrolysis, the γ-form of 6-PGL is a 'dead branch', resulting in an accumulation of the highly electrophilic compound. G6PDH is only able to hydrolyse the δ-form, but by doing so it prevents its conversion into the γ-form.

6-PG is subsequently oxidised and decarboxylated to ribulose 5-phosphate (Rul-5-P) by 6-phosphogluconate dehydrogenase, while again reducing $NADP^+$ to NADPH. Pentose phosphate isomerase finally converts Rul-5-P into ribose 5-phosphate (Rib-5-P), although this step can also be considered to be part of the non-oxidative part of PPP.

1.5.2. Non-oxidative PPP

In the non-oxidative part of the PPP, pentose phosphate epimerase (PPE) converts Rul-5-P into xylulose 5-phosphate (X-5-P). The enzyme transketolase (TKT) transfers two carbon atoms from X-5-P to Rib-5-P, producing glyceraldehyde 3-phosphate (GA-3-P) and sedoheptulose 7-phosphate (S-7-P). Transaldolase (TAL) can subsequently transfer three of the carbon atoms from S-7-P to GA-3-P, producing fructose 6-phosphate (Fru-6-P) and erythrose 4-phosphate (E-4-P). TKT can catalyse another reaction, where two carbon atoms from X-5-P are transferred to E-4-P, producing Fru-6-P and GA-3-P.

The end products from three molecules of Rul-5-P through the non-oxidative part of the PPP are one molecule of GA-3-P and two molecules of Fru-6-P. In bloodstream form trypanosomes only the oxidative part of the PPP, including PPI is active, while the whole PPP is operational in procyclic trypanosomes (Cronin *et al.*, 1989; Colasante *et al.*, 2006).

1.5.3. Functions of PPP

The PPP has several important functions, such as the production of reducing equivalents in the form of NADPH, which can protect the parasite during oxidative stress (Barrett, 1997). In *T. cruzi*, the connection between resistance against oxidative stress and activity of G6PDH and 6PGDH—two enzymes that produce the protecting NADPH—has been demonstrated (Igoillo-Esteve and Cazzulo, 2006; Mielniczki-Pereira *et al.*, 2007). In this context, a genetic null mutant of the glucose transporter in *Leishmania mexicana* was also more sensitive to oxidative stress (Rodriguez-Contreras *et al.*, 2007).

The production of Rib-5-P is also an important function of the PPP in many organisms, as this metabolite can be used to produce phosphoribosylpyrophosphate, an important intermediate in nucleotide biosynthesis. The non-oxidative branch in procyclic trypanosomes is also important in provision of key carbohydrate precursors and interconnecting pentose phosphates with glycolytic intermediates.

Most of the PPP enzymes appear to be targeted to the glycosome, suggested by the presence of PTS sequences. However, experiments also show a dual localisation of the PPP enzymes, here they are most abundant in the cytosol. Of the total cellular activity, 85 % of PGL and 55 % of G6PDH were located in the cytosol (Heise and Opperdoes, 1999; Duffieux *et al.*, 2000). The localisation of 6PGDH was inconclusive, but indicates a larger abundance in the cytosol (Heise and Opperdoes, 1999). It has been reported that transketolase has a PTS (Colasante *et al.*, 2006) and most of this enzyme is found in the cytosol with a small proportion also found in glycosomes (Veitch *et al.*, 2004; Stoffel *et al.*, 2011).

1.6. Redox metabolism

Another characteristic of the divergent biochemistry of trypanosomatids is the mechanism by which it regulates its redox balance. Where most organisms use glutathione as the central thiol to control cellular redox, trypanosomatids use trypanothione or N^1,N^8-bis(glutathionyl)-spermidine, which consists of two glutathione molecules conjugated to a spermidine linker (Fairlamb *et al.*, 1985). Trypanothione is central in maintaining cellular redox metabolism in trypanosomatids (Krauth-Siegel and Comini, 2008) and is more efficient than glutathione as it can form intramolecular disulphide bonds more rapidly (Olin-Sandoval *et al.*, 2010). Interestingly, the trypanocidal drug eflornithine acts as a suicide inhibitor of ornithine decarboxylase

(Bacchi *et al.*, 1983), an enzyme involved in the synthesis of polyamines and ultimately trypanothione (Figure 1.7). Untargeted metabolomics shows that treatment of *T. brucei* with a sub-lethal dose of eflornithine leads to significant changes in concentrations of polyamines, i.e. putrescine levels are depleted (Vincent *et al.*, 2012).

1.6.1. Ornithine biosynthesis

Given the effects of eflornithine on ornithine decarboxylase, it was considered that ornithine biosynthesis is a good drug target. It has been assumed that arginase was the source of ornithine in *T. brucei*, as in other eukaryotes (Figure 1.7).

The gene coding for arginase in the related species *Leishmania* has been identified and studied in detail (da Silva *et al.*, 2002, 2008, 2012; Riley *et al.*, 2011), but *T. brucei* does not have a syntenic homologue of this gene (Vincent, 2011). However, the *T. brucei* genome does harbour a different putative gene with high sequence similarity to other eukaryotic arginases. The syntenic partner of this gene was putatively annotated in *Leishmania* as an ureohydrolase, the group to which arginase also belongs.

The *T. brucei* gene was putatively annotated as arginase in early genome databases, although this annotation was changed in a later update to agmatinase, another ureohydrolase. However, *T. brucei* has found to have negligble arginase activity (Vincent *et al.*, 2012). Sequence alignment of the latter gene with known arginases from different species demonstrated the absence of key active site residues (Vincent, 2011).

Interestingly, following treatment of *T. brucei* with eflornithine, the accumulation of ornithine is closely correlated to the accumulation of *N*-acetylornithine (Vincent *et al.*, 2012). This brings up the suggestion that *T. brucei* produces ornithine from glutamine, similar to a common pathway in prokaryotes (Figure 1.8). In contrast, further investigation by (Vincent, 2011) demonstrated that *T. brucei* does not use glutamine to produce ornithine, although a putative *N*-acetylornithine deacetylase gene was identified. The putative arginase and *N*-acetylornithine deactylases genes are investigated in more detail in chapter 5. It seems that much of the trypanosome's supply of ornithine is via uptake from its environment, although in ornithine-free conditions, arginine can be converted to ornithine, albeit by an unknown route (Vincent, 2011).

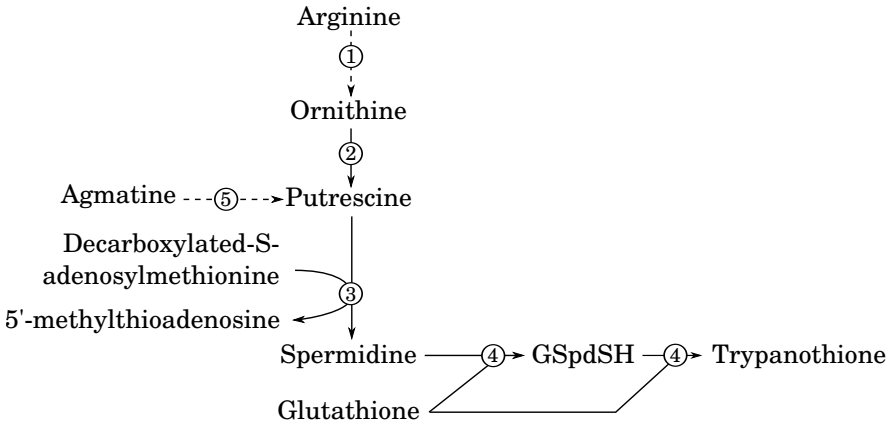

Figure 1.7.: The trypanothione biosynthetic pathway. Trypanothione consists of two glutathione molecules conjugated to a spermidine linker, produced in a two-step reaction by trypanothione synthase. *Leishmania* spp. have a functional arginase that can produce ornithine, which is lacking in *Trypanosoma brucei*. GSpdSH, glutathionylspermidine. *1:* arginase; *2:* ornithine decarboxylase; *3:* spermidine synthase; *4:* trypanothione synthase; *5:* agmatinase.

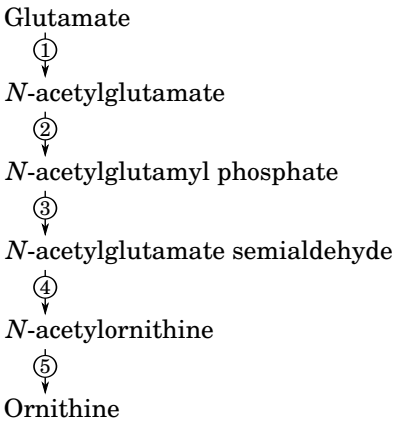

Figure 1.8.: Ornithine biosynthetic pathway from glutamate. Reaction *1: N*-acetylglutamate synthase; *2: N*-acetylglutamate kinase; *3: N*-acetyl-γ-glutamyl phosphate reductase; *4: N*-acetylornithine transaminase; *5: N*-acetylornithine deacetylase.

1.7. Metabolomics

To study metabolic pathways one can apply the analysis of all small molecules in a given biological sample, called metabolomics (Creek *et al.*, 2012a). The aim of metabolomics is not only to study the complete metabolic content (Mr <1200) of cells or other defined systems, but also to do this in an unbiased and high-throughput manner. Of all the "omics" techniques, metabolomics could be described as being closest to the phenotype.

Where in the other "omics", entities are studied that more or less follow the same basic structure (for example a deoxyribose-backbone with four types of bases in DNA), the complement of metabolites (or "metabolome", as introduced by Tweeddale *et al.*, 1998) is very heterogeneous in chemicophysical properties. Metabolites extend over a broad range in mass, volatility, charge, stability, thermolability etc. Due to the heterogeneity of the metabolome, there is not a single technique that can be used to measure all metabolites. Several techniques have been developed and all have their own biases against certain metabolites alongside other (dis)advantages.

The main techniques used in metabolomics are mass spectrometry (MS) and nuclear magnetic resonance (NMR) spectroscopy. MS is often hyphenated with gas chromatography (GC) or liquid chromatography (LC) to resolve complex biological mixtures, increasing the resolution and decreasing ion suppression (Villas-Bôas *et al.*, 2005). There also exist a variety of mass-spectrometers, differing in methods of ionisation (Vestal, 2001), detection and mass analysis (McLuckey and Wells, 2001). MS generally has a high sensitivity and resolution, but lacks quantitative accuracy. NMR spectroscopy on the other hand, has a lower sensitivity and resolution, but an outstanding quantitative accuracy and reproducibility (Pan and Raftery, 2007). Additionally, as NMR is typically not hyphenated to a separation technique, it has no bias for or against volatile, heavy or charged compounds.

Metabolomics has been used successfully many times in the study of Kinetoplastids (Creek *et al.*, 2012a). For example, NMR has been used to study anaerobic glycolysis of *T. brucei* (Mackenzie *et al.*, 1982, 1983), but more recently in a series of studies on central carbon metabolism in the procyclic form of this parasite (Besteiro *et al.*, 2002; Coustou *et al.*, 2006, 2008; Ebikeme *et al.*, 2010). The mode of action of the drugs eflornithine and nifurtimox on *T. brucei* were investigated with LC-MS (Vincent *et al.*, 2012), while central carbon metabolism was investigated in *Leishmania* (Saunders *et al.*, 2010).

1.8. Systems biology of metabolism

Trypanosomal metabolism has for long been the subject of investigation due to its unique characteristics and the hope of identifying potential drug targets, with particular focus on both the metabolites (e.g. trypanothione) and enzymes (e.g. ornithine decarboxylase). However, most of these studies are about defining the characteristics of the object of interest in isolation, while their role is performed in real biological systems.

1.8.1. Why modelling metabolism?

Real systems in biology are mathematically complex, and would be impossible to study as a whole without the use of modelling. Models are simplified abstractions of reality, that aim to provide a deeper understanding of the real system. An important reason for the complexity of biological systems is that they are hierarchical, both in time scales and material structures. The time it takes for a compound to react with an enzyme is separated by many orders of magnitude from the time it takes for a full cell-division. And the material structures range from low-weight molecular compounds that make up metabolism to whole organisms and even populations. Focusing only on metabolism reduces the time scale and limits the scope of the analysis to the enzymes and their metabolites, whereby you are no longer looking at the real system, but rather at a model.

A second reason for the complexity of biological systems is that they are highly connected. Enzymes interact with metabolites, but also with other enzymes, which are themselves the product of transcription and translation. In this respect, RNA and DNA can also interact with each other, with enzymes and metabolites. All these interactions can theoretically be described by mathematical equations, with various levels of detail. Again, only focusing on metabolism reduces the complexity of the system, but results in a simplified model.

Mathematical modelling of metabolism allows the investigation of the constituent parts of metabolism within a biological context, by using mathematics to describe the interactions within the network and focusing on the part of system important for the particular research question. An important feature of using modelling while studying biological systems is the constant iterative cycle between the real biological system and the model.

1.8.1.1. Metabolic control analysis

An important example of why the modelling of metabolism is required, and not just the study of enzymes in isolation, is the subject of metabolic control analysis. In a landmark paper in 1973, Kacser and Burns showed that the accepted dogma of one rate-limiting step in a metabolic pathway is incorrect. Rather than one enzyme that controls the flux through a pathway, the control is distributed through all the enzymes that are part of the pathway. Not all enzymes have the *same* control on the pathway, enzymes can have a near-zero control or even a negative control, but all control is shared.

The control of an enzyme can be quantified with the control coefficient:

$$C_{v_i}^{J} = \frac{d \ln J}{d \ln V_{max,i}}, \tag{1.1}$$

where J is the metabolic flux through the pathway, vi represent reaction i and $V_{\mathrm{max,i}}$ is the activity of enzyme i. The control coefficient can theoretically obtain a number between 0 and 1. If the control-coefficient $C_{v_i}^{J}$ of enzyme i is zero, then any changes in the activity $V_{\mathrm{max,i}}$ of enzyme i has no effect on the flux J through the pathway. If the control-coefficient $C_{v_i}^{J}$ of enzyme i is 1, then any changes in the activity $V_{\mathrm{max,i}}$ of enzyme i lead to an equal change of the flux J through the pathway. All enzymes combined share all control over the flux through the pathway, such that

$$\sum_{i=1}^{n} C_{v_i}^{J} = 1, \tag{1.2}$$

where n is the total number of enzymes in the pathway. From this it becomes clear that the control coefficient can only be calculated, and only has meaning, when enzymes are studied as part of a pathway rather than in isolation.

1.8.2. Top-down versus bottom-up

Two broad approaches have emerged to allow the study of metabolism in recent years: top-down and bottom-up (Figure 1.9 and Bruggeman and Westerhoff, 2007). The main difference in the two approaches is primarily dictated by what data is used to generate the mathematical models.

The top-down approach to modelling generates large networks with limited detail, starting by generating data that describes (a large part of) the whole system. These data sets can for instance be gene expression profiles, protein-protein interactions or untargeted metabolomics (Kell, 2004; Chandrasekaran and Price, 2010). Subsequently, it is attempted to make connections between the measured entities from a data set. From gene expression profiles for instance, one can generate a metabolic map describing all active metabolic pathways by connecting all expressed enzymes in a particular life-cycle stage. Because of the size and nature of the underlying data sets, the models generated from a top-down approach are typically large but only describe the stoichiometry of the network.

The main objective of top-down models is to discover how the observed systemic behaviour can be explained from the structure of the network. For instance a model of all active metabolic pathways in a particular life-cycle of a cell can be used to identify critical reactions, so called choke points, that can pin-point to important enzymes and potential drug targets (Lee *et al.*, 2009).

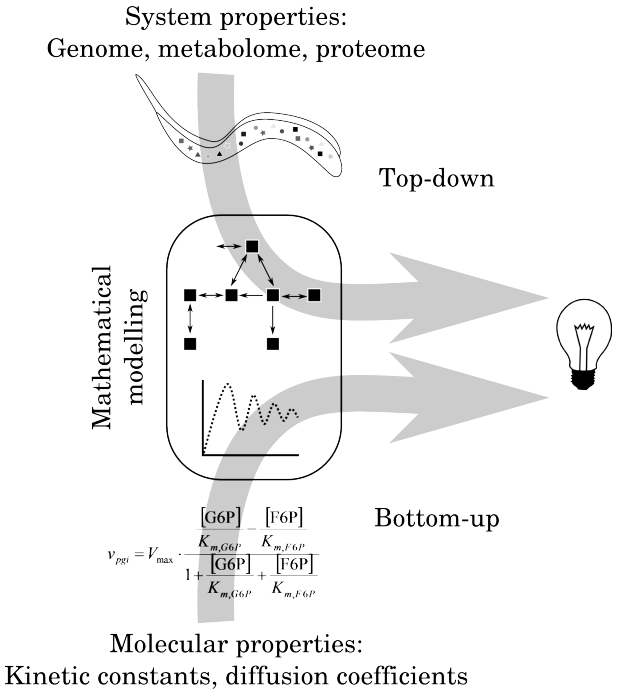

Figure 1.9.: Top-down versus bottom-up systems biology. Top-down systems biology starts with knowledge about systemic properties and applies the use of mathematical models to gain new understanding of the network. Typically large datasets (e.g. genome data) are generated while large networks are constructed that connect entities within the dataset. Bottom-up systems biology on the other hand starts with the properties of the system's components, integrates those components into a model and studies the emerging behaviour of the system. Top-down models are typically large scale descriptions of the stoichiometry of a model, while bottom-up models are typically detailed small scale models describing part of the whole network.

The second approach to modelling is bottom-up, typically generating smaller models with much more detail than in a top-down approaches (Figure 1.9 and Snoep *et al.*, 2006). One starts with studying the constituent parts of the system in great detail, e.g. the kinetics of a particular enzyme in isolation. Detailed descriptions of the different entities are then connected to generate a bottom-up models. The size of such models is restricted due to the complexity of the description of the parts and the lack of experimental data. For a bottom-up model of a metabolic pathway, one would typically need to measure many parameter values.

The main objective of such bottom-up models is to predict what systemic behaviour emerges from the combination of its constituent parts. An example is the use of a detailed model of glycolysis in muscle cells to understand the rapid inactivation of this system after contraction (Schmitz *et al.*, 2010).

However, there is no strict separation between the two approaches to modelling. The future potential of systems biology is based on the integration of both modelling approaches. An ambitious aim, but one that logically flows from the developments seen in the last decades, is the construction of a Silicon Cell (Westerhoff, 2001). In the future, this *in silico* representation of life would span all levels in cell biology, from genomes to proteomes, metabolomes and beyond, and might also eventually include spatial effects. The hope is that such *in silico* cells can be used for personalised medicine, where computationally the best combination of drugs can be found using a personalised *in silico* description of life. It is clear that this approach can only function with a combination of top-down and bottom-up approaches.

1.8.3. Generation of a dynamic model

To get a better understanding of what a dynamic model of metabolism exactly is, it is good to look at how a dynamic model is generated. The construction of a dynamic model can be separated in four steps (Figure 1.10):

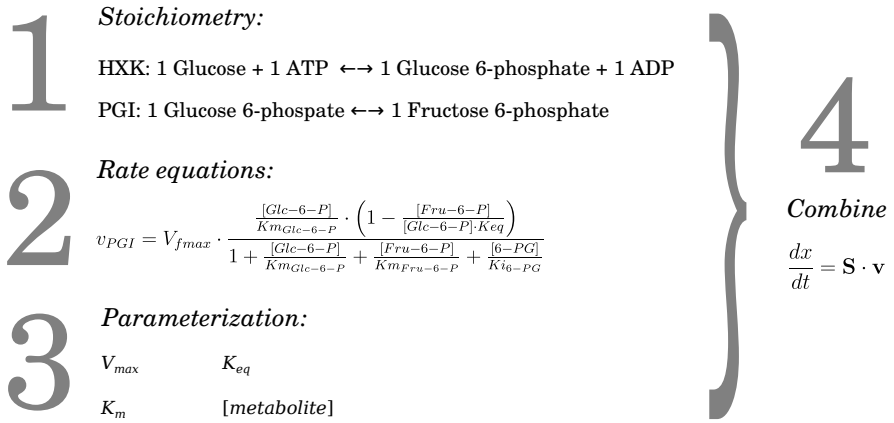

Figure 1.10.: Four-step construction of a dynamic model of metabolism. The first step constitutes of describing the stoichiometry of the system to be modelled: what enzymes convert what metabolites in what quantities? Shown are two reactions of glycolysis: HXK, hexokinase; PGI, phosphoglucose isomerase. The second step is to provide rate equations for each reaction step, which will allow for simulation of the dynamics of the system. The Michaelis-Menten equation for PGI is given as an example. The third step is the parametrisation of the rate equations declared in step 2, but also includes the metabolite concentrations at $t = 0$, and typically also the volume of the system. In the fourth and final step, all this information is gathered to form a set of ordinary differential equations.

1. **Description of the system and its stoichiometry.** All the constitutive parts of the system need to be listed and the topology of the network connecting the parts needs to be described. In models of metabolism, the parts are metabolites and the links are the enzymes. The outcome of this step is the stoichiometry matrix S, where S_{ij} is positive if metabolite i is a product of reaction j and negative if metabolite i is a substrate of reaction j.

2. **Description of rate equations for the reactions in matrix S.** The complexity of the rate equations can vary from standard mass-action kinetics, to complex kinetics involving specific binding constants for each substrate. Typically, Michaelis-Menten type of equations are used. The results is vector v, where v_j is the rate equation of reaction j.

3. **Parametrisation of the rate equations.** The parameters used in the rate equations in vector v have to be given. In a model of metabolism, these are typically the kinetic constants for the enzymes. These values can be obtained experimentally, by characterising the enzymes *in vitro,* or computationally, by fitting the parameter values to an available data set. For experimental determination of parameter values it is important that the assays performed *in vitro* are close to the *in vivo* conditions, as differences in pH, temperature and metabolite concentrations can have major effects on the results. For a model of central carbon metabolism in yeast, all kinetic parameters were measured in one *in vivo*-like buffer.

4. **Combination of all information.** The final step of model building is the combination of the three previous steps. Multiplication of matrix S with parametrised vector v results in a set of ordinary differential equations that describe the changes in the metabolites over time.

The primary output of a simulation of a dynamic model of metabolism are the concentrations of the metabolites and the reaction rates as a function of time (Figure 1.11). Most models will eventually reach a state where the rates and concentrations of metabolites do not change any more; such a system is then said to be in steady-state. A time-course simulation can be performed while checking for every time-step, to determine whether the model has reached steady-state, but this can also be directly calculated algebraically.

More advanced analysis of a dynamic model of metabolism is the metabolic control analysis mentioned above, where the contribution of each reaction to the control of the pathway is calculated. Additionally, dynamic models exist of formulae and parameter

values that can easily be altered and therefore the effect of a range of parameter values or the presence or absence of particular reactions can easily be tested.

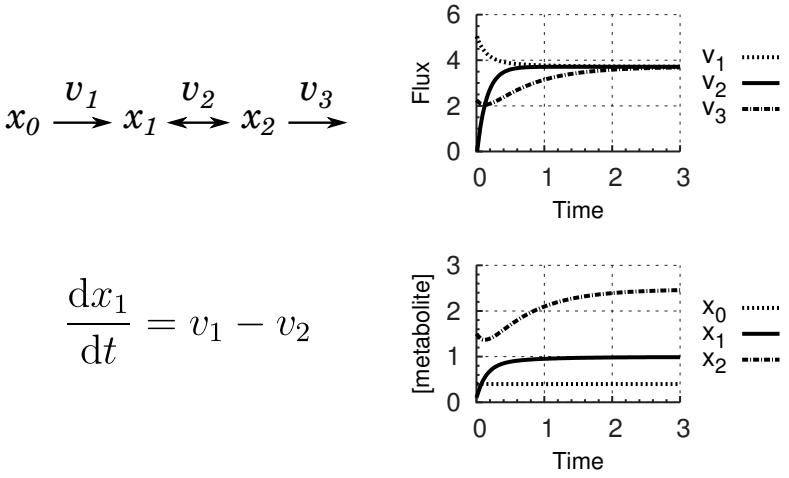

Figure 1.11.: Example of output from a time-course simulation. A time-course simulation is performed with a conceptual model containing three metabolites (x_i) and three reactions (v_i). Metabolite x_0 is a source with a fixed concentration. The ordinary differential equation of metabolite x_1 is given, and describes the change in concentration as a function of the rates of reactions v_1 and v_2. The output of the time-course simulation is the flux through the three reactions and the metabolite concentrations over time. Note that the metabolite concentrations converge after three time-units, indicating that a steady-state is reached.

1.8.4. Applications of dynamic models

Dynamic models of metabolism have been around for many years. The first comprehensive models of metabolic pathways were published in the 70s, after the development of computers (Garfinkel *et al.*, 1970) and the arrival of recombinant technologies made dynamic modelling more accessible (Heinrich and Rapoport, 1974; Westerhoff and Palsson, 2004). Since then, a large number of models have been published, describing a variety of metabolic processes from accumulation of mucopolysaccharides during development of *Dictyostelium discoideum* (Loomis and Thomas, 1976), to central carbon metabolism in erythrocytes (Joshi and Palsson, 1989). The basis of dynamic models of metabolism has not changed much over these years, but what has changed is the accuracy, amount of detail and scope of such models.

1.8.4.1. Dynamic models of glycolysis

The most-studied and best-characterised biochemical pathway is glycolysis, not unexpected for a pathway so essential for almost all organisms. The enzymes of glycolysis have been studied extensively for almost a century, and since the 1960s many dynamic models, particularly of yeast glycolysis, have been constructed (e.g. Boiteux *et al.*, 1975; Schellenberger and Hervagault, 1991; Teusink *et al.*, 2000), providing a wealth of knowledge for the modelling of glycolysis in other systems.

The early models of glycolysis were focused on oscillations in metabolite concentrations that were observed in yeast cultures (Peringer *et al.*, 1974; Richter *et al.*, 1975). These models were phenomenological and perhaps early examples of (small-scale) top-down systems biology, as the observation of systemic oscillations was followed by attempts to describe this behaviour with mathematical equations. With the development of metabolic control analysis, bottom-up approaches were starting to be used to generate mechanistic models that describe the enzyme kinetics underlying glycolysis (Cortassa and Aon, 1994; Teusink *et al.*, 2000), following the scheme described in Figure 1.10. A model of glycolysis in yeast was for instance instrumental to demonstrate the aforementioned risk of the turbo design of glycolysis (Teusink *et al.*, 1998).

The model of yeast glycolysis by Teusink *et al.* (2000) was the first yeast glycolytic model that did not involve any fitting of parameter values, where parameter values are estimated by fitting the outcome from the dynamic model to observed metabolite concentrations or fluxes, in attempt to have the model mimic reality. In contract, the Teusink-model was purely based on the measurements of enzyme kinetics. Therefore, the model was an evaluation whether the dynamics of yeast glycolysis can indeed be understood from the underlying kinetics. Teusink *et al.* (2000) concluded that the *in vitro* kinetics did not satisfactorily describe the *in vivo* activity for all the glycolytic enzymes: the steady-states observed in the laboratory could not be replicated with the mathematical model. Only significant changes to some parameter values would lead to a satisfactory description. This discrepancy between outcome of the Teusink-model and experimental observations was often observed under different growth conditions, as commented by van Eunen *et al.* (2012).

Extensive scrutiny of the Teusink-model eventually led to the substantial improvement of model predictions by: (i) measuring all kinetic parameters under *in vivo*-like conditions that resemble the intracellular environment, and (ii) including appropriate allosteric regulation (van Eunen *et al.*, 2012). It transpired that kinetic parameters measured under optimised assay conditions (van Eunen *et al.*, 2010) were sometimes

substantially different from kinetic parameters measured in an assay buffer specifically formulated to mimic *in vivo* conditions. The formulation of an *in vivo*-like reaction buffer for the kinetic characterisation of all enzymes in a metabolic model is therefore recommended. Allosteric regulation of HXK and G3PDH were not included in the previous model (Teusink *et al.*, 2000), but measurement of these improved model predictions substantially. Although it is implausible to test every enzyme for any potential allosteric regulator, it is important to keep the possibility of allosteric regulation in mind when there is a difference in the outcome of modelling and experiments.

1.8.4.2. Dynamic models of PPP

In contrast to glycolysis, the PPP has been the subject of dynamic modelling to a lesser extent. In particular the PPP in erythrocytes has been modelled using enzyme kinetics (Schuster *et al.*, 1988; Joshi and Palsson, 1989; Mulquiney and Kuchel, 1999a). Erythrocytes are particularly suitable for the application of kinetic models of metabolism, as their set of metabolic pathways is reduced to only the bare minimum to survive. Erythrocytes have no functional citric acid cycle, but solely rely on glycolysis and the PPP for energy.

Schuster *et al.* (1989) used a kinetic model of glycolysis and the PPP in erythrocytes to study deficiencies of enzymes responsible for the first reaction of the PPP, G6PDH. The PPP is the only source of reducing energy to keep glutathione reduced, and deficiencies in G6PDH in erythrocytes are the most widespread enzymopathies, present in more than 400 million people worldwide (Cappellini and Fiorelli, 2008). G6PDH deficiency can cause haemolytic anaemia in response to infections or exposure to certain chemicals or medications. In an approach that already gives a flavour of the aim of *silicon cells*, i.e. personalised medicine, Schuster *et al.* (1989) measured the kinetic parameters of G6PDH variants in patients and included these patient-specific values in a generic model of erythrocyte metabolism. In this study, both mathematical prediction and wet-lab experimentation, which involved the exposure of erythrocytes from the patients to the reducing agent methylene blue, correlated well with the clinical manifestation of the disease in the individual patients. Schuster *et al.* (1989) indicated that increases in the rate of ATP utilisation within the erythrocyte can aggravate the symptoms of G6PDH, culminating in the advice to give special attention to prescribing drugs that activate energy-consuming reactions to G6PDH-deficient patients.

Another model of erythrocyte glycolysis and PPP was published by Mulquiney and Kuchel (1999a). This model has yielded new insights into the regulation of

2,3-bisphosphateglycerate (2,3-BPG), an important modulator of haemoglobin oxygen affinity (Benesch and Benesch, 1967; Gerber *et al.*, 1973). Metabolic control analysis with this dynamic model has, among others, demonstrated how the flux through 2,3-BPG changes in response to changing energy demands placed on the cell (Mulquiney and Kuchel, 1999b). Reaction rates within the Mulquiney-model of erythrocyte energy metabolism are defined with great detail, with more than twice as many parameter values per reaction in comparison to the Schuster-model. pH effects and the binding of magnesium to ATP are also taken into account. It is worth noting, however, that larger and more detailed models are not by definition *better* models, as the increased complexity might work against the principle reason why they are used in the first place: to simplify reality.

1.8.5. Dynamic model of trypanosomal glycolysis

Glycolysis in the bloodstream form of *T. brucei* has been studied using dynamic models. In 1997, Bakker *et al.* (1997) established that trypanosomal glycolysis can be understood from the kinetics of the underlying enzymes. This model has become an example of a well-curated model of metabolism and has been improved multiple times by incorporating new data (Bakker *et al.*, 1997, 1999a; Helfert *et al.*, 2001; Albert *et al.*, 2005).

1.8.5.1. Stoichiometric analysis of trypanosomal glycolysis

Analysis of the stoichiometry of the model demonstrated the existence of five moiety conservations (Bakker *et al.*, 1997; Albert *et al.*, 2005). The stoichiometry of the model network, and the partial glycosomal localisation in particular, results in five groups of metabolites whose combined concentrations within the group are conserved (Table 1.1). The metabolites of moieties 1–3 are involved in reactions as co-factors, transferring high-energy organic phosphate (moieties 1 and 2) or electrons (moiety 3). Moiety 4 is a result of the Gly-3-P:DHAP antiporter, where each Gly-3-P in the cytosol can only be transformed in DHAP and vice versa. Possibly the most interesting of all moieties is the conserved sum of bound-phosphates within the glycosome, moiety 5 (Table 1.1). Note that inorganic phosphate (Pi) is not part of the conserved moiety, even though it is involved in the production of 1,3-BPGA (Figure 1.5). The concentration of inorganic phosphate has been set as a fixed metabolite, reflecting an intracellular homoeostasis of inorganic phosphate (Bakker, 1998). Allowing Pi to transport cross the glycosomal and cytosolic membrane, by the addition of transport reactions to the glycolytic model, does

not result in a different conserved sum. Moreover, the inorganic phosphate concentration is not limiting to the rate of the steady-state flux (Bakker, 1998), supporting the fixation of inorganic phosphate and thereby assuming rapid diffusion of inorganic phosphates from the environment into the glycosome.

Moiety	Conserved metabolites
1	ATP_g + ADP_g + AMP_g
2	ATP_c + ADP_c + AMP_c
3	$NADH_g$ + NAD_g
4	Gly-3-P_c + $DHAP_c$
5	Glc-6-P_g + Fru-6-P_g + 2 Fru-1,6-BP_g + $DHAP_g$ + GA-3-P_g + 1,3-$BPGA_g$ + Gly-3-P_g + 2 ATP_g + ADP_g

Table 1.1.: Conserved moieties in the glycolysis model. The stoichiometry of the model results in five groups of metabolites, whose combined concentration within the group remains constant.

Mode	Overall reaction	Individual reactions
1	Glc_e + O_2 + 2 Pi_g → 2 Pyr_e + 2 Pi_c	$GlcT_c$, $GlcT_g$, HXK_g, PGI_g, PFK_g, ALD_g, TPI_g, 2 $GAPDH_g$, 2 PGK_g, 2 $PGAT_g$, 2 $PGAM_c$, 2 ENO_c, 2 PYK_c, 2 $PyrT_c$, 2 $G3PDH_g$, 2 GDA_g, 2 GPO_c, 2 $ATPu_c$
2	Glc_e + Pi_g → Pyr_e + Gly_e + Pi_c	$GlcT_c$, $GlcT_g$, HXK_g, PGI_g, PFK_g, ALD_g, $GAPDH_g$, PGK_g, $PGAT_g$, $PGAM_c$, ENO_c, PYK_c, $PyrT_c$, $G3PDH_g$, GK_g, $ATPu_c$
3	Gly_e + O_2 + Pi_g → Pyr_e + Pi_c	TPI_g, $GAPDH_g$, PGK_g, $PGAT_g$, $PGAM_c$, ENO_c, PYK_c, $PyrT_c$, $G3PDH_g$, 2 GDA_g 2 GPO_g, – GK_g, $ATPu_c$

Table 1.2.: Elementary modes of the original glycolysis model. Three elementary modes are listed as the overall reactions plus the individual enzyme-catalysed reactions with their relative flux weight. Mode 1 is known as aerobic glycolysis, mode 2 is anaerobic glycolysis, while mode 3 is glycerol oxidation.

Elementary mode analysis is a tool that allows to identify so-called elementary modes: the simplest subsets of reaction in the system that can support a steady state (Schuster *et al.*, 1999). The model of glycolysis supports three elementary modes (Table 1.2). In the absence of oxygen the only possible elementary mode is anaerobic glycolysis, mode 2. During anaerobic glycolysis, equimolar amounts of glycerol and pyruvate are produced,

as discussed in Section 1.3. This requires glycerol kinase to work far from equilibrium, in order to balance the NAD^+ and NADH within the glycosome. The first dynamic model of trypanosomal glycolysis demonstrated how mode 2 is not only possible from model's stoichiometry, but also from the enzyme kinetics involved (Bakker *et al.*, 1997).

1.8.5.2. Metabolic control analysis of trypanosomal glycolysis

Metabolic control analysis of the model of trypanosomal glycolysis provided additional interesting insights. The glucose transporter present on the glycosomal membrane has the highest control over the glycolytic flux, followed by ALD, G3PDH, GAPDH and PGK (Bakker *et al.*, 1999a,b). This is of particular interest as erythrocytes, sharing the same living space as bloodstream form *T. brucei* in the mammalian host, deficient in ALD, GAPDH and PGK show no clinical symptoms in 95 % of the cases (Schuster and Holzhütter, 1995). Indeed, experiments where the glucose transporter was inhibited confirmed a potent trypanocidal effect (Haanstra *et al.*, 2011).

A additional prediction that arose from the kinetic model of trypanosomal glycolysis was that the glycosomal compartmentalisation of glycolysis is essential to prevent the aforementioned turbo effect, as described in (Section 1.3.1). This effect was predicted by the model in 2000 by Bakker *et al.*, but only experimentally confirmed by Haanstra *et al.* in 2008.

The model has been improved from the first publication (Bakker *et al.*, 1997) to the latest curation (Albert *et al.*, 2005). In the first model, the kinetic parameters where taken from the literature, where almost each enzyme was assayed in a unique assay buffer. Albert *et al.* (2005) measured all enzyme activities from cultured parasites, bringing more uniformity into the sources of parameter values. Nonetheless, dynamic modelling of glycolysis in yeast has shown the importance of measuring all parameter values in the same *in vivo*-like buffer (van Eunen *et al.*, 2012).

1.9. Aim: extension of the dynamic model of trypanosomal metabolism

With the success of the dynamic model of trypanosomal glycolysis, the next step is to extend this model with additional pathways. An extended model of trypanosomal metabolism will allow the further exploration of the peculiar physiological properties of *T. brucei*. The ambitious aim of producing a Silicon Trypanosome was raised by Bakker *et al.* (2010). This Silicon Trypanosome would be "[...] a comprehensive, experiment-based, multi-scale mathematical model of trypanosome physiology [...]" and comparable to the Silicon Cell (Snoep, 2005) and Virtual Liver projects (Abbott, 2010).

However, because of the complexity of metabolic pathways and the lack of available data on kinetic parameters, Silicon Cell initiatives depend upon exploiting the modularity of metabolic models, such that basic models can be extended by the sequential addition of new reactions, pathways and sub-models. This bottom-up approach allows coupling of models of different pathways to create ever larger representations of the network under scrutiny (Snoep *et al.*, 2006).

Based on these observations, the aims of this project were to:

1. Extend the current model of glycolysis in bloodstream form *T. brucei* with the PPP, as a step intp the direction of the Silicon Trypanosome.

2. Test hypotheses deriving from the model extension with wet-lab experimentation in an iterative cycle between model building and experimental testing.

3. Elucidate parts of the peculiar trypanosomal metabolism by using reverse genetics, enzyme analyses and metabolomics.

Chapter 2

Methods

2.1. Trypanosome growth

2.1.1. Culturing *T. brucei*

Bloodstream form trypanosomes were cultured in HMI-9 medium (Hirumi and Hirumi, 1989) at 37 °C and 5 % CO_2, unless otherwise stated. HMI-9 was routinely obtained from Gibco, but was made from scratch for growth on fructose, where glucose was absent (Chapter 6). For metabolomics experiments, parasites were routinely grown in CMM, a medium that contains less components than HMI-9 but supports a similar growth (appendix A; unpublished; Dr Darren Creek, University of Glasgow). The advantages of using CMM in metabolomics experiments is the reduced background signal and reduced HEPES concentration that could otherwise block the mass-spectrometer needle. Culture medium was supplemented with 10 % FBS Gold (PAA) or 10% certified tetracycline-free FBS (Biosera) for the inducible genetic mutants.

Cell densities of trypanosome cultures were typically kept between $0.5 \cdot 10^4$ and $2 \cdot 10^6$ cells ml^{-1}. Wild-type strain 427 was cultured in the absence of antibiotics; 2T1 cells were cultured with 0.5 μg ml^{-1} phleomycin and 0.2 μg ml^{-1} puromycin; transfected 2T1 cells (Alsford and Horn, 2008) with 0.5 μg ml^{-1} phleomycin and 2.5 μg ml^{-1} hygromycin; *6PGDH*^{RNAi} cells (derived from 427 WT, generated by Dr Vincent P Alibu, University of Glasgow) with 10 μg mL^{-1} hygromycin, 5 μg ml^{-1} G418 and 0.2 μg ml^{-1} phleomycin. Tetracycline was used at 1 μg ml^{-1}.

Stabilates were routinely made from parasite cultures, by resuspending parasites to a density of around $1 \cdot 10^6$ ml^{-1} in HMI-9 with 15 % glycerol. Aliquots of 1 ml were wrapped in cotton wool and frozen at −80 °C before transferring to liquid nitrogen for long-term storage. Stabilates were revived by harvesting the cells by centrifugation (10 minutes, 3000*g*, 4 °C) and resuspending the cells in HMI-9 with 20 % FBS. Appropriate antibiotics were added in subsequent passages.

2.1.2. Transformation of parasites

Stable transformation of parasites was performed as described previously (Burkard *et al.*, 2007). For each transformation, $4 \cdot 10^7$ cells of a mid-log culture were resuspended in 100 µl transfection buffer (Schumann Burkard *et al.*, 2011) and 10 µl H_2O containing 10 µg linearised DNA, followed by electroporation of the parasites in 2-mm gap cuvettes (Bio-Rad) with the proprietary program X-001 of the Amaxa Nucleofector II (Lonza, Germany). Cells were subsequently diluted in HMI-9 and appropriate antibiotics were added 6 hours post transformation. Stable clones were selected by serial dilutions on 96-wells plates. If fewer than 30 % of the wells contained live cells after 14 days, then the populations were considered to be clonal (calculated for a 96-well plate using a Poisson distribution).

2.1.3. AlamarBlue assays

Toxicitiy of compounds were assessed by alamarBlue assays (Räz *et al.*, 1997). Parasites were incubated in a 96-wells plate at a density of $4 \cdot 10^4$ cells ml^{-1} and a 1:2 serial dilution of the desired drug in a final volume of 200 µl per well. Parasites were incubated for 48 hours at 37 °C, 5 % CO_2, followed by addition of 20 µl 0.49 mM resazurin (Sigma) in PBS, pH 7.4 and incubation for another 24 hours. Fluorescence was measured on a FLUOstar OPTIMA (BMG Labtech, Germany) fluorescence spectrometer, with $\lambda_{excitation}$ = 544 nm and $\lambda_{emission}$ = 590 nm.

2.1.4. Cell extracts

For enzymatic assays on cell extracts, $2 \cdot 10^8$ cells were harvested in mid-log phase by centrifugation at 1,900*g* for 10 minutes, and washed twice in PBS. Subsequently, the

cells were resuspended in 1 mL lysis buffer (PBS, 150 mM NaCl, 0.1 % Triton X-100 and cOmplete™ EDTA-free Protease Inhibitor Cocktail (Roche)), incubated on ice for 1 hour and briefly vortexed every 15 minutes. Cell debris was removed by centrifugation (30 minutes, 16,100g, 4 °C) and the remaining supernatant was kept on ice until further use. The protein content of cell-extracts was determined via a Bio-Rad protein assay, based on the method by Bradford (1976).

2.2. Molecular biology

2.2.1. PCR

Polymerase chain reactions were typically performed in 25 µl volumes GoTaq DNA polymerase (Promega) according to provided standard protocols. High-fidelity polymerase chain reactions were typically performed in 50 µl volumes with Phusion Hi-Fi polymerase (New England Biolabs) according to provided standard protocols. Primers used in this study are listed in Table 2.1.

2.2.2. Plasmid generation

Various plasmids were routinely obtained by digestion and ligation with restriction enzymes. An overview of plasmids used in this study is given in Table 2.2. Maps of the different plasmids generated in this study are given in Figure 2.1 and Figure 2.2.

For the generation of plasmids, DNA was amplified with a proofreading polymerase and subsequently incubated with 1 U Taq polymerase and 0.3 mM dNTP to obtain A-overhangs. These amplicons were ligated into intermediate cloning vector pGEM-T Easy (Promega) via TA-cloning. Plasmids were typically transformed in DH5α (Invitrogen) for growth on Luria broth agar plates or in Luria broth with the appropriate antibiotic (ampicillin 100 µg ml^{-1}; kanamycin 50 µg ml^{-1}). Plasmids were extracted from overnight cultures using commercial miniprep kits (Qiagen or Macherey-Nagel).

Gene	Description	Sequence	Restriction sites	Identifier
Ribokinase	Recombinant expression, fwd	GATCAAGCTTTATTTTGCATTCCTTCACCTCAGCA	HindIII	MB0331
"	Recombinant expression, rev	CGCGGATCCTAGATGAGTGCTGCCGGCGTTAAGAGC	BamHI	MB0413
"	RK^{RNAi}, fwd	GATCGGGCCCGGTACCAATAGTGTTTTCGCCCAACG	ApaI, Acc65I	MB0316
"	RK^{RNAi}, rev	GATCTCTAGAGGATCCCCCTTCTCGCCAATAACGTA	XbaI, BamHI	MB0317
"	Δ*rk::HYG/PAC*, 5' UTR, fwd	GATCGCGGCCGCGGTCTTCCAGCACGGAAGGT	NotI	MB0473
"	Δ*rk::HYG/PAC*, 5' UTR, rev	GATCTCTAGAGTGATGATGATGGGCAATGC	XbaI	MB0474
"	Δ*rk::HYG/PAC*, 3' UTR, fwd	GATCGGGCCCATGCATGACGCACGTGTGGATTGAGA	ApaI, NsiI	MB0475
"	Δ*rk::HYG/PAC*, 3' UTR rev	GATCGGGCCCCTCGAGGAACCTCCCATGTCTTACAG	ApaI, XhoI	MB0476
"	Δ*rk::HYG/PAC::*RK^{i}, re-exp, fwd	GCAAGCTTATGAGTGCTGCCGGCGTTAA	HindIII	MB0567
"	Δ*rk::HYG/PAC::*RK^{i}, re-exp, fwd	GCGGATCCCTATATTTTGCATTCCTTCA	BamHI	MB0568
"	Δ*rk* integration, primer A	AGGTGCGGTTTGTTCGTTTC	n/a	MB0046
"	Δ*rk* integration, primer B	CTGAGCGATTCCCCAACCT	n/a	MB0468
"	Δ*rk* integration, primer E	TCACCCACACGCCCATATGGCCG	n/a	MB0386
"	Δ*rk* integration, primer F	ATATGGATCCAATAGTGTTTTCGCCCAACG	n/a	MB0469
Arginase	Recombinant expression, fwd & Δ*arg* primer Y	GATCCATATGTTCTCCAAGTTCCTGAT	NdeI	MB0542
"	Recombinant expression, rev & Δ*arg* primer Z	GATCGCGGCCGCTCAATGATCGGGGTACGGAT	NotI	MB0544
"	Δ*arg::HYG/PAC*, 5' UTR, fwd	GATCGCGGCCGCTGTCAAAGGGGAGAGAAAC	NotI	MB0536
"	Δ*arg::HYG/PAC*, 5' UTR, rev	GATCTCTAGACCGAGTCGATTGGCCCAATC	XbaI	MB0550
"	Δ*arg::HYG/PAC*, 3' UTR, fwd	GATCATGCATGTCATTCAAGGCTGCGTCAG	NsiI	MB0538
"	Δ*arg::HYG/PAC*, 3' UTR rev	GATCCTCGAGCAGCCCCTTTCAAGATGTGT	XhoI	MB0551
"	Δ*arg* integration, primer A	TGTGAAGGGGATAAGGAAGC	n/a	MB0540
"	Δ*arg* integration, primer B	TCGCGTGGTGATTGAAGAAA	n/a	MB0529
"	Δ*arg* integration, primer E	GCCTGTTCTTCCTTTGCG	n/a	MB0625
"	Δ*arg* integration, primer F	GATCGGGCCCGGTACCTGGGTAACCGTCAAGTGTCA	n/a	MB0314

Table 2.1.: Oligonucleotides used in experiments. Underlined nucleotides indicate restriction sites.

Gene	Description	Sequence	Restriction sites	Identifier
N-acetylornithine deacetylase	Recombinant expression, fwd	GCGGATCCATGAACTGCAGAGAGTGGTT	BamHI	MB0555
"	Recombinant expression, rev	GCAAGCTTCTACAAATGCGGTTTTCTTC	HindIII	MB0556
"	Δ*nao::HYG/PAC*, 5' UTR, fwd	GCGCGGCCGCTCGAGATTTGCAGACGTTTGCTCCG	NotI, XhoI	MB0559
"	Δ*nao::HYG/PAC*, 5' UTR, rev	GCCGCCGGCGTCTAGAGTTTATAGGTGGCCTATCCT	XbaI	MB0560
"	Δ*nao::HYG/PAC*, 3' UTR, fwd	GCGGGCCCGAGACACAGATCGTTGTGTT	ApaI	MB0561
"	Δ*nao::HYG/PAC*, 3' UTR rev	GCGGGCCCTCGAGAAGTGATAAAGCTAATAATA	ApaI, XhoI	MB0562
"	Δ*nao* integration, primer A	TGGGGTGTGGTAATGGAT	n/a	MB0603
"	Δ*nao* integration, primer B	CTGTTAGAGTGAAGGGGT	n/a	MB0605
"	Δ*nao* integration, primer E	AGTTGTTTTCCTCAGTCCC	n/a	MB0604
"	Δ*nao* integration, primer F	TTCTCATTTTGCTTCGTCGT	n/a	MB0606
Nicotinamidase	Recombinant expression, fwd	GGTATTGAGGGTCGCATGTCTACATCCCGCATTAC	n/a	MB0682
"	Recombinant expression, rev	AGAGGAGAGTTAGAGCCTCAGAAGCTGGAAAGGTCTG	n/a	MB0683
"	NAM^{RNAi}, fwd	GGGGACAAGTTTGTACAAAAAAGCAGGCTAATTAATCGCGTTGTCGGAG	n/a	MB0684
"	NAM^{RNAi}, rev	GGGGACCACTTTGTACAAGAAAGCTGGGTGCTGGAAAGGTCTGTGCTTC	n/a	MB0685
Hygromycin	Knockout integration, primer C	GGTGAGTTCAGGCTTTTTCAT	n/a	MB0416
"	Knockout integration, primer G	CGTCCGAGGGCAAAGGAATA	n/a	MB0415
Puromycin	Knockout integration, primer D	TGAGGAAGAGTTCTTGCAGC	n/a	MB0419
"	Knockout integration, primer H	TTCTACGAGCGGCTCGGCTT	n/a	MB0422

Table 2.1 – (continued)

Gene	Identifier	Description	Parent
Ribokinase	pMB-G67	*RK*$^{\mathrm{RNAi}}$	pRPa$^{\mathrm{iSL}}$
"	pMB-G97	Δ*rk::HYG* knockout	pTBT
"	pMB-G98	Δ*rk::PAC* knockout	pTBT
"	pMB-G102	Recombinant expression	pET28a(+)
"	pMB-G130	Re-expressor for Δ*rk::HYG/PAC::RK*^{i}	pHD1336
Arginase	pMB-G122	Δ*arg::HYG* construct	pTBT
"	pMB-G123	Δ*arg::PAC* construct	pTBT
"	pMB-G131	Recombinant expression	pET28a(+)
N-acetylornithine deacetylase	pMB-G124	Recombinant expression	pET28a(+)
	pMB-G126	*Δnao::HYG* construct	pTBT
"	pMB-G127	*Δnao::PAC* construct	pTBT
Nicotinamidase	pMB-G170	Recombinant expression	pET30 Xa/Lic
"	pMB-G171	*NAM*^{RNAi}	pGL2084

Table 2.2.: Plasmids produced in this study.

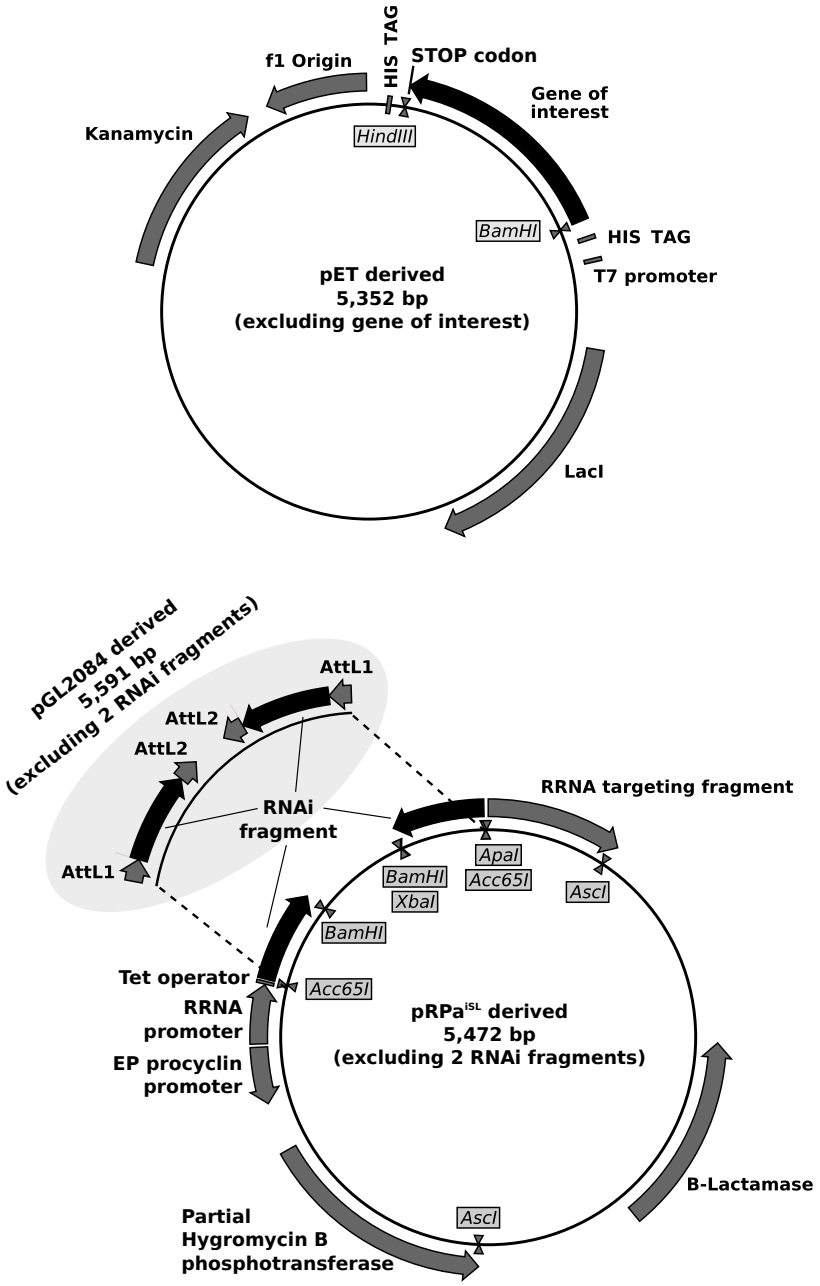

Figure 2.1.: Plasmid maps as generated in this study (1). Coding sequences and other features are indicated by grey arrows. Cloned fragments are indicated by black arrows. Restriction sites used for cloning or linearisation of the constructs are shown. Plasmids pMB-G102, 124, 131 and 170 are derived from pET, pMB-G67 is derived from pRPa^{iSL}, while pMB-G171 is derived from pGL2084. pGL2084 is similar to pRPa^{iSL}, but contains AttL1 and AttL2 sites to allow for Gateway cloning (Nathaniel Jones, University of Glasgow). For transfection, pRPa^{iSL} and pGL2084 derived plasmids are linearised at the AscI sites.

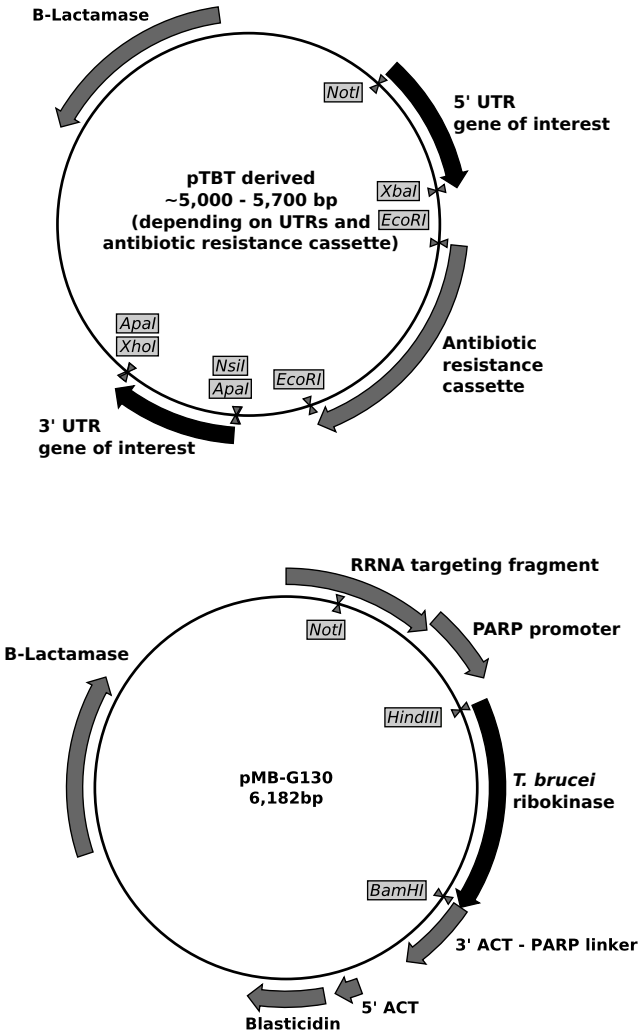

Figure 2.2.: Plasmid maps as generated in this study (2). Coding sequences and other ... are indicated by grey arrows. Cloned fragments are indicated by black arrows. Restriction sites used for cloning or linearisation of the constructs are shown. Plasmids pMB-97, 98, 122, 123, 126 and 127 are derived from pTBT. pTBT derived plasmids are linearised at the NotI and XhoI restriction sites, while pMB-G30 is linearised at the NotI site.

2.2.2.1. Plasmids for recombinant protein overexpression

Vector pET28a(+) (Merck) was used for overexpression of ribokinase (RK), putative arginase (ARG) and *N*-acetylornithine deactylase (NAO). RK was amplified with primers MB0331 and MB0413 (Table 2.1) and cloned at the HindIII and BamHI sites to generate plasmid pMB-G102 (Table 2.2); ARG was amplified with primers MB0542 and MB0544 and cloned at the NdeI and NotI sites to generate plasmid pMB-G131; NAO was amplified with primers MB0555 and MB0556 and cloned at the BamHI and HindIII sites to generate plasmid pMB-G124.

The expression vector for recombinant nicotinamidase (pMB-G170, Table 2.2) was generated with a ligation-independent cloning kit (pET30a Xa/Lic, Merck Millipore),

in an effort to speed up the generation of expression vectors. The reverse primer for nicotinamidase also contained a stop-codon (TAG), leading to N-terminal 6xHIS-tagged nicotinamidase.

2.2.2.2. RNA interference constructs

The vector pRPa^{iSL} in combination with the cell line 2T1 were used for the ablation of transcript by RNA interference (Alsford and Horn, 2008). A detailed description of the cloning of RNAi fragments into pRPa^{iSL} is given in (Alsford and Horn, 2008). The pRPa^{iSL} / 2T1 system is optimised for stable transfection and expression of a stem-loop RNAi construct. The pRPa^{iSL} vector integrates in a targeted locus in 2T1 cells, disturbing a puromycin resistance gene while complementing a hygromycin resistance gene. Correct integration of the pRPa^{iSL} construct can subsequently be monitored by the gain of hygromycin resistance and the loss of puromycin resistance. The gene fragment to be used in the RNAi vector was selected with the RNAit program (Redmond *et al.*, 2003).

A ligation-independent version (pGL2084) of the pRPa^{iSL}plasmid was used for generation of the nicotinamidase RNAi construct (pMB-G171), kindly provided by Nathaniel Jones (University of Glasgow).

2.2.2.3. Gene knockout constructs

Vector pGL1688, based on pTBT (Cross *et al.*, 2002), was used for generating of knockout constructs. The 5' and 3' untranslated regions (UTRs) adjacent to the genes of interest were cloned at the NotI and XbaI (5') and ApaI (3') restriction sites on pGL1688. pGL1688 originally included a coding sequence for hygromycin resistance, which was swapped at the EcoRI restriction sites with a coding sequence for puromycin acetyltransferase. Knockout constructs were linearised by restriction digest with NotI and XhoI, prior to transfection.

Constructs for the tetracycline-inducible expression of ribokinase were generated by cloning the full ribokinase gene at the HindIII and BamHI sites of pHD1336 (Alibu *et al.*, 2005). Prior to transfection of trypanosomes with the tetracycline-inducible construct, first the tetracycline-repressor was introduced by transfection with pHD1313 (Alibu *et al.*, 2005). Both plasmids were linearised with NotI prior to transfection.

2.2.3. Northern blot

Northern blots were performed according to standard procedures. Certified RNA-free equipment was used and equipment was sprayed with RNaseZap (Ambion) or treated with DEPC. RNA was extracted using Trizol (Invitrogen), and 20 µg was run on a formaldehyde (16 %), Na_2HPO_4 (18 mM), NaH_2PO_4 (2 mM) and agarose (1 %) gel, blotted on a Hybond-N (Amersham) nylon membrane and probed with Easytides ^{32}P-dATP (Perkin Elmer), incorporated in the gene of interest using a one-cycle polymerase reaction (PrimeIT, Stratagene).

2.3. Protein expression

2.3.1. Overexpression

Protein overexpression was performed in BL21(DE3) *E. coli* (Stratagene), by inoculating 1 litre of lysogeny broth (30 µg ml^{-1} kanamycin) with an overnight culture. The large culture was incubated at 37 °C in an orbital shaker, until an OD600 of 0.6 was reached. Overexpression was induced by addition of 1 mM IPTG for 4 hours at 37 °C. Cells were harvested by centrifugation (4500g, 30 minutes, room temperature) and stored at −20 ˚C.

2.3.2. Purification

Small scale purification was performed on Ni-NTA spin columns (Qiagen) following supplier's protocols. Large scale purification was done by immobilised metal affinity chromatography (IMAC), kindly performed by Alan Scott (University of Glasgow). Cells were lysed in bacterial protein extraction reagent (Thermo Scientific) and sonicated. Purification was performed under native (non-denaturating) conditions, by using increasing concentrations of imidazole (50 mM for the wash step, 500 mM for the elution). The N-terminal polyhistidine-tags bind to the nickel ions that are immobilised in the column. Proteins retained in the column by non-specific and low affinity binding are washed away by imidazole (50 mM), that competitively interacts with the nickel ions. A high concentration of imidazole (500mM) is used to elute the polyhistidine-tagged protein from the column. The eluate was dialysed twice in 100 volumes 50 mM Tris HCl, 100 mM NaCl, pH 7.2 at 4 °C and stored at −80 °C with 50 % glycerol.

2.4. Enzyme assays

To standardise kinetic measurements of *T. brucei* enzymes, a pseudo-*in vivo* reaction buffer was developed within the SilicoTryp project (unpublished; Dr Alejandro Leroux, University of Heidelberg, Germany). This ST buffer is designed to mimick *in vivo*-like conditions, regarding pH, concentrations of salts, phosphate, tonicity etc. (Table 2.3). All kinetic measurements within the SilicoTryp project are to be measured in this buffer.

Component	Concentration (mM)
K^+	95
Na^+	15
Cl^-	120
PO_4^{3-}	10
Mg^{2+}	10
EDTA	1

Table 2.3.: SilicoTryp assay buffer. Pseudo-*in vivo* reaction buffer as used within the SilicoTryp project. Assays are performed at pH 7 and 37 °C. The pH of the assay buffer is adjusted with KOH after all other metabolites used in the enzyme assay are added.

2.4.1. Ribokinase

The ribokinase activity was measured spectrophotometrically by a coupled enzyme assay at 340 nm (Figure 2.3). Ablation of NADH was monitored at 340 nm and the change of absorption over time was converted to change of NADH concentration using a molar extinction coefficient of 6,220 M cm^{-1}. The stoichiometry of the coupled enzyme assay dictates that changes in NADH concentration correspond to equal changes in ribose concentration, i.e. the change in NADH concentration is a measure of the ribokinase activity. The measured ribokinase activity was normalised against the quantity of ribokinase used in the assay, as determined from the protein sample by Bradford assay, to obtain the enzyme's specific activity. A similar approach was used for the reverse reaction, where NADPH production was monitored at 340 nm, corresponding to consumption of Rib-5-P (Figure 2.3).

The forward (ribose consuming) reaction was assayed in 1 ml ST buffer, 20 mM ribose, 5 mM ATP, 5 mM PEP, 0.2 mM NADH, 2 U PK and 2 U lactate dehydrogenase. The

reverse (ribose producing) reaction was assayed in 1 ml ST buffer, 20 mM Rib-5-P, 5 mM ADP, 5 mM glucose, 0.2 mM $NADP^+$, 2 U HXK and 2 U G6PDH. The signal was corrected for background activity using assays with no ribose or Rib-5-P was added.

2.4.2. Hexokinase

The hexokinase activity was measured spectrophotometrically by a coupled enzyme assay at 340 nm (Figure 2.3). The phosphorylation of glucose was measured by monitoring the production of NADPH, while dephosphorylation of glucose was measured by monitoring the production of NADH. Conversion from NADPH and NADH concentrations to activities was performed as described in Section 2.4.1.

The phosphorylation of glucose was assayed in 1 ml ST buffer, 20 mM glucose, 5 mM ATP, 0.2 mM $NADP^+$ and 2 U glucose 6-phosphate dehydrogenase. Fresh cell extract was added at 5 µg whole cell protein per assay. The dephosphorylation of glucose 6-phosphate was assayed in 1 ml ST buffer, 25 mM Glc6P, 5 mM ADP, 0.2 mM NAD and 2 U glucose dehydrogenase. Fresh cell extract was added at 25 µg whole cell protein per assay.

2.4.3. Glucose-6-phosphatase assay

The activity of glucose-6-phosphatase was measured spectrophotometrically by a coupled enzyme assay at 340 nm (Figure 2.3). The phosphorylation of glucose was measured by monitoring the production of NADH, conversion from NADH concentrations to specific activities was performed as described in Section 2.4.1. Assays were performed in 1 ml ST buffer, 0.2 mM NAD^+, 5 mM glucose 6-phosphate and 2 U glucose dehydrogenase. Fresh cell extract was added at 25 µg per assay, and absorbance measurements were corrected with a control sample without glucose 6-phosphate.

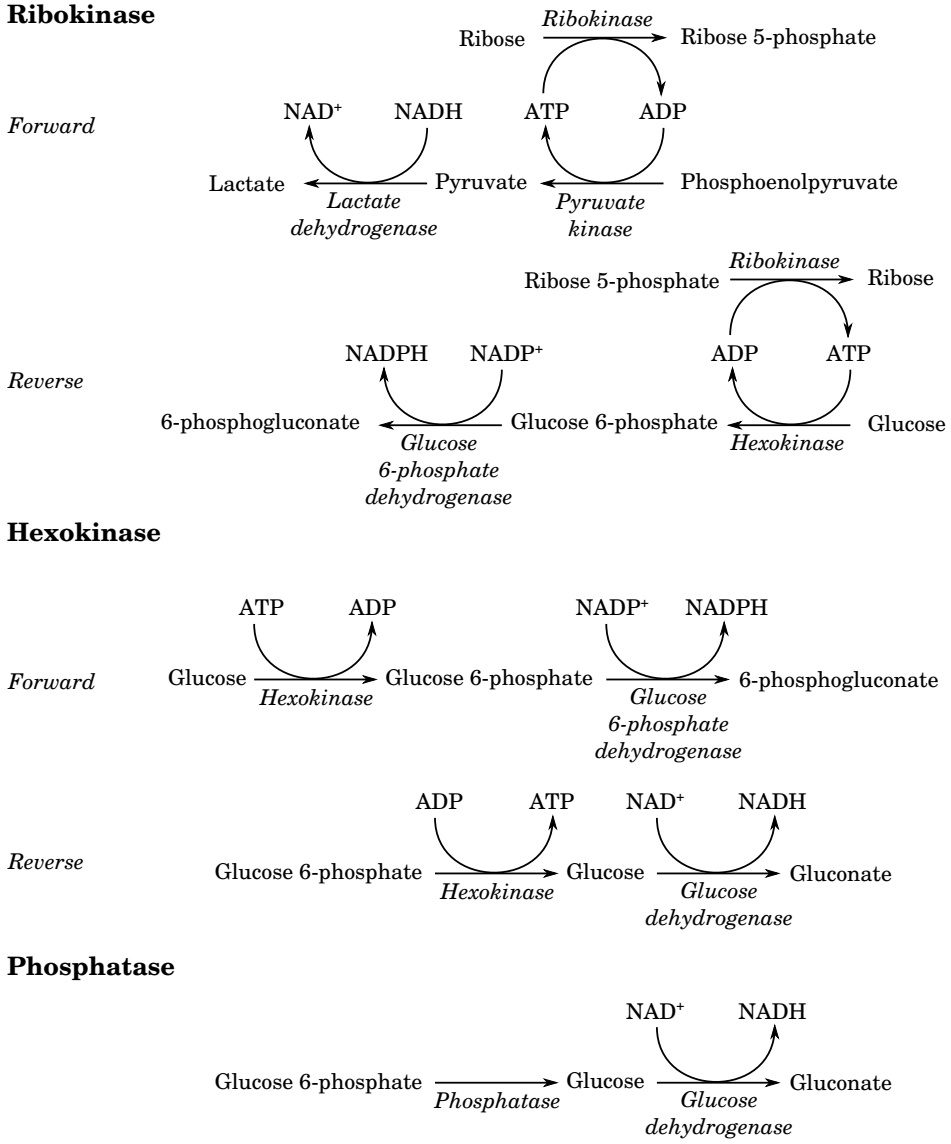

Figure 2.3.: Coupled enzyme assays. Overview of the coupled enzyme assays used in this study. Changes in NADPH and NADH correspond to the activity of the reaction of interest, and are measured at 340 nm. Extinction coefficients and the quantity of protein added to the assay are subsequently used to calculate specific activities.

2.5. Western blotting

For Western blot analysis, $3 \cdot 10^6$ parasites were harvested by centrifugation, washed in PBS, resuspended in 30 µl Laemmli buffer (Laemmli, 1970) and stored at –80 °C before analysis. Samples were boiled for 10 minutes at 95 °C and 20 µL was separated on SDS-PAGE (Novex 4–20 % Tris-glycine, Invitrogen) at 125 V and transferred to a nitrocellulose membrane (Hybond-ECL, Amersham, USA) at 150 mA for 4 hours. Membranes were blocked for 2 hours at room temperature with 5 % milk in PBS-T (PBS with 0.05 % Tween-20), washed three times with PBS-T, and probed with primary

antibody in 1 % milk in PBS-T overnight at 4 °C. After three washes with PBS-T, the membrane was incubated with secondary antibody in 1 % milk in PBS-T for 2 hours at room temperature. After five washes with PBS-T, horseradish peroxidase activity was measured with SuperSignal HRP substrate (Merck, Germany).

2.5.1. Ribokinase polyclonal antibody

A polyclonal antibody (pAB) for *T. brucei* ribokinase (pAB-TbRK) was raised in rabbits by GenicBio, Hong Kong, using recombinant ribokinase. The antibody was purified from serum by protein A-chromatography, and the ELISA titer was determined at >1:192,000. The antibody was further purified by affinity-chromatography. For this, recombinant *T. brucei* ribokinase was immobilised on column with a mixture of Affi-Gel 10 and 15 activated affinity medium following supplier's protocol (Bio-Rad). 15.5 mg of recombinant ribokinase in PBS was coupled to 2 ml of Affi-Gel mixture overnight at 4 °C.

The protein A-purified serum was loaded on the ribokinase-column and a series of different solutions were used to find the optimal elution conditions. The first ten elution volumes were acid elutions with 100 mM glycine-HCl pH 2.5, the second ten elution volumes were base elutions with 100 mM ethanolamine pH 11.5, while the and last ten elution volumes were chaotrophic elutions with 3.5 M $MgCl_2$, 20 mM TrisHCl pH 7.5. A dot blot was used to select the optimal elution fractions, and the final magnesium elutions were used for subsequent Western blots.

The purified pAB-TbRK was used at a final dilution of 1:1,000. The secondary antibody used for detection of pAB TbRK was goat anti-rabbit IgG peroxidase conjugate (Calbiochem). A cross-reacting band larger than 80 kDa was observed in all Western blots using pAB-TbRK, while *T. brucei* RK is expected to show a band at 38 kDa. The cross-reacting band was constant in all genetic mutants, even when the 38 kDa-band disappeared. The identity of the cross-reacting band is unknown.

2.6. Metabolomics

2.6.1. Metabolomics enzyme assay sampling

The idea behind the metabolomics enzyme assay is discussed in detail in chapter 5. Briefly, it consists of incubation of a recombinant enzyme in a complex mixture of metabolites and the measurement of changes in the metabolite mixture using mass-spectrometry. Commercial yeast extract (Sigma) was used as a complex metabolite mixture. Around 1 mg of yeast extract was resuspended in 200 µl of 75 % acetonitrile / H_2O and briefly vortexed to denature the proteins. Denatured protein and other debris were pelleted (16,100g, 5 minutes) and the supernatant was dried under vacuum. The remaining metabolites were resuspended in 100 µl 40 mM MOPS pH 7, 20 mM $MgCl_2$. The final assay volume of 100 µl contained 1:4 diluted metabolite mixture, one of the two cofactor mixtures (each cofactor at 100 µM, Table 2.4) and 2 µl of purified recombinant protein of interest.

The enzyme was allowed to react for 30 minutes at 37 °C and the reaction was subsequently quenched by the addition of 400 µL ice-cold acetonitrile. Samples were vortexed, centrifuged at 16,100g for 6 minutes at 4 °C, and transferred to glass chromatography vials. Control samples were prepared by addition of the enzyme of interest after the addition of acetonitrile. Samples were stored at −80 ˚C under argon prior to analysis by mass-spectrometry.

Mixture 1	Mixture 2
NAD	NADH
NADP	NADPH
ADP	ATP
GDP	GTP
CoA	Acetyl-CoA
FMN	FMN
FAD	FAD
PP	PP
TPP	TPP
Biotin	Biotin

Table 2.4.: Cofactor mixtures used in metabolomics enzyme assays. All cofactors were used at a final concentration of 0.1 mM.

2.6.2. Parasite metabolite extraction

Samples for metabolic profiling were taken from cultures in log phase growth (around $1–2 \cdot 10^6$ cells ml^{-1}). Five biological replicates were obtained by sampling from independent cultures on separate days. For each replicate, $4 \cdot 10^7$ cells were rapidly cooled to 4 °C by submersion of a 50 mL Corning flask in a dry ice-ethanol bath, and kept at 4 °C for all subsequent steps. The samples were centrifuged (1250*g*, 10 minutes) and the supernatant discarded. Cell lysis and protein denaturation was achieved by addition of 200 µl of ice-cold chloroform:methanol:water (ratio 1:3:1 v/v/v) plus internal standards followed by vigorous shaking for 1 hour at 4 °C. Metabolite extracts were centrifuged (16,000*g*, 4 °C, 2 minutes), the supernatant collected and stored under argon at −80 °C until further analysis.

2.6.3. Internal and authentic standards

During sampling, internal standards are added to the extraction solvent at a concentration of 1 µM. These internal standards (theophylline, 5-fluorouridine, Cl-phenyl cAMP, *N*-methyl glucamine, canavanine and piperazine) have been selected as they are expected to be present in the *T. brucei* and *E. coli* samples. With each experiment, a set of authentic standards were run on the mass spectrometer, a full list is given in Section D.1. These standards have been selected to cover a wide range of chemical properties, and among others function as a training set that is used in the retention time prediction that is performed during analysis (Creek *et al.*, 2011). Standards were prepared at 10 µM in three mixtures, according to the list of Section D.1, to prevent isobaric compounds and likely fragments within each group, as described by Creek *et al.* (2011).

2.6.4. Liquid chromatography-mass spectrometry

All samples were separated by HPLC with either a ZIC®-HILIC or ZIC®-pHILIC column (Merck). HILIC stands for hydrophilic interaction liquid chromatography, and separation of compounds is based on their interactions with the hydrophilic stationary phase in the chromatographic column. HILIC is able to separate polar compounds and commonly recommended for LC-MS based metabolomics analysis (Creek *et al.*, 2012a). The stationary phase in HILIC is silica based, while the stationary phase in pHILIC is polymer based, giving pHILIC an extended pH stability range. As metabolites can have different charges depending on the pH, and the analytes are measured based on mass-

to-charge ratio, analysis of the sample at different pHs therefore allows to extend the coverage of the measured analytes. In this project, I tried to use both columns as much as possible.

The injection volume was 10 µl and the HPLC gradient was as follows: flow rate 100 µl $\cdot$ min^{-1}; solvent A: 20 mM ammonium carbonate in H_2O; solvent B: acetonitrile; 80 % B (0 min); 20 % B (30 min); 5 % B (32 min); 5 % B (38 min); 80 % B (40 min); 80 % B (47 min). The HPLC column was coupled to an Exactive Orbitrap mass spectrometer (Thermo) as mass detector. The Exactive was run with rapid switching between positive and negative mode, and data was acquired at 50,000 resolution; spray voltages +4.5 kV and −3.5 kV; capillary voltage 40 V and 30 V; tube voltage 70 V; skimmer voltage 20 V and 18 V; ESI probe temperature 150 °C; capillary temperature 275 °C; shealth gas 40 units; auxilliary gas 5 units and sweep gas 1 unit.

2.6.5. Data analysis

Raw LC-MS data was converted to peakML format with msconvert (Kessner *et al.*, 2008), and metabolite peaks were picked using xcms with a mass accuracy of 2 parts per million; peak width 5−100 seconds; signal-to-noise ratio of 5 and minimal intensity of 1000 (Smith *et al.*, 2006). The peak list was aligned, filtered and reduced using mzMatch, with grouping window of 30 sec and 5 parts per million, a relative standard deviation filter of 0.5, noise filter of 0.8, intensity filter of 3000, 3 minimum detections and a retention-time window of 6 sec for related peaks (Scheltema *et al.*, 2011). Retention time correction, mass calibration, metabolite and related peak identification and comparative analysis were all performed using default settings of version 14 of the Excel-based macro system IDEOM (Creek *et al.*, 2012a).

Manual curation of the metabolomics data sets consisted of the confirmation of peak shape and intensity, and the identification of fragments based on both retention time and relational id as provided by mzMatch (Scheltema *et al.*, 2011).

Significantly changed metabolites were selected by using rank products (Breitling *et al.*, 2004), which is a non-parametrical statistical method that was developed to detect differentially expressed genes in microarray experiments. Rank products are based on the rank of fold-changes, where metabolites that are consistently increased among all replicates receive a higher rank than metabolites that only show random variation (Table 2.5). Subsequently, it is calculated how consistent the obtained rank products are by comparison to typically 10,000 random permutations of the same data set. From this

comparison, a false discovery rate (FDR) is calculated, as described in (Armengaud *et al.*, 2004). An FDR of < 5% means that only 5% or less of the metabolites up to this position is expected to be observed by change (false positives), the remaining being metabolites that are significantly affected (true positives). The strength of rank product analysis is that it looks at the whole data set for each replicate, and takes both the fold change (rank position) and reproducibility (product of ranks) into account.

A

Fold change			
Metabolite	Repl. 1	Repl. 2	Repl. 3
A	3.0	2.5	2.0
B	2.9	2.7	1.7
C	1.0	1.3	1.6

→

B

Rank lists			
	Repl. 1	Repl. 2	Repl. 3
Rank 1	A	B	A
Rank 2	B	A	C
Rank 3	C	C	B

↙

C

	Ranks multiplication	Rank product
A	$1/3 \cdot 2/3 \cdot 1/3$	$1/9$
B	$2/3 \cdot 1/3 \cdot 3/3$	$2/9$
C	$3/3 \cdot 3/3 \cdot 2/3$	$2/3$

Table 2.5.: Main principles of rank product analysis. A simplified overview of rank product analysis. In three replicate experiments (1–3), three metabolites (A–C) are measured and compared between a treated and untreated sample. The fold changes of the three metabolites are given (Table A). Rank lists are made for each replicate, where the metabolites are ordered by the size of the fold change, with the highest fold change on top (Table B). The rank values of each replicate are divided by the total number of measured metabolites and subsequently multiplied for each metabolite (Table C). The resulting number is the rank product, metabolites with the lowest rank product have the largest and most significant fold changes throughout the replicates.

2.7. Computational methods

2.7.1. Model description

The dynamic model described in chapter 5 is based on the curated model of trypanosomal glycolysis (Albert *et al.*, 2005; Haanstra *et al.*, 2008) first published by (Bakker *et al.*, 1999a). The equations were rewritten to contain the equilibrium constants and rapid

reversible reactions for the transport steps, as described by (Achcar *et al.*, 2012). These alterations did not affect the model outcome. A few additional modifications in the kinetic equations are listed below. A full description of the model is provided as Copasi and SBML files on the supplementary CD-ROM.

2.7.1.1. Generic rate equations

Most of the rate equations for 2-substrate-2-product reactions follow the generic form:

$$v_{c/g} = V_{max,c/g} \cdot \frac{\frac{[S1]_{c/g}}{K_{m,S1}} \cdot \frac{[S2]_{c/g}}{K_{m,S2}} \cdot \left(1 - \frac{\Gamma_{x,c/g}}{K_{eq,x}}\right)}{\left(1 + \frac{[S1]_{c/g}}{K_{m,S1}} + \frac{[P1]_{c/g}}{K_{m,P1}}\right) \cdot \left(1 + \frac{[S2]_{c/g}}{K_{m,S2}} + \frac{[P2]_{c/g}}{K_{m,P2}}\right)} \tag{2.1}$$

while rate equations for reactions with one substrate and one product typically follow:

$$v_{c/g} = V_{max,c/g} \cdot \frac{\frac{[S1]_{c/g}}{K_{m,S1}} \cdot \left(1 - \frac{\Gamma_{x,c/g}}{K_{eq,x}}\right)}{1 + \frac{[S1]_{c/g}}{K_{m,S1}} + \frac{[P1]_{c/g}}{K_{m,P1}}} \tag{2.2}$$

where S1 and S2 are the substrates while P1 and P2 are the products. Subscripts *c/g* indicates that separate equations are used for cytosolic and glycosomal reactions. *Keq* is the equilibrium constant, and $\Gamma_{x,c/g}$ specifies the ratio of substrates and products and is defined as:

$$\Gamma_{c/g} = \frac{[P1]_{c/g} \cdot [P2]_{c/g}}{[S1]_{c/g} \cdot [S2]_{c/g}}, \tag{2.3}$$

for Eq. (2.1), and

$$\Gamma_{c/g} = \frac{[P]_{c/g}}{[S1]_{c/g}} \tag{2.4}$$

for Eq. (2.2).

2.7.1.2. Modified glycolysis equations

The equations in the last model of glycolysis have been modified by using reversible rate equations for hexokinase, phosphofructokinase and pyruvate kinase, which were modelled previously as irreversible reactions. Hexokinase now follows Eq. (2.1) and Eq. (2.3).

Phosphofructokinase is modelled with reversible ordered bi-bi kinetics with mixed inhibition by fructose 1,6-bisphosphate (Fru-1,6-BP) (Cronin and Tipton, 1987):

$$v_{PFK,g} = V_{max,g} \cdot \frac{K_{ii}}{[Fru-1,6-BP]_g + K_{ii}} \cdot \frac{\frac{[Fru-6-P]_g \cdot [ATP]_g}{K_{m,Fru-6-P} \cdot K_{m,ATP}} \cdot \left(1 - \Gamma_{PFK,g} / K_{eq,PFK}\right)}{\frac{K_{s,ATP}}{K_{m,ATP}} + \frac{[ATP]_g}{K_{m,ATP}} + \frac{[Fru-6-P]_g}{K_{m,Fru-6-P}} + \frac{[Fru-6-P]_g \cdot [ATP]_g}{K_{m,Fru-6-P} \cdot K_{m,ATP}} + \frac{[ADP]_g}{K_{m,ADP}} + \frac{[Fru-1,6-BP]_g \cdot [ADP]_g}{K_{is} \cdot K_{m,ADP}}}, \tag{2.5}$$

where $\Gamma_{PFK,g}$ follows Eq. (2.3), K_{ii} and K_{is} describe the mixed inhibition by Fru-1,6-BP and are also taken from Cronin and Tipton (1987).

Pyruvate kinase is modelled reversibly with cooperativity for phosphoenolpyruvate (PEP):

$$v_{PK,c} = V_{max,c} \cdot \frac{\left(\frac{[PEP]_c}{K_{PEP}}\right)^n \cdot \frac{[ADP]_c}{K_{m,ADP}} \cdot \left(1 - \Gamma_{PK,c} / K_{eq,PK}\right)}{\left(1 + \left(\frac{[PEP]_c}{K_{PEP}}\right)^n + \frac{[Pyr]_c}{K_{m,Pyr}}\right) \cdot \left(1 + \frac{[ADP]_c}{K_{m,ADP}} + \frac{[ATP]_c}{K_{m,ATP}}\right)}, \tag{2.6}$$

where $\Gamma_{PK,c}$ follows Eq. (2.3) and

$$K_{PEP} = K_{m,PEP} \cdot \left(1 + \frac{[ATP]_c}{K_{i,ATP}} + \frac{[ADP]_c}{K_{i,ADP}}\right). \tag{2.7}$$

The known inhibition of phosphoglucose isomerase by the pentose phosphate pathway intermediate 6-phosphogluconate (6-PG) was included as described by Marchand *et al.* (1989):

$$v_{PGI,g} = V_{max,g} \cdot \frac{\frac{[Glc-6-P]_g}{K_{m,Glc-6-P}} \cdot \left(1 - \Gamma_{PGI,g} / K_{eq,PGI}\right)}{1 + \frac{[Glc-6-P]_g}{K_{m,Glc-6-P}} + \frac{[Fru-6-P]_g}{K_{m,Fru-6-P}} + \frac{[6-PG]_g}{K_{i,6-PG}}}, \tag{2.8}$$

where $\Gamma_{PK,c}$ follows Eq. (2.4).

2.7.1.3. Rate equations of PPP extension

The reactions of the ATP:ADP antiporter, glucose-6-phosphate dehydrogenase, 6-phosphogluconate dehydrogensae, and ribokinase were modelled with Eq. (2.1) and Eq. (2.3). Glucose-6-phosphatase, pentose phosphate isomerase and trypanothione reductase were modelled with Eq. (2.2) and Eq. (2.4).

For the 6-phosphogluconolactonase reaction both the spontaneous hydrolysis as well as the enzyme-catalysed reaction were included (Miclet *et al.*, 2001):

$$v_{PGL,c/g} = V_{max,c/g} \cdot \frac{\frac{[6-PGL]_{c/g}}{K_{m,6-PGL}} \cdot \left(1 - \Gamma_{PGL,c/g}/K_{eq,PGL}\right)}{1 + \frac{[6-PGL]_{c/g}}{K_{m,6-PGL}} + \frac{[6-PG]_{c/g}}{K_{m,6-PG}}} + k \cdot V_{c/g} \cdot \left([6-PGL]_{c/g} - \frac{[6-PG]_{c/g}}{K_{eq,PGL}} \right), \tag{2.9}$$

where k is the rate constant of spontaneous hydrolysis and $V_{c/g}$ is the volume of the relative compartment, which are 5.4549 and 0.2451 µl per mg protein for the cytosol and glycosome, respectively (Opperdoes *et al.*, 1984).

Glycosomal and cytosolic oxidation of NADPH and trypanothione are modelled with mass-action kinetics:

$$v_{c/g} = k \cdot [S]_{c/g},$$

where k is the mass-action constant.

2.7.1.4. Rate equation of fructose extension

To allow the model to use fructose instead of glucose (see chapter 6), the hexokinase reaction (Eq. (2.1)) was amended to include competitive inhibition:

$$v_{c/g} = V_{max,c/g} \cdot \frac{\frac{[S1]_{c/g}}{K_{m,S1}} \cdot \frac{[S2]_{c/g}}{K_{m,S2}} \cdot \left(1 - \frac{\Gamma_{x,c/g}}{K_{eq,x}}\right)}{\left(1 + \frac{[S1]_{c/g}}{K_{m,S1}} + \frac{[P1]_{c/g}}{K_{m,P1}}\right) \cdot \left(1 + \frac{[S2]_{c/g}}{K_{m,S2}} + \frac{[P2]_{c/g}}{K_{m,P2}} + \frac{[IS2]_{c/g}}{K_{i,IS2}} + \frac{[IP2]_{c/g}}{K_{i,IP2}}\right)} \tag{2,10}$$

where IS2 is the inhibiting substrate (glucose in the case of the fructose-phosphorylating hexokinase, and *vice versa*), and IP2 is the inhibiting product (glucose 6-phosphate in the case of the fructose-phosphorylating hexokinase, and fructose 6-phosphate in case of the glucose-phosphorylating hexokinase) and K_i are the inhibitor constants of IS2 and IP2.

2.7.1.5. Kinetic parameters

The kinetic parameters in the rate equations mentioned above were predominantly derived from literature. If no parameters of the *T. brucei* enzyme were available,

parameters from related species were used. If necessary, K_{eq} values were corrected to pH 7. All parameter values are listed in Table 3.2. Distributions of parameters used in uncertainty modelling are given in appendix B.

2.7.1.6. Metabolite concentrations

The extension of the model with the glycosomal pentose phosphate pathway led to an extension of the conserved moiety of phosphorylated glycosomal metabolites (Table 1.1) as compared to earlier model versions (Bakker *et al.*, 1999a). The new conserved sum was chosen such that extension of the glycolysis model with the glycosomal PPP and ribokinase results in similar steady state concentrations of glycolytic metabolites in both models. The conserved sum of NADPH in the cytosol and glycosome was arbitrarily chosen as 2 mM, while the conserved sum of trypanothione was chosen as 0.38 mM (Fairlamb *et al.*, 1987).

2.7.2. Simulations

The model was initially constructed and simulations were performed in PySCeS 0.7.8 (Olivier *et al.*, 2005) or COPASI 4.8 (Hoops *et al.*, 2006). SBML and Copasi files are provided on the supplementary CD-ROM. Some of the simulations were performed while taking uncertainty into account. Each simulation exists of a 1000 individual runs, where in each run all parameter values are sampled simultaneously. The parameter distributions are described in more detail in appendix B. A tool was developed in-house by Dr Fiona Achcar, that is responsible for the random sampling of parameter values, calculations of steady states or time-course simulations, and subsequent collation of the results from all individual runs (Achcar *et al.*, 2012).

Chapter 3

Extensions of the model of trypanosomal metabolism

A detailed dynamic model of *T. brucei* glycolysis was constructed and successfully applied to address questions regarding unique characteristics of trypanosomal glycolysis (Bakker *et al.*, 1997, 1999a, 2000; Helfert *et al.*, 2001; Albert *et al.*, 2005).

In this Chapter, the model of trypanosomal glycolysis is extended with the PPP. Hypotheses that derived from the newly constructed models were experimentally tested, and the results were subsequently used to update the model.

3.1. Introduction

An ambitious aim in systems biology is the generation of the "Silicon Cell", a mathematical description of life at a cellular level by integration of information from the genome, transcriptome, proteome, metabolome and observed phenotype (Snoep, 2005). Because of the complexity of biological systems, the most tractable way to construct such a large-scale model is by applying a modular approach (Snoep *et al.*, 2006). Smaller models, describing only part of the biological system, are coupled to create ever larger *in silico* representations of life.

3.1.1. Towards an *in silico* trypanosome

The dynamic model of bloodstream form *T. brucei* glycolysis, constructed by Bakker *et al.* (1997), is an example of a model that describes part of a biological system. This model describes the kinetics of the enzymes that form glycolysis, which is partly compartmentalised in a unique organelle called the glycosome, and is the sole energy source of bloodstream form trypanosomes. Trypanosomal glycolysis has been a front runner in systems biology, due to the relative simplicity of the network and the availability of a comprehensive and uniform set of kinetic parameters. This model of glycolysis has aided to address a number of questions, including what reaction steps control the glycolytic flux—they were found to be different from erythrocytes, offering potential as drug targets (Bakker *et al.*, 1999a,b)—and the significance of the loss of some feedback regulation, (Bakker *et al.*, 2000; Haanstra, 2009; Gualdrón-López *et al.*, 2012b).

In spite of the successes of the model of glycolysis, it only covers a small part of metabolism. For instance, even though the majority of glycolytic flux is directed towards the excretion of pyruvate, it does branch into other essential pathways such as the PPP. The PPP is an important source of NADPH that is used in reductive biosynthesis and to maintain cellular redox homoeostasis, particularly under oxidative stress. An important factor in the oxidative stress protection is the unique and essential thiol trypanothione, with its biosynthesis implicated in the mode-of-action of trypanocidal drugs (Bacchi *et al.*, 1983). The biological importance of redox metabolism renders the PPP as a natural extension of the current available model.

In a collaborative project called SilicoTryp, funded within the large systems biology programme SysMO (Booth, 2007), the model of trypanosomal glycolysis is now

extended to incorporate pathways that are involved in redox metabolism (Bakker *et al.*, 2010). Besides *horizontal* extension of the model of metabolism with additional metabolic pathways, the model is also extended *vertically* by the inclusion of gene transcription and translation, making progress towards a "silicon trypanosome". In this Chapter I will deal with the *horizontal* extension of the glycolytic model with additional pathways.

3.1.2. Trypanosomal PPP

The PPP, branching off glycolysis at the point of Glc-6-P, is an essential pathway that provides NADPH for redox metabolism and Rib-5-P for nucleotide biosynthesis. Genetic mutants and inhibitor studies have demonstrated the importance of the PPP for trypanosome survival (Hanau *et al.*, 1996; Dardonville *et al.*, 2003).

In the bloodstream form of *T. brucei* only the oxidative part of the PPP is present (Figure 1.6), and the PPP is localised to both the cytosol and glycosomes, as indicated by subcellular localisation studies (Duffieux *et al.*, 2000; Heise and Opperdoes, 1999; Stoffel *et al.*, 2011), proteomic analyses (Colasante *et al.*, 2006; Vertommen *et al.*, 2008) and subcellular targeting-sequence-based predictions (Opperdoes and Szikora, 2006).

3.1.3. Aim

Because of the importance of the PPP for trypanosome survival (Hanau *et al.*, 1996; Dardonville *et al.*, 2003), and the partial glycosomal localisation of this pathway, it was decided to extend the original model of trypanosomal glycolysis with the PPP. Such an extended mechanistic model will allow to study the characteristics and (dynamic) behaviour of both glycolysis and the PPP in more detail (as shown in Chapter 6). The extended model is a step forwards towards a silicon trypanosome (Bakker *et al.*, 2010).

In this chapter, I will extend the current model of trypanosomal glycolysis with the PPP using enzyme kinetics, both from literature and wet-lab experimentation. This progress follows an iterative cycle, where model predictions are tested by experimentation, and the results from experimentation is subsequently used to inform the model building process. The results section commences with a brief description of a method that has been developed in our laboratory that allows to take uncertainty of the parameter values into account. Although this is not a prerequisite for most of the remaining chapter, it

does demonstrate that observed behaviour of a dynamic model is not purely based on particularly selected parameter values.

3.2. Results

3.2.1. Modelling glycolysis including uncertainty of the parameters

Kinetic models of metabolism require quantitative knowledge of detailed kinetic parameters (e.g. maximum reaction rates, enzyme affinities for substrates and regulators). However, our knowledge about these parameters is often limited. When the parameters are measured, various sources of error can affect the results: experimental noise at the technical and biological levels, systematic bias introduced by parameters being measured *in vitro* instead of *in vivo* or by the choice of specific experimental conditions (pH, temperature, ionic strength, etc.). Moreover, a substantial number of important parameters have never been measured and the estimates included in models are based either on values measured in closely related species or on the general distribution of similar parameters (Borger *et al.*, 2006). Few general methods for dealing with this uncertainty have been suggested (Wang *et al.*, 2004; Tran *et al.*, 2008; Murabito *et al.*, 2011; Mišković and Hatzimanikatis, 2011).

The model of glycolysis in *T. brucei* was adapted to include this uncertainty of parameter values, prior to further extension. In order to specify the uncertainty of each parameter value, Dr Fiona Achcar (University of Glasgow) and I gathered all available information relating to the sources of the values used in the model. Information included data on how kinetics were measured, the number of replicates and the standard error of mean values when available, additional calculations used to estimate the parameter from the observed values, and any "corrections" for additional factors such as temperature or pH. For this purpose, we created the SilicoTryp Wiki[1], a MediaWiki-based website dedicated to the detailed documentation of the sources of parameters used in the latest version of the model of glycolysis in *T. brucei*. Each reaction is described on its own page, which contains the rate equation and the detailed references and calculations for each parameter (see Figure 3.1 for an example). From the information collected, probability distributions could be inferred for each parameter, as described in Chapter C.

Dr Fiona Achcar developed methodology to handle the random sampling of parameters (Figure 3.1) and analysed the implications of parameter uncertainty on the model of trypanosomal glycolysis in more detail (Section E, Achcar *et al.*, 2012). In the remainder of this chapter this strategy will be used to demonstrate that the observed dynamic

[1] http://silicotryp.ibls.gla.ac.uk/wiki/

behaviour is not a function of a chosen set of parameter values. Error bars in this chapters represent interquartile ranges of the model results.

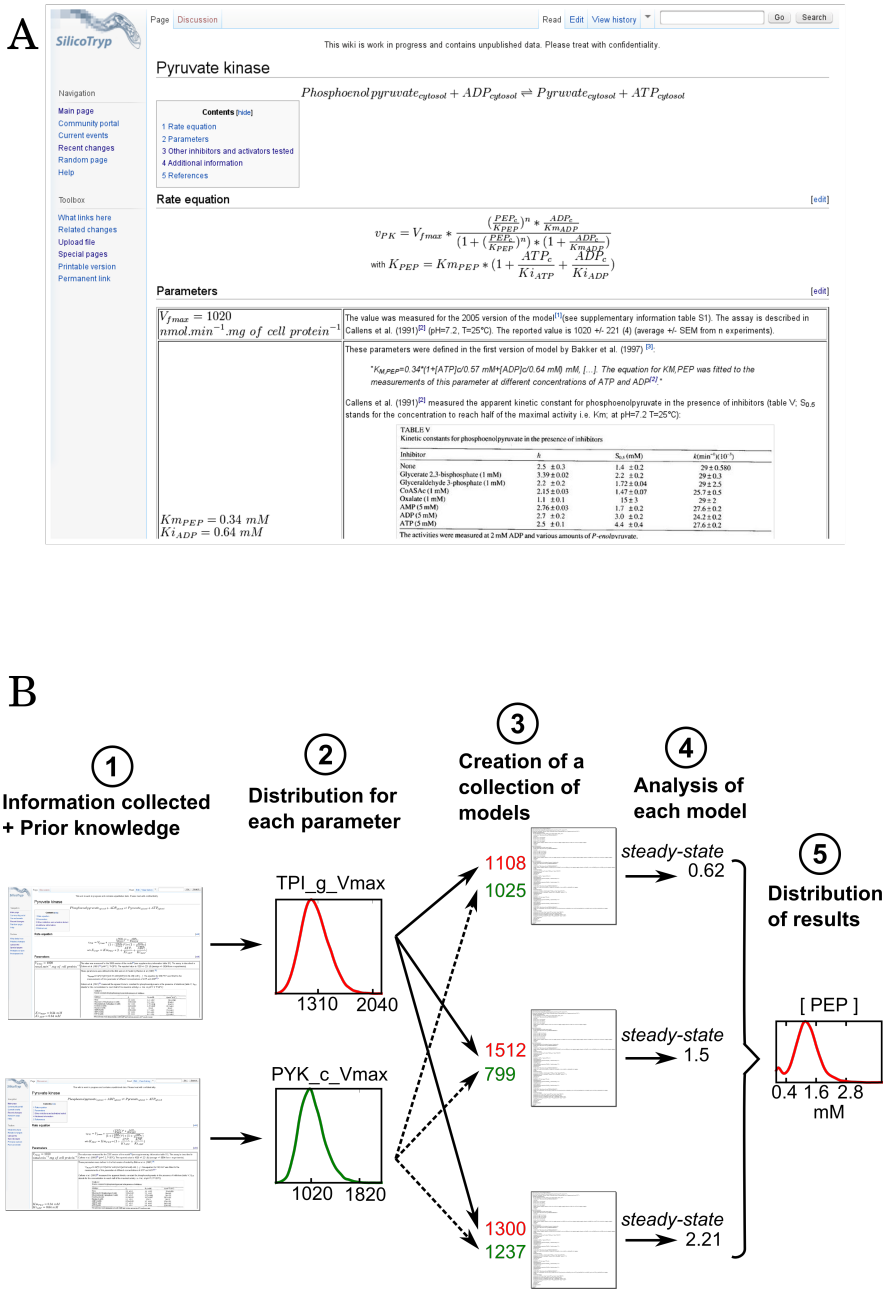

Figure 3.1.: Overview of modelling with uncertainty. *A:* Example of a page on the SilicoTryp wiki. *B:* Schematic overview of modelling with uncertainty in 5 steps. *1:* Collection of information on parameter uncertainty, together with any relevant prior knowledge. *2:* Distributions are described for each parameter value. *3:* A collection of models is generated, by random sampling of parameter values. Each model has a unique combination of parameter values. *4:* All generated models are analysed one by one. *5:* The outcome from all model simulations are combined to give a distribution of outcomes. Figure courtesy of Dr Fiona Achcar, University of Glasgow.

3.2.2. Stepwise extension with the PPP

The latest model of glycolysis in *T. brucei* was extended with the PPP. The extensions were divided into modules and added to the original model of glycolysis in a stepwise approach, what allowed extensive scrutiny of each module. Figure 3.2 and Figure 3.3 give an overview of all model versions considered in this Chapter. Table 3.1 describes the stoichiometry of all reactions, while Table 3.2 and gives all parameter values. The rate equations used are described in Chapter 2, Copasi and SBML files of the model are supplied on the supplementary CD-ROM. Stoichiometric analyses of each module are described in the appropriate section.

The original model of glycolysis was changed on a few points. A number of reactions that were modelled with irreversible rate equations (HXK, PFK and PYK). The rate equations for these reactions were replaced with reversible rate equations, using parameter values from literature (Table 3.2 for parameter values, see Methods for rate equations). It was decided not to change the assumption of the existence of an intracellular inorganic phosphate homoeostasis. As described in 1.8.5.1, inorganic phosphate is not limiting the rate, it is not involved in the rate equation for GAPDH, and inorganic phosphate is not a member of the conserved moiety of bound phosphates in the cytosol. The incorporation of transport reactions over the glycosomal and cytosolic membrane does therefore not affect the model, and I decided to keep the structure of the glycolysis module identical to the well tested original model of glycolysis (except from the aforementioned reversibility).

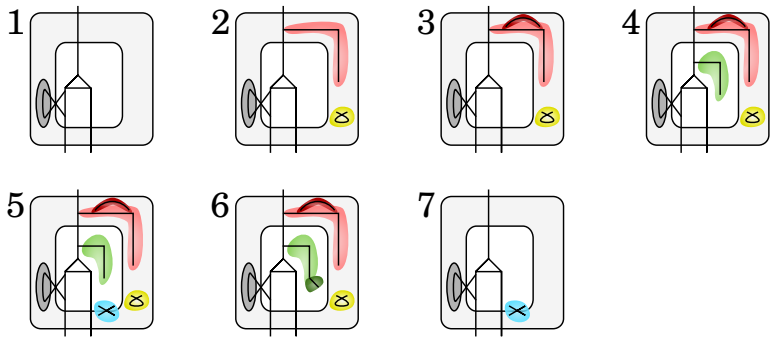

Figure 3.2.: Overview of different versions of models described in this Chapter. Coloured pathways refer to modules from Figure 3.3.

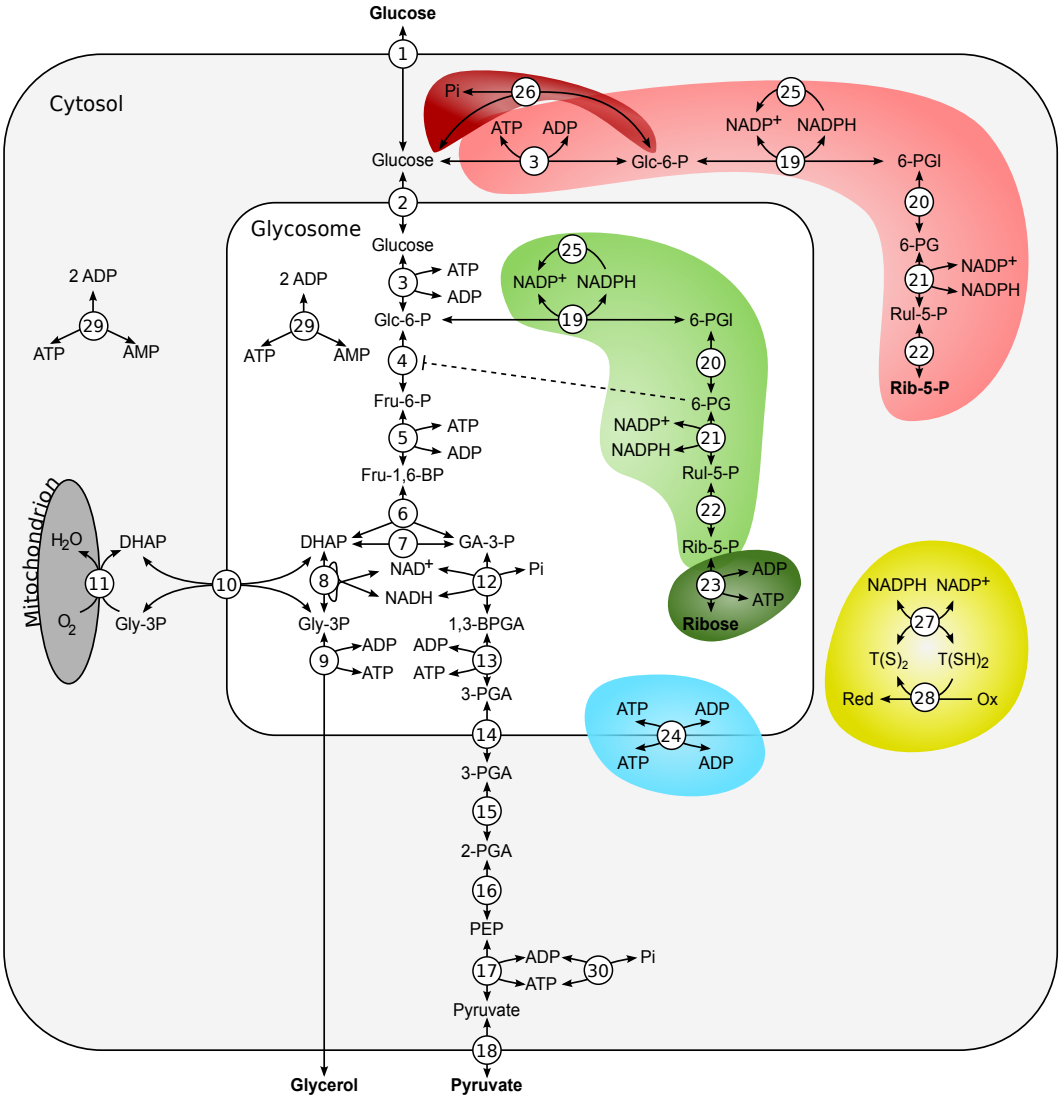

Figure 3.3.: Overview of metabolic pathways modelled in this Chapter. Detailed scheme of the glycolytic model with extensions including the glycosomal and cytosolic PPP. Reactions are indicated by numbers: *1*: glucose transport over the cell membrane ($GlcT_c$); *2*: glucose transport over the glycosomal membrane ($GlcT_g$); *3*: hexokinase ($HXK_{c/g}$); *4*: phosphoglucose isomerase (PGI_g); *5*: phosphofructokinase (PFK_g); *6*: aldolase (ALD_g); *7*: triosephosphate isomerase (TIM_g); *8*: glycerol-3-phosphate dehydrogenase ($G3PDH_g$); *9*: glycerol kinase (GK_g); *10*: Gly-3-P/DHAP antiporter (GDA_g); *11*: glycerol-3-phosphate oxidase (GPO_c); 12: glyceraldehyde 3-phosphate dehydrogenase ($GAPDH_g$); *13*: phosphoglycerate kinase (PGK_g); *14*: 3-PGA transporter ($PGAT_g$); *15*: phosphoglycerate mutase ($PGAM_c$); *16*: enolase (ENO_c); *17*: pyruvate kinase (PYK_c); *18*: pyruvate transport ($PYRT_c$); *19*: glucose-6-phosphate dehydrogenase ($G6PDH_{c/g}$); 20: phosphogluconolactonase ($PGL_{c/g}$); *21*: 6-phosphogluconate dehydrogenase ($6PGDH_{c/g}$); *22*: pentosephospate isomerase ($PPI_{c/g}$); *23*: RK (RK_g); *24*: ATP/ADP antiporter ($ATPT_g$); *25*: NADPH utilisation ($NADPHu_{c/g}$); *26*: G6PPase ($G6PP_c$); *27*: trypanothione reductase (TR_c); *28*: trypanothione oxidation (TOX_c); *29*: adenylate kinase ($AK_{c/g}$); *30* ATP utilisation ($ATPu_c$). Extensions to the original model of glysolysis that correspond to the modules in Table 3.1 are indicated by coloured shapes. Boundary metabolites with fixed concentrations are in bold, Rib-5-P in the glycosome is a boundary metabolite in model versions where no RK is present. Pink: cytosolic PPP; red: G6PP; yellow: TR; light-green: glycosomal PPP; dark-green: RK; blue: ATPT.

Module	Reaction	Reaction stoichiometry
Glycolysis	$GlcT_c$	**$Glucose_e$** $\rightarrow$ $Glucose_c$
	$GlcT_g$	$Glucose_c \leftrightarrow Glucose_g$
	HXK_g	$Glucose_g + ATP_g \leftrightarrow Glc\text{-}6\text{-}P_g + ADP_g$
	PGI	$Glc\text{-}6\text{-}P_g \leftrightarrow Fru\text{-}6\text{-}P_g$
	PFK	$Fru\text{-}6\text{-}P_g + ATP_g \leftrightarrow Fru\text{-}1,6\text{-}BP_g + ADP_g$
	ALD	$Fru\text{-}1,6\text{-}BP_g \leftrightarrow DHAP_g + GA\text{-}3\text{-}P_g$
	TIM	$DHAP_g \leftrightarrow GA\text{-}3\text{-}P_g$
	GAPDH	$GA\text{-}3\text{-}P_g + NAD_g +$ **Pi_g** $\leftrightarrow 1,3\text{-}BPGA_g + NADH_g$
	PGK	$1,3\text{-}BPGA_g + ADP_g \leftrightarrow 3\text{-}PGA + ATP_g$
	PGAT	$3\text{-}PGA_g \leftrightarrow 3\text{-}PGA_c$
	PGAM	$3\text{-}PGA_c \leftrightarrow 2\text{-}PGA_c$
	ENO	$2\text{-}PGA_c \leftrightarrow PEP_c$
	PYK	$PEP_c + ADP_c \leftrightarrow Pyruvate_c + ATP_c$
	PyrT	$Pyruvate_c \rightarrow$ **$Pyruvate_e$**
	G3PDH	$DHAP_g + NADH_g \leftrightarrow NAD_g + Gly\text{-}3\text{-}P_g$
	GDA	$DHAP_c + Gly\text{-}3\text{-}P_g \leftrightarrow DHAP_g + Gly\text{-}3\text{-}P_c$
	GPO	$Gly\text{-}3\text{-}P_c + 0.5\ O_2 \rightarrow DHAP_c$
	GK	$Gly\text{-}3\text{-}P_g + ADP_g \leftrightarrow$ **$Glycerol_e$** $+ ATP_g$
	ATPu	$ATP_c \rightarrow ADP_c +$ **Pi_c**
	AK_g	$2\ ADP_g \leftrightarrow ATP_g + AMP_g$
	AK_c	$2\ ADP_c \leftrightarrow ATP_c + AMP_c$
G6PP	G6PP	$Glc\text{-}6\text{-}P_c \leftrightarrow Glucose_c +$ **Pi_c**
Cytosolic PPP	HXK_c	$Glucose_c + ATP_c \leftrightarrow Glc\text{-}6\text{-}P_c + ADP_c$
	G6PDH	$Glc\text{-}6\text{-}P_c + NADP_c \leftrightarrow 6\text{-}PGL_c + NADPH_c$
	PGL	$6\text{-}PGL_c \leftrightarrow 6\text{-}PG_c$
	6PGDH	$6\text{-}PG_c + NADP_c \leftrightarrow Rul\text{-}5\text{-}P_c + NADPH_c +$ **CO_2**
	PPI	$Rul\text{-}5\text{-}P_c \leftrightarrow$ **Rib-5-P_c**
	NADPHu	$NADPH_c \rightarrow NADP_c$
Trypanothione cycle	TR	$TS_{2,c} + NADPH_c \leftrightarrow T(SH)_{2,c} + NADP_c$
	TOX	$T(SH)_{2,c} \rightarrow TS_{2,c}$
Glycosomal PPP		Reactions and kinetics identical to cytosolic PPP, but pathway entirely localised in the glycosome.
RK	RK	$Rib\text{-}5\text{-}P_g + ADP_g \leftrightarrow$ **$Ribose_g$** $+ ATP_g$
ATPT	ATPT	$ATP_c + ADP_g \leftrightarrow ATP_g + ADP_c$

Table 3.1.: Model stoichiometry. The modules and their subsequent reactions, as depicted in Figure 3.3. Bold characters indicate external metabolites whose concentrations are kept constant.

Table 3.2.: Kinetic parameters of the reactions related to the PPP. For dual localised reactions, subscript c and g indicate cytosolic or glycosomal localisation. Where needed, parameter values were corrected to pH 7 and/or 25 °C.

Enzyme	Parameter	Value	Unit	Ref.
$GlcT_c$	V_{max}	111.7	nmol min^{-1} mg $protein^{-1}$	Achcar *et al.*, 2012
	$K_{m,Glc}$	1	mM	Bakker *et al.*, 1999b
	α	0.75	dimensionless	Bakker *et al.*, 1997
$GlcT_g$	k	250,000	dimensionless	Achcar *et al.*, 2012
HXK	$V_{max,g}$	1,775	nmol · min^{-1} · mg $protein^{-1}$	This Chapter
	$V_{max,c}$	154 [2]	nmol · min^{-1} · mg $protein^{-1}$	This Chapter
	K_{eq}	759 [3]	dimensionless	Fromm *et al.*, 1964
	$K_{m,Glc}$	0.1	mM	Bakker *et al.*, 1997
	$K_{m,ATP}$	0.12	mM	Nwagwu and Opperdoes, 1982
	$K_{m,Glc\text{-}6\text{-}P}$	12	mM	This Chapter
	$K_{m,ADP}$	0.13	mM	Nwagwu and Opperdoes, 1982
PGI	V_{max}	1,305	nmol · min^{-1} · mg $protein^{-1}$	Albert *et al.*, 2005
	K_{eq}	0.457	dimensionless	Achcar *et al.*, 2012
	$K_{m,Glc\text{-}6\text{-}P}$	0.4	mM	Helfert *et al.*, 2001
	$K_{m,Fru\text{-}6\text{-}P}$	0.12	mM	Helfert *et al.*, 2001
	$K_{i,6\text{-}PG}$	0.14	mM	Marchand *et al.*, 1989
PFK	V_{max}	1,708	nmol · min^{-1} · mg $protein^{-1}$	Albert *et al.*, 2005
	K_{eq}	1,035	dimensionless	Voet *et al.*, 1999
	Kii	15.8	mM	Cronin and Tipton, 1987
	Kis	10.7	mM	Cronin and Tipton, 1987
	$K_{s,ATP}$	0.0393	mM	Cronin and Tipton, 1987
	$K_{m,ATP}$	0.0648	mM	Cronin and Tipton, 1987
	$K_{m,Fru\text{-}6\text{-}P}$	0.999	mM	Cronin and Tipton, 1987
	$K_{m,ADP}$	1	mM	[4]
ALD	V_{max}	560	nmol · min^{-1} · mg $protein^{-1}$	Albert *et al.*, 2005
	K_{eq}	0.084	dimensionless	Achcar *et al.*, 2012
	$K_{m,GA\text{-}3\text{-}P}$	0.067	mM	Callens *et al.*, 1991
	$K_{i,GA\text{-}3\text{-}P}$	0.098	mM	Callens *et al.*, 1991
	$K_{m,Fru\text{-}1,6\text{-}BP}$	0.009	mM	Callens *et al.*, 1991
	$K_{m,DHAP}$	0.015	mM	Callens *et al.*, 1991
	$K_{i,ATP}$	0.68	mM	Callens *et al.*, 1991
	$K_{i,ADP}$	1.51	mM	Callens *et al.*, 1991
	$K_{i,AMP}$	3.65	mM	Callens *et al.*, 1991

[2] Model 1 and 7 do not have a cytosolic HXK.

[3] Corrected to pH 7 and/or 25 °C.

[4] No value available, assumed to be significantly higher than $K_{m,ATP}$, as ADP was shown to activate the enzyme under particular conditions (Cronin and Tipton, 1987).

Enzyme	Parameter	Value	Unit	Ref.
TPI	V_{max}	999.3	nmol · min^{-1} · mg protein^{-1}	Albert *et al.*, 2005
	K_{eq}	0.046	dimensionless	Achcar *et al.*, 2012
	$K_{m,DHAP}$	1.2	mM	Lambeir *et al.*, 1987
	$K_{m,GA-3-P}$	0.25	mM	Lambeir *et al.*, 1987
GAPDH	V_{max}	720.9	nmol · min^{-1} · mg protein^{-1}	Albert *et al.*, 2005
	K_{eq}	0.066	dimensionless	Achcar *et al.*, 2012
	$K_{m,GA-3-P}$	0.15	mM	Lambeir *et al.*, 1991
	K_{m,NAD^+}	0.45	mM	Lambeir *et al.*, 1991
	$K_{m,1,3-BPGA}$	0.1	mM	Lambeir *et al.*, 1991
	$K_{m,NADH}$	0.02	mM	Lambeir *et al.*, 1991
G3PDH	V_{max}	465	nmol · min^{-1} · mg protein^{-1}	Albert *et al.*, 2005
	K_{eq}	17,085	dimensionless	Achcar *et al.*, 2012
	$K_{m,DHAP}$	0.1	mM	Marché *et al.*, 2000
	$K_{m,NADH}$	0.01	mM	Marché *et al.*, 2000
	$K_{m,Gly-3-P}$	2	mM	Marché *et al.*, 2000
	K_{m,NAD^+}	0.4	mM	Marché *et al.*, 2000
GPO	V_{max}	368	nmol · min^{-1} · mg protein^{-1}	Fairlamb and Bowman, 1977
	$K_{m,Gly-3-P}$	1.7	mM	Fairlamb and Bowman, 1977
GK	V_{max}	200	nmol · min^{-1} · mg protein^{-1}	Bakker *et al.*, 1997
	K_{eq}	0.000837	dimensionless	Achcar *et al.*, 2012
	$K_{m,Gly-3-P}$	3.83	mM	Králová *et al.*, 2000
	$K_{m,ADP}$	0.56	mM	Králová *et al.*, 2000
	$K_{m,Gly}$	0.44	mM	Králová *et al.*, 2000
	$K_{m,ATP}$	0.24	mM	Králová *et al.*, 2000
PGK	V_{max}	2,862	nmol · min^{-1} · mg protein^{-1}	Albert *et al.*, 2005
	K_{eq}	3,377	dimensionless	Achcar *et al.*, 2012
	$K_{m,1,3-BPGA}$	0.003	mM	Albert *et al.*, 2005
	$K_{m,ADP}$	0.1	mM	Misset and Opperdoes, 1987
	$K_{m,3-PGA}$	1.62	mM	Misset and Opperdoes, 1987
	$K_{m,ATP}$	0.29	mM	Misset and Opperdoes, 1987
3PGAT	k	250	dimensionless	Achcar *et al.*, 2012
PGAM	V_{max}	225	nmol · min^{-1} · mg protein^{-1}	Albert *et al.*, 2005
	K_{eq}	0.17	dimensionless	Achcar *et al.*, 2012
	$K_{m,3-PGA}$	0.15	mM	Chevalier *et al.*, 2000
	$K_{m,2-PGA}$	0.16	mM	Chevalier *et al.*, 2000
ENO	V_{max}	598	nmol · min^{-1} · mg protein^{-1}	Albert *et al.*, 2005
	K_{eq}	4.17	dimensionless	Achcar *et al.*, 2012
	$K_{m,2-PGA}$	0.054	mM	Hannaert *et al.*, 2003a
	$K_{m,PEP}$	0.24	mM	Hannaert *et al.*, 2003a

Enzyme	Parameter	Value	Unit	Ref.
PYK	V_{max}	1,020	nmol · min^{-1} · mg protein^{-1}	Albert *et al.*, 2005
	K_{eq}	10,800	dimensionless	Achcar *et al.*, 2012
	n	2.5	dimensionless	Callens *et al.*, 1991
	$K_{m,ADP}$	0.114	mM	Barnard and Pedersen, 1988
	$K_{i,ATP}$	0.57	mM	Barnard and Pedersen, 1988
	$K_{i,ADP}$	0.64	mM	Barnard and Pedersen, 1988
	$K_{m,PEP}$	0.34	mM	Barnard and Pedersen, 1988
	$K_{m,ATP}$	15	mM	Achcar *et al.*, 2012
	$K_{m,Pyr}$	50	mM	Achcar *et al.*, 2012
PYRT	V_{max}	230	nmol · min^{-1} · mg protein^{-1}	Helfert *et al.*, 2001
	$K_{m,Pyr}$	1.96	mM	Wiemer *et al.*, 1992
ATPu	k	50	dimensionless	Bakker *et al.*, 1997
AK	$k_{1,c/g}$	480	dimensionless	Achcar *et al.*, 2012
	$k_{2,c/g}$	1,000	dimensionless	Achcar *et al.*, 2012
GDA	k	600	dimensionless	Achcar *et al.*, 2012
G6PDH	$V_{max,c/g}$	8.4	nmol · min^{-1} · mg protein^{-1}	Cronin *et al.*, 1989; Heise and Opperdoes, 1999
	K_{eq}	5.02	dimensionless	Goldberg *et al.*, 1993
	$K_{m,Glc-6-P}$	0.058	mM	Cordeiro *et al.*, 2009
	$K_{m,6-PGL}$	0.04	mM	Thorburn and Kuchel, 1985 [5]
	$K_{m,NADP^+}$	0.0094	mM	Cordeiro *et al.*, 2009
	$K_{m,NADPH}$	0.0001	mM	Thorburn and Kuchel, 1985 [5]
PGL	$V_{max,g}$	5	nmol · min^{-1} · mg protein^{-1}	Cronin *et al.*, 1989; Duffieux *et al.*, 2000
	$V_{max,c}$	28	nmol · min^{-1} · mg protein^{-1}	Cronin *et al.*, 1989; Duffieux *et al.*, 2000
	K_{eq}	20,000	dimensionless	Casazza and Veech, 1986
	$K_{m,6-PGL}$	0.05	mM	Igoillo-Esteve *et al.*, 2007 [6]
	$K_{m,6-PG}$	0.05	mM	[7]
	k	0.055	min^{-1}	Schofield and Sols, 1976
6PGDH	$V_{max,c/g}$	10.6	nmol · min^{-1} · mg protein^{-1}	Cronin *et al.*, 1989
	K_{eq}	47	dimensionless	Villet and Dalziel, 1969
	$K_{m,6-PG}$	0.0035	mM	Hanau *et al.*, 1996
	$K_{m,Rul-5-P}$	0.03	mM	Hanau *et al.*, 1996
	$K_{m,NADP^+}$	0.001	mM	Hanau *et al.*, 1996
	$K_{m,NADPH}$	0.0006	mM	Hanau *et al.*, 1996

[5] Parameter from red blood cells. K_m for Glc-6-P and $NADP^+$ are in the same range for *T. brucei* and red blood cells.

[6] Parameter from *Trypanosoma cruzi*.

[7] No value available. The affinity is assumed to be similar for the substrate and the product.

Enzyme	Parameter	Value	Unit	Ref.
PPI	$V_{max,c/g}$	72	nmol · min^{-1} · mg protein^{-1}	Cronin *et al.*, 1989 [8]
	K_{eq}	5.6	dimensionless	Goldberg and Tewari, 1995
	$K_{m,Rul-5-P}$	4	mM	Igoillo-Esteve *et al.*, 2007 [6]
	$K_{m,Rib-5-P}$	1.4	mM	Igoillo-Esteve *et al.*, 2007 [6]
TR	V_{max}	252	nmol · min^{-1} · mg protein^{-1}	Krieger *et al.*, 2000
	K_{eq}	434	dimensionless	Fairlamb and Cerami, 1992 [9]
	$K_{m,TS2}$	0.0069	mM	Jones *et al.*, 2010 [10]
	$K_{m,TSH2}$	0.0018	mM	
	$K_{m,NADPH}$	0.00077	mM	Jones *et al.*, 2010 [10]
	$K_{m,NADP^+}$	0.081	mM	
TOX	k	2-200	µl · min^{-1} · mg protein^{-1}	[11]
NADPHu	$k_{c/g}$	2	µl · min^{-1} · mg protein^{-1}	[12]
G6PPase	V_{max}	28	nmol · min^{-1} · mg protein^{-1}	This Chapter
	K_{eq}	263	dimensionless	Atkinson *et al.*, 1961
	$K_{m,Glc-6-P}$	5.6	mM	McLaughlin, 1986 [13]
	$K_{m,Glc}$	5.6	mM	McLaughlin, 1986
ATP:ADP antiporter	V_{max}	1.5	nmol · min^{-1} · mg protein^{-1}	[14]
	K_{eq}	1	dimensionless	[15]
	$K_{m,ATPc/g}$	0.02	mM	[15]
	$K_{m,ADPc/g}$	0.02	mM	[15]
RK	V_{max}	5	nmol · min^{-1} · mg protein^{-1}	This Chapter
	K_{eq}	0.0035	dimensionless	Table 4.3
	$K_{m,Rib-5-P}$	0.39	mM	Table 4.3
	$K_{m,Rib}$	0.51	mM	Table 4.3
	$K_{m,ADP}$	0.25	mM	Table 4.3
	$K_{m,ATP}$	0.24	mM	Table 4.3

[8] No reliable localisation data available, assumed to be equally distributed in glycosomal and cytosol.

[9] Calculated from redox potential of trypanothione.

[10] Ratio of K_m values of reduced and oxidised trypanothione are assumed to be similar to the ratio of K_m values of reduced and oxidised glutathione for glutathione reductase.

[11] Varies depending on oxidative stress

[12] Fitted to result in a total PPP flux of 1.2 nmol · min^{-1} · mg protein^{-1}, the PPP flux in *T. cruzi* and *L. mexicana* without induced oxidative stress (Maugeri *et al.*, 2003; Maugeri and Cazzulo, 2004).

[13] The average of the two types of acid phosphatases in *T. rhodesiense* were used as a first estimate.

[14] No specific value available. See Figure 1.4.

[15] The hypothetical ATP/ADP antiporter was given arbitrary kinetic constants. The K_{eq} of 1 reflects the assumption of facilited transport, i.e. not driven by an external source of Gibbs free energy.

3.2.2.1. Cytosolic PPP

As the first stepwise extension, the cytosolic PPP (Figure 3.2, model 2) was added to the glycolysis model (model 1). Two key enzymes of the non-oxidative PPP, PPE and TKT, are not expressed in the bloodstream form of the parasite (Cronin *et al.*, 1989; Stoffel *et al.*, 2011), rendering Rib-5-P the end product of the cytosolic PPP branch. The concentration of Rib-5-P is fixed in the model, implicitly reflecting its continuous utilisation as a precursor for nucleotide biosynthesis, or other potential undefined roles in the cell (Constantinides *et al.*, 1990). The equations and parameters used to describe the kinetics of the enzymes were based on *in vitro* studies (Table 3.2).

An elementary mode analysis was performed on the structure of model 2. A total of twelve elementary modes were observed (Table 3.3). The first three modes are identical to the modes observed in the original glycolysis model Table 1.2. The fourth mode is gluconeogenesis from glycerol to glucose, possible in model 2 but not in the original glycolysis model due to the reversibility of the HXK and PFK introduced in model 2. Elementary modes 8–12 consist of a combination of similar modes as 1–3 with an additional mode through the PPP (Table 3.3). In modes 5 and 6, oxidative glycolysis generates 2 ATP_c, similar to mode 1. Where ATP_c in mode 1 is subsequently consumed by ATPu, in modes 5 and 6 ATP_c is invested in the cytosolic PPP. Comparably, ATP_c generated by non-oxidative glycolysis in modes 7 and 8 are used by the cytosolic PPP (cf. mode 2); while ATP_c for the cytosolic PPP in modes 9–12 are generated by glycerol oxidation (cf. mode 3). In modes 5, 7, 9 and 11, NADPH generated by the cytosolic PPP is consumbed by the generic NADPH utilising reaction, while in modes 6, 8, 10 and 12, the NADPH is consumed by the specific TOX reaction. Model 2 has seven conserved moieties, of which moieties 1–5 are identical to the original model of glycolysis (Table 1.1).

In model 2, Glc-6-P is produced by HXK, an enzyme that was initially assumed to be strictly localised to the glycosomes of *T. brucei*, based on fractionation experiments (Visser and Opperdoes, 1980). An absence of cytosolic HXK would pose a problem for the provision of Glc-6-P to the cytosolic G6PDH. However, enzymes targeted to the glycosome are already fully folded in the cytosol (Walton *et al.*, 1995), indicating that glycosomal enzymes are likely to have a residual activity in the cytosol. The majority of the activity of the glycolytic enzymes is localised in the glycosome, preventing the turbo-explosion that is observed when all of the glycosomal enzymes are localised in the cytosol (Figure 1.4 and Bakker *et al.*, 2000; Haanstra *et al.*, 2008), but more detailed analysis of a partial cytosolic localisation of glycolysis in *T. brucei* is currently ongoing (Dr Fiona Achcar, University of Glasgow). Additionally, *T. brucei* HXK has a strong

tendency to stick to membranes (Guerra-Giraldez *et al.*, 2002), indicating that the strict glycosomal localisation found in fractionation experiments are likely an artifact.

Mode	Overall reaction	Individual reactions
1	$Glc_e + O_2 + 2\ Pi_g \rightarrow 2\ Pyr_e + 2\ Pi_c$	$GlcT_c$, $GlcT_g$, HXK_g, PGI_g, PFK_g, ALD_g, TPI_g, 2 $GAPDH_g$, 2 PGK_g, 2 $PGAT_g$, 2 $PGAM_c$, 2 ENO_c, 2 PYK_c, 2 $PyrT_c$, 2 $G3PDH_g$, 2 GDA_g, 2 GPO_c, 2 $ATPu_c$
2	$Glc_e + Pi_g \rightarrow Pyr_e + Gly_e + Pi_c$	$GlcT_c$, $GlcT_g$, HXK_g, PGI_g, PFK_g, ALD_g, $GAPDH_g$, PGK_g, $PGAT_g$, $PGAM_c$, ENO_c, PYK_c, $PyrT_c$, $G3PDH_g$, GK_g, $ATPu_c$
3	$Gly_e + O_2 + Pi_g \rightarrow Pyr_e + Pi_c$	TPI_g, $GAPDH_g$, PGK_g, $PGAT_g$, $PGAM_c$, ENO_c, PYK_c, $PyrT_c$, $G3PDH_g$, 2 GDA_g, 2 GPO_g, $-GK_g$, $ATPu_c$
4	$2\ Gly_e + O_2 \rightarrow Glc_e$	$-2\ GK_g$, $-2\ GDA_g$, $-2\ GPO_c$, TPI_g, $-ALD_g$, $-PFK_g$, $-PGI_g$, $-HXK_g$, $-GlcT_g$, $-GlcT_c$
5	$3\ Glc_e + 2\ Pi_g + O_2 \rightarrow 2\ Pyr_e + 2\ Rib5P_c + CO_2$	$GlcT_c$, $GlcT_g$, HXK_g, PGI_g, PFK_g, ALD_g, TPI_g, 2 $GAPDH_g$, 2 PGK_g, 2 $PGAT_g$, 2 $PGAM_c$, 2 ENO_c, 2 PYK_c, 2 $PyrT_c$, 2 $G3PDH_g$, 2 GDA_g, 2 GPO_c, 2 HXK_c, 2 $G6PDH_c$, 2 PGL_c, 2 $6PGDH_c$, 2 PPI_c, 4 $NADPHu_c$
6	$3\ Glc_e + 2\ Pi_g + O_2 \rightarrow 2\ Pyr_e + 2\ Rib5P_c + CO_2$	$GlcT_c$, $GlcT_g$, HXK_g, PGI_g, PFK_g, ALD_g, TPI_g, 2 $GAPDH_g$, 2 PGK_g, 2 $PGAT_g$, 2 $PGAM_c$, 2 ENO_c, 2 PYK_c, 2 $PyrT_c$, 2 $G3PDH_g$, 2 GDA_g, 2 GPO_c, 2 HXK_c, 2 $G6PDH_c$, 2 PGL_c, 2 $6PGDH_c$, 2 PPI_c, 4 TOX_c
7	$2\ Glc_e + Pi_g \rightarrow Pyr_e + Gly_e + Rib5P_c + CO_2$	$GlcT_c$, $GlcT_g$, HXK_g, PGI_g, PFK_g, ALD_g, $GAPDH_g$, PGK_g, $PGAT_g$, $PGAM_c$, ENO_c, PYK_c, $PyrT_c$, $G3PDH_g$, GK_g, HXK_c, $G6PDH_c$, PGL_c, $6PGDH_c$, PPI_c, 2 $NADPHu_c$
8	$2\ Glc_e + Pi_g \rightarrow Pyr_e + Gly_e + Rib5P_c + CO_2$	$GlcT_c$, $GlcT_g$, HXK_g, PGI_g, PFK_g, ALD_g, $GAPDH_g$, PGK_g, $PGAT_g$, $PGAM_c$, ENO_c, PYK_c, $PyrT_c$, $G3PDH_g$, GK_g, HXK_c, $G6PDH_c$, PGL_c, $6PGDH_c$, PPI_c, 2 TOX_c
9	$3\ Gly_e + Pi_g + 2\ O_2 \rightarrow Pyr_e + Rib5P_c + CO_2$	2 TPI_g, $GAPDH_g$, PGK_g, $PGAT_g$, $PGAM_c$, ENO_c, PYK_c, $PyrT_c$, $G3PDH_g$, 4 GDA_g, 4 GPO_g, $-3\ GK_g$, $-ALD_g$, $-PFK_g$, $-PGI_g$, $-HXK_g$, $-GlcT_g$, HXK_c, $G6PDH_c$, PGL_c, $6PGDH_c$, PPI_c, 2 $NADPHu_c$
10	$3\ Gly_e + Pi_g + 2\ O_2 \rightarrow Pyr_e + Rib5P_c + CO_2$	2 TPI_g, $GAPDH_g$, PGK_g, $PGAT_g$, $PGAM_c$, ENO_c, PYK_c, $PyrT_c$, $G3PDH_g$, 4 GDA_g, 4 GPO_g, $-3\ GK_g$, $-ALD_g$, $-PFK_g$, $-PGI_g$, $-HXK_g$, $-GlcT_g$, HXK_c, $G6PDH_c$, PGL_c, $6PGDH_c$, PPI_c, 2 TOX_c
11	$Gly_e + Glc_e + Pi_g + O_2 \rightarrow Pyr_e + Rib5P_c + CO_2$	TPI_g, $GAPDH_g$, PGK_g, $PGAT_g$, $PGAM_c$, ENO_c, PYK_c, $PyrT_c$, $G3PDH_g$, 2 GDA_g, 2 GPO_g, $-GK_g$, $GlcT_c$, HXK_c, $G6PDH_c$, PGL_c, $6PGDH_c$, PPI_c, 2 $NADPHu_c$
12	$Gly_e + Glc_e + Pi_g + O_2 \rightarrow Pyr_e + Rib5P_c + CO_2$	TPI_g, $GAPDH_g$, PGK_g, $PGAT_g$, $PGAM_c$, ENO_c, PYK_c, $PyrT_c$, $G3PDH_g$, 2 GDA_g, 2 GPO_g, $-GK_g$, $GlcT_c$, HXK_c, $G6PDH_c$, PGL_c, $6PGDH_c$, PPI_c, 2 TOX_c

Table 3.3.: Elementary mode analysis of model 2. Twelve elementary modes are listed as the overall reactions plus the individual enzyme-catalysed reactions with their relative flux weight. Mode 1–3 are identical to mode 1–3 in the original model of glycolysis (Table 1.2), mode 4 is gluconeogenesis from glycerol.

Moiety	Conserved metabolites
1	$ATP_g + ADP_g + AMP_g$
2	$ATP_c + ADP_c + AMP_c$
3	$NADH_g + NAD^+{}_g$
4	$Gly\text{-}3\text{-}P_c + DHAP_c$
5	$Glc\text{-}6\text{-}P_g + Fru\text{-}6\text{-}P_g + 2\ Fru\text{-}1,6\text{-}BP_g + DHAP_g + GA\text{-}3\text{-}P_g + 1,3\text{-}BPGA_g + Gly\text{-}3\text{-}P_g + 2\ ATP_g + ADP_g$
6	$NADPH_c + NADP^+{}_c$
7	$T(SH)_{2,c} + TS_{2,c}$

Table 3.4.: Conserved moieties in model 2. The stoichiometry of the model results in five groups of metabolites, whose combined concentration within the group remains constant.

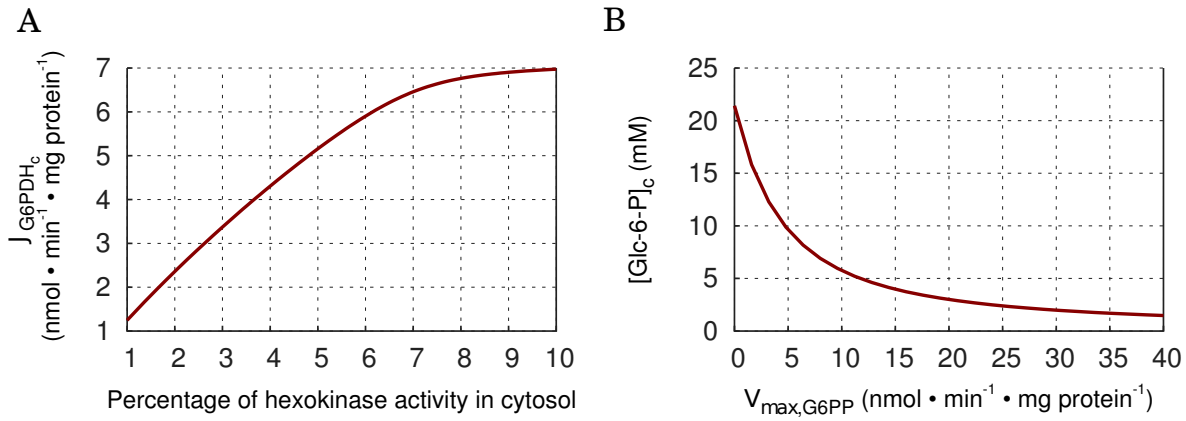

Figure 3.4.: Scans of parameter values related to the cytosolic PPP. *A:* The steady-state flux through cytosolic G6PDH (J_{G6PDH_C}) at variable cytosolic HXK activity. The percentage of cytosolic HXK activity was scanned from 1 to 10 % of the total HXK activity in the fixed parameter model 2. *B:* The steady-state concentration of cytosolic Glc-6-P at variable G6PPase activity. The activity of G6PPase ($V_{max,G6PP}$) was scanned from 0 to 40 nmol $\cdot$ min^{-1} $\cdot$ mg protein^{-1} in the fixed parameter model 3.

The distribution of glycosomal and cytosolic HXK activity was scanned in model 2, and affects the flux through the PPP as anticipated (Figure 3.4). For subsequent simulations, the cytosolic HXK activity was set at 10 % of the total HXK activity in fixed parameter models, or sampled from a uniform distribution between 1 and 10 percent in models were uncertainty was taking into account.

3.2.2.2. Prevention of cytosolic Glc-6-P accumulation

Simulations of model 2 resulted in a high risk of accumulation of Glc-6-P in the cytosol (25 % of the models have a cytosolic Glc-6-P concentration over 20 mM), while a steady state concentration of 2.9 mM has been reported (Hammond and Bowman, 1980b). I postulated that the cytosolic Glc-6-P does not accumulate because of its consumption by other pathways beside PPP. Glc-6-P can be used in GDP-mannose biosynthesis (Kuettel *et al.*, 2012), residual activity of cytosolic localised glycolysis and potentially dephosphorylated by glucose-6-phosphatase (G6PPase, Seed *et al.*, 1967; McLaughlin, 1986). Model 2 was extended with a Glc-6-P utilising reaction, generating model 3. The G6PPase activity was assayed in wild-type parasite cell extracts, and a value of 28 ± 6.7 nmol · min^{-1} · mg $protein^{-1}$ was measured. In simulations, the G6PPase activity was sampled from an uniform distribution between 1 and 40 nmol · min^{-1} · mg $protein^{-1}$, because of uncertainty about the cytosolic availability of the total measured G6PPase activity and other fluxes using Glc-6-P.

In previous versions of the glycolytic model (Albert *et al.*, 2005), HXK was modelled as an irreversible reaction with a very low affinity for Glc-6-P ($K_{m,Glc\text{-}6\text{-}P}$ = 12 mM). Both the irreversibility and the low affinity of Glc-6-P exacerbate the accumulation of Glc-6-P in the cytosol. It has been reported that Glc-6-P up to a concentration of 50 mM does not inhibit *T. brucei* HXK (Nwagwu and Opperdoes, 1982; Hara *et al.*, 1997; Morris *et al.*, 2006), however, all these experiments were assaying the phosphorylation of glucose by HXK. No data could be found in literature where the dephosphorylation of Glc-6-P by *T. brucei* HXK was assayed. In comparison, HXK from *T. cruzi* is said to be insensitive to Glc-6-P, even though a $K_{i,Glc\text{-}6\text{-}P}$-value of 1.45 mM was measured (Urbina and Crespo, 1984), and HXK from *L. mexicana* has a $K_{i,Glc\text{-}6\text{-}P}$ of 0.43 mM (Pabón *et al.*, 2007).

I therefore decided to measure the affinity constant of Glc-6-P by assaying the dephosphorylation of Glc-6-P. *T. brucei* cell extracts were used in the assay, and a $K_{m,Glc\text{-}6\text{-}P}$-value of 2.7 ± 1.3 mM was measured, significantly lower than previously assumed (>50 mM, Nwagwu and Opperdoes, 1982; Hara *et al.*, 1997; Morris *et al.*, 2006). The discrepancy with previous experiments could be explained by the use of cell extracts instead of purified recombinant enzyme and the use of an *in vivo*-like assay buffer. Additionally, *T. brucei* has two isoforms of HXK (HXK1 and HXK2) that form a complex *in vivo* (Joice *et al.*, 2012). The *in vivo* formation of heterohexamers of HXK1 and HXK2 might be responsible for the regulation of Glc-6-P sensitivity. Morris *et al.* (2006) used only recombinant HXK1 to test the inhibition of glucose phosphorylation by 50 mM of Glc-6-P, while the assembly of recombinant HXK heterohexamers has already demonstrated to affect the affinity of hexokinse to ATP (Chambers *et al.*, 2008).

Steady-state calculations of the further extended models 5 and 6 (see below) with the updated kinetics for HXK resulted in a cytosolic Glc-6-P concentration of 1.6–2.2 mM, more in concordance with the previously measured concentration of 2.9 mM (Hammond and Bowman, 1980b).

3.2.2.3. Oxidative stress regulates flux through PPP

Simulations of model 3 showed that oxidative stress regulates the flux through the cytosolic PPP (Figure 3.6A). Increasing the rate of the trypanothione oxidising reaction (TOX) enhanced the flux through the PPP to a maximum of 4.7 ± 1.8 % of the total glucose uptake (Figure 3.5). A similar increase in the PPP flux upon oxidative stress has been measured in *T. cruzi* (Maugeri and Cazzulo, 2004).

An increase in oxidative stress in model 3 decreases the ratio of reduced over oxidised trypanothione (Figure 3.6B), and methodologies are being developed in our laboratory to measure both this ratio and the absolute levels (Dr Dong-Hyun Kim, University of Glasgow). In comparison, the ratio of reduced over oxidised glutathione in proliferating *Plasmodium* cells is kept in the range of 10–100 (Müller, 2004). In the mathematical models, a k_{TOX}-value of 2 $\mu l \cdot min^{-1} \cdot mg\ protein^{-1}$ was chosen to represent a healthy proliferating trypanosome under low oxidative stress, corresponding to a ratio of reduced over oxidised trypanothione of 29 (Figure 3.6B). A low PPP flux in healthy proliferating trypanosomes is supported by the experimental observation that almost all glucose consumed is excreted as either pyruvate or glycerol (Grant and Fulton, 1957; Haanstra *et al.*, 2012).

The steady state flux through the cytosolic PPP is much lower than the maximum capacity of the PPP enzymes. Even the dehydrogenases, which have the lowest activity in the cytosolic PPP, use only 16–20 % of their full capacity at low oxidative stress (Figure 3.5). This overcapacity of PPP activity renders the parasite capable of a rapid response to sudden bursts of oxidative stress. Simulation of a sudden burst of oxidative stress revealed that the parasite can, theoretically, restore its redox balance in around a minute (Figure 3.6C and D). At low oxidative stress, the steady state concentrations and fluxes in glycolysis were comparable to those in the original model, suggesting that the small cytosolic PPP flux barely disturbed the system. High oxidative stress does not affect the total glucose flux, but reallocates flux from glycerol and pyruvate into the PPP (Figure 3.5).

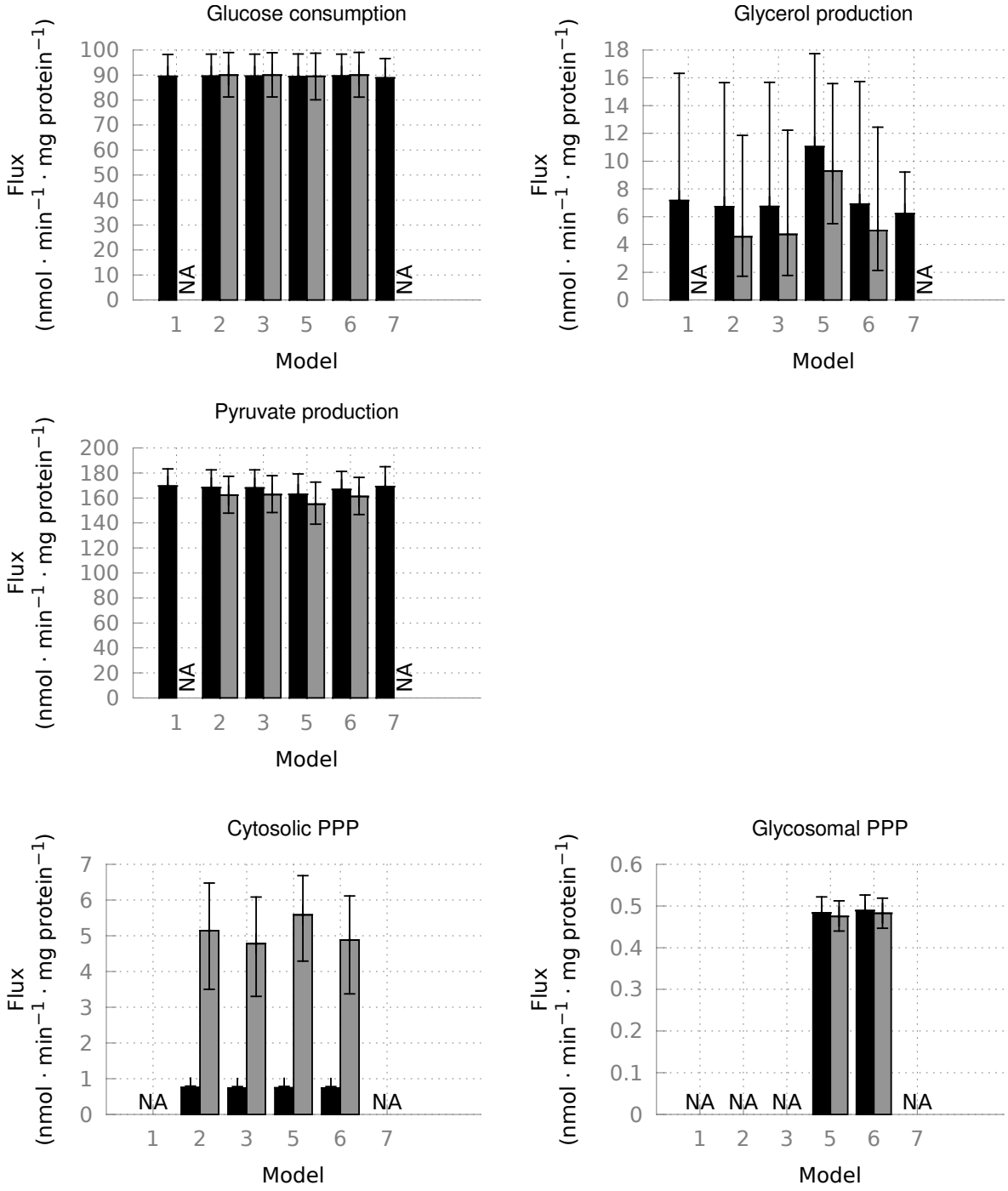

Figure 3.5.: Steady-state fluxes of the various model versions. Steady state fluxes of all model versions that reach a steady state, at standard conditions (black, k_{TOX} = 2 µl · min^{-1} · mg protein^{-1}) and if cytosolic PPP is maximised (grey, k_{TOX} = 200 µl · min^{-1} · mg protein^{-1}). Error bars indicate interquartile ranges. NA denotes 'Not Applicable' for branches that are absent from certain model version, $[Glc]_e$ is 5 mM in all models. The glucose consumption flux is distributed over the production of glycerol and pyruvate and the two branches of the PPP. Note that ALD generates two trioses from every hexose, such that the fluxes through the trioses glycerol and pyruvate are double the hexose flux. The errors bars indicated interquartile ranges as a result of the uncertainty modelling. The large error bars for glycerol production are a result of its low flux and the smaller uncertainties assigned to the fluxes through the other pathways.

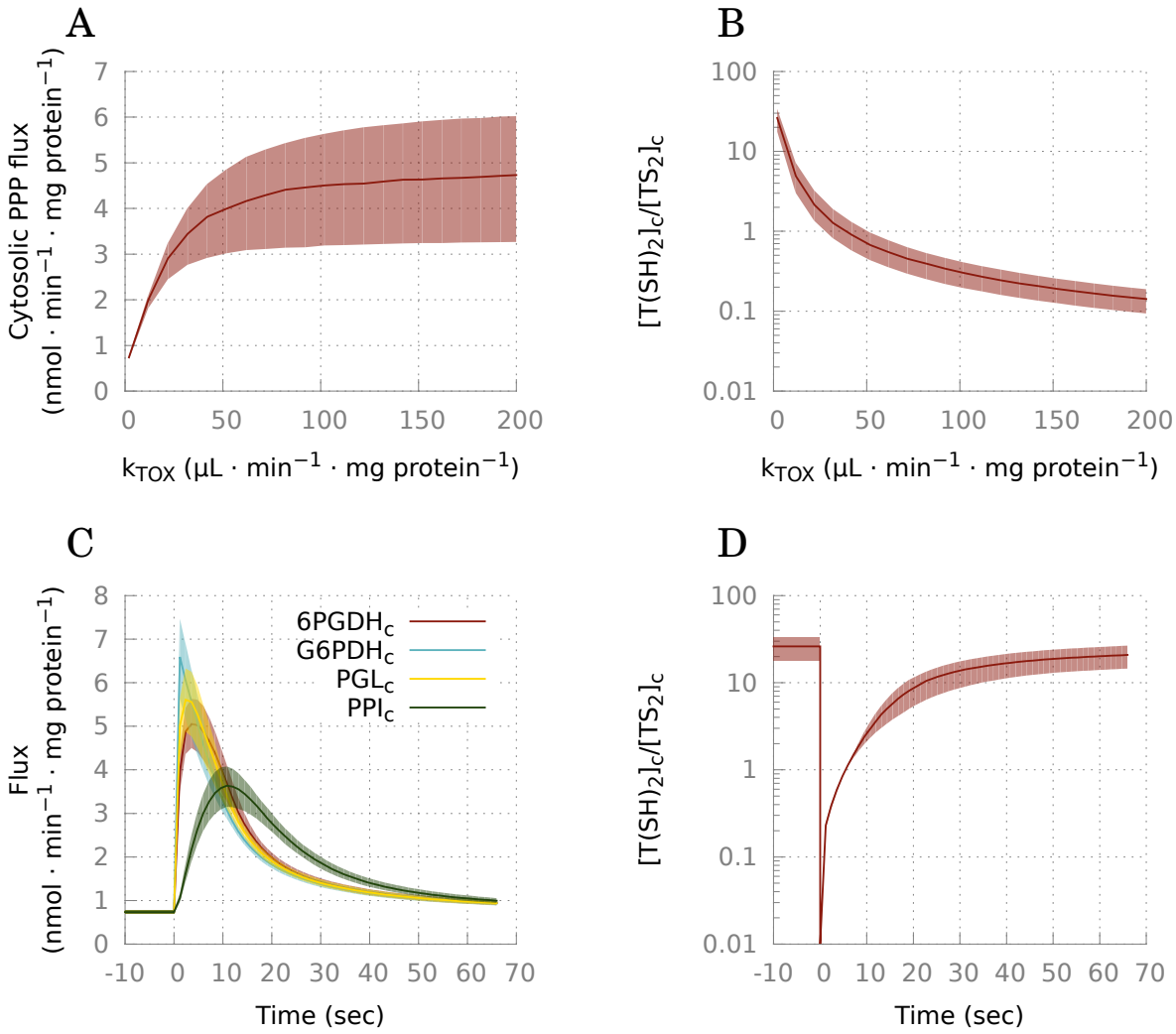

Figure 3.6.: Simulations of oxidative stress. Steady state calculations and time-course simulations of model 3, at Glc_e = 5 mM and k_{TOX} = 2 µl · min^{-1} · mg protein^{-1}, unless stated otherwise. Solid lines indicate medians, shaded areas show interquartile ranges. *A:* The steady state flux through the cytosolic PPP as a function of the oxidative stress by varying the kinetic constant k_{TOX}. *B:* The ratio of reduced trypanothione over oxidised trypanothione as a function of oxidative stress. *C:* Fluxes through the cytosolic PPP enzymes as a function of time upon sudden oxidative stress. During the whole time-course, k_{TOX} = 2 µl · min^{-1} · mg protein^{-1}. The system is removed from steady state at t = 0, by setting 99 % of the cytosolic NADPH and trypanothione pools to the oxidised form. Shown is the relaxation of the cytosolic PPP fluxes. *D:* From the same simulation as panel C, the ratio of reduced trypanothione over oxidised trypanothione is shown.

Experimental confirmation of the simulation of a sudden burst of oxidative stress would be extremely challenging. Nonetheless, the capability of trypanosomes to deal with continuous stress has been investigated experimentally. Penketh and Klein (1986) demonstrated that *T. brucei* can metabolise 20 µM H_2O_2 in a uniform manner for at least one hour. H_2O_2 is metabolised at 5 nmol · min^{-1} · mg protein^{-1} (assuming that one

trypanosome represents $1.01 \cdot 10^{-11}$ g protein; Opperdoes *et al.*, 1984) and requires one NADPH + H^+ per H_2O_2. The PPP produces two NADPH + H^+ per glucose consumed, translating the 5 nmol $\cdot$ min^{-1} $\cdot$ mg $protein^{-1}$ H_2O_2 metabolism to a PPP flux of 2.5 nmol $\cdot$ min^{-1} $\cdot$ mg $protein^{-1}$. At this PPP flux, the ratio of reduced over oxidised trypanothione is 19 (Figure 3.6B), that falls within the expected range of 10–100.

3.2.3. Further extension with the glycosomal PPP

The second round of model building consisted in extending model 3 further with the glycosomal branch of the PPP (model 4). The structure of the glycosomal PPP is identical to the cytosolic PPP, with Rib-5-P as the end-product of the PPP. Similar to in the cytosolic PPP (Section 3.2.2.1), Rib-5-P in the glycosome is fixed to represent utilisation in the glycosome (as interestingly, enzymes of nucleotide biosynthesis can be found in the glycosome (Colasante *et al.*, 2006; Opperdoes and Szikora, 2006; Vertommen *et al.*, 2008)) or transport of Rib-5-P over the glycosomal membrane and subsequent utilisation in the cytosol.

Elementary mode analysis immediately indicated an obvious problem. Model 4 has the same elementary modes as model 3 (Table 3.3). No additional modes through the glycosomal PPP are present. This is in contrast with the assumption that the PPP is a functional pathway in the glycosome. Analysis of the stoichiometry of the model also showed that model 3 had lost the conserved moiety of bound phosphates in the glycosome (Table 3.4, moiety 5). A dynamic time-course simulation indicates the serious implications of this so-called phosphate "leak" (Figure 3.7). In model 4, the conversion of glucose to Rib-5-P drains phosphates from this previously conserved moiety of bound phosphates (Figure 3.7), with lethal consequences. The depletion of bound phosphates renders the model incapable of supporting a flux through glycolysis, as bound phosphates first need to be invested in the early steps of glycolysis before they can be balanced by the later steps of glycolysis.

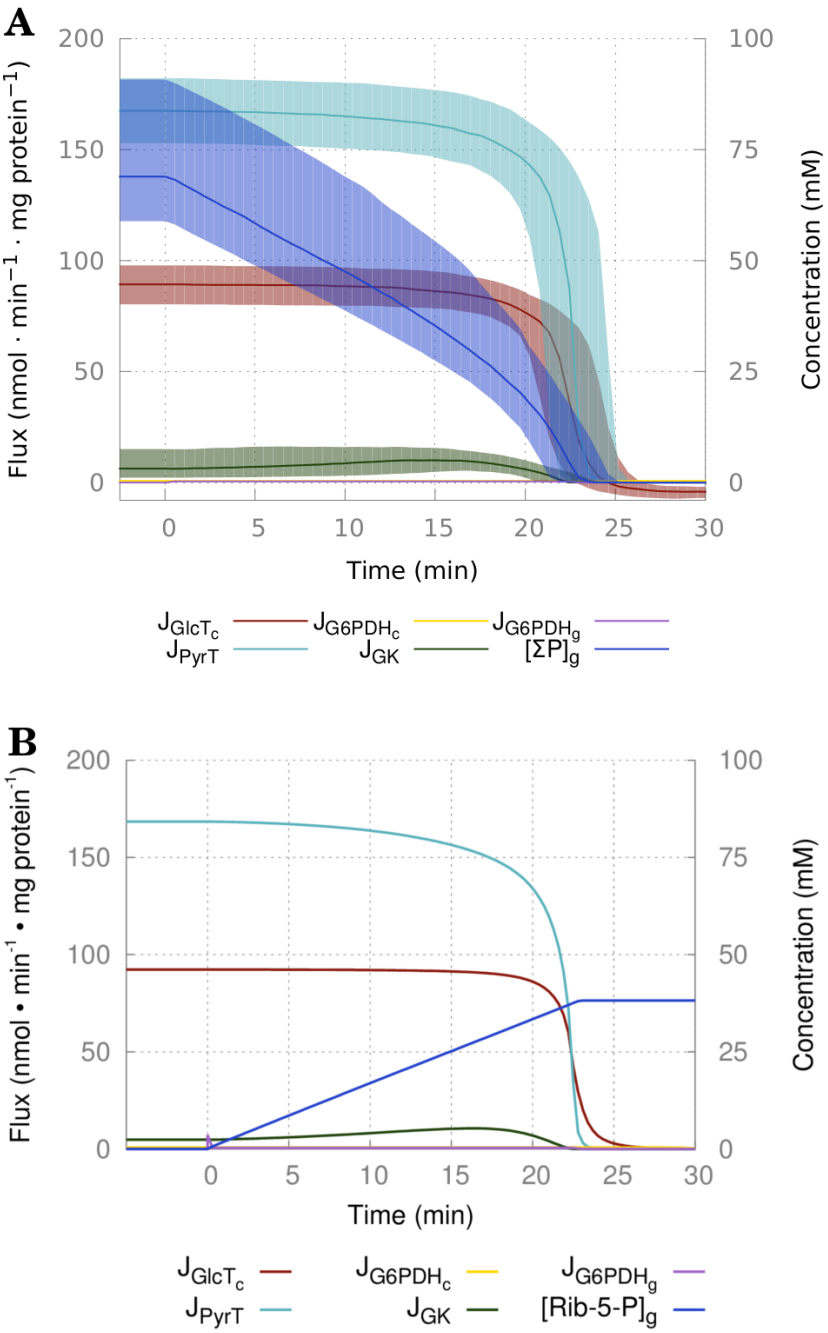

Figure 3.7.: A 'phosphate leak' introduced by the glycosomal PPP. Time course simulation of model 4, in which the reactions of the glycosomal PPP are switched on at $t = 0$ by increasing their V_{max} value from zero to the value given in Table 3.2. Glc_e is 5 mM and $k_{TOX} = 2\ \mu l \cdot min^{-1} \cdot mg\ protein^{-1}$. *A:* Solid lines indicate medians, shaded areas show interquartile ranges. Concentrations and fluxes at $t = 0$ correspond to the steady state values of model 3. Fluxes (J) are plotted on the left y-axis and are indicative of glucose uptake ($GlcT_c$), glycerol (GK) and pyruvate production (PyrT) and the two branches of PPPs ($G6PDH_{c/g}$). The sum of bound phosphates in the glycosome (ΣP_g), as exists in the model of glycolysis (Table 1.1, moiety 5), is plotted on the right y-axis. Within 25 minutes, all bound phosphates within the glycosome are depleted and all metabolic fluxes subsequently drop to zero. *B:* The same time-course simulation is shown in model 4, where glycosomal Rib-5-P is not a fixed metabolite. Accumulation of Rib-5-P drains phosphates from the conserved moiety of bound phosphates in the glycosome, resulting to identical loss of glycolytic flux, identical to in panel A.

The phosphate leak is not a problem introduced by the decision to fix the concentration of Rib-5-P. When the concentration of Rib-5-P is allowed to change in model 4, still no elementary modes are supported through glycosomal PPP. Time-course simulation of a model with a non-fixed Rib-5-P demonstrates a similar ablation of all fluxes (Figure 3.7). Additional allowing Rib-5-P to transport over the glycosomal membrane does not give different results, as such a transporter has the same effect as a fixed Rib-5-P concentration: the dissipation of bound phosphates from the glycosome.

Several possibilities to restore the balance of phosphorylated metabolites were considered, some of which were discarded immediately. For instance, extension of the PPP with its non-oxidative branch would return phosphorylated metabolites to glycolysis at the level of Fru-6-P and GA-3-P. The aforementioned absence of PPE and TKT in the bloodstream form, however, precludes this option. Comprehensible glycosomal proteomics data (Colasante *et al.*, 2006; Vertommen *et al.*, 2008) and searches of the genome for genes with a PTS sequence (Opperdoes and Szikora, 2006) have indicated the presence of even more enzymes in the glycosome in addition to the glycolytic and PPP enzymes discussed here. However, inclusion of most of these additional reactions in a mathematical model would require many more hypothetical reactions to be added.

Another model that deals with compartmentalisation of phosphates is the model of the Calvin-Benson cycle in plants (Petterson and Ryde-Petterson, 1988). In this model, inorganic phosphate is translocated across the mitochondrial membrane in exchange for triose-phosphates. Similar translocators, either exchanging phosphates for triose-phosphates or ribose-phosphates, can not prevent the glycosomal phosphate leak observed in model 4. As described in Section 1.3, inorganic phosphate is not part of the conserved moiety of bound phosphates in the glycosome, and therefore transport reactions involving inorganic phosphate do not influence the conserved moiety.

Two options could be less readily excluded on the basis of current knowledge and were analysed in more detail. The first option consists of an ATP:ADP antiporter operative across the glycosomal membrane (model 5). If involved in ATP import into the glycosome, its result would be a return of bound phosphates to the glycosome. Although the presence of a glycosomal ATP:ADP antiporter has not been demonstrated in trypanosomes, the general feasibility of such a transporter is indicated by the existence of a peroxisomal adenine nucleotide transporter in yeast (van Roermund *et al.*, 2001).

A second option is further conversion of Rib-5-P to ribose with the concomitant phosphorylation of ADP by RK (model 6), rendering not Rib-5-P but ribose as the end-product of the glycosomal PPP. The *T. brucei* genome contains a gene putatively annotated as coding for RK (Tb11.03.0900), which is investigated in detail in Chapter 4.

The two options presented here are of a different nature. The RK option maintains the conserved moiety of phosphorylated metabolites in an extended version, while the ATP:ADP antiporter breaks the conserved moiety altogether and introduces extra degrees of freedom. Both options can be seen as representatives of two classes of solutions, where one maintains the phosphate balance (RK class solutions), while the other provides net import of bound phosphates into the glycosome (antiporter class solutions). To investigate the various options further I constructed alternative kinetic models.

3.2.3.1. Glycosomal ATP:ADP antiporter requires tight regulation

First, a dynamic model was constructed to test the hypothesis that an ATP:ADP antiporter in the glycosomal membrane could sustain the intraglycosomal balance of phosphorylated metabolites (model 5). Indeed, the ATP:ADP antiporter successfully rescued the model from the phosphate leak, enabling a steady flux through all branches and no accumulation or depletion of any metabolites (Figure 3.5).

However, a strict separation of the glycosomal and cytosolic ATP and ADP pools is essential to prevent a deadly accumulation of sugar-phosphates, or "turbo explosion" (discussed in more detail in Section 1.3). Briefly, it was demonstrated that a model of *T. brucei* glycolysis without glycosomal localisation exhibits the dangerous turbo effect (Bakker *et al.*, 2000; Haanstra *et al.*, 2008), shown in Figure 3.8A and B as "model 1, no glycosome". To investigate if the ATP:ADP antiporter also risks the turbo effect, a model consisting of only glycosomal glycolysis and the ATP:ADP antiporter was generated (model 7), to allow comparison with (Haanstra *et al.*, 2008).

Simulations indicated that the presence of an ATP:ADP antiporter indeed mimics the absence of a glycosomal localisation of glycolysis: increasing the glucose concentration results in an accumulation of Fru-1,6-BP (Figure 3.8A and B, cf. model 1 without glycosome and model 7). The ATP:ADP antiporter allows bound phosphates to accumulate in the glycosome, as there is no longer a conserved sum of bound phosphates within the glycosome. This allows accumulation of Fru-1,6-BP without depleting the ATP that is required to fuel HXK and PFK.

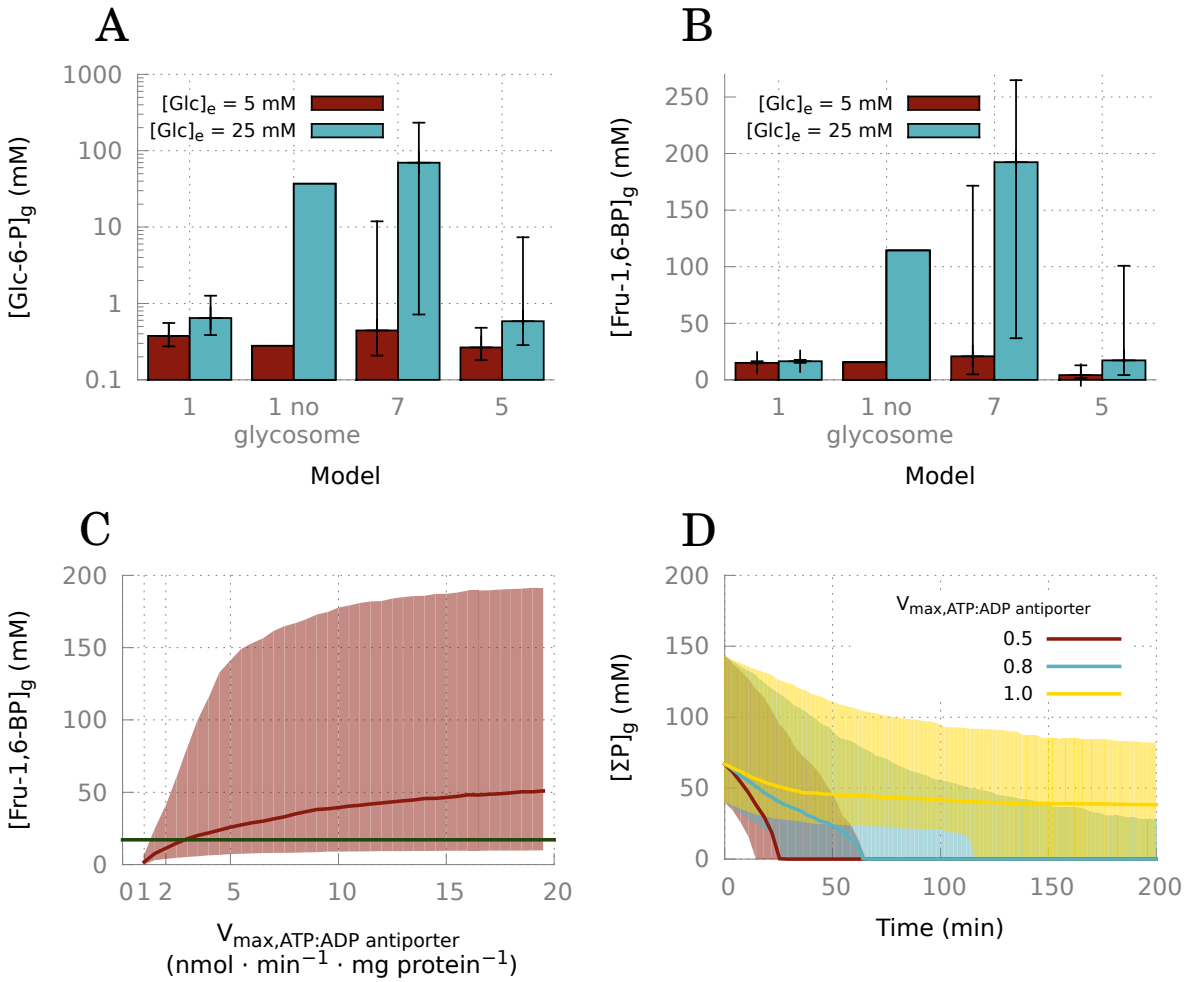

Figure 3.8.: ATP:ADP antiporter mimics turbo-state. *A-B:* Concentrations of glycosomal Glc-6-P and fructose 1,6-bisphosphate are depicted (i) in model 1, (ii) in a modified version of model 1, in which the glycosomal compartmentalisation of glycolysis has been removed (Haanstra *et al.*, 2008), (iii) in the presence of an ATP:ADP antiporter, without any further extensions (model 7), and (iv) when both branches of the PPP and the ATP:ADP antiporter are active (model 5). *C:* Increasing the activity of the ATP:ADP antiporter ($V_{max,ATP:ADP\ antiporter}$) in model 5 leads to a high risk of accumulation of hexose phosphates. The green line indicates the concentration of fructose 1,6-bisphosphate in the original model of glycolysis (17.2 mM, panel B, model 1). Glc_e in this simulation is 25 mM. *D:* Time course simulation of model 5 at 25 mM external glucose and various values for the $V_{max,ATP:ADP\ antiporter}$ parameter. Plotted is the concentration of glycosomal phosphates (ΣP as in Figure 3.7, moiety 5 in Table 1.1). ATP:ADP antiporter activity values below 1 nmol · min^{-1} · mg $protein^{-1}$ result in depletion of glycosomal phosphates (cf. Figure 3.7). k_{TOX} = 2 µl · min^{-1} · mg $protein^{-1}$ in all models. Solid lines indicate medians, shaded areas and error bars show interquartile ranges, as derived from the uncertainty modelling.

When the cytosolic and glycosomal branches of the PPP are added to this model (Figure 3.8A and B, model 5), the accumulation of sugar-phosphates seems to be reduced. This is due to the increased utilisation of Glc-6-P in the glycosome via the PPP, which prevents the accumulation of glycolytic intermediates. However, this situation is dependent on the activity of the ATP:ADP antiporter, for which there is no experimental

data available. When the activity of the antiporter is set at a low value (around 1 nmol $\cdot$ min^{-1} $\cdot$ mg protein^{-1}), no accumulation of sugar-phosphates is observed (Figure 3.8C). However, when the activity of the antiporter increases slightly, there is a high risk of accumulation of sugar-phosphates (Figure 3.8C). On the other hand, a reduced antiporter activity is unable to prevent the depletion of bound phosphates from the glycosome (Figure 3.8D). The activity of the transporter would therefore only be allowed to fluctuate in a narrow range (Figure 3.8C and D).

3.2.3.2. Glycosomal RK in reverse

A second hypothesis to restore the balance of phosphorylated metabolites postulates the presence of a RK enzyme in the glycosome (model 6). The *T. brucei* genome contains a gene putatively annotated as coding for RK, which has previously been localised to glycosomes (Colasante *et al.*, 2006; Opperdoes and Szikora, 2006; Vertommen *et al.*, 2008). I hypothesised that RK in the glycosomes catalyses the transfer of phosphates from Rib-5-P to ADP, forming ATP and ribose. The thermodynamically favoured direction of the RK reaction under standard conditions is the phosphorylation of ribose (Tewari *et al.*, 1988). However, I reasoned that the supply of Rib-5-P through the glycosomal PPP might direct the reaction towards ATP production. Defining the RK in the direction of ribose production, the equilibrium constant is 0.0035 (Table 4.2) and is defined as:

$$K_{eq} = \frac{[Rib]^{\circ} \cdot [ATP]^{\circ}}{[Rib5P]^{\circ} \cdot [ADP]^{\circ}}, \tag{3.1}$$

where $^{\circ}$ indicates the state at thermodynamic equilibrium. When a reaction is studied in isolation, the direction of the direction is determined by:

$$\Delta G = \Delta G^{\circ} - RT \cdot \ln \frac{[Rib] \cdot [ATP]}{[Rib5P] \cdot [ADP]}, \tag{3.2}$$

where ΔG is the Gibbs free energy, R is the gas constant and T is temperature in Kelvin. When ΔG is larger than 0, the reaction will go produced ribose, while a ΔG smaller than 0 will result in production of ribose 5-phosphate. To produce ribose: Eq. (3.2) can be expanded to:

$$0 > RT \cdot \ln K_{eq} - RT \cdot \ln \frac{[Rib] \cdot [ATP]}{[Rib5P] \cdot [ADP]} \tag{3.3}$$

$$0 > K_{eq} - \frac{[Rib] \cdot [ATP]}{[Rib5P] \cdot [ADP]} \tag{3.4}$$

$$K_{eq} > \frac{[Rib] \cdot [ATP]}{[Rib5P] \cdot [ADP]} \tag{3.5}$$

$$[Rib5P] > \frac{[Rib] \cdot [ATP]}{K_{eq} \cdot [ADP]} \tag{3.6}$$

In isolation, the Rib-5-P concentration has to be higher than the product of ribose and ATP over the product of K_{eq} and ADP. Assuming an ATP over ADP ratio of 2 (Bakker *et al.*, 2000) and an K_{eq} of 0.0035:

$$[Rib5P] \gtrsim 571 \cdot [Rib] \tag{3.7}$$

Assuming a ribose concentration of 0.1 mM, the concentration of Rib-5-P needs to be greater than 57.1 mM to produce more ribose. However, a steady-state calculation of model 6 demonstrates that the ratio of ATP over ADP has decreased to 0.6, such that the Rib-5-P concentration has to be 181-fold higher than the ribose concentration.

A similar situation is seen for the glycosomal glycerol kinase, which thermodynamically favours the direction of glycerol 3-phosphate production under standard conditions (Janson and Cleland, 1974), but has been shown to support a flux in the reverse direction, purely based on mass action of its substrates and products when glycerol 3-phosphate levels accumulate under anaerobiosis (Krakow and Wang, 1990).

The K_{eq} of glycerol kinase (in the direction of glycerol production) is even smaller than the K_{eq} of ribose: 0.000837. In a similar calculation as for RK (Eq. (3.1)–Eq. (3.6)):

$$[Gly3P] \gtrsim 2389 \cdot [Gly]\,, \tag{3.8}$$

the Gly-3-P needs to be 2389 times as high as the glycerol concentration to allow the production of glycerol. Again, simulation of the model demonstrates that the ATP over ADP ratio has changed. The steady-state ratio of ATP over ADP in model 1 with the GPO reaction switched off (V_{max} set to zero, to simulate anaerobiosis) is 0.07, such that the Gly-3-P concentration only needs to be 410-fold higher than the glycerol concentration.

3.2.3.3. Conserved moieties in model 6

The stoichiometry of model 6 was analysed to confirm that the presence of glycosomal RK indeed results in an extension of the conserved moiety of bound phosphates in the glycosome, as discussed in 3.2.3. In addition to the conserved moieties observed in the original model (Table 1.1) and model 2 (Table 3.4), two new conserved moieties are present in model 6 (Table 3.5). Moiety 5 is extended to also include the pentose phosphates, while moiety 8 consists of the glycosomal NADPH and $NADP^+$.

Moiety	Conserved metabolites
1	ATP_g + ADP_g + AMP_g
2	ATP_c + ADP_c + AMP_c
3	$NADH_g$ + $NAD^+{}_g$
4	Gly-3-P_c + $DHAP_c$
5	Glc-6-P_g + Fru-6-P_g + 2 Fru-1,6-BP_g + $DHAP_g$ + GA-3-P_g + 1,3-$BPGA_g$ + Gly-3-P_g + 2 ATP_g + ADP_g + 6-PG_g + 6-PGL_g + Rul-5-P_g + Rib-5-P_g
6	$NADPH_c$ + $NADP^+{}_c$
7	$T(SH)_{2,c}$ + $TS_{2,c}$
8	$NADPH_g$ + $NADP^+{}_g$

Table 3.5.: Conserved moieties in model 6. The stoichiometry of the model results in five groups of metabolites, whose combined concentration within the group remains constant.

3.2.3.4. Glycosomal RK is potentially essential

To confirm the presence of a functional RK enzyme, the gene was cloned and successfully expressed in *E. coli*, as described in Chapter 4. Characterisation of the catalytic activity yielded kinetic parameters which were used to update the model. Attempts to measure RK activity in whole cell extracts were unsuccessful due to high background activity in the form of non-specific NADH changes, similar as experienced by Olin-Sandoval *et al.* (2012). Therefore, the activity of RK was scanned in model 6 (Figure 3.9), and in the fixed parameter model the V_{max} value was set at a value that results in limited control over the fluxes and metabolite concentrations (5 nmol $\cdot$ min^{-1} $\cdot$ mg $protein^{-1}$). In uncertainty modelling, the RK activity was sampled form a log normal distribution with a mean of 10 nmol $\cdot$ min^{-1} $\cdot$ mg $protein^{-1}$.

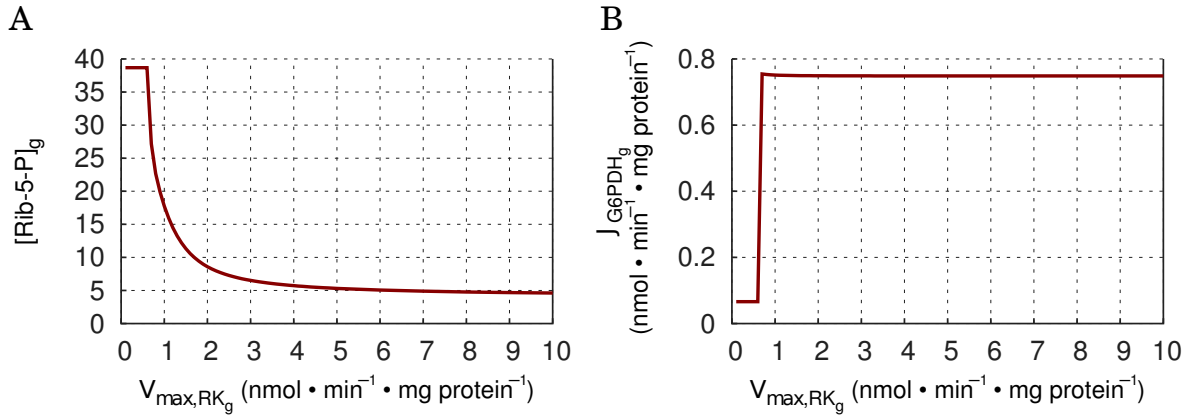

Figure 3.9.: Scan of RK activity. Steady state concentration of glycosomal Rib-5-P (*A*) and steady state flux of glucose-6-phosphate dehydrogenase (*B*) in model 6 at various RK activities ($V_{max,RKg}$).

Simulations show that the RK hypothesis indeed rescues the parasite from the phosphate leak. Since the model without RK failed to reach steady state, I postulated that RK is an essential gene for *T. brucei*. RK was ablated from *T. brucei* by gene knockdown and attempted gene knockout, as discussed in Chapter 4. The combined results of reverse genetics on RK as described in Chapter 4 suggested that the RK gene is essential to *T. brucei*, but only a small amount of RK is required for survival.

The discrepancy between *in vivo* and *in silico* data is potentially the result of the presence of additional reactions within the glycosome. Inhibition of RK and depletion of RK are only lethal to the parasite if RK would be the only reaction in the glycosome that can be involved in recovering the bound phosphates that are 'leaked' via the glycosomal PPP. Instead of a unique solution to the phosphate leak, the RK solution rather represents a class of solutions, that all regulate the glycosomal bound-phosphate balance in a similar approach. Proteomics has shown the presence of more enzymes in the glycosome (Colasante *et al.*, 2006; Vertommen *et al.*, 2008). However, the aforementioned gaps in our current knowledge of the glycosomal proteome precludes detailed *in silico* analysis of all these reactions. Elementary mode analysis on the glycosomal proteome data from Colasante *et al.*, 2006; Vertommen *et al.*, 2008 indicates that many additional reactions and potential transporters would need to be added, for which there is no experimental proof (Chapter B).

Nonetheless, the model with ribokinase is a valuable example of solutions to the phosphate leak that are based on restoring the phosphate balance, and it is useful to use this model to study the effects of this class of solutions.

3.2.3.5. Increased ribose levels are lethal *in silico*, but not *in vivo*

Additional analysis of model 6 suggests that *T. brucei* should be sensitive to increasing concentrations of external ribose. This becomes clear from the Eq. (3.7), where the concentration of Rib-5-P should be 571-fold higher than the concentration of ribose. This ratio is decreased, when the ATP/ADP ratio is reduced (as explained in 3.2.3.2), but still more Rib-5-P than ribose should be present. An dynamic simulation demonstrates than an accumulation of intracellular ribose would inhibit the dephosphorylation of Rib-5-P, having detrimental effects on the glycolytic flux (Figure 3.10). The model predicts that ribose needs to accumulate to a concentration of 9 mM to reduce the glycolytic flux by 50 %, which has been shown to be sufficient to kill the parasites (Haanstra *et al.*, 2011). There is no experimental data available on the intracellular or intraglycosomal ribose concentration.

The ribose sensitivity of the parasites was investigated by alamarBlue assay, but ribose concentrations up to 50 mM had little effect on the parasite (Figure 3.11). Analysis of the alamarBlue data suggests an IC_{50} value of 17 mM, however, it becomes apparent from the data that other phenomena are also playing a role at these concentrations. Incubation with the not natural-occuring sugar lyxose showed a similar response as ribose, while lyxose is not a substrate for RK (see section 4.1.2). This suggests that the isotonicity of the high sugar concentrations affects the parasites. Additionally, the ribose concentration in the alamarBlue is the extracellular concentration, it remains unclear what intracellular, and more important, intraglycosomal concentration of ribose is reached.

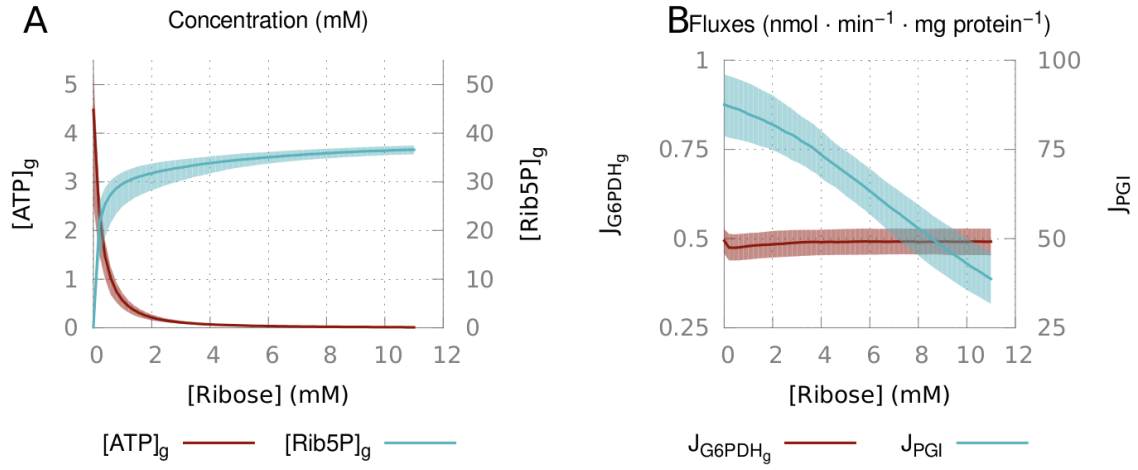

Figure 3.10.: Ribose sensitivity in the extended model. Steady state concentrations (*A*) and fluxes (*B*) of model 6 at various concentrations of ribose. Solid lines indicate medians, shaded areas show interquartile ranges. Increasing ribose concentration results in a depletion of ATP and accumulation of Rib-5-P in the glycosome. While the glycosomal PPP flux (J_{G6PDH_g}) remains mostly unaffected, the glycolytic flux (J_{PGI}) is strongly reduced.

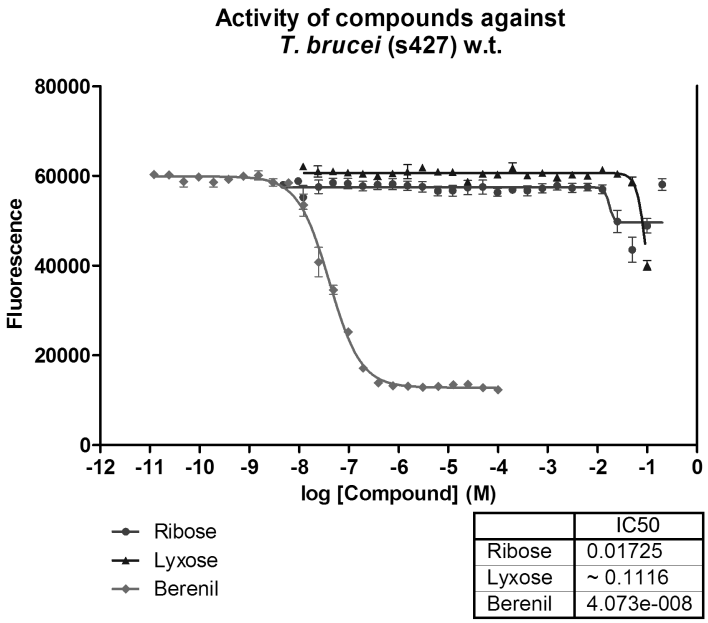

Figure 3.11.: Sensitivity to extracellular ribose. An alamarBlue assay with berenil as positive control failed to demonstrate toxicity. The reduced fluorescence at high concentration of ribose is non-specific and is also observed with other sugars, as the rarely naturally occurring lyxose.

3.3. Discussion

In this Chapter, I successfully extended the previous model of trypanosomal glycolysis with the PPP. The original model containing 21 reactions was expanded by adding 11 new reactions, of which 6 are localised in two compartments, roughly doubling the number of kinetic and concentration parameters, from 120 to 200 in total. The stepwise extension and cycles between *in silico* and *in vivo* experiments has been crucial in this model building process. Extension of the successful, albeit small, model of trypanosomal glycolysis resulted very easily in models incapable of reaching steady state, extreme accumulation of metabolites, or other non-physiological results.

I demonstrated (i) how the overcapacity of the cytosolic PPP allows it to respond rapidly to an oxidative stress and (ii) how two classes of solutions are theoretically capable of repairing the phosphate leak that is introduced by the presence of the glycosomal phosphate leak. The first class is the net import of bound phosphates into the glycosome, demonstrated here as an ATP:ADP antiporter. Such an antiporter requires tight regulation within a narrow range that should be tuned to the PPP flux, which indicates possible allosteric regulation by NADPH. The second class of solutions was the extension of the conserved moiety of bound phosphates in the glycosome, demonstrated here with a glycosome RK. When RK would be the sole responsible reaction for balancing the bound phosphates glycosome, it would be an essential enzyme. However, genetic mutants generated in Chapter 4 will demonstrate that ablation of RK activity is not lethal, supporting that RK merely represents an example of a solution where the bound phosphates are balanced within the glycosome.

Ribose sensitivity as predicted by the extended model was not observed in wet-lab experiments. The insensitivity of RK to ribose is in contrast to the sensitivity of glycerol kinase to glycerol. In anoxic environments, glycerol kinase also functions far away from its thermodynamic equilibrium (Hammond and Bowman, 1980a), however, glycerol kinase is sensitive for its product (glycerol) at low concentrations (0.8 mM inhibits 50 % of the glycolytic flux, Fairlamb *et al.*, 1977).

I cannot exclude that this is due to a limited uptake of ribose into the glycosome, although active uphill secretion from the glycosome or out of the cell seems unlikely. While the addition of the dual-localised PPP to the original model of glycolysis is a significant extension, the glycosome contains still more pathways that will add to the complexity and indicate the necessity of further model extensions (Parsons, 2004; Colasante *et al.*, 2006; Michels *et al.*, 2006; Vertommen *et al.*, 2008). Taking these pathways and enzymes fully into account might be important to fully understand the glycosomal phosphate balance.

Although the predicted glycosomal proteome gives insight into some of the enzymes potentially present in the glycosome, it does currently not provide enough information on stoichiometry and kinetics to allow incorporating them into the model.

The recent finding of channels across the glycosomal membrane (Gualdrón-López *et al.*, 2012a,c) could have major implications for the hypotheses explored in this chapter. Transport of sugar-phosphates across the glycosomal membrane would affect the phosphate balance, although it remains to be confirmed what precise metabolites are capable and incapable of transversing the glycosomal membrane via these channels. The implications of the presence of such glycosomal channels are currently being investigated with the use of dynamic modelling (Dr Fiona Achcar, University of Glasgow).

Including the uncertainty of the model parameters in our simulations demonstrates that the observed dynamics of the model are reproducible and are not artifacts of certain narrowly chosen sets of parameter values. Additionally to uncertainty of model parameters, I also demonstrated uncertainty of network stoichiometry. The ATP:ADP antiporter and RK are representatives of two classes of solutions to the phosphate leak, but neither model can be excluded based on current biological knowledge and simulations.

Potential problems in our models only became apparent once I deviated from the standard conditions: the increase of external glucose from 5 to 25 mM indicated how the ATP hypothesis would require very tight regulations, while the insensitivity of RK for external ribose indicates how additional pathways must be involved in balancing the glycosomal phosphates. Our results reveal that it is crucial for newly constructed models to be stressed and scrutinised thoroughly, by not only looking at the behaviour under standard conditions, but also by examining the model under physiologically relevant extreme conditions.

Chapter 4

The role of a putative *T. brucei* ribokinase

In the previous chapter it was predicted that RK might play a crucial role in retaining the balance of bound phosphates within the glycosome. In this chapter, *T. brucei* RK is studied in more detail, and predictions that arose from mathematical modelling in the previous chapter are tested.

4.1. Introduction

The construction of a mathematical model of the PPP in *T. brucei* has lead to the prediction that RK plays an essential role in retaining the balance of bound phosphates in the glycosome, as explained in chapter 3. Briefly, the sole addition of the glycosomal branch of the oxidative PPP to a model of *T. brucei* glycolysis resulted in a so-called phosphate leak. ATP committed in the early reactions of glycolysis is balanced within the glycosome by the production of ATP in the subsequent reactions of glycosomal glycolysis. An imbalance appears when ATP is used to produce glucose 6-phosphate that is used in the PPP, as the absence of the non-oxidative branch of the PPP in bloodstream form *T. brucei* results in Rib-5-P as the end-product of the PPP. This phosphate imbalance can potentially be solved by the presence a glycosomal RK, as detailed in chapter 3.

In classical biochemical textbooks, RK is introduced as an enzyme that catalyses the phosphorylation of ribose to provide Rib-5-P. Rib-5-P can be used in nucleotide biosynthesis, or when the non-oxidative branch of the PPP is present, as a carbon source (Anderson and Cooper, 1969). The Gibbs free energy of reaction favours the phosphorylation of ribose under standard conditions, as $\Delta G^{\circ} = -13.9$ kJ / mol at pH 7 and 25 °C, calculated from the Gibbs free energies of ATP (Banks and Vernon, 1970) and ribose hydrolysis (Tewari *et al.*, 1988). I postulated that the role of *T. brucei* glycosomal RK is to dephosporylate Rib-5-P, effectively catalysing the reverse reaction of a traditional RK, and as such restoring the glycosomal phosphate balance by producing ATP.

The *T. brucei* genome contains a gene that has been putatively annotated as RK (Tb427tmp.03.0090). This gene is homologues to other kinases, and shows synteny with the RK previously characterised in the related kinetoplastid *Leishmania major*. The gene Tb427tmp.03.0090 codes for a 35 kDa protein with a type 1 peroxisomal targeting sequence (PTS-1) located at the C-terminus: cysteine-lysine-isoleucine (Opperdoes and Szikora, 2006). Tb427tmp.03.0090 is expressed in both life-cycle stages, as demonstrated by transcriptomics (Siegel *et al.*, 2010) and proteomics (Colasante *et al.*, 2006; Vertommen *et al.*, 2008). Additionally, high-throughput phenotyping using RNA interference has categorised the knockdown of RK as resulting in a "significant loss of fitness" (Alsford *et al.*, 2011).

The glycosomal localisation of RK in bloodstream form *T. brucei* seems counterintuitive, considering the traditional roles of RK in nucleotide biosynthesis or when ribose is used as an alternative carbon source. The glycosome does not contain DNA, and the absence of the non-oxidative PPP precludes the use of ribose in glycolysis. Nonetheless, the

purine salvage and *de novo* pyrimidine biosynthetic pathways are partly localised in the glycosome, with the remainder localised in the cytosol (reviewed by Michels *et al.*, 2000). Additionally, the PPP is an important source of reducing equivalents for the glycosome in the form of NADPH. It is important to note here that the presence of a peroxisomal targeting sequence does not mean sole localisation in the glycosome, demonstrated by G6PDH equally localised in the glycosome and cytosol (Heise and Opperdoes, 1999) and transketolase with a dual localisation in *Leishmania mexicana* (Veitch *et al.*, 2004).

The reversible-RK hypothesis is potentially supported by metabolomics experiments. When bloodstream form *T. brucei* are fed with uniformly labelled ^{13}C-glucose, it is suggested that ^{13}C(u)-labelled ribose is excreted (unpublished; Dr Jana Anderson, Dr Darren Creek, University of Glasgow). The identify of ribose in those experiments has not been confirmed with authentic standards, and even the presence of labelled ribose does not necessarily mean that ribose is produced by RK in the glycosome, as it is possible that ribose is produced by the PPP that is co-localised in the cytosol. Nonetheless, it does indicate the possibility for reversibility of RK.

In this chapter, the kinetics of *T. brucei* RK are characterised and genetic mutants are generated in an effort to scrutinise the hypothesis that RK does prevents the phosphate leak in the glycosome of bloodstream form *T. brucei*.

4.2. Results

4.2.1. Putative *T. brucei* RK gene has a typical RK sequence

The *T. brucei* gene Tb427tmp.03.0090 is putatively annotated as a RK, based on sequence similarity to other RK sequences. The gene is syntenic with the *Leishmania major* gene LmjF.27.0420, whose RK activity has been demonstrated previously (Ogbunude *et al.*, 2007). An interesting difference between *L. major* and *T. brucei* RK is the absence of a PTS-1 signal in LmjF.27.0420. Nonetheless, *L. major* RK has a predicted PTS-2 signal (Opperdoes and Szikora, 2006), which could still guarantee glycosomal localisation.

The Tb427tmp.03.0090 gene has additionally high identity with ribokinases from both eukaryotes and prokaryotes (Figure 4.2). Structural alignment of Tb427tmp.03.0090 with *E. coli* RK (1RK2) indicates that the active site is highly conserved, and that the differences between the two amino sequences are not located near the binding pockets (Figure 4.1). The function of the extra amino acids around positions 160 and 200 remains unclear, but these are also observed in *L. major* RK (Figure 4.2). The Tb427tmp.03.0090 nucleotide sequence of our lab strain was identical to the publicly available reference sequence for strain 427 at the TriTrypDB database (Aslett *et al.*, 2009).

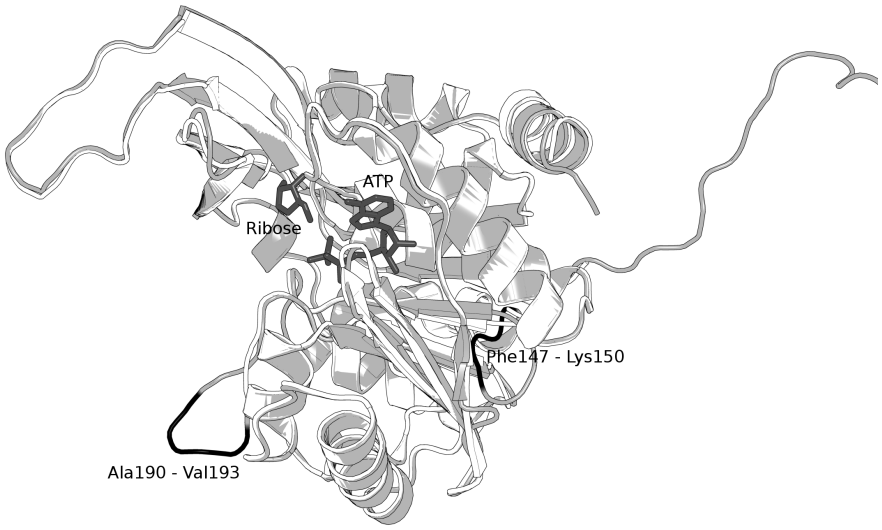

Figure 4.1.: Structural alignment of *T. brucei* to *E. coli* RK. Amino acid alignment of Tb427tmp.03.0090 (green) to the crystal structure of *E. coli* RK (blue, Protein DataBank, structure 1RK2, subunit A). Ribose and ADP were co-crystalised with 1RK2 and are shown in red. The N-terminal, which is longer in *T. brucei* than in *E. coli* (Figure 4.2), is located at the opposite site from the ribose and ATP binding sites. In orange are the loops around residues 160 and 200, also not located near the binding pockets.

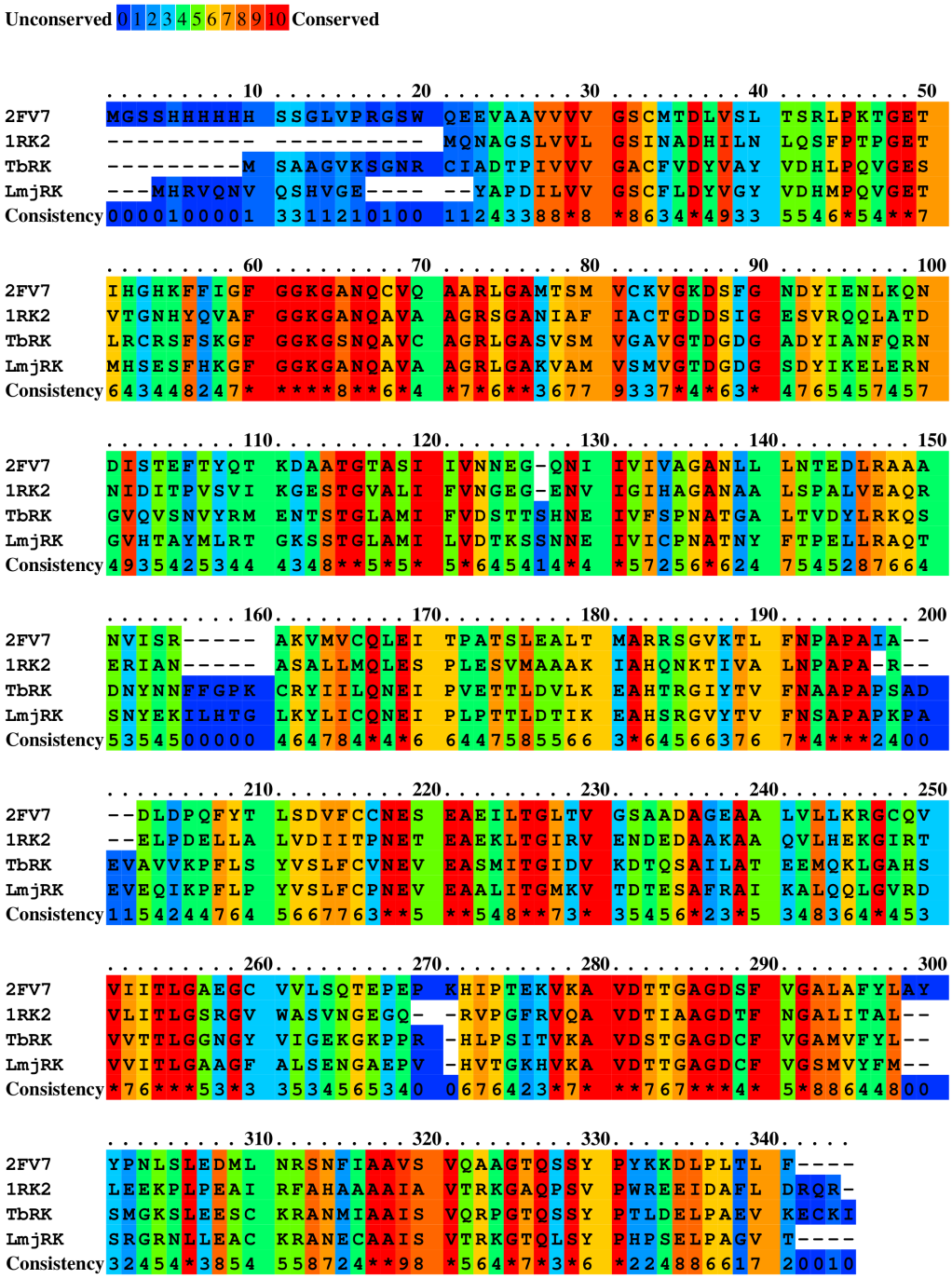

Figure 4.2.: Protein sequence alignment of ribokinases. Sequences 2FV7 and 1RK2 are human and *E. coli* ribokinases, respectively, with elucidated crystal structures (from the Protein Data Bank, http://www.rcsb.org). LmjRK is *Leishmania major* gene LmjF.27.0420, while TbRK is *T. brucei* gene Tb427tmp.03.0090. Protein sequences were aligned with PRALINE (Heringa, 1999). Regions with high conservation are typically located around the binding pocket. The regions around residues 65, 115 and 190 are situated around the ribose binding pocket, while the regions around residues 250, 280 and 320 are located around the ATP binding site.

4.2.2. Kinetic characterization of recombinant *T. brucei* RK

To study the putative *T. brucei* RK in greater detail, an N-terminal polyhistidine-tagged recombinant version of the Tb427tmp.03.0090 protein was heterologously expressed in *E. coli.* Purification of the recombinant RK by immobilised metal affinity chromatography (IMAC) gave a protein of approximately 39 kDa (Figure 4.3) and a typical yield of 10 mg $\cdot$ l^{-1} bacteria culture.

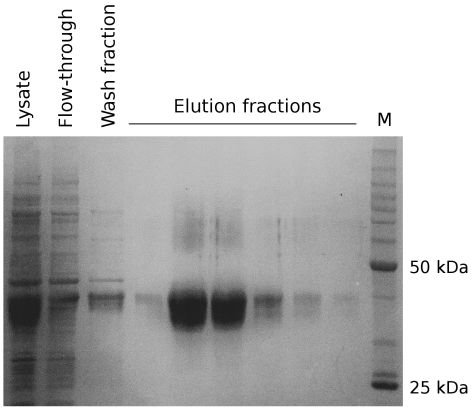

Figure 4.3.: Protein gel of recombinant RK **purification.** After heterologous expression of *T. brucei* RK in *E. coli*, recombinant protein was purified with IMAC and fractions from the purification process were separated on SDS-PAGE and stained with Coomassie. The wash fraction eluted with 50 mM imidazole, while the elution fractions eluted with 500 mM imidazole. M indicates protein marker. Purification and gel performed by Alan Scott (University of Glasgow).

The recombinant RK was assayed in both the direction of Rib-5-P dephosphorylation and ribose phosphorylation, by a coupled enzyme assay (Figure 2.3), as described in Section 2.4.

Substrate	V_{max}(µmol $\cdot$ min^{-1} $\cdot$ mg $protein^{-1}$)
Ribose	2.5 ± 0.37
2-deoxyribose	2.3 ± 0.4
Arabinose	ND
Erythrose	0.36 ± 0.1
Fructose	ND
Lyxose	ND
Threose	ND
Xylose	ND
Xylulose	ND

Table 4.1.: Phosphorylation of different substrates by RK. Activity was measured at 25 °C with a substrate concentration of 5 mM and by coupling ADP production to pyruvate kinase and lactate dehydrogenase (Figure 2.3). n = 3. ND is not detected.

	k_{cat} (s^{-1})		V_{max} ($\mu mol \cdot min^{-1} \cdot mg\ protein^{-1}$)	
Direction	25 °C	37 °C	25 °C	37 °C
Forward (Rib-5-P forming)	1.6 ± 0.24	3.2 ± 0.43	2.5 ± 0.37	4.9 ± 0.66
Reverse (Ribose forming)	0.014 ± 0.0036	0.026 ± 0.0050	0.022 ± 0.0056	0.040 ± 0.0077

Table 4.2.: Activity of recombinant *T. brucei* RK. Both the forward and reverse direction were assayed (Figure 2.3). The enzyme was saturated with 10 mM ribose and 5 mM ATP in the forward direction, and 10 mM Rib-5-P and 5 mM ADP in the reverse direction (Figure 2.3). $n = 3$.

	K_m (mM)				
Organism	Ribose	ATP	Rib-5-P	ADP	Reference
T. brucei	0.15 ± 0.03	0.26 ± 0.10	0.39 ± 0.15	0.25 ± 0.09	This study
L. major	0.3 ± 0.04	0.2 ± 0.02	NA	NA	Ogbunude *et al.*, 2007
E. coli	0.11 ± 0.02	NA	NA	NA	Maj and Gupta, 2001
H. sapiens	2.17	0.07	NA	NA	Park *et al.*, 2007

Table 4.3.: Affinity constants of RK. The affinity constants of *T. brucei* RK for its substrates and products. Ribose and ATP were assayed in the direction of ribose phosphorylation, while Rib-5-P and ADP were assayed in reverse. $n = 3$. NA = not available.

T. brucei RK has a high specificity for ribose (Table 4.1). Of the pentoses tested as substrates, only significant activity with 2-deoxyribose was observed. RK is also capable of phosphorylating erythrose, albeit at a 86 % reduced rate.

The assays were performed at both 25 °C and 37 °C, as the current mathematical model of trypanosomal bloodstream form metabolism operates at 25 °C (Albert *et al.*, 2005), while future versions of the model will be operating at the *in vivo*-like temperature of 37 °C. It is apparent from the results that the preferred direction of the RK reaction is in the direction of ribose phosphorylation (Table 4.2), as expected from the thermodynamic equilibrium. Increasing the temperature by 12 °C doubled the activity.

The affinity constants (K_m) of the substrates in both reaction directions were determined by measuring the activity at various substrate concentrations. The K_m values were subsequently determined via nonlinear regression. The K_m values of ribose and ATP were comparable to other ribokinases (Table 4.3), while no affinity constants of Rib-5-

P and ADP for any organism have been reported previously. The affinity constants of Rib-5-P and ADP were in the similar range as those of ribose and ATP.

Attempts were made to measure the specific activity of RK in bloodstream form *T. brucei*, using the same coupled enzyme assay and *T. brucei* cell extracts. However, significant background ATPase activity in these assays precluded the calculation of the RK activity, as also encountered when specific activities of enzymes in *T. cruzi* extracts were measured (Olin-Sandoval *et al.*, 2012).

4.2.3. Ablation of *T. brucei* RK by RNA interference

To assess the role and essentiality of RK in *T. brucei,* an RK^{RNAi} cell line was generated to ablate the RK activity by RNA interference (RNAi). The $pRPa^{SLi}$/2T1 plasmid and cell line system was used to facilitate reliable transfection and expression of a stem-loop allow selection of a stem-loop construct (Alsford and Horn, 2008).

Ablation of the RK transcript, induced by the addition of 1 $\mu g \cdot ml^{-1}$ tetracycline, did not result in a growth phenotype (Figure 4.4). The ablation of the RK transcript and protein was confirmed by both northern blot and western blot (Figure 4.5). The loss of RK activity from the cells could not be assayed, due to the aforementioned significant background in the assay.

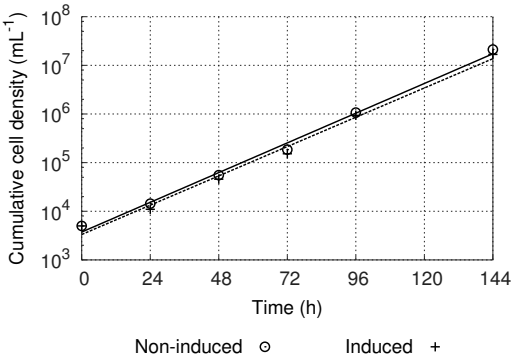

Figure 4.4.: Growth curve of RK^{RNAi}. A culture of RK^{RNAi} was kept at a cell density in between $2 \cdot 10^4$ and $2 \cdot 10^6$ cells per mL. Induced (plus-sign) is cultured in the presence of 1 $\mu g \cdot ml^{-1}$ tetracycline, while non-induced (circle) is the control. No change in growth could be observed.

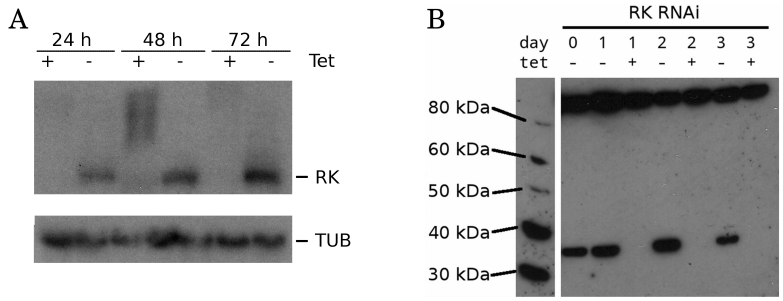

Figure 4.5.: Northern and western blot of RK^{RNAi}. Presence of RK transcript (*A*) and protein (*B*) in RK^{RNAi} after induction with tetracycline (tet) at 1 $\mu g \cdot ml^{-1}$ tetracycline. Tubulin (TUB) was used as a loading control in the northern blot, while a cross-reacting band around 90 kDa was used as loading control in the western blot.

	IC_{50}(nM)			
Compound	Induced	Non-induced	Fold change	*p*
Methylene blue	46.3 ± 1.88	33.4 ± 4.26	1.39	0.0085
Diminazene	78.7 ± 3.43	71.9 ± 10.6	1.09	0.35

Table 4.4.: AlamarBlue assays of 7-days induced RK^{RNAi}. IC_{50} values from 3 alamarBlue assays, using methylene blue to mimic oxidative stress, and diminazene as a control. Errors are standard deviations. *p*-value is from a Student's *t*-test, two-tailed, equal variance.

With Rib-5-P as a reactant for RK, I wondered whether ablation of RK has an effect on the parasite's capability to deal with oxidative stress, as the PPP is an important source of NADPH. The effect of methylene blue on RK^{RNAi} was investigated with an alamarBlue assay. Methylene blue readily reacts with NADPH, so not directly increasing the oxidative stress, but rather mimicking the more oxidised state of the parasite under oxidative stress. Surprisingly, RK^{RNAi} induced for 7 days had a significantly higher IC_{50} value for methylene blue, although the difference was only 1.39-fold. (Table 4.4).

4.2.4. Limited changes in metabolome of RK^{RNAi}

The effect of ablation of RK on the metabolome on the parasite was investigated by untargeted metabolomics. The metabolites of 72 hours induced and non-induced RK^{RNAi} were extracted and analysed by liquid chromatography-mass spectrometry (LC-MS), using pHILIC chromatography and high resolution accurate mass spectrometry with fast polarity switching. The data was deconvoluted and analysed using the mzMatch/IDEOM pipeline.

Measured mass	Retention time (min)	Predicted formula	Isomers	Putative metabolite	Fold change	FDR
237.04597	4.37	$C_{13}H_{24}N_4O_{11}P_2$	1	CDP-N-dimethylethanolamine	2.02	0.00388
219.05341	7.11	$C_{11}H_9NO_4$	2	8-Methoxykynurenate	1.80	0.00927
247.06910	17.64	$C_9H_{13}NO_7$	1	N-Succinyl-L-glutamate	1.77	0.00279
363.05790	18.18	$C_{10}H_{14}N_5O_8P$	5	Guanosine 3'-phosphate	1.75	0.00485
151.04938	13.13	$C_5H_5N_5O$	3	Guanine	1.65	0.00489
207.05337	7.06	$C_{10}H_9NO_4$	6	4-(2-Aminophenyl)-2,4-dioxobutanoate	1.65	0.00851
145.01977	15.46	$C_5H_7NO_2S$	2	(S)-4-amino-4,5-dihydro-2-thiophenecarboxylate	1.64	0.00328
145.07388	16.71	$C_6H_{11}NO_3$	9	[FA oxo,amino(6:0)] 3-oxo-5S-amino-hexanoic acid	1.62	0.0290
161.05106	7.07	$C_6H_{11}NO_2S$	1	Allylcysteine	1.55	0.0254
193.07390	4.67	$C_{10}H_{11}NO_3$	10	Phenylacetylglycine	1.48	0.0398
174.07937	7.07	$C_{10}H_{10}N_2O$	4	Indole-3-acetamide	1.46	0.0283
200.00857	13.92	$C_4H_9O_7P$	4	Erythrulose 1-phosphate	1.42	0.0282
886.55673	3.48	$C_{47}H_{83}O_{13}P$	19	[PI (38:4)] 1-octadecanoyl-2-(5Z,8Z,11Z,14Z-eicosatetraenoyl)-sn-glycero-3-phospho-(1'-myo-inositol)	-1.09	0.0369
488.10748	16.86	$C_{14}H_{26}N_4O_{11}P_2$	1	CDP-choline	-1.20	0.0256
337.09449	16.28	$C_{11}H_{19}N_3O_7S$	3	S-(Hydroxymethyl)glutathione	-1.28	0.0130
144.12628	10.26	$C_7H_{16}N_2O$	2	1-(3-aminopropyl)-4-aminobutanal	-1.29	0.0241
335.13294	15.9	$C_{12}H_{21}N_3O_8$	3	Thr-Thr-Asp	-1.31	0.0118
187.08443	7.15	$C_8H_{13}NO_4$	6	6-Acetamido-2-oxohexanoate	-1.36	0.0184
113.05897	9.95	$C_4H_7N_3O$	1	Creatinine	-1.39	0.00383
259.18954	14.62	$C_{12}H_{25}N_3O_3$	2	Leu-Lys	-1.45	0.0119
112.02730	10.09	$C_4H_4N_2O_2$	2	Orotate (Fragment)	-1.47	0.00215
230.01912	17.07	$C_5H_{11}O_8P$	16	D-Ribose 5-phosphate	-1.57	0.00253
320.05079	18.21	$C_8H_{17}O_{11}P$	1	Octulose 8-phosphate	-1.93	<0.0001

Table 4.5.: Changes in metabolite concentrations in RK^{RNAi}. Putatively identified metabolites that changed significantly (rank product FDR<0.05) in 72 hours induced RK^{RNAi}. Metabolites are ranked by fold changes. Measured mass as mass-to-charge ratio (m/z); number of isomers as predicted from IDEOM databases. Negative fold changes indicate decreased metabolites.

A total of 372 metabolites could putatively be identified in this experiment (mzMatch output and IDEOM sheets are provided on CD-ROM). Of these putative metabolites, the

levels of 23 were significantly changed in the induced RK^{RNAi} cell line (based on rank product, FDR<0.05, Table 4.5).

Comparative metabolomics experiments with this set-up routinely results in seemingly significant changes in particularly peptides and lipids. The high heterogeneity and similarity between the different lipids and peptides only allow identification into subgroups, such as phosphatidyl-cholines, or fatty acids. When a large number of metabolites are studied, some of them will show a significant change just by chance. Therefore, changes in lipids and peptides are only monitored for general changes, switches from one subgroup to another, but are ignored otherwise for further analysis.

Overall, only limited changes are observed in RK^{RNAi} metabolism: none of the metabolites change by twofold or more.

4.2.5. RK mainly produces Rib-5-P

From the remaining significantly changed metabolites, the most striking is the decreased level of Rib-5-P. Although the pHILIC column used in the liquid chromatography step allows a comprehensive coverage of metabolism, it is not particularly effective in separating sugar-phosphate isomers. The identified Rib-5-P therefore represents a mixture of pentose phosphates. Nevertheless, the decrease in Rib-5-P in the induced cell line proposes that RK is mainly involved in producing Rib-5-P, instead of consuming Rib-5-P. This does not necessarily contradict the reverse-RK hypothesis. The reverse-RK hypothesis dictates that the loss of RK results in an accumulation of Rib-5-P. However, this accumulation can be overshadowed by a decrease in Rib-5-P in the much larger cytosol.

In comparison, a genetic null mutant in the glucose transporter of *Leishmania mexicana* up regulated a number of proteins, including RK (Feng *et al.*, 2011). The null mutant is unable to produce Rib-5-P via the PPP due to a limited uptake of glucose and compensates this by increasing the amount of RK present.

4.2.6. *T. brucei* produces octulose 8-phosphate from Rib-5-P

Interesting from the metabolomics data is that the decrease in Rib-5-P is accompanied with a decrease in octulose 8-phosphate. Routinely, the two uncommon sugar-phosphates octulose 8-phosphate and nonulose 9-phosphate are being identified in metabolomics

experiments on *T. brucei* in our lab (Creek *et al.*, 2012b). Labelling patterns of octulose 8-phosphate upon ^{13}C(u)-glucose labelling suggest that octulose 8-phosphate is produced by a ligation of a pentose phosphate and a triose phosphate (a subsequent phosphatase reaction than cleavages one of the two phosphates). This reaction could be performed by fructose-1,6-bisphosphate aldolase, as demonstrated in our lab (Ashleigh Fleming, University of Glasgow). According to this scheme, a decrease in Rib-5-P *in situ* leads to a decrease in octulose 8-phosphate, and this was observed in the RK^{RNAi} cell line.

The nonulose 9-phosphate that is observed in *T. brucei* extracts is produced by a ligation of a hexose phosphate and a triose phosphate, according to ^{13}C(u)-glucose labelling (Creek *et al.*, 2012b). The RK^{RNAi} metabolomics supports this hypothesis, as the nonulose 9-phosphate does not change (fold change 1.18, FDR 0.61), and the production of nonulose 9-phosphate is therefore unlikely to be related to Rib-5-P or octulose 8-phosphate.

Interestingly, erythrulose 1-phosphate was increased in the RK^{RNAi} cell line. The opposing trends of erythrulose 1-phosphate and Rib-5-P levels suggest that the two sugar-phosphates can react with each other. The accumulation of erythrulose 1-phosphate could be a result of the reduced availability of Rib-5-P. The connection remains unclear, an aldolase reaction ligating the two sugar-phosphate results in a nonulose 9-phosphate, but this is contradicted by labelling studies (Creek *et al.*, 2012b).

4.2.7. Unable to knockout RK

Ablation of a gene's transcript by RNA interference does not typically result in a complete loss of the protein of interest. It was therefore attempted to generate a null mutant for the RK gene (*Δrk*), by replacing the Tb427tmp.03.0090 gene with antibiotic selection markers via homologous recombination with neighbouring non-coding sequences .

To construct *Δrk*, untranslated regions (UTRs) adjacent to Tb427tmp.03.0090 were cloned into plasmid pTBT (Cross *et al.*, 2002), containing either puromycin N-acetyltransferase or hygromycin phosphotransferase as antibiotic selection markers (Figure 4.6). Wild-type bloodstream form *T. brucei* were transfected with both constructs separately, generating *Δrk::HYG/RK* when one RK allele was replace by a hygromycin resistance gene, and *Δrk::PAC/RK* when replaced by a puromycin resistance gene. Independent clones were selected after transfection by plating out various dilutions

on 96-wells plates. Correct integration of the selection markers was verified by PCR (Figure 4.6).

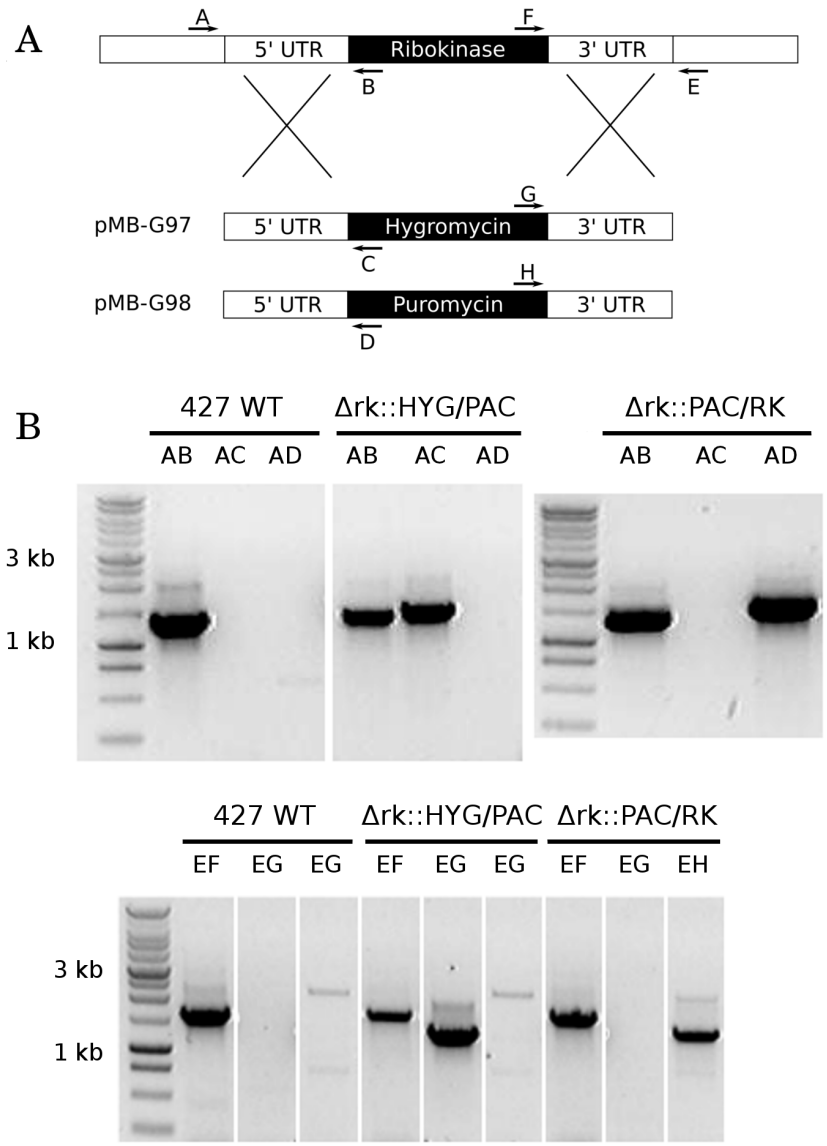

Figure 4.6.: PCR confirming targeted replacement of RK gene. *A:* Strategy of PCR confirming gene replacement. Arrows and letters indicate primers. A PCR with primersets AB and EF indicates presence of the endogenous RK gene, primer sets AC and EG indicate replacement of RK with a hygromycin resistance gene, while primer sets AD and EH indicate replacement of RK with a puromycin resistance gene. Primer sequence are in Table 2.1. *B:* PCR of wild-type 427, Δ*rk::HYG/RK* and Δ*rk::PAC/RK*, with primers as indicated in *A*. The selection markers succesfully replace the endogenous RK gene.

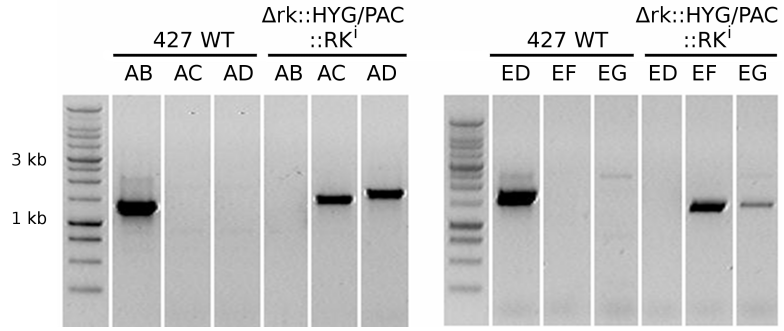

Figure 4.7.: PCR confirmation of Δ*rk::HYG/PAC::RK^{i}*. Genomic DNA from 427 WT and Δ*rk::HYG/PAC::RK^{i}* were amplified with primers described in Figure 4.6. The endogenous RK is absent in Δ*rk::HYG/PAC::RK^{i}* (primers AB and ED), replaced with hygromycin (primers AC and EF) and puromycin (primers AD and EG).

However, numerous attempts of transfection with the other resistant marker were invariably unsuccessful, no parasites survived the selection with both hygromycin and puromycin. Selection for only the antibiotic from the second transfection round gave rise to mutants where the selection marker from the first round of transfection was replaced by the second selection marker.

Being unable to remove both RK alleles, it was decided to generate a conditional RK knockout instead. An exogenous copy of the RK gene, placed under control of a tetracycline inducible promoter, was introduced to the parasites prior to replacement of the endogenous copies of RK. The RK gene was amplified from genomic DNA and cloned into pHD1336, that contains a tetracycline inducible PARP promotor (as pHD678 with blasticidin, Biebinger *et al.*, 1997). The construct was transfected in strain 449 *T. brucei*, which is derived from strain 427 and expresses the T7 polymerase and tetracycline-repressor required by pHD1336 (Biebinger *et al.*, 1997). Clones were selected by blasticidin resistance. Subsequently, the endogenous RK gene was replaced by resistance genes in two rounds of transfection, while the expression of the exogenous

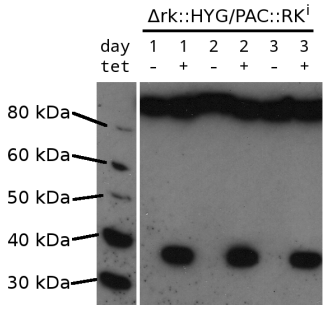

Figure 4.8.: Western blot of RK in RK re-expressor. Δ*rk::HYG/PAC::RK^{i}* strain parasites were cultured in the absence and presence of tetracycline (tet). Subsequently, presence of the *T. brucei* RK protein was investigated by Western blot. An unidentified cross-reacting band around 90 kDa was used as loading control.

RK was continuously induced by the presence of tetracycline. PCR confirmed the successful replacement of the endogenous RK *Δrk::HYG/PAC::RK*^{i}.

Subsequently, expression of the inducible copy of RK was halted by the removal of tetracycline from the culture. Cells were washed in medium without tetracycline and subsequently cultured in HMI-9 without tetracycline, supplemented with certified tetracycline-free fetal bovine serum (FBS, BioSera). Surprisingly, no growth effect was observed when the expression of the exogenous RK was halted by the absence of tetracycline, while Western blot confirmed the disappearance of RK from the culture (Figure 4.8).

In an alternative approach, Spitznagel *et al.* (2009) constructed an RNAi mutant for alanine aminotransferase in a strain lacking one of the endogenous alleles, and were able to ablate enough activity to observe a phenotype. Loss of one endogenous allele in an RNAi mutant has the potential to enhance the knockdown of the gene of interest, as even less transcript would be available for translation. I attempted a similar approach, by transfection of the *RK*^{RNAi} with the construct used in the generation of *Δrk::PAC/RK*. Identical to all other generated RK mutants, no growth phenotype could be observed.

4.3. Discussion

4.3.1. *T. brucei* RK can work both ways

Heterologues expression, purification and characterisation confirmed the RK activity of the gene Tb427tmp.03.0090 from *T. brucei*. The kinetic parameters are comparable to those measured on ribokinases in other species, but here I report the first affinity constants of Rib-5-P and ADP. In chapter 3, mathematical modelling predicted that the role of *T. brucei* RK in the glycosome is to dephosphorylate Rib-5-P in order to prevent a glycosomal phosphate leak. I demonstrate here that *T. brucei* RK is indeed capable of dephosphorylating Rib-5-P.

Metabolomics experiments on a genetic mutant ablated of RK showed a significant decrease in the level of Rib-5-P (1.57-fold decrease, FDR 0.00253, based on rank product), suggesting that the depleted RK would normally produce Rib-5-P. However, it is likely that any changes in Rib-5-P concentration in the cytosol mask changes that are observed in the glycosome, due to the size difference of the two compartments.

4.3.2. RK is potentially essential, but low levels suffice

The attempts to generate RK knock-out mutants suggested that RK is an essential, as a full knockout could not be obtained, even as deletion of single RK alleles were successful. However, both RK^{RNAi} and $\Delta rk::HYG/PAC::RK^{i}$ show no growth phenotype upon ablation of RK transcript and protein from northern and western blots. Additionally, metabolomics on RK^{RNAi} only indicated minor changes in a small number of metabolite levels. This suggests that potentially low levels of RK are still present in the RK^{RNAi} and $\Delta rk::HYG/PAC::RK^{i}$ cell lines. RNAi in *T. brucei* does often not result in complete ablation of the protein of interest, especially for very stable proteins, while inducible expression of an exogenous gene has the risk of leaky expression. The amount of residual activity of RK in the genetic mutants is unknown, as I was unable to assay RK from extracts, although the western blot is compelling to show ablation of the protein.

In a recent high-throughput RNAi screen, the knockdown of RK in both bloodstream form and procyclic form *T. brucei* resulted in a growth loss (Alsford *et al.*, 2011). However, in *T. brucei* RNAi, the gene fragment used in the RNA construct, culture conditions and method used in scoring fitness can all conspire to create discrepant results, especially if, as appears to be the case, levels of knockdown need to reach a high threshold

for an effect to be detectable. For alanine aminotransferase, too, RNAi failed to yield a growth phenotype while gene knockout indicated essentiality (Spitznagel *et al.*, 2009).

Interestingly, RK^{RNAi} seemed to be better protected against oxidative stress, although only by a small fold change. When, at least in the cytosol, no Rib-5-P is produced from ribose by RK, then the PPP might be activated to compensate. An increased flux through the PPP would result in increased production of NADPH. Consequently, ablation of RK actually improves the oxidative state of the cell.

4.3.3. The importance of uncommon metabolites

Metabolomics on RK^{RNAi} mutants furthermore demonstrated that the uncommon metabolite octulose 8-phosphate is likely produced from Rib-5-P, as previously predicted from labelling patterns of octulose 8-phosphate (Creek *et al.*, 2012b). The uncommon metabolite nonulose 9-phosphate is not linked to Rib-5-P or octulose 8-phosphate, as no changes were observed. Erythrulose 1-phosphate, another uncommon metabolite, was increased in the RK^{RNAi}, but the connection with ablation of RK remains unclear.

The importance of these metabolites for trypanosomes remains a mystery. The production of octulose and nonulose phosphates can be catalysed by already identified enzymes within the glycosome such as ALD and TAL, due to substrate promiscuity. The presence of these unknown metabolites can therefore be seen as "errors" of an "underground metabolism" (D'Ari and Casadesus, 1998), but perhaps they play an essential role in the glycosomal compartmentalisation of metabolism.

In Chapter 3 I demonstrated how rigid the structure of glycosomal metabolism is: there are very strict stoichiometric rules that need to be adhered to in the small volume of a glycosome, and already a small leak in the system will quickly lead to its demise. Perhaps the presence of an underground metabolism, with metabolites and reactions linking up at maybe a smaller scale and rate than the majority of the flux, provides the system with more flexibility and degrees of freedom. However, an important factor here is the localisation of the metabolites, as it is not expected that metabolism in the cytosol suffers from a rigid structure.

4.3.4. RK alone is unlikely to prevent the glycosomal phosphate leak

While the mathematical model predicted an essential role of RK in *T. brucei* glycosomes in the prevention of the phosphate leak, the experimental data provided here is inconclusive. However, as discussed in 3.2.3.4, a glycosomal RK is only an example of a number of solutions that belong to the same class, where the conserved moiety of bound phosphates within the glycosome is extended by additional reactions within the glycosome. My data presented here suggests that indeed RK on its owh is preventing the phosphate leak, but is rather involved in a complex dance with other enzymes present in the glycosome to balance the bound-phosphates (Colasante *et al.*, 2006; Opperdoes and Szikora, 2006; Vertommen *et al.*, 2008).

Notably, phosphoenolpyruvate carboxykinase (PEPCK) and arginine kinase (ArgK) are present in the glycosome (Colasante *et al.*, 2006; Opperdoes and Szikora, 2006; Vertommen *et al.*, 2008), both using ATP (Hunt and Köhler, 1995; Pereira *et al.*, 2002). Potentially, the effects of ablation of RK^{RNAi} in the glycosome are buffered by other glycosomal kinases. PEPCK is part of the succinate fermentation pathway, which is supposed to have very limited activity in the bloodstream form of the parasite. The activity of PEPCK, however, is 1.5 nmol $\cdot$ min^{-1} $\cdot$ mg protein^{-1}(Hart *et al.*, 1984), higher than the flux through the glycosomal PPP. Arginine kinase appears to be an isolated enzyme (there are no other enzymes reported in the glycosome that use either arginine or arginine phosphate), although the cytosol could be a source of arginine. It is thought that arginine kinase plays a role in management of energy reserves in trypanosomatids (Pereira *et al.*, 2002), and additional work is required to better understand the role of arginine-phosphate in trypanosome metabolism.

Combined with the potential importance of the uncommon metabolites routinely identified in our datasets, it perspires that glycosomal metabolism might be more complex than initially thought when glycosomes received their name.

Chapter 5

Studying enzyme function with metabolomics

It is important to know, when studying the metabolism of a particular organism, which enzymes are present and what reactions they catalyse. Although the genome sequence, with the help of various bioinformatics approaches, can suggest which enzymes are present, these putative annotations require experimental validation. In this chapter I use metabolomics to study the putative function of three *T. brucei* enzymes.

5.1. Introduction

Computational models are valuable tools to study the behaviour of metabolic networks; however, the power of these models is restricted by how comprehensive the knowledge of the parameters is. While *in silico* models of metabolism exist with different degrees of abstraction, from stoichiometric models to detailed kinetic models, they all depend on the knowledge of which reactions are happening within the cell. This combination of all (catalysed) metabolic reactions has been called the "reactome" by (Joshi-Tope, 2004) (or "catalome" by (Sun *et al.*, 2006)). However, our current knowledge of the reactome is far from complete. An estimated 30–40 % of catalytic activities are currently "orphan", meaning that the activity has been detected, but no gene has been annotated as being responsible for these activities in any organism (Chen and Vitkup, 2007). Even in a well characterised model organism, such as *E. coli*, 40 % of the genes have no experimentally confirmed function (Keseler *et al.*, 2009), while 60–70 % of the predicted protein coding genes in trypanosomatids remain unannotated (Choi and El-Sayed, 2012). This problem of incomplete and unreliable annotation has been recognised, and has for instance led to the establishment of the Enzyme Function Initiative that aims to address this problem with a structure based strategy (Gerlt *et al.*, 2011).

Bioinformatics approaches are helpful in the functional identification of genes by studying nucleotide sequences using tools, such as BLAST[1] and Pfam[2] domain searches, but sequence analysis alone is often not sufficient to elucidate the function of a gene. Particularly for enzymes, sequence similarity is rarely sufficient to annotate the substrate specificity. An example of this are the enzymes melamine deaminase and atrizine chlorohydrolase which have 98% identical amino acid sequences (Seffernick *et al.*, 2001). Only 9 out of 475 amino acids are different, but no detectable activity could be measured with either enzyme for the other enzyme's natural substrate. Although this might appear an exceptional example, an additional problem with incorrect annotations is that they are propagated through the genome databases (Furnham *et al.*, 2009). Once a gene has been annotated incorrectly, that incorrect annotation is used to (incorrectly) annotate other genes by sequence similarity (Schnoes *et al.*, 2009).

Evidently, sequence analysis alone is not sufficient for reliable gene annotations; there is a requirement for experimental data on the gene products, even if just to confirm the function predicted from sequence analysis. The detailed characterisation of enzyme functions has traditionally been performed with targeted assays, where each assay is optimised to measure one particular catalytic activity at the same time. However, as

[1] http://blast.ncbi.nlm.nih.gov/
[2] http://pfam.sanger.ac.uk/

demonstrated by the example of melamine deaminase and atrizine chlorohydrolase, an untargeted approach is required to be able to evaluate the full catalytic potential of enzymes. Furthermore, to fully describe the reactome it is imperative to also take substrate promiscuity into account. While most enzymes have one substrate that can be converted to product with a high rate, they often also have affinity and activity to other (related) molecules. To address the wide range of potential catalytic activities of uncharacterised enzymes, traditional enzyme assays have been scaled-up by the development of microarray-based enzyme assays (Sun *et al.*, 2006; Northen *et al.*, 2008). While these arrays can now monitor many reactions at the same time, they are still only capable of measuring a finite number of reactions that are specified by the array's design.

5.1.1. Metabolomics for elucidation of enzyme function

The use of metabolomics has been proposed as an untargeted approach to study enzyme functions (Saito *et al.*, 2006; Baran *et al.*, 2009; Saito *et al.*, 2010). Metabolites are common substrates and products of enzyme activities, and with the current advances in metabolomics it is now possible to measure metabolites in a sensitive and high-throughput manner. More precisely, two general approaches have been proposed to aid the functional elucidation of unannotated enzymes: (i) metabolomics enzyme assays, where a purified enzyme of interest is studied in isolation; and (ii) metabolic profiling, where a genetic mutant of the enzyme of interest is phenotyped by metabolomics (Figure 5.1).

The metabolomics enzyme assay, is based on measuring changes in levels of metabolites in a complex mixture of metabolites when incubated with the enzyme of interest (Saito *et al.*, 2006). For this, the enzyme needs to be isolated from the organisms, what is often easiest accomplished by heterologous expression of a recombinant version of the enzyme and subsequent purification from the expression host. The complex mixture typically consists of whole cell extracts, with all of the original enzyme activity eliminated.

Metabolic profiling is performed on genetic mutants that are defective in the enzyme of interest (Saghatelian *et al.*, 2004). This can be obtained by knockout of the gene of interest, or knockdown of its transcript by RNA interference (RNAi), although the latter might not lead to sufficient ablation of functional enzyme to show a metabolic effect. Subsequently, the metabolome from the genetic mutant is extracted and compared to wild-type extracts.

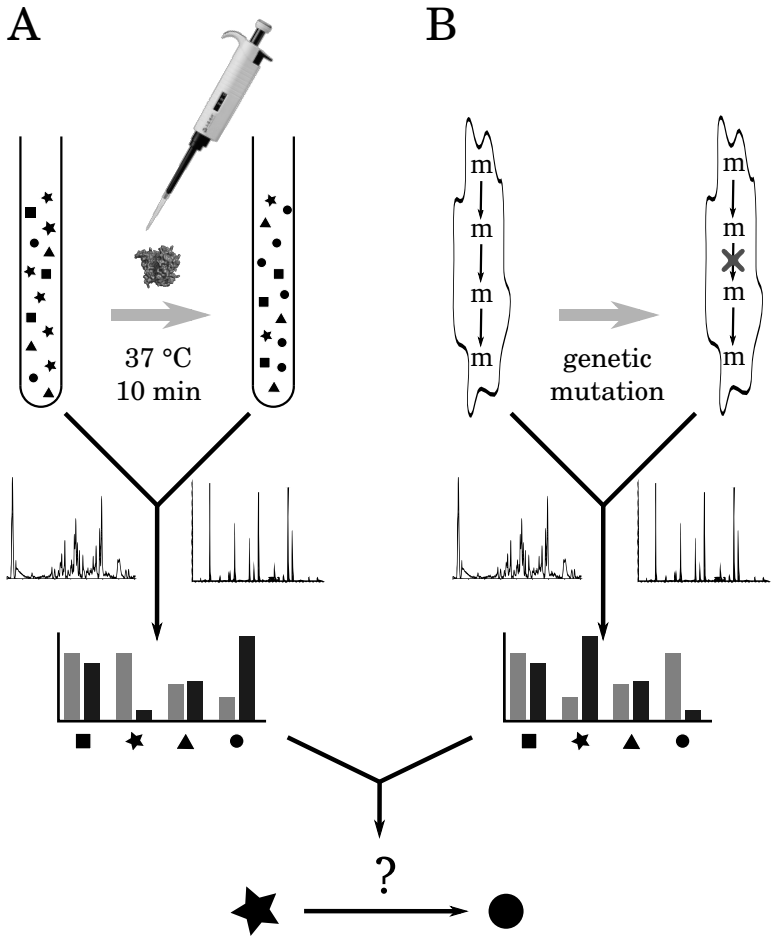

Figure 5.1.: The use metabolomics in functional elucidation of enzymes. *A:* In the metabolomics enzyme assay, a complex mixture of metabolites (depicted by various shapes) is incubated with a purified enzyme. The contents of the two samples are compared by mass spectrometry, generating an overview of changes in metabolite levels. *B:* In metabolic profiling, an organism containing an unknown pathway, with unknown enzymes, connecting unknown intermediates (m). A genetic mutant is generated in one of the unknown enzymes and the metabolome is compared to a wild-type cell via mass-spectrometry. As in *A*, an overview of changed metabolite levels is given. Both the metabolomics enzyme assay and metabolic profiling methods suggest that the star metabolite is converted to the circle metabolite by the previously uncharacterised enzyme.

In the simplest case, only one metabolite increases and one decreases in both approaches. This does not necessarily mean that these are the substrate and product of the enzyme catalysed reaction: a plausible chemical transformation needs to connect the increased and decreased metabolites. As will become clear from the results below, however, typically that many more metabolites change between conditions, complicating elucidation of the enzyme's function.

These metabolomic approaches have been applied successfully: e.g. Saito *et al.* (2006) used metabolomics enzyme assays to study the characterised YbhA and YbiV proteins from *E. coli* and found phosphotransferase and phosphatase activities against different sugars. In 2009, the same group (Saito *et al.*, 2009) characterised *E. coli* YihU as a novel hydroxybutyrate dehydrogenase, this time using both metabolomics enzyme assays and metabolic profiling.

The changes observed depend on the presence or absence of the enzyme of interest. While this might seem trivial, not all observed changes in metabolites are necessarily related to the presence of the enzyme. Mass spectrometry provides the ability to compare a large number of metabolites, typically thousands per sample. When two conditions are compared, a number of these measured metabolites will show significant changes that originate from biological and experimental variation, rather than from differences in the two conditions.

Additionally, the enzyme can have the ability to affect a multitude of metabolites due to substrate promiscuity and moonlighting, the effects that an enzyme can have multiple, potentially entirely unrelated functions. An example is cytochrome P450 170A1 that has recently been found to be able to catalyse both monooxygenase and terpene synthase activity (Zhao and Waterman, 2011). The two functions do not have to be catalytic activities, aldolase in the parasite *Echinococcus granulosus* for example is also involved in key processes as motility, differentiation, invasion and development (Lorenzatto *et al.*, 2012).

In metabolic profiling, the results can be even more ambiguous. A genetic mutation of an enzyme of interest will likely affect its substrate and product levels, but these changes may then by themselves affect levels of other metabolites. Alternatively, the cell might react by homoeostatic regulation, such that the levels of substrate and product of the enzyme of interest do not change. Although this might complicate the elucidation of the enzyme function, it is anticipated that rigorous analysis of the results allows us to infer new knowledge about the enzyme of interest.

In this chapter I applied the two strategies of enzyme metabolomics and metabolic profiling to the products of three *T. brucei* genes that are predicted to be enzymatically active, but have no confirmed activity: a putative arginase, *N*-acetylornithine deacetylase, and nicotinamidase.

5.2. Results

Three *T. brucei* genes of interest were investigated with a metabolomics approach. All three genes have been given putative annotations in genome databases, but have not been confirmed experimentally. For identification purposes, the proteins are here indicated by the abbreviations for the putative functions: gene Tb427.08.1910 codes for putative *N*-acetylornithine deacetylase (NAO), gene Tb427.08.2020 codes for a putative arginase (ARG), and genes Tb427tmp.160.2540 and Tb427tmp.160.2600 code for putative nicotinamidases (NAM).

5.2.1. A putative *T. brucei* arginase without arginase activity

In *T. brucei*, the loss of polyamine biosynthesis results in a growth-arrest. This is the mode of action of eflornithine, the only clinically used trypanocidal drug with a known mode of action (Poulin *et al.*, 1992). Eflornithine inhibits the enzyme ornithine decarboxylase (ODC) and thereby prevents the production of putrescine from ornithine. It was speculated that this makes the production of ornithine, as a substrate for ODC, a potential drug target. In most eukaryotes, ornithine is produced from arginine by arginase, but our lab showed that a gene putatively annotated in the *T. brucei* genome as an arginase does not have arginase or the related agmatinase activity (Vincent, 2011). I therefore decided to elucidate the function of this gene (ARG) by a metabolomics approach.

5.2.1.1. Recombinant ARG binds to an *E. coli* chaperone

For the investigation of the enzymatic activity of the putative arginase, a polyhistidine-tagged recombinant version of the protein was heterologously expressed in *E. coli*. Purification of the recombinant ARG by immobilised metal affinity chromatography gave two bands on a protein gel, with sizes of approximately 40 kDa and 110 kDa (Figure 5.2). Further purification by gel-filtration and ion-exchange chromatography (Alan Scott, University of Glasgow) did not improve the purity of the protein (Figure 5.2). Both bands were excised from the gel and the identity of the proteins was investigated by proteomics (Dr Richard Burchmore, University of Glasgow). The 40 kDa band was identified as *T. brucei* ARG, while the 110 kDa band is a complex of ARG and chaperone protein DnaK, a 70 kDa heat shock protein (Hsp70) involved in the correct folding of proteins (Langer *et al.*, 1992). The DnaK must be of *E. coli* origin as ARG was the

only *T. brucei* gene heterologously expressed. The presence of DnaK with the purified enzyme was ignored for further experiments, as DnaK is assumed to have no metabolic activity, although it can not be excluded that the presence of DnaK affects the activity of ARG. *T. brucei* also has endogenous heat shock proteins that have sequence similarity to the *E. coli* DnaK found in the proteomics analysis. This suggests that ARG might also form a complex with heat shock proteins *in vivo*.

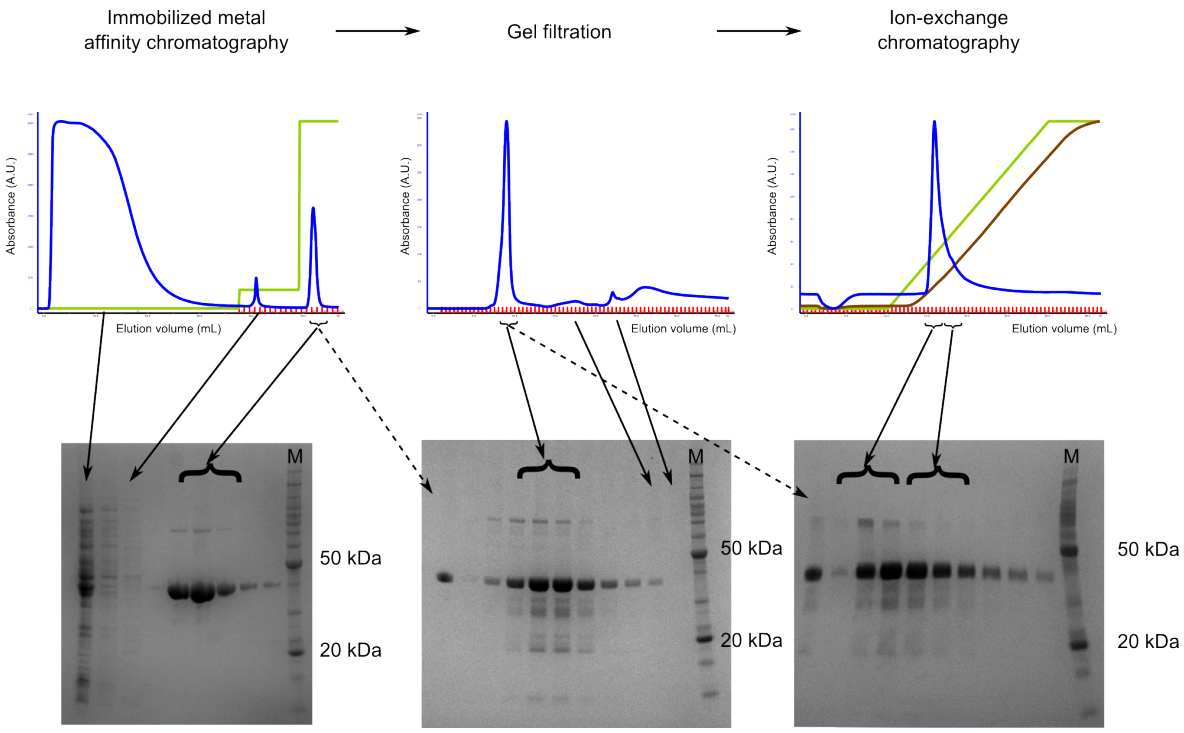

Figure 5.2.: Purification of recombinant ARG. Heterologously expressed ARG was sequentially purified over immobilised metal affinity chromatography, gel filtration and ion-exchange chromatography. The black lines in the graphs on top show the elution profiles from the chromatography system, as absorbance measured at 280 nm. Below are Coomassie blue stained SDS-PAGE gels with different fractions of the purification process. Purification fractions and gel samples are matched by arrows, dashed arrows indicate what sample was used for further purification. The 40 kDa band is ARG, while the 110 kDa is a complex of ARG and DnaK, as demonstrated by proteomics.

5.2.1.2. ARG is a potential tryptophan oxygenase

The activity of the recombinant ARG was investigated using a metabolomics enzyme assay. Purified ARG was incubated in a complex mixture of metabolites in the form of commercial yeast extract, with the addition of either of two cofactor mixtures (Table 5.1). The two cofactor mixtures differ in the presence of the reduced or oxidised, and phosphorylated or dephosphorylated forms of some of the components. It was anticipated

that, when the cofactors are involved, the catalysed reaction could be steered to the thermodynamically preferred direction depending on the cofactor mixture.

Attempts were made to use *T. brucei* extracts as complex metabolite mixtures, but resulted in a reduced number of detected metabolites, showed no significant changes upon incubation with the enzymes, and was therefore deemed unnecessarily tedious in comparison to the use of commercial yeast extract. Consequently, it was decided to use commercial yeast extracts for future metabolomics enzyme assays, at least as a first approach, with the possibility to generate trypanosome extracts if desired.

The enzyme was allowed to react in the complex metabolite mixture for 10 minutes at 37 °C, the reaction was quenched by the addition of ice-cold 75% acetonitrile, after which the samples were analysed by LC-MS. The results were compared to a control sample, where ARG was added after the acetonitrile quench.

Data deconvolution and filtering by mzMatch and IDEOM resulted in the putative identification of 865 metabolites, almost half of which were di-, tri- or tetra-peptides (IDEOM sheet on supplementary CD-ROM). It can be expected from the large number of peptides measured that a number of these will show significant changes purely by chance, as discussed in the introduction of this chapter.

The number of significantly changed metabolites (based on rank product, FDR<0.05) was more than fourfold higher in samples with cofactor mixture 1; 76 putative metabolites changed significantly in mixture 1, while 30 changed significantly in mixture 2 (Section D.3). Additionally, the individual fold-changes of metabolites were roughly 2.5-fold higher in samples with cofactor mixture 1. The differences between the two cofactor mixtures implies the involvement of the mixture 1-specific cofactors NAD^+, $NADP^+$, ADP, GDP and/or CoA.

Mix 1	NAD^+	$NADP^+$	ADP	GDP	CoA	FMN	FAD	PP	TPP	Biotin
Mix 2	NADH	NADPH	ATP	GTP	Acetyl-CoA	FMN	FAD	PP	TPP	Biotin

Table 5.1.: Contents of cofactor mixtures. The two cofactor mixtures prepared shared many components, while some are varied between their oxidised and reduced form, or phosphorylated and dephosphorylated forms. All concentrations were at 0.1 mM.

Measured mass	Retention time (min)	Predicted formula	Isomers	Putative metabolite	Fold change Mix 1	Fold change Mix 2	Indole	Quinoline
290.09005	9.26	$C_{14}H_{14}N_2O_5$	2	N2-Malonyl-D-tryptophan	24.4	5.43	×	
205.03770	5.63	$C_{10}H_7NO_4$	2	6-Hydroxykynurenate	21.8	3.35		×
211.04837	7.11	$C_9H_9NO_5$	5	5-(2'-Formylethyl)-4,6-dihydroxypicolinate [a]	9.25	4.17		
246.10058	9.28	$C_{13}H_{14}N_2O_3$	4	N-Acetyl-D-tryptophan	8.76	1.96 [b]	×	
189.04258	5.82	$C_{10}H_7NO_3$	6	Kynurenate	5.80	1.74		×
145.05282	6.89	C_9H_7NO	7	1(2H)-Isoquinolinone	4.06	1.36 [b]		×
173.04773	5.99	$C_{10}H_7NO_2$	4	2-Quinolinecarboxylic acid	3.95	1.49		×
236.07972	10.45	$C_{11}H_{12}N_2O_4$	2	L-Formylkynurenine [a]	3.87	1.82		
145.05281	5.53	C_9H_7NO	7	3-Methyleneoxindole	3.53	1.34 [b]	×	
174.07932	10.97	$C_{10}H_{10}N_2O$	4	Indole-3-acetamide	3.48	1.96 [b]	×	
252.07440	12.08	$C_{11}H_{12}N_2O_5$	1	5-Hydroxy-N-formylkynurenine [a]	3.00 [b]	1.58		
248.07931	6.16	$C_{12}H_{12}N_2O_4$	1	5-Hydroxyindoleacetylglycine	2.65	1.43 [b]	×	
182.08442	8.27	$C_{12}H_{10}N_2$	1	Harman	2.04	-1.06 [b]	×	
172.06372	5.76	$C_{10}H_8N_2O$	1	Indole-3-acetonitrile oxide	2.00	1.25 [b]	×	
198.07940	8.74	$C_{12}H_{10}N_2O$	4	Harmalol	1.71	1.21 [b]	×	
204.08995	10.55	$C_{11}H_{12}N_2O_2$	6	L-Tryptophan	-4.50	-1.28 [b]	×	

[a] Not indoles or quinolines, but related to tryptophan metabolism.
[b] Non-significant change (rank product FDR>0.05).

Table 5.2.: Changes in indoles and quinolines in ARG assay. Indoles, quinolines and tryptophan related metabolites that changed significantly (rank product, false discovery rate (FDR)<0.05, n=3) in at least one of the two cofactor mixtures. Measured mass as mass-to-charge ratio (m/z); number of isomers as predicted from IDEOM databases. Negative fold-changes indicate decreased metabolites.

Approximately one third of the significant changes were in lipids and peptides. No trend could be observed in the changes of lipids from one class to another, while the largest decreases in peptides contained tryptophan (Figure 5.3). Of the remaining metabolites, a large fraction were indoles, quinolines or related to the indolic amino acid tryptophan (Figure 5.4). While all indoles and quinolines increased in both reaction mixtures, only tryptophan decreased during the assay (Table 5.2). Ionisation of metabolites by mass spectrometry typically results in fragmentation of some analytes, however, likely ionisation fragments have already been filtered out as much as possible, based on retention time, peak shape and chemical formula (cf. Table 5.2 and Section D.3). Nonetheless, it cannot be excluded that fragmentation has occurred before column

chromatography, what would result in fragments of the same metabolite entering the mass-spectrometer at different times.

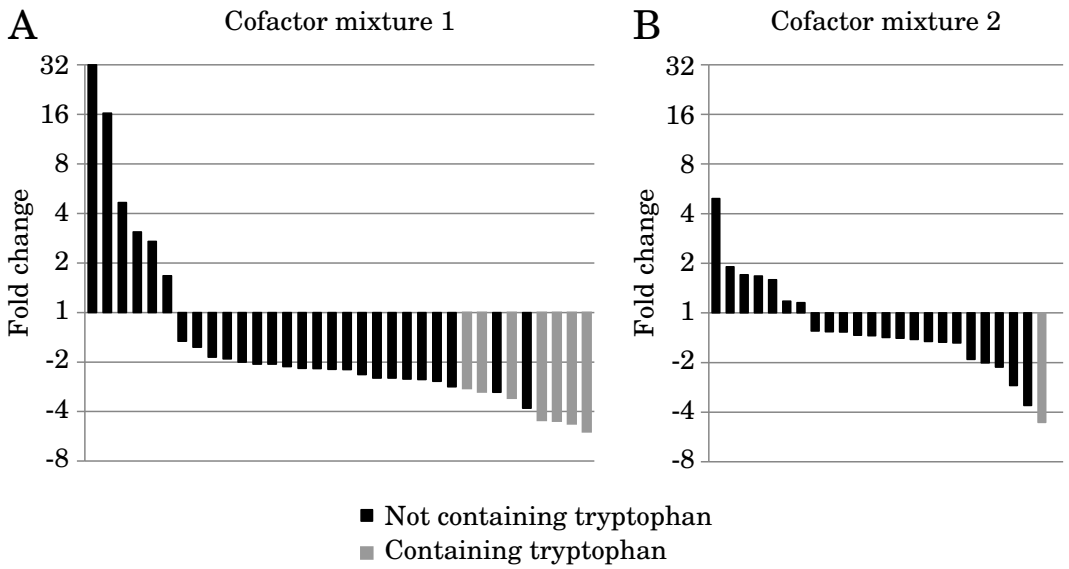

Figure 5.3.: Peptide changes in ARG metabolomics assay. Fold changes of significantly changed peptides (rank product, FDR<0.05) are shown for cofactor mixture 1 (*A*) and mixture 2 (*B*). Grey bars indicate peptides that contain tryptophan, while black bars indicate peptides that do not contain tryptophan.

The pattern of increased and decreased metabolites suggests that tryptophan is a substrate for ARG, while the indoles and quinolines are products. While the results suggest promiscuity of ARG, it is difficult to imagine an enzyme that uses one substrate to generate a wide range of products. It is possible that other substrates were decreased as well, but not detected in our data set.

Four of the increased indole-related compounds are the direct products of an EC-number assigned reaction that uses tryptophan as a substrate (Figure 5.5). Two of the reactions are oxygenases, members of a class of oxidoreductases that oxidise a substrate by the transfer of oxygen from molecular oxygen (O_2). Oxidation by dioxygenases often involves cleavage of aromatic rings in the substrate. The two non-oxygenase reactions are acyltransferases. This suggests that ARG might have a moonlighting function, where it is capable to catalyse two unique reactions, albeit here with additional promiscuity.

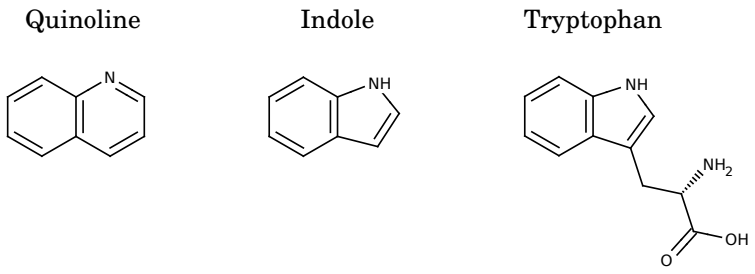

Figure 5.4.: Chemical structure of quinoline, indole and tryptophan.

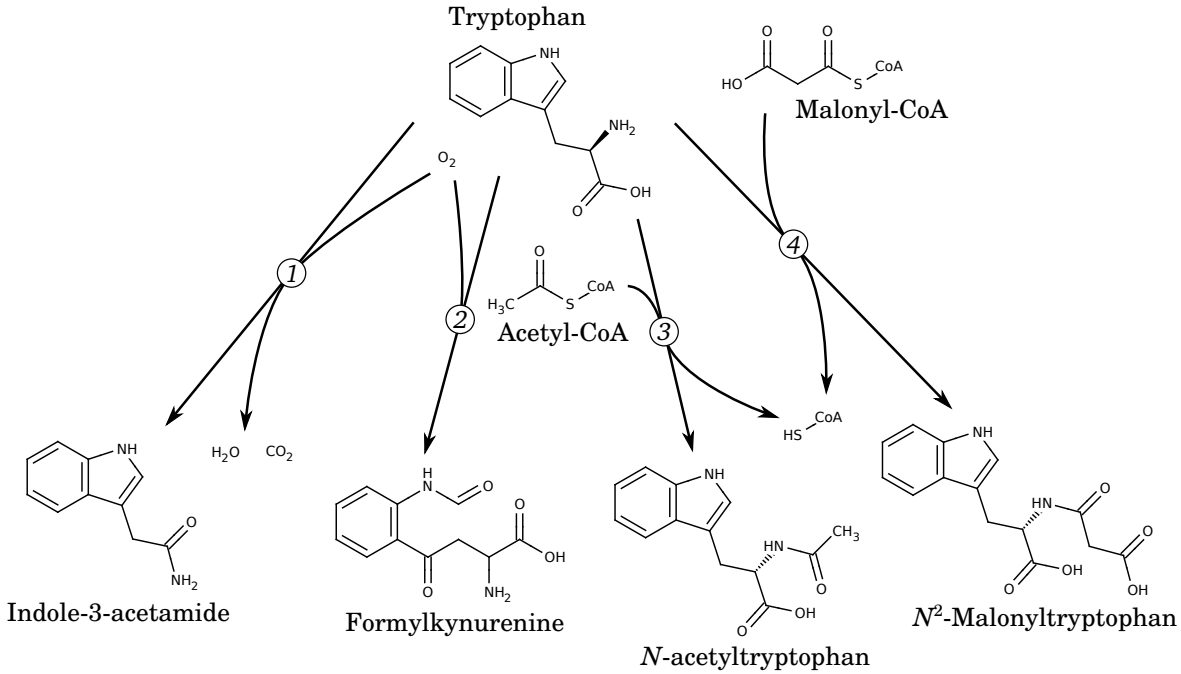

Figure 5.5.: Potential substrate-product pairs from ARG metabolomics assay. Metabolites on the bottom can all be produced from tryptophan by an EC-number assigned reaction. Reaction *1:* tryptophan 2-monooxygenase (EC 1.13.12.3); *2:* tryptophan 2,3-dioxygenase (EC 1.13.11.11); *3:* tryptophan N-acetyltransferase (EC 2.3.1.34); *4:* tryptophan N-malonyltransferase (EC 2.3.1.112).

Interestingly, the BRENDA[3], KEGG [4] and MetaCyc [5] databases indicate that most of the potential (EC-number assigned) reactions do not involve the cofactors that are provided in the two cofactor mixtures. FAD has been identified as a cofactor of tryptophan 2-monooxygenase (Hutcheson and Kosuge, 1985), but is present in both mixtures. Although the $NAD(P)^+$ present in cofactor mixture 1 might not directly take part in the catalysed reaction, it does increase the oxidation potential of the assay buffer. Also, although the assay buffer is pH 7, potentially the presence of the different cofactor mixtures caused a shift in the pH of the final assay mixture. The pH of the final assay mixtures was not determined, but could provide useful information, possible even more by measuring the pH before and after the incubation with purified enzyme.

5.2.1.3. ARG null mutant is less susceptible to trypanocidals

The ARG gene was further investigated by metabolic profiling. An ARG null mutant was generated by replacement of the endogenous ARG gene with antibiotic resistance genes by homologous recombination of the flanking regions. Clones were selected by applying the appropriate drug pressure, and successful replacement of the ARG gene by

[3]http://www.brenda-enzymes.info/
[4]http://www.genome.jp/kegg/
[5]http://metacyc.org/

a resistance gene was confirmed by PCR (Figure 5.6). Both alleles of ARG could readily be replaced, generating the genotypic strain Δ*arg::HYG/PAC*, hereafter referred to as Δ*arg*.

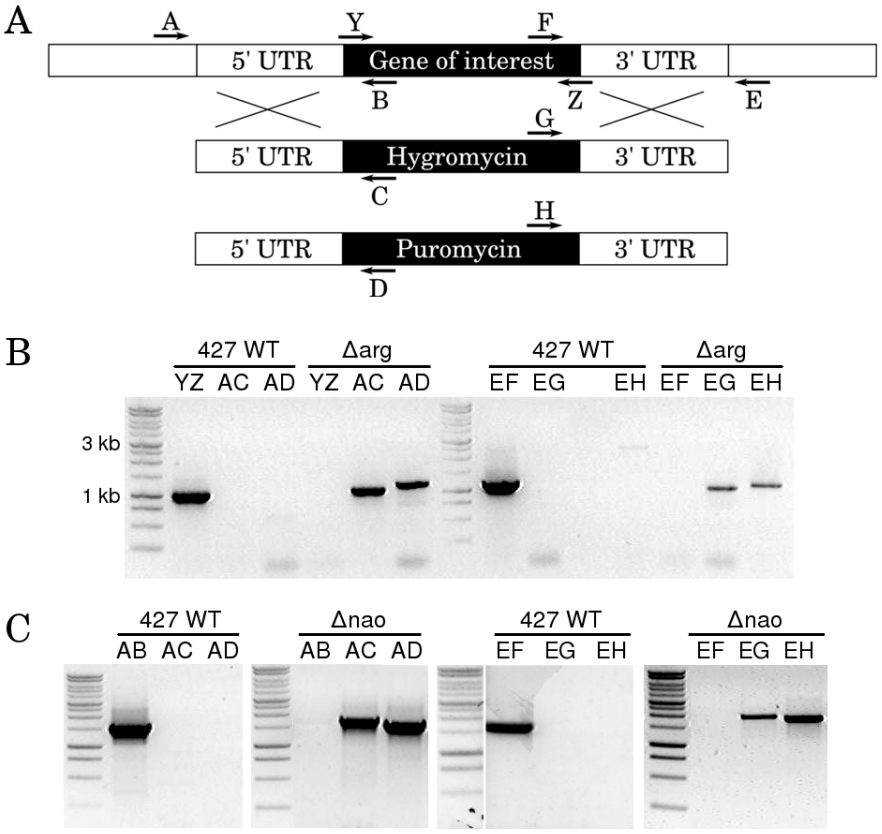

Figure 5.6.: Confirmation of genetic mutants by PCR. *A:* The strategy of PCRs used to confirm gene replacement. Arrows and letters indicate primers. PCR with primersets AB and EF indicates presence of the endogenous gene, primersets AC and EG indicate replacement of the endogenous gene with a hygromycin resistance gene, while primersets AD and EH indicate replacement of the endogenous gene with a puromycin resistance gene. Primers YZ indicates the presence of the endogenous gene. Primers A, B, E, F, Y and Z are unique for each gene of interest, all primer sequences are given in Table 2.1. *B:* PCR of wild-type 427 and Δ*arg*, with primers as indicated in *A*. *C:* PCR of wild-type 427 and Δ*nao*, with primers as indicated in *A*. Primerset AB for Δ*arg* did not amplify from wild-type 427 genomic DNA, and could therefore not be used to indicate gene replacement. Instead, the full gene was amplified (primerset YZ).

The Δ*arg* strain was maintained in HMI-9 medium in the presence of hygromycin and puromycin. Only a minor growth phenotype could be observed, likely due to the presence of the antibiotics (Figure 5.7). Antibiotics were removed from the culture medium prior to further experiments. AlamarBlue assays were performed with a selection of trypanocidals to investigate drug sensitivity and Δ*arg* is slightly less sensitive for most of the drugs (Table 5.3).

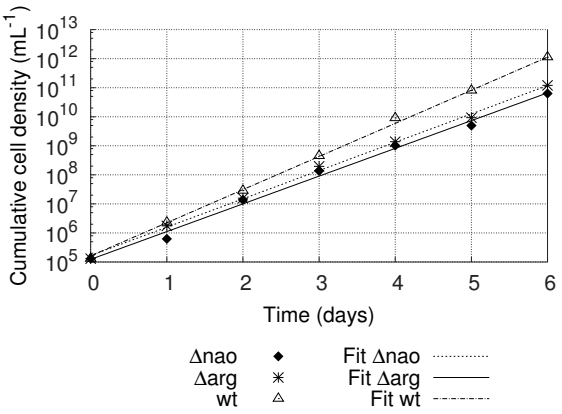

Figure 5.7.: Growth curves of various genetic mutants generated in this chapter. Cell densities were routinely kept between $1 \cdot 10^4$ and $2 \cdot 10^6$, cumulative cell counts are plotted, lines are fitted exponential growth curves.

Compound	Medium	IC_{50} (nM) WT	IC_{50} (nM) Δ*arg*	Ratio WT/ Δ*arg*	*p*-value
Suramin	HMI-9	37 ± 0.72	39 ± 10	1.1	0.86
	CMM	32 ± 4.1	30 ± 2.5	1.1	0.71
Melarsen oxide	HMI-9	11 ± 0.98	7.0 ± 2.3	0.66	0.021
	CMM	10 ± 2.9	15 ± 1.6	0.69	0.24
DFMO	HMI-9	23 ± 2.8 µM	49 ± 1.9 µM	0.48	0.0018
	CMM	12 ± 1.6 µM	21 ± 2.4 µM	0.59	0.027
Berenil	HMI-9	29 ± 3.5	48 ± 4.6	0.61	0.019
	CMM	16 ± 1.6	13 ± 3.3	1.2	0.48
5-fluorouracil	HMI-9	21 ± 3.1 µM	35 ± 2.6 µM	0.59	0.018
	CMM	1.5 ± 3.3 µM	2.2 ± 4.3 µM	0.70	0.28
Methylene blue	HMI-9	23 ± 5.3	92 ± 6.6	0.25	0.00021
	CMM	24 ± 3.7	53 ± 9.4	0.46	0.037

Table 5.3.: Toxicity of various trypanocidals in Δ*arg* and wild-type parasites. AlamarBlue assays were used to determine IC_{50} values in both Δ*arg* and wild-type (WT) parasites, in both HMI-9 and CMM culture medium. SEM; $n \geq 3$; Student's *t*-test, two-tailed, unequal variance.

5.2.1.4. ARG null mutant affects phosphocholines, PPP and methionine metabolism

The metabolome of Δ*arg* parasites was measured and compared to wild-type during growth in CMM medium, a reduced medium formulation optimised for high-quality metabolomics experiments (unpublished; Dr Darren Creek, University of Melbourne). The growth in CMM medium was similar to growtn in HMI-9 medium. The samples

were analysed by LC-MS, and two complementary runs were performed with hydrophilic interaction chromatography using ZIC-HILIC and ZIC-pHILIC columns, in an attempt to increase the coverage of the metabolome. The metabolomics data was deconvoluted and analysed with the mzMatch/IDEOM pipeline.

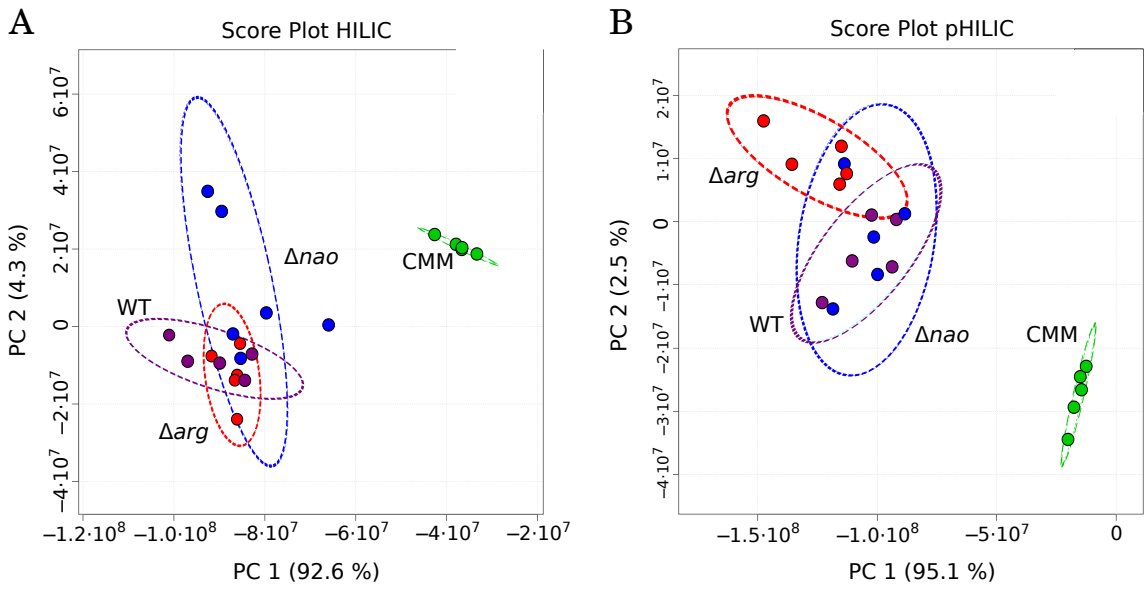

Figure 5.8.: Correlation of metabolomes of different genetic mutants. The correlation of the metabolomes of wild-type, Δ*nao* and Δ*arg* was compared by principle component analysis using all basepeaks. Depicted are the score plots of the first two principal components of the ZIC-HILIC (*A*) and ZIC-pHILIC (*B*) chromatography runs. Dotted lines are the 95% confidence interval. There is no clear separation between wild-type (WT), Δ*nao* and Δ*arg* samples. Medium samples (CMM) are well separated from the parasite samples.

A principal component analysis (PCA) was performed on all potential basepeaks identified from the samples. PCA is a mathematical procedure that reduces multidimensional data, which in metabolomics data sets is based on the numerous metabolites compared. PCA transforms the data points to a reduced number of principle components (PC) in such a way that the first principle component accounts for most of the variability within the data set. PCA is often utilised as an initial step prior to further analysis, to visualise general trends between the different samples in a data set (Sumner *et al.*, 2003).

PCA analysis of all potential basepeaks identified from the samples showed that the metabolome of Δ*arg* is barely distinguishable from the metabolome of wild-type parasites (Figure 5.8). Looking at individual metabolites, around 70 metabolites change significantly (Section D.4), with almost half of the changes in lipids. Within the lipids, a shift was observed from ether phosphatidylcholines (PC) to PCs with an ester group (Figure 5.9). Ether lipids are synthesised from dihydroxyacetone phosphate, while

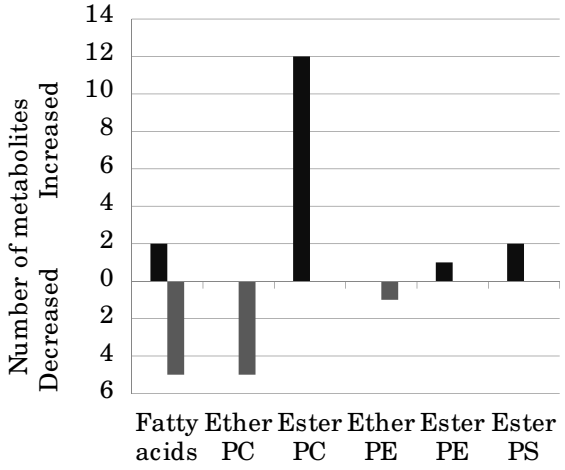

Figure 5.9.: Changes in lipid concentrations of Δ*arg*. The number of lipids and fatty acids that either increased or decreased significantly in the Δ*arg* strain (rank product, FDR<0.05). Grouped by fatty acids, ether and ester phosphatidylcholines (PC), ether and ester phosphatidylethanolamine (PE) and ester phosphatidylserine.

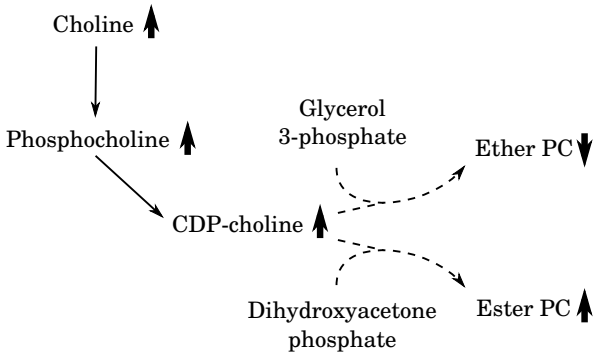

Figure 5.10.: Biosynthetic pathway of phosphatidylcholines. Thin lines indicate reactions, dashed line represents multiple reactions, and bold arrows indicate an increase or decrease of the metabolite in Δ*arg*. PC: phosphatidylcholine.

glycerol 3-phosphate is the precursor for ester lipids (Figure 5.10). Concordant to a turnover of PCs is the increase in precursors of PCs: choline, phosphocholine and CDP-choline (Figure 5.11).

Most of the remaining changes are orientated around two pathways: the PPP (PPP) and methionine metabolism (Figure 5.11). Most intermediates of the PPP are increased in the Δ*arg* strain. An increase in metabolic intermediates can have various causes: (i) impaired ability to use the end-product of the pathway; (ii) increased availability of the pathway's substrate; (iii) activation of the pathway as a secondary effect. Additionally, changes in one metabolite can have knock-on effect and cause additional metabolites in the same pathway to change. These possibilities can complicate the identification of the primary effect of the loss of the gene of interest.

The increase in PPP intermediates is accompanied by an increase in NADPH (Section D.4). The PPP can be activated at increase of oxidative stress (see Chapter 3, and Maugeri

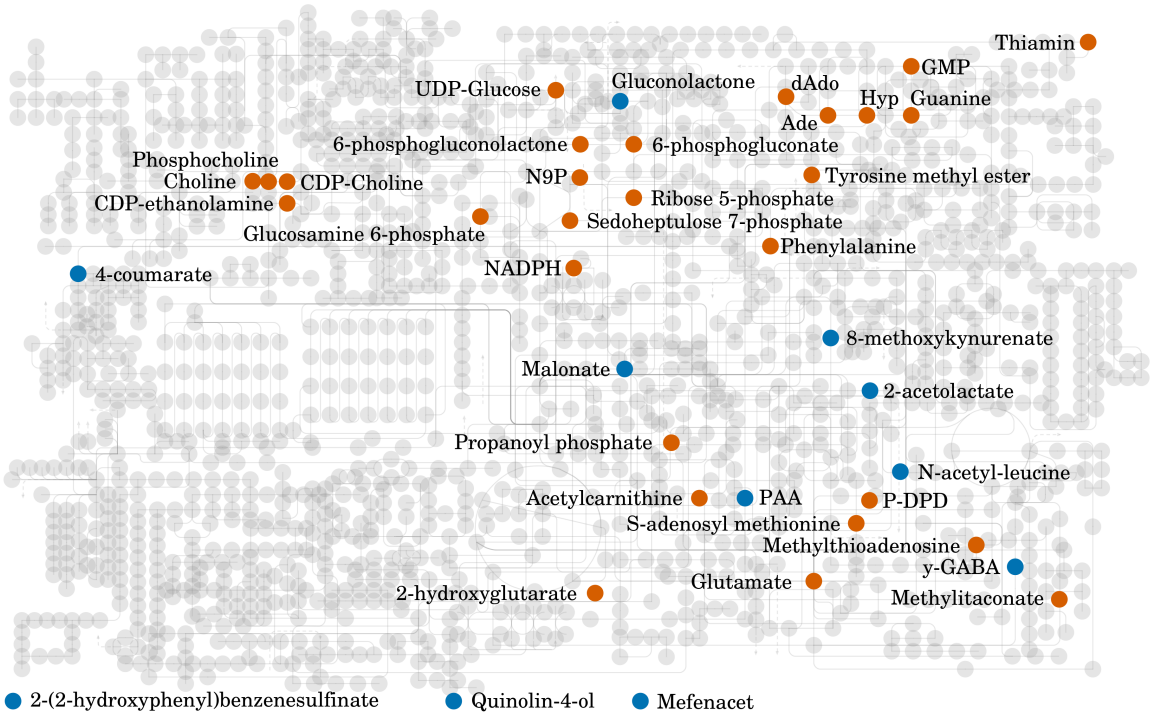

Figure 5.11.: Schematic map of metabolite changes in Δ*arg*. Metabolic changes are painted on a non-species specific metabolic map, based on KEGG IDs (Yamada *et al.*, 2011). Increased metabolite concentrations are in red, decreased in blue. At the bottom are metabolite that are not part of, or closely related, to any pathway. Ade: adenine; dAdo: deoxyadenosine; y-GABA: gamma-glutamyl-gamma-aminobutyraldehyde; Hyp: hypoxanthine; N9P: nonulose 9-phosphate P-DPD, 4-hydroxy-2,3-pentanedione-5-phosphate; PAA, phenylacetic acid.

et al., 2003; Maugeri and Cazzulo, 2004), but that does not seem to be the cause here. The higher NADPH level of the parasites renders them less susceptible to methylene blue and many other drugs that are suspected to increase oxidative stress (Table 5.3). It seems that the loss of ARG requires the parasites to compensate by augmenting their PPP, with the increased oxidative stress protection as a side-effect, rather than an activation of the PPP due to oxidative stress.

Besides NADPH, the PPP also provides Rib-5-P that can be used in nucleotide biosynthesis. Phosphoribosylpyrophosphate (PRPP) is produced from Rib-5-P while the phosphoribosyl-group can subsequently be transferred to a nucleobase (e.g. adenine) to form a monophosphate nucleoside (e.g. AMP). Besides adenine, also hypoxanthine and guanine were increased upon the loss of ARG (Figure 5.11).

The second major pathway affected in the Δ*arg* strain is methionine metabolism: metabolites as S-adenosyl methionine (SAM) and methylthioadenosine (MTA) are increased in Δ*arg*. Interestingly, there is a connection with the original proposed annotation of ARG as an arginase, as decarboxylated SAM is used in the biosynthesis of spermidine from the putrescine that is produced from ornithine. However, no significant changes in arginine, ornithine, *N*-acetylornithine, or other polyamines were observed. Adenine is a by-product of methylthioadenosine degradation, potentially connecting the changes in methionine metabolism to the changes in nucleobases and PPP intermediates. SAM connects to phosphatidylcholine metabolism, as CDP-ethanolamine can be converted to PC in a series of biochemical reactions.

While connections can be drawn between the metabolic changes, it remains unclear what exactly is the primary effect of loss of ARG. Furthermore, there seems to be very little overlap with the results of the metabolomics enzyme assay with recombinant ARG. The only change related to tryptophan metabolism is the decrease of 8-methoxykynurenate, but neither this metabolite nor close neighbours in tryptophan metabolism seem to be involved in any of the other changed metabolites in Δ*arg*.

5.2.1.5. Different functions suggested for ARG

The metabolomics enzyme assay suggested that ARG has a function related to tryptophan or other indoles, with an indication of a potential oxygenase function. While the metabolic profiling uncovered significant changes in a number of metabolites, and these changes are potentially connected to each other, it did not provide support for a tryptophan-related function. Moreover, I was unable from the metabolic profiling to

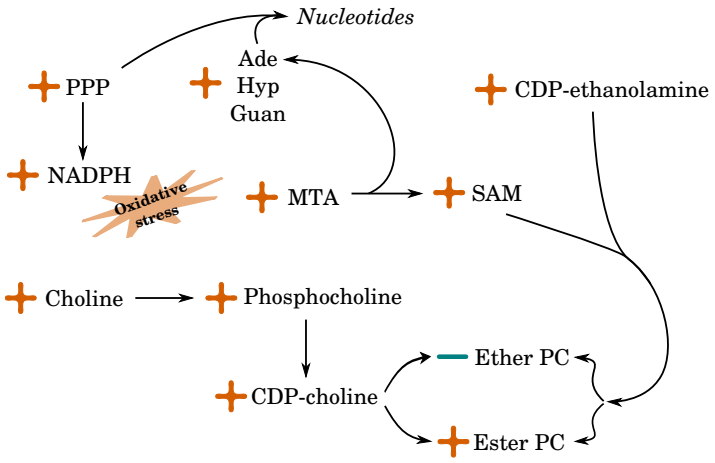

Figure 5.12.: Possible connection of observed changes in Δ*arg*. Arrows do not necesarily represent one reaction. Direction of the arrow indicates a hypothetical causative connection.

distinguish between the primary effect of ARG loss, the secondary effect and potential compensatory changes.

Especially the lack of concordance between the numerous tryptophan related changes in the metabolomics assay and only 8-methoxykynurenate changing upon loss of ARG seems problematic to pinpoint the function of ARG.

5.2.2. Putative *N*-acetylornithine deacetylase

From earlier metabolomics experiments it became apparent that treatment of *T. brucei* with eflornithine results in similar changes in levels of ornithine as of *N*-acetylornithine (Vincent *et al.*, 2012). As *T. brucei* lacks arginase activity there is a possibility that *N*-acetylornithine is part of an alternative ornithine biosynthetic pathway (see 1.6.1, and Vincent, 2011). The *T. brucei* genome contains a gene that has been putatively annotated as an *N*-acetylornithine deacetylase (NAO, Tb427.08.1910), and this gene is investigated here in more detail.

5.2.2.1. Metabolomics assay confirms deacetylase function

For the metabolomics assay with NAO, a polyhistidine-tagged recombinant version of the NAO gene was heterologously expressed in *E. coli* and purified with immobilised metal affinity chromatography. Purification yielded a single band on SDS-PAGE of approximately 45 kDa. A metabolomic enzyme assay was performed as described above for ARG. The number of significantly changed metabolites (rank product, FDR<0.05)

was roughly 2.5-fold higher in cofactor mixture 1, with 65 changes compared to 23 changes in mixture 2 (Supplement 1.1.4). Unlike in the ARG assay, however, there was little difference in fold-changes in metabolites that were significantly changed in both mixtures (Table 5.4), suggesting that none of the mixture-specific cofactors were required.

The changed metabolites propose that NAO is an *N*-acyl-amino acid deacetylase with a broad substrate specificity. Javid-Majd and Blanchard (2000) have characterised *E. coli N*-acetylornithine deacetylase and found a similar substrate specificity: the highest activities were found using *N*-formylmethionine and *N*-acetylmethionine, while also numerous of other acetylated amino acids could function as substrates. Interestingly, four of the consistent changed metabolites were related to kynurenine (Table 5.4). In the ARG assay, a number of kynurenine related metabolites were all increased, while the kynurenine related changes in the NAO assay are decreased. This further questions the significance of the kynurenine related changes that were observed in the ARG assay. The only consistently increased metabolite in the NAO assay is fumarate. The reason for this increase remains unclear, as no other fumarate related metabolites are changing.

Measured mass	Retention time (min)	Predicted formula	Isomers	Putative metabolite	Fold change	
					Mix 1	Mix 2
116.01107	6.26	$C_4H_4O_4$	3	Fumarate	5.20	4.18
252.07445	12.14	$C_{11}H_{12}N_2O_5$	1	5-Hydroxy-N-formylkynurenine	-1.36	-1.69
189.04255	5.82	$C_{10}H_7NO_3$	6	Kynurenate	-1.50	-2.47
264.07438	5.95	$C_{12}H_{12}N_2O_5$	1	Diformylkynurenine	-1.58	-1.56
173.10506	5.73	$C_8H_{15}NO_3$	5	N-Acetyl-L-leucine	-1.67	-1.61
205.03768	5.66	$C_{10}H_7NO_4$	2	6-Hydroxykynurenate	-2.03	-5.29
207.08962	5.68	$C_{11}H_{13}NO_3$	6	N-Acetyl-L-phenylalanine	-2.18	-2.18
177.04598	5.94	$C_6H_{11}NO_3S$	3	N-Formyl-L-methionine	-3.62	-4.20
191.06129	5.89	$C_7H_{13}NO_3S$	1	N-Acetylmethionine	-4.88	-3.85

Table 5.4.: Significantly changed metabolites in NAO assay. Metabolites that showed significant changes in both cofactor mixtures are shown. Measured mass as mass-to-charge ratio (m/z); number of isomers as predicted from IDEOM databases. Negative fold-changes indicate decreased metabolites.

5.2.2.2. Metabolome of NAO null mutant shows limited changes

An NAO null mutant (Δ*nao*) was generated as described previously for ARG (Figure 5.6 and Figure 5.7). The metabolome of the Δ*nao* strain was measured by LC-MS and compared to wild-type parasites. Principal component analysis demonstrated limited separation of the null mutant from wild-type parasites (Figure 5.8). This is further supported by studying the putative metabolites: only 26 putatively identified metabolites changed significantly (rank product, FDR<0.05, Supplement 1.1.5).

Of the significantly changed metabolites, only *N*-acetylmethionine was also changed in the enzyme metabolomics assay (cf. and Table 5.4 and Table 5.5). In Δ*nao*, methionine did not change significantly, but the decrease in 5'-methylthioadenosine (MTA) could be connected to the loss of NAO (Figure 5.13). *N*-acetylmethionine, however, is not a classical source for methionine synthesis, as it is normally produced from cysteine via cystathionine and homocysteine. *N*-acetylornithine does not change, with non-significant fold-changes of 0.73 and 1.21 from the analysis with ZIC-HILIC and ZIC-pHILIC chromatography respectively. Also ornithine does not change significantly, with fold-changes of 1.08 and 1.19.

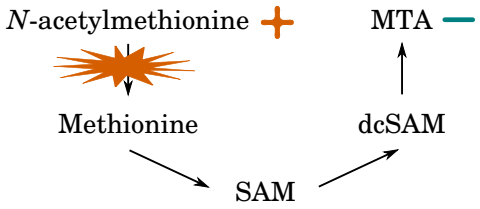

Figure 5.13.: Potential connection between changes in *N*-acetylmethionine and MTA. Levels of *N*-acetylmethionine are increased in Δ*nao*, while methylthioadenosine (MTA) is decreased. The star indicates the perturbation of *N*-acetylornithine deacetylase. SAM: *S*-adenosyl-methionine; dcSAM: decarboxylated SAM.

Chromatography	Measured mass	Retention time (min)	Predicted formula	Isomers	Putative metabolite	Fold change	FDR
pHILIC	154.00305	12.32	$C_3H_7O_5P$	3	Propanoyl phosphate	-1.46	0.0381
	135.05453	9.92	$C_5H_5N_5$	1	Adenine	-1.63	0.0427
	112.02734	8.59	$C_4H_4N_2O_2$	2	Uracil	-1.73	0.0487
	297.08976	7.36	$C_{11}H_{15}N_5O_3S$	2	*5'-Methylthioadenosine*	-1.78	0.00161
	247.06925	17.94	$C_9H_{13}NO_7$	1	N-Succinyl-L-glutamate	-2.12	0.0162
	339.99585	19.67	$C_6H_{14}O_{12}P_2$	14	D-Fructose 1,6-bisphosphate	-2.79	<0.0001
HILIC	191.06171	5.94	$C_7H_{13}NO_3S$	1	N-Acetylmethionine	2.97	0.000284
	297.08978	11.33	$C_{11}H_{15}N_5O_3S$	2	*5'-Methylthioadenosine*	-1.50	0.0189
	422.08255	17.26	$C_{12}H_{23}O_{14}P$	5	Trehalose 6-phosphate	-2.13	0.0206

Table 5.5.: Metabolic changes in Δ*nao*. Significantly changed metabolites (rank product, FDR<0.05, n=5) in Δ*nao* compared to wild-type. Peptides, lipids and fatty acids are not shown (see Supplement). Results are ordered by LC-column, and by fold-change. Measured mass as mass-to-charge ratio (m/z); number of isomers as predicted from IDEOM databases. Negative fold-changes indicate decreased metabolites.

The limited metabolomic response to loss of NAO is not completely unexpected if NAO is indeed an *N*-acetylornithine deactylase. The *T. brucei* genome contains a putative aminoacylase gene (Tb427tmp.01.3000), that would be able to compensate for the loss of NAO. In bacteria, heterologous expression of an aminoacylase was able to complement mutants defective in *N*-acetylornithine deacetylase activity (Sakanyan *et al.*, 1993). Although bacteria NAO and aminoacylase both have broad substrate specificities, they do differ substantially in deacetylating capacity depending on the amino acid. While NAO has the highest activities with *N*-formyl- and *N*-acetyl-methionine (Javid-Majd and Blanchard, 2000), aminoacylase has the highest activity with *N*-acetyl-alanine (Sakanyan *et al.*, 1993).

To annotate *T. brucei* NAO as *N*-acetylornithine deacetylase, however, can be misleading, as the highest activity is not observed with *N*-acetylornithine. In bacteria the NAO gene (ArgE) is located in the *argECBH* operon, together with other enzymes involved in arginine biosynthesis (Meinnel *et al.*, 1992), providing rationale for this annotation. *T. brucei* on the other hand does not produce ornithine via a similar pathway from glutamate (Vincent, 2011), suggesting that NAO might have an alternative role in *T. brucei*. Aminoacylases do not tend to have extreme thermodynamic equilibria, with a

typical equilbrium constant under standard conditions in the range of 3−33 (Goldberg *et al.*, 2004). The function of NAO could therefore easily be in either direction, the acetylation or deacetylation of (acetylated) amino acids.

5.2.2.3. NAO does not affect eflornithine sensitivity

Treatment of parasites with the ornithine decarboxylase inhibitor eflornithine results in changes in *N*-acetylornithine that correlate with changes in ornithine, as shown by Vincent (2011). It was therefore anticipated that the knockout of NAO might affect the eflornithine sensitivity of the parasite. Sensitivity assays by alamarBlue showed a significant but limited reduction in IC_{50} value (Table 5.6).

	IC_{50}(μM)			
Medium	WT	Δ*nao*	Ratio	*p*
HMI-9	49.4 ± 4.2	36.1 ± 6.4	0.73	0.016
CMM	20.8 ± 5.4	15.8 ± 6.9	0.76	0.28

Table 5.6.: Eflornithine sensitivity of Δ*nao*. Drug sensitivity to eflornithine (20 mM – 4.8 nM) was assayed by alamarBlue in two types of medium and compared between wild-type and Δ*nao* strain parasites. SD, $n \geq 3$, Student's *t*-test, two-tailed, unequal variance.

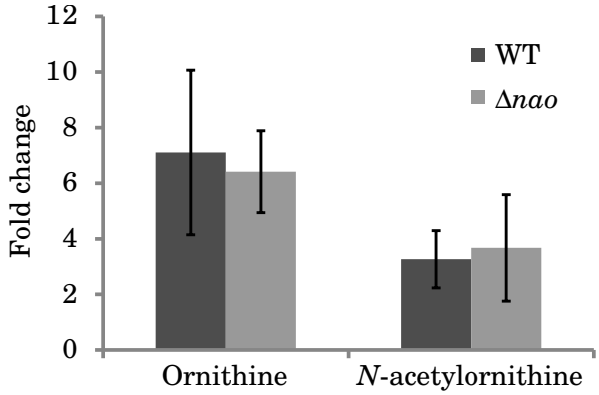

Figure 5.14.: Changes in metabolites upon eflornithine treatment. The fold change of ornithine and *N*-acetylornithine in Δ*nao* is similar to the fold change in wild-type cells, upon a 5 hour treatment with 500 μM eflornithine (WT data from Vincent *et al.*, 2012, measured with an identical experimental setup). Error bars are standard deviations.

The metabolome of eflornithine treated parasites was determined by treatment of Δ*nao* cells with DFMO for 5 hours prior to metabolite extraction. The metabolome was compared to wild-type parasites treated in an identical experiment (Vincent *et al.*, 2012). Calculating fold changes between treated and untreated parasites reduces the technical

variability and allows to compare the two separate experiments. No significant changes in the response to DFMO in wild-type parasites (Figure 5.14).

5.2.3. Putative nicotinamidase

Metabolomics experiments in our lab showed interesting changes in nicotinamide levels in parasites upon treatment with the drug SDG66, a compound designed with a P2-motif for recognition by the P2-transporter (Barrett *et al.*, 1995), and a nitro group for potential oxidative toxicity. Upon treatment with SDG66, untargeted metabolomics by an identical approach as used in this thesis demonstrated that nicotinate levels increased significantly, while nicotinamide levels decreased (Dr Pui Ee Wong, University of Glasgow). Although addition of nicotinamide did not rescue the parasites from the trypanocidal effects of SDG66, it does suggest involvement of nicotinamidase in the drug action of SDG66 (Figure 5.15). The *T. brucei* genome contains putatively annotated nicotinamidase (NAM) genes, and it was therefore decided to investigate these further.

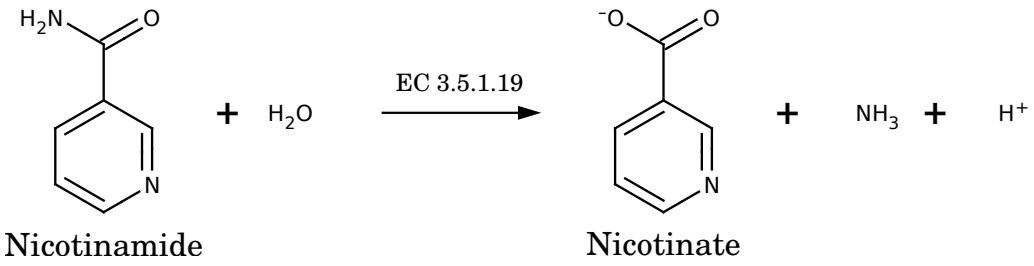

Figure 5.15.: Reaction catalysed by nicotinamidase.

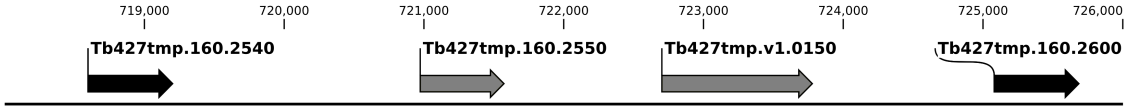

Figure 5.16.: Nicotinamidase gene within the *T. brucei* strain 427 genome. The two nicotinamidase genes (black) are separated by two putative genes (grey). Tb427tmp.160.2550 is annotated as "ribosomal protein S7, putative", while Tb427tmp.v1.0150 is annotated as "hypothetical protein, conserved".

5.2.3.1. Nicotinamidase function confirmed by metabolomics enzyme assay

There are two copies of the nicotinamidase gene in the *T. brucei* genome (Tb427tmp.160.2540 and Tb427tmp.160.2600), with 100 % sequence identity (Figure 5.16). For heterologous expression, the NAM gene was amplified and cloned

into pET-30 Xa/LIC. Expression and purification resulted in a protein of approximately 24 kDa.

The NAM enzyme was investigated by a metabolomics assay identical to ARG and NAO. Data deconvolution by mzMatch and IDEOM resulted in the putative identification of 652 metabolites. In concordance with the ARG and NAO assays, cofactor mixture 1 resulted in more significantly changed metabolites in comparison to cofactor mixture 2, with 45 and 29 changes respectively, while the fold-changes themselves were comparable in both mixtures (Table 5.7).

Striking in the list of significantly changed metabolites is the combination of an increase in nicotinate (average peak intensity from $10 \cdot 10^5$ to $28 \cdot 10^5$) and a decrease in nicotinamide (average peak intensity from $30 \cdot 10^5$ to $2.4 \cdot 10^5$). These are the substrate and product of nicotinamidase, confirming the activity of NAM. *T. brucei* nicotinamidase is also capable of hydrolysing amino groups from other substrates. This is demonstrated by the decrease in *N*-acetyl-beta-alanine and increase in 2-acetolactate, and similar for succinamate and succinate, however, nicotinamide and nicotinate showed the largest fold changes. Nicotinamidases are known to hydrolyse the drug pyrazinamide (Hu *et al.*, 2007; Zhang *et al.*, 2008; Fyfe *et al.*, 2009), a compound highly related to nicotinamide and only differing in an additional nitrogen in the aromatic ring. The changes in succinamate and N-acetyl-beta-alanine potentially show an even further reduced specificity of nicotinamidase.

Crystallography of yeast nicotinamidase has characterised the binding and activation of zinc to the enzyme (Hu *et al.*, 2007). No zinc was specifically added to the growth medium and assay buffer during the study of *T. brucei* NAM, but it is plausible that the yeast extract used in both the LB growth medium and the complex metabolite mixture contains zinc. The mass of zinc is too low to be detected with our mass spectrometry instruments.

5.2.3.2. Attempt to ablate NAM by RNA interference

A knockdown mutant by RNAi was generated for NAM instead of a knockout. The two *T. brucei* nicotinamidase genes (Tb427tmp.160.2540 and Tb427tmp.160.2600) are located in close proximity to one another on chromosome 9, but are separated by two other genes (Figure 5.16). The 5' and 3' UTR of the two nicotinamidase genes are also identical, suggesting that the gene has been duplicated. A knockout strategy where each copy is targeted individually is impossible due to the identical UTRs. Replacing the

Measured mass	Retention time (min)	Predicted formula	Isomers	Putative metabolite	Fold change	
					Mix 1	Mix 2
123.03210	7.46	$C_6H_5NO_2$	4	Nicotinate	2.81	2.64
309.10597	17.27	$C_{11}H_{19}NO_9$	5	N-Acetylneuraminate	2.45	1.32
132.04224	6.13	$C_5H_8O_4$	16	2-Acetolactate	1.94	1.18 [a]
222.06736	22.74	$C_7H_{14}N_2O_4S$	4	L-Cystathionine	1.92	1.10 [a]
116.01094	6.12	$C_4H_4O_4$	3	Fumarate	1.51 [a]	1.91
147.05319	16.64	$C_5H_9NO_4$	14	L-Glutamate	1.83	1.12 [a]
189.06379	7.16	$C_7H_{11}NO_5$	4	N-Acetyl-L-glutamate	1.79	1.00 [a]
118.02663	6.43	$C_4H_6O_4$	7	Succinate	1.64	1.14 [a]
133.03753	17.59	$C_4H_7NO_4$	4	L-Aspartate	1.57	1.05 [a]
308.15822	27.02	$C_{12}H_{24}N_2O_7$	2	Fructoselysine	1.38	-1.10 [a]
345.04732	15.69	$C_{10}H_{12}N_5O_7P$	3	3',5'-Cyclic GMP	1.27	1.10 [a]
135.05462	14.54	$C_5H_5N_5$	1	Adenine	1.24 [a]	1.25
131.05820	6.58	$C_5H_9NO_3$	14	N-Acetyl-beta-alanine	-1.41	-1.22 [a]
189.10014	6.23	$C_8H_{15}NO_4$	5	2 -(Butylamido)-4-hydroxybutanoic acid	-1.27 [a]	-1.43
117.04262	6.74	$C_4H_7NO_3$	5	Succinamate	-1.43	-1.22 [a]
72.05753	5.66	C_4H_8O	4	Butanal	-1.23 [a]	-1.64
129.15178	11.08	$C_8H_{19}N$	2	Octylamine	-1.89	-1.64
147.05316	7.70	$C_5H_9NO_4$	14	N-hydroxy-N-isopropyloxamate	-1.25 [a]	-1.75
145.15790	43.66	$C_7H_{19}N_3$	1	Spermidine	-2.11	-1.43 [a]
122.04802	8.63	$C_6H_6N_2O$	4	Nicotinamide	-17.7	-10.0

[a] Non-significant change (rank product FDR>0.05).

Table 5.7.: Significantly changed metabolites in NAM assay. Shown are metabolites that changed significantly in at least one of the two mixtures (rank product FDR<0.05), excluding peptides and lipids. Measured mass as mass-to-charge ratio (m/z); number of isomers as predicted from IDEOM databases. Negative fold-changes indicate decreased metabolites.

whole region, however, would additionally replace the two genes in between. Although these two genes are annotated as hypothetical and putative, I decided that the risk of an effect by disturbing those genes was undesired. Instead, RNA interference was used to ablate the NAM protein. Both NAM transcripts would be targeted equally due to the identical sequences.

The *NAM*^{RNAi} strain was constructed by amplification and cloning of a 544 bp fragment in the pRPaSLi plasmid (as explained in 2.2.2), and subsequent transfection of 2T1 parasites. Successful integration of the construct was confirmed by the gain of hygromycin resistance, and puromycin sensitivity. Induction of RNA interference by addition of tetracycline to the culture medium did not result in a growth phenotype of *NAM*^{RNAi} (Figure 5.7), however, Northern blot failed to provide conclusive evidence of knockdown of the NAM transcript (Figure 5.17). A ^{32}P labelled dATP was used to generate a radioactive probe from the whole RK gene. After probing the Northern blot, clear bands could only be identified in the tetracycline-induced samples. However, these bands were much further to the bottom of the blot than expected from the expected molecular weight of NAM transcript. NAM has a comparable molecular weight to tubulin, that had been used as a control to confirm presence of transcript in all samples (Figure 5.17). As the tubulin control did indicate transcript in all samples, and the low-molecular weight bands after probing with NAM only occurred after addition of tetracycline, I hypothesised that the bands visualised with the NAM probe are the expressed RNAi fragments, and not the endogenous NAM transcripts. This suggests that NAM might not be expressed in this cell line, even though it has been demonstrated to been expressed previously. Additional experiments with alternative techniques, like quantitative PCR combined with reverse-transcription, would be required to further investigate this hypothesis.

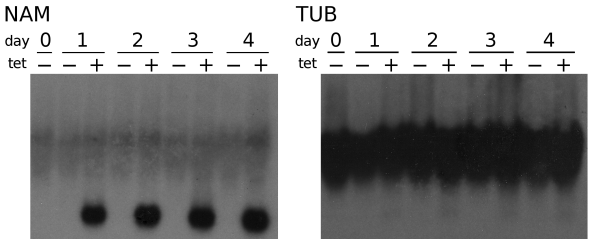

Figure 5.17.: Northern blot of *NAM*^{RNAi}. RNA samples were taken before and 0, 1, 2, 3 and 4 days after induction of RNAi with tetracycline (tet). Northern blot was probed with the full NAM gene or with a full tubulin (TUB) gene as control. RNA ladder was not visible. The tubulin genes are approximately 1.3 kb, the NAM gene is 615 bp. The NAM probe is only visible in samples with tetracycline, while the TUB blot, although overexposed, indicates equal loading of all samples.

The NAM^{RNAi} strains was investigated by metabolic profiling comparable to the Δarg and Δnao strains. RNAi was induced in independent cultures for 8 days prior to sampling, and the metabolome was compared between induced and non-induced NAM^{RNAi}. Samples were run only over a ZIC-HILIC column prior to mass spectrometry.

The metabolome of NAM^{RNAi} showed very limited changes after 8 days of induction (Table 5.8). Possible explanations for this result are that (i) NAM is not expressed in *T. brucei*, such that ablation has no effect (although Alsford *et al.* (2011) found NAM to be an abundant transcript); (ii) the level of NAM transcript was not reduced at all, or only by an insignificant amount (the Northern blot was inconclusive); (iii) NAM is expressed in *T. brucei*, and the transcript level was significantly reduced by RNA interference, but the parasite adapts to the loss of NAM. However, the absence of proof that NAM was ablated in the parasites renders it impossible to infer why virtually no changes are observed.

While metabolic profiling did not provide any support for the elucidation of the function of *T. brucei* NAM, the metabolomics enzyme assay provided reasonable support for the functional annotation of NAM as a nicotinamidase.

Measured mass	Retention time (min)	Predicted formula	Isomers	Putative metabolite	Fold change	FDR
126.00820	12.02	$C_2H_7O_4P$	2	2-Hydroxyethylphosphonate	1.87	0.00054
297.08964	9.81	$C_{11}H_{15}N_5O_3S$	2	5'-Methylthioadenosine	1.63	0.00153
174.01642	7.84	$C_6H_6O_6$	3	cis-Aconitate	1.44	0.0267
147.03534	12.12	$C_5H_9NO_2S$	1	Thiomorpholine 3-carboxylate	1.38	0.0114
205.07376	5.90	$C_{11}H_{11}NO_3$	5	Indolelactate	1.38	0.0138
161.05108	10.38	$C_6H_{11}NO_2S$	1	allylcysteine	1.33	0.0275
173.06876	10.45	$C_7H_{11}NO_4$	6	N-Acetyl-L-glutamate 5-semialdehyde	1.31	0.0469
245.61693	29.44	$C_{18}H_{33}N_7O_9$	2	Arg-Thr-Thr-Asp	1.30	0.0371
763.51473	5.67	$C_{43}H_{74}NO_8P$	24	[PE (16:0/22:6)] 1-hexadecanoyl-2-(4Z,7Z,10Z,13Z,16Z,19Z-docosahexaenoyl)-sn-glycero-3-phosphoethanolamine	1.26	0.0459
189.08240	8.16	$C_8H_{15}NO_2S$	1	Prenyl-L-cysteine	1.26	0.0438
191.06153	5.88	$C_7H_{13}NO_3S$	1	N-Acetylmethionine	1.25	0.05
248.17771	5.16	$C_{16}H_{24}O_2$	13	[FA (16:4)] 4,7,10,13-hexadecatetraenoic acid	-1.27	0.0493
713.53575	5.88	$C_{40}H_{76}NO_7P$	5	PC(14:1(9Z)/P-18:1(11Z))	-1.31	0.0354
509.38484	9.81	$C_{26}H_{56}NO_6P$	8	LysoPC(O-18:0)	-1.32	0.0182
214.13167	14.89	$C_{10}H_{18}N_2O_3$	2	Val-Pro	-1.33	0.0377
181.04097	15.67	$C_5H_{11}NO_4S$	1	DL-Methionine sulfone	-1.33	0.0401
272.08383	5.18	$C_{19}H_{12}O_2$	2	7,8-benzoflavone	-1.38	0.0237

Table 5.8.: Metabolic changes in NAM^{RNAi}. All significantly changed metabolites are shown, including lipids and peptides. Measured mass as mass-to-charge ratio (m/z); number of isomers as predicted from IDEOM databases. Negative fold-changes indicate decreased metabolites.

5.3. Discussion

In this chapter I demonstrated the use of metabolomics in the investigation of unknown enzyme functions, and obtained mixed results.

5.3.1. Complicated metabolite changes observed in *T. brucei* ARG elucidation

A putative *T. brucei* arginase (ARG) did not demonstrate ureohydrolase activity, in line with previous investigations in the absence of arginase activity in *T. brucei* (Vincent, 2011). The metabolomics assay with ARG, where a recombinant version of ARG was incubated in a complex metabolite mixture, suggested instead a function related to the metabolism of tryptophan, indoles and quinolines. The large number of significantly changed metabolites complicates elucidation of the function of the enzyme of interest.

Substrate promiscuity of the enzyme could be the cause of numerous increases and decreases of metabolites. These increasing and decreasing metabolites due to substrate promiscuity can then be paired up to show the same chemical transformation for each pair. This was observed in the metabolomics assay with nicotinamidase: three pairs of metabolites showed opposite changes upon incubation with nicotinamidase, where the three increased compounds were the deaminated products of the three decreased compounds. In ARG however, the many increases in indoles and quinolines only seemed to be related to a decrease in tryptophan, what cannot be explained by substrate promiscuity.

While enzymes can have multiple functions in the cell, a phenomenon known as "moonlighting", it seems unlikely for one enzyme to be able to produce such a variety of products from one substrate, bringing up the suggestion that the purified ARG was contaminated with *E. coli* enzymes that would react with tryptophan. Although a number of tryptophan-related metabolites changed in the NAO assay, those changes were in the opposing direction compared to the ones observed in the ARG assay, arguing against contamination with *E. coli* enzymes as a recurring problem. In the NAM assay, none of the significant changes seem to be related to tryptophan. Overall, this supports that the consistent increases in indoles and quinolines in the ARG assay are specific for ARG, although the mechanism for this remains unclear. The different indoles and quinolines are not products of fragmentation by the mass spectrometer, as the retention times of the

compounds vary significantly, but it can not be excluded that the indoles and quinolines are fragments formed before the samples are run on the liquid chromatography system.

In contrast to the many changes in indoles and quinolines observed in the metabolomics assay, none of these metabolomics changes were present in the metabolic profiling of a *T. brucei* ARG null mutant. The loss of ARG seems to activate the PPP, resulting in increased NADPH production that makes the parasites less susceptible to oxidative stress. The activation of the PPP is potentially related to an increase in nucleobases, methionine metabolism and a switch of ether phosphatidylcholines to ester phosphatidylcholines. Although a network can be drawn connecting the changes observed upon loss of ARG, it is not clear whether those connections are causal, and which of the changes are the primary effect of loss of ARG. Curiously, there seems to be very limited overlap between the metabolomics assay and metabolic profiling results for ARG.

5.3.2. Should NAO be annotated as N-acetylornithine deacetylase?

While the analysis of ARG resulted in confusing results, the picture was clearer for the analysis of NAO. *T. brucei* NAO seems to be a broad substitute range *N*-acylamino acid deacetylase. The greatest changes were observed in *N*-acetylmethionine and *N*-formylmethionine, similar to NAO characterised from *E. coli* (Javid-Majd and Blanchard, 2000). The metabolic profiling of a NAO null mutant showed limited changes in the metabolome. It has been demonstrated that a *N*-acetylornithine deactylase null mutant of yeast can be compensated by the expression of an aminoacylase (Sakanyan *et al.*, 1993). Potentially the same happens in *T. brucei*, as the gene Tb427.01.3000 has been putatively annotated as aminoacylase.

While *T. brucei* NAO demonstrates the same broad substitute range as *E. coli* NAO, it remains debatable whether *T. brucei* NAO should be annotated as *N*-acetylornithine deacetylase. *E. coli* NAO is located in an operon with other enzymes of the glutamate-to-arginine biosynthetic pathway, indicating a specific function of *E. coli* NAO in deacetylation of *N*-acetylornithine, even though higher affinities are observed for *N*-acetylmethionine and *N*-formylmethionine. However, *T. brucei* does not produce arginine from glutamate, suggesting that it might play a different role in the parasites metabolism. Because of the broad substrate range it might be advisable to annotate *T. brucei* NAO as an “aminoacylase”, and define different aminoacylases to different classes depending on substrate specificity. This will need to be established empirically by assaying different aminoacylases.

5.3.3. NAM also seems to have a broader substrate range than predicted

Of the three *T. brucei* enzymes studied the putative nicotinamidase yielded the clearest results in the metabolomics assay. The most significant increases and decreases observed where in the natural substrate and product of nicotinamidase. Additionally, a number of other amines were decreased, while two of those could be paired by an increase of their deaminated form. This suggests a broader substrate specificity than typically given for nicotinamidases, that are known to be able to deaminate pyrazinamide as well.

5.3.4. Improvements on metabolomics enzyme function elucidation

The use of metabolomics in the elucidation of the three aforementioned *T. brucei* enzymes has brought to light a number of potential improvements to the experimental set-up used here.

While each assay was performed with two different cofactor mixtures, only ARG showed significant changes in the fold-changes of individual metabolites between the two mixtures. Surprisingly, mixture 1 consistently changed more metabolites, even in the NAO and NAM assays. It would be advisable also to include an assay where none of the oxidising, reducing, phosphorylating and dephosphorylating cofactors are added. Additionally, the effect of incubation of the metabolite mixture in the presence of cofactors, but without enzyme, might highlight changes occurring in the metabolite mixture due to the reducing potential of the cofactors, rather than the addition of the enzyme.

The numerous changes in the ARG metabolomics enzyme assay brings up the problem of carry-over of *E. coli* enzymes from the purification. It would therefore be informative to have an *E. coli* extract undergo the Ni^{2+} purification used here without heterologous expression of a recombinant protein, and to use the different fractions in a metabolomics enzyme assay. This addresses the potential affinity of *E. coli* proteins to the nickel-column, however, it is also possible that *E. coli* proteins bind to the recombinant protein and therefore co-elute simultaneously. The experimental approach could be improved by introducing point mutations at the active site of the enzyme, as predicted from sequence alignments. This would act as a suitable negative control. Nonetheless, the absence of similar significant changes of tryptophan related metabolites in the NAO and NAM

metabolomics enzyme assays suggest that the observed changes in the ARG assay are not due to contamination by *E. coli* protein binding to the column during purification.

For the metabolic profiling of knockouts, although the experiments typically consists of five biological replicates, it would be informative to use different clones for each replicate. Potentially, the clone used in the metabolic profiling has changed in an additional way, that is not typical for the loss of the gene of interest. Comparison of only one clone to wild-type parasites might therefore be misleading. This can be prevented by the use of RNAi mutants instead of null mutants, as the knockdown is induced independently for each replicate. However, RNAi has the risk that multiple transcripts are targeted and knocked-down. Additionally, the NAM results demonstrated that knockdown of the gene of interest might not be sufficient to result in changes in the metabolome.

Finally, the complexity of metabolomics experiments will always include variables that introduce uncertainty as to the interpretation of results. The combination of metabolomics enzyme assay and metabolic profiling helps to identify potential catalytic activities, however, it remains crucial to validate the putative function by a more classical enzyme assay, to provide higher certainty about the correct annotation.

Chapter 6

Why does the loss of 6PGDH kill trypanosomes?

The second enzyme of the PPP, 6PGDH, has been identified as a potential drug target in *T. brucei*, thriving the synthesis of potent inhibitors of this enzyme. It has been assumed that ablation of 6PGDH activity is lethal to the parasites as a result of a reduced glycolytic flux. However, this has not been confirmed experimentally, and it is plausible that the glycosomal localisation of glycolysis and the PPP in *T. brucei* affects the mode-of-action of 6PGDH ablation. The extended model generated in previous chapters is used in this chapter to investigate the effects of a loss of 6PGDH activity, and preliminary experimental results are shown that support the model predictions. This is an example of how the model generated in Chapter 3 can be used to investigate the behaviour of trypanosomal metabolism.

6.1. Introduction

Most of the current drugs against Human African trypanosomiasis are difficult to administer, unacceptably toxic, and relatively expensive when considering the impoverished state of most patients (Barrett *et al.*, 2007). It is anticipated that the parasites' divergent biochemistry will enable development of novel therapies for the disease.

6PGDH has been identified as a potential drug target, due to its divergent amino-acid sequence (Barrett and Le Page, 1993), and, as part of the PPP, as an important source of NADPH required by the parasite to maintain cellular redox potential and protect against oxidative stress (LePage and Barrett, 1990). The potential of 6PGDH as a drug target was confirmed when inhibition of 6PGDH was shown to be lethal to the parasite (Hanau *et al.*, 1996). Subsequently, effort has been made to design more potent and specific inhibitors of 6PGDH (Bertelli *et al.*, 2001; Pasti *et al.*, 2003; Dardonville *et al.*, 2003; Dardonville and Gilbert, 2003; Dardonville *et al.*, 2004). Although 6PGDH plays an important role in maintaining the cellular redox potential, it has been assumed that inhibition of 6PGDH is lethal to the parasite by a different mechanism.

Inhibition of 6PGDH leads to the accumulation of its substrate 6-phosphogluconate (6-PG), a potent inhibitor of the enzyme PGI (PGI, Figure 6.1A). PGI is part of the glycolytic pathway, and responsible for the isomerisation of glucose 6-phosphate to fructose 6-phosphate. Inhibition of 6PGDH activates a positive feedback loop: accumulation of 6-phosphogluconate causes inhibition of PGI, resulting in an increase of glucose 6-phosphate. Accumulation of glucose 6-phosphate directs the flux towards the PPP, consequently increasing the concentration of 6-PG even more (Figure 6.1B).

The activation of this feedback loop, and the deadly consequences of loss of 6PGDH activitiy, have been demonstrated previously. Bewley and Lucchesi (1975) described the lethality of *Drosophila* null mutants of 6PGDH and attributed this to the absence of a functional PPP. In 1977, however, Hughes and Lucchesi showed that an additional loss of glucose-6-phosphate dehydrogenase (G6PDH) rescues 6PGDH null mutants (Figure 6.1C). The absence of G6PDH activity prevents a flux through the PPP and the subsequent accumulation of 6PG. Similar results were obtained for yeast (Lobo and Maitra, 1982).

More recently, it was shown that the loss of 6PGDH inhibited growth of lung cancer cells, while no changes in NADPH and ribose 5-phosphate production were observed (Sukhatme and Chan, 2012). Possibly, NADPH levels are maintained by enhanced

glutaminolysis. Loss of G6PDH on the other hand did not affect cell growth, and rescued proliferation of cells deficient in 6PGDH. Moreover, growth on fructose instead of glucose also restored the proliferation of 6PGDH knockdown cells. Fructose bypasses the PPP, while any remaining inhibition of PGI does not affect the flux from fructose to the lower part of glycolysis (Figure 6.1D).

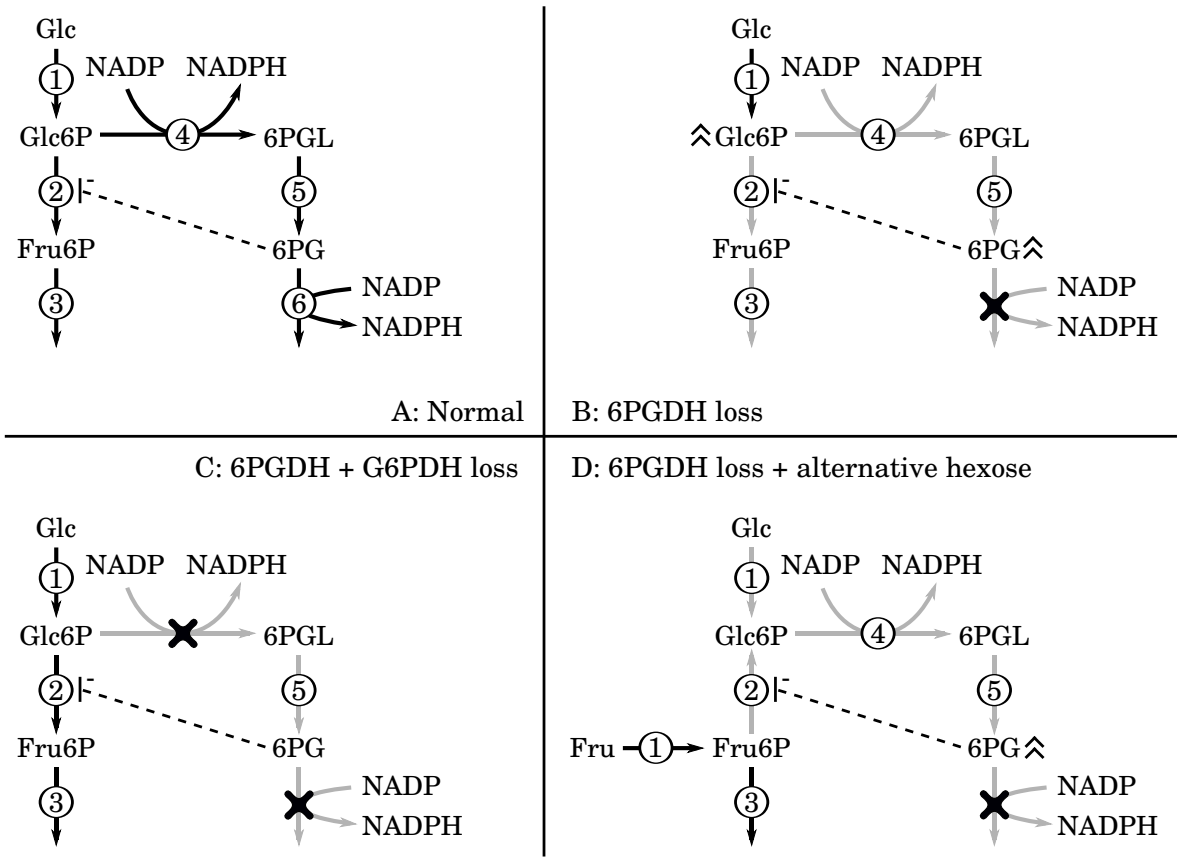

Figure 6.1.: Schematic overview of positive feedback loop of 6PGDH inhibition. Overview of the first reactions of both glycolysis and the PPP. Black arrows represent reactions with a flux, grey arrows are reactions with a reduced flux. Crosses indicate loss of activity and chevrons indicate accumulation of a metabolite. *A:* Distribution of fluxes in normal conditions, both glycolysis and PPP are active. *B:* Loss of 6PGDH activity results in accumulation of 6PG that inhibits PGI and forms a positive feedback loop. Glycolysis is inhibited. *C:* Loss of both 6PGDH and G6PDH activity prevents a flux through the PPP, preventing accumulation of 6PG. Glycolysis is restored. *D:* Loss of 6PGDH activity with an alternative source of hexose (here fructose), bypasses PGI. Any accumulation of 6PG does not affect the flux through the lower part of glycolysis. *1:* HXK, can use phosphorylate glucose and fructose; *2:* PGI; *3:* PRK; *4:* G6PDH; *5:* PGL; *6:* 6PGDH.

The same lethal mechanism is thought to be effective in *T. brucei* by analogy, as 6PG is also an inhibitor of *T. brucei* PGI (Marchand *et al.*, 1989). However, trypanosomal metabolism has some unique characteristics, including the compartmentalisation of part of glycolysis and PPP in the glycosome. It remains undetermined whether these peculiarities might affect the response of *T. brucei* to the loss of 6PGDH.

The construction of a dynamic model including both glycolysis and the PPP in *T. brucei* (Chapter 3) now allows us to test his hypothesis *in silico.* In this chapter, the effect of ablation of 6PGDH is investigated by both mathematical modelling and wet-lab experimentation.

6.2. Results

6.2.1. 6PGDH loss in *T. brucei* does not inhibit PGI

The mathematical model of trypanosomal glycolysis was extended in chapter 3 with the PPP, creating two classes of models. Model 5 includes an ATP:ADP antiporter across the glycosomal membrane, while model 6 includes a glycosomal ribokinase (Figure 6.2). Both models were analysed here.

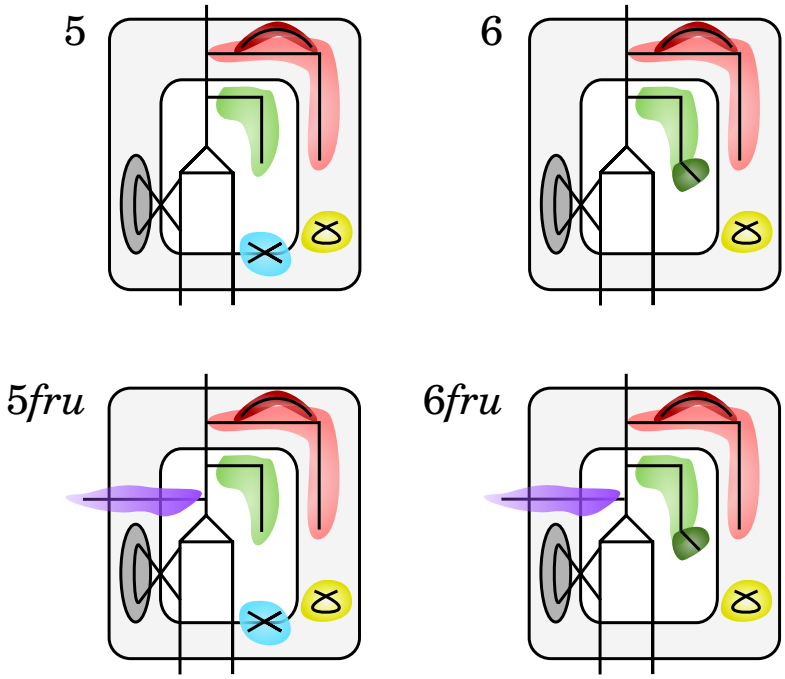

Figure 6.2.: Schematic overview of model versions considered. Model 5 and 6 are identical to model 5 and 6 in chapter 3 (Figure 3.3), models 5*fru* and 6*fru* include the transport and phosphorylation of fructose (shown in purple).

The activity of 6PGDH ($V_{max,6PGDHc/g}$) was scanned and model 5 and 6 behave similar to the ablation of 6PGDH. The activity of 6PGDH can be reduced by 90 % without any apparent effects on fluxes or metabolite concentrations (Figure 6.1). When the activity of 6PGDH is reduced below 1 nmol $\cdot$ min^{-1} $\cdot$ mg protein^{-1}, 6-PG accumulates both in the glycosome and the cytosol (Figure 6.1B and D). An increasing fraction of the models fails to reach steady-state (within 1000 modelled minutes, Figure 6.1B and D), due to the extreme accumulation of 6-PG.

The two models behave differently at very low 6PGDH activity, as the glycosomal concentration of 6-PG is constrained in model 6 (moiety 6, Table 3.5). The fraction of model 6 that reaches steady state at near-absent 6PGDH activities increases, but the

steady-state that is calculated with these low 6PGDH activities have a very low glycolytic flux (Figure 6.1A). Nonetheless, those states would never be reached, as knockdown or inhibition of 6PGDH would already have caused a lethal accumulation of 6-PG.

In an attempt to isolate the inhibition of PGI by 6-PG, the glycosomal concentration of 6-PG was scanned in model 1, consisting of only glycolysis and no PPP (Figure 6.3C). A 6-PG concentration of 400 mM is required to inhibit the glycolytic flux by 50 %, which results in a growth arrest of the trypanosomes (Haanstra *et al.*, 2011). This concentration is only obtained when the cytosolic 6-PG has already accumulated to extremely high levels (model 5), or are not obtained at all (model 6). Inhibition of glycolysis is therefore an unlikely explanation for the lethality of 6PGDH ablation, as the parasite would have burst from extreme 6-PG levels already.

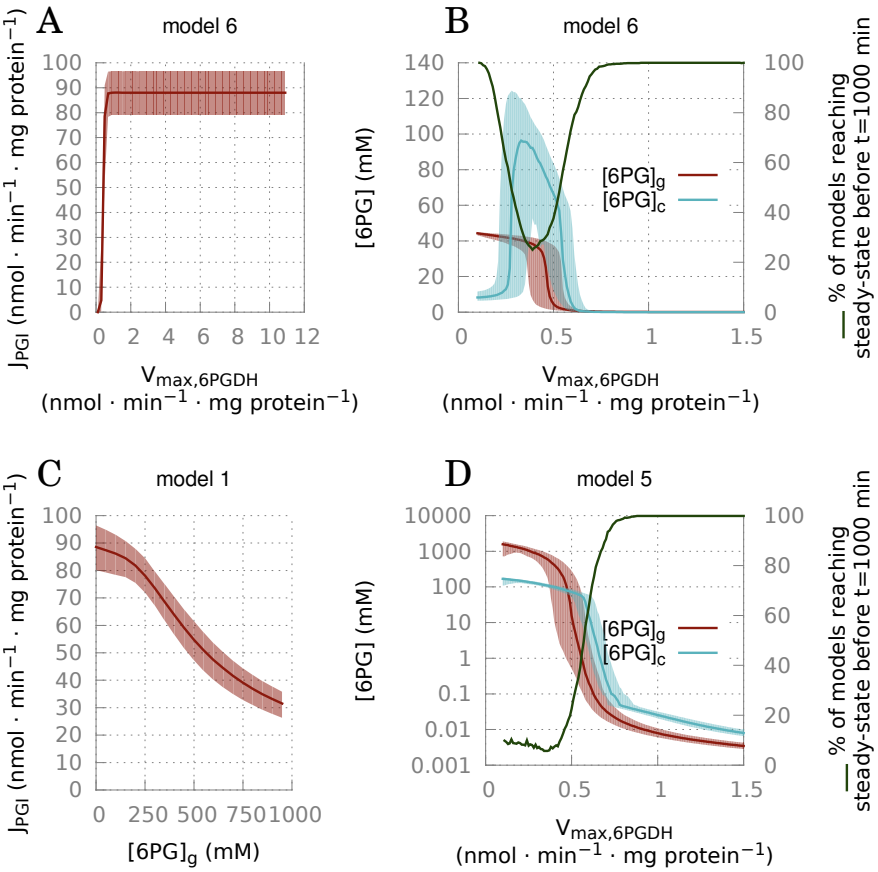

Figure 6.3.: Effects of ablation of 6PGDH. *A:* The effect of knockdown of 6PGDH on the flux through glycolysis is simulated by reducing $V_{max,6PGDH}$ in model 6 with k_{TOX} = 2 µl · min^{-1} · mg protein^{-1}. Model 5 gives similar results. *B* and *D:* Very low activity of 6PGDH results in accumulation of 6-PG in the glycosome (red lines) and cytosol (blue lines). The green lines indicate the percentage of models that do not reach steady-state within 16 hours. When no steady-state is reached, the concentration at *t* = 1000 min is plotted. *C:* A scan of the glycosomal concentration of 6-PG in model 1 demonstrates that a glycosomal 6-PG concentration of around 400 mM is required for a lethal 50 % reduction in glycolytic flux.

While a 90 % reduction of 6PGDH (1.06 nmol $\cdot$ min^{-1} $\cdot$ mg protein^{-1}) does not seem to affect the glycolytic flux and metabolites, it does affect the capability to deal with oxidative stress. The reduced activity of 6PGDH hinders the PPP to quickly react to oxidative stress. It was demonstrated in chapter 3 that oxidative stress activates the PPP, increasing the production of NADPH, with PPP enzymes working closer to their maximum activity (Figure 3.6). Inhibition of the PPP would limit the capabilities to increase the PPP flux and therefore increases the parasites sensitivity to oxidative stress.

Based on these results, it is suggested that inhibition of PGI by accumulation is unlikely to be the cause of the lethality of 6PGDH depletion. More likely is that rather the explosive accumulation of 6-PG, or the impaired PPP flux and associated increased sensitivity to oxidative stress are what kills the parasite.

6.2.2. Fructose is unable to rescue 6PGDH loss *in silico*

Sukhatme and Chan (2012) showed that 6PGDH deficient tumours could retain their proliferation by growth on fructose, bypassing PGI. *T. brucei* is also able to use fructose as carbon source (Kiaira and Njogu, 1989), as the hexose transporter and hexokinase of *T. brucei* are able to transport (Fry *et al.*, 1993) and catalyse the phosphorylation of fructose (Morris *et al.*, 2006). By analogy, it was tested whether *T. brucei* could be rescued from depletion of 6PGDH by growth on fructose.

Model 5 and 6 were both extended with the fructose transport and utilising reactions, and are denoted as model 5*fru* and model 6*fru*. Parameter values were derived from literature (Table 6.1), and the rate equations of hexokinase were changed to allow both the use of fructose and glucose as substrates, but also include competitive inhibition between the two substrates (see Methods for rate equations).

Reaction	Parameter	Value	Unit	Ref
FruT	V_{max}	69.1 / 195	nmol · min^{-1} · mg protein^{-1}	Fry *et al.*, 1993 [a]
	$K_{m,Fru}$	3.91	mM	Fry *et al.*, 1993
	α	0.75	dimensionless	b
HXK	$V_{max,c}$	1775	nmol · min^{-1} · mg protein^{-1}	b
(Fru)	$V_{max,g}$	154	nmol · min^{-1} · mg protein^{-1}	b
	$K_{m,Fru}$	0.35	mM	Morris *et al.*, 2006
	$K_{m,Fru\text{-}6\text{-}P}$	12	mM	b
	$K_{m,ATP}$	0.116	mM	b
	$K_{m,ADP}$	0.126	mM	b
	K_{eq}	631	dimensionless	Banks and Vernon, 1970
	$K_{i,Glc}$	0.1	mM	c
	$K_{i,Glc\text{-}6\text{-}P}$	12	mM	c
HXK	$K_{i,Fru}$	0.35	mM	c
(Glc)	$K_{i,Fru\text{-}6\text{-}P}$	12	mM	c

a: A value of 69.1 was measured from ex vivo trypanosomes, a value of 125 is used in simulations, fitted to the net ATP production of glucose-grown models.
b: No value measured for fructose (6-phosphate). Assumed to be similar to the value for glucose (6-phosphate).
c: Competitive inhibitor, K_i is identical to K_m.

Table 6.1.: Parameter values of fructose extension. Additional parameter values, all other parameter values used in the models are shown in Table 3.2. Hexokinase can use two substrates, glucose (Glc) and Fructose (Fru).

The steady-state flux through pyruvate kinase, responsible for net ATP production, is more than halved when fructose is used instead of glucose (Figure 6.4B, 76 vs 188 nmol · min^{-1} · mg protein^{-1}). The lower flux originates from the difference in the measured transport capacity for fructose and glucose: the glucose transporter V_{max} is 111.7 nmol · min^{-1} · mg protein^{-1} and K_m is 1 mM, while those numbers for fructose are 69.1 nmol · min^{-1} · mg protein^{-1} and 3.91 mM. A 50% reduction in ATP production results in a growth arrest (Haanstra *et al.*, 2011), contradicting that *T. brucei* can readily use fructose as carbon source and indicating that the measured fructose transport capacity is incompatible with the dynamic model. The current model of trypanosomal metabolism is based on enzyme activities from culture parasites, while the fructose transport activity is measured from *ex vivo* trypanosomes. Additionally, it is possible that the parasite adapts to growth in fructose by up-regulating its hexose transporters. A fructose transport V_{max} of 190 nmol · min^{-1} · mg protein^{-1} is required to achieve a similar steady state pyruvate kinase flux as when glucose is used (Figure 6.4B).

Ablation of 6PGDH in the fructose models leads to a similar accumulation of 6-PG (Figure 6.4A). The accumulation of 6-PG is dependent on the activity of the fructose transporter, an activity of less than 150 nmol · min^{-1} · mg protein^{-1} does

not lead to accumulation of 6-PG when the 6PGDH activity is reduced to 0.2 nmol · min^{-1} · mg $protein^{-1}$(Figure 6.4A). However, ATP production is also significantly lower (Figure 6.4B). The model therefore predicts that fructose is unlikely to rescue from the explosive accumulation of 6-PG when 6PGDH is ablated.

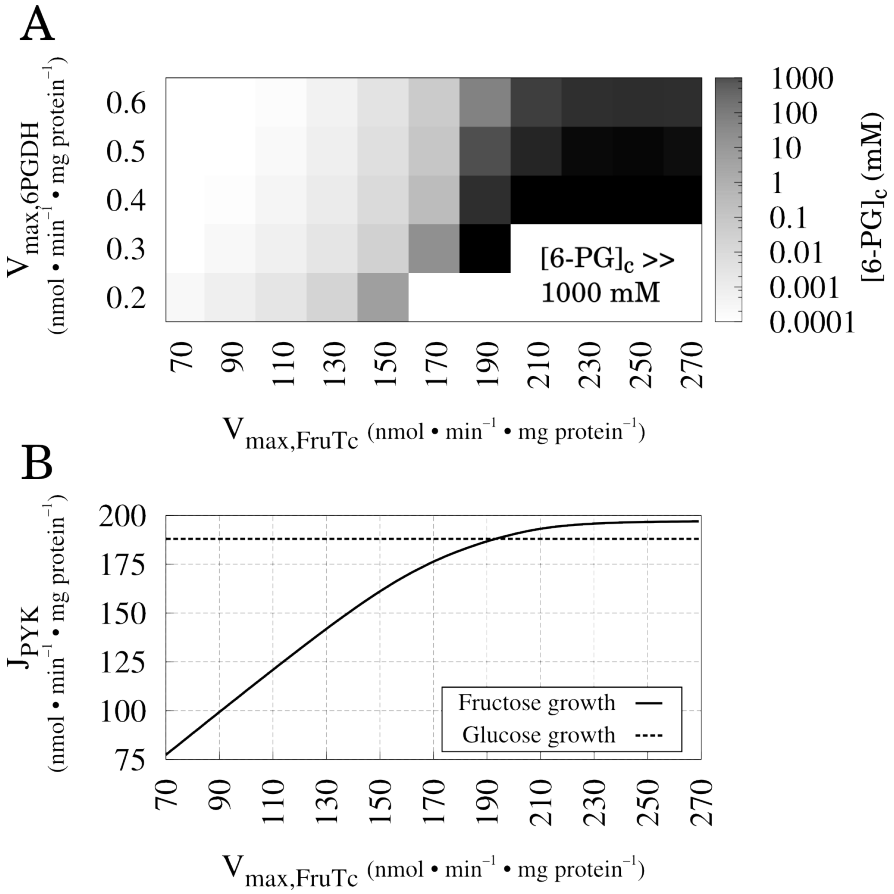

Figure 6.4.: Simulations of the fructose model. Results shown are for model 6, simulations with model 5 give similar results. *A:* Heat-map of steady-state cytosolic 6-phosphogluconate (6-PG) concentration at various fructose transporter (FruTc) and 6PGDH (6PGDH) activities. A steady-state could not be calculated for the combination of parameters in the bottom right corner, due to continuous extreme accumulation of 6-PG. *B:* Steady-state flux through pyruvate kinase (PYK) in model 6 with no ablated 6PGDH activity, at different fructose transporter activities. Solid line is result from model 6*fru*, dashed line is the steady-state flux in model 6 (using glucose).

6.2.3. Preliminary experimental results on ablation of 6PGDH

The model prediction that fructose is not able to rescue the ablation of 6PGDH in trypanosomes was tested experimentally. A $6PGDH^{RNAi}$ line was generated in our group (Dr Vincent Alibu). Induction of the RNA interference by the addition of tetracycline resulted in reduced levels and activities of 6PGDH (Dr Vincent Alibu).

Reduced levels of 6PGDH are lethal for bloodstream *T. brucei*, as shown in Figure 6.5. I tested whether the growth of *T. brucei* on fructose would rescue from the reduction in 6PGDH activity. Parasites were routinely grown in the glucose-medium and transferred to fructose-medium upon induction of the RNA interference. The growth rate of *T. brucei* on fructose was slightly lower than on glucose (Figure 6.5) but $6PGDH^{RNAi}$ parasites did not survive in either glucose or fructose medium upon reduction in the 6PGDH level (Figure 6.5).

The slightly lower growth could be indicative that the ATP production is lower in parasites grown on fructose, however, additional and more rigorous experiments are required to confirm this. A reduced flux is contradictory to the findings of Kiaira and Njogu (1989), who showed that *ex vivo* trypanosomes produce more pyruvate when grown on fructose instead of glucose.

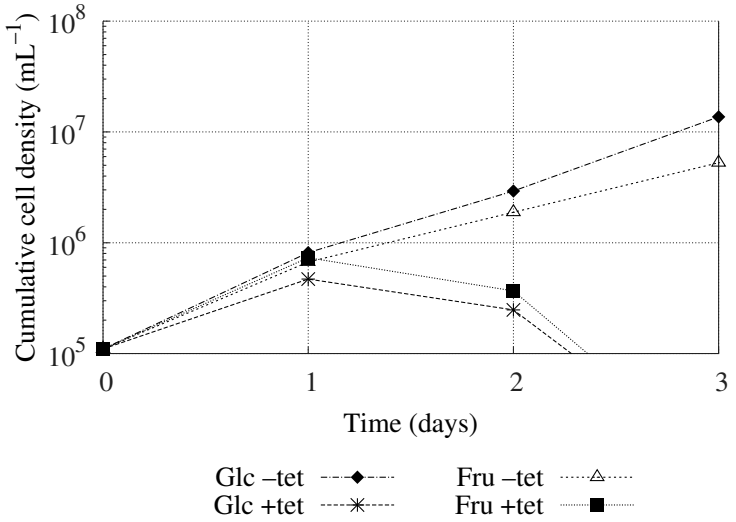

Figure 6.5.: Growth curve of $6PGDH^{RNAi}$ on glucose and fructose. $6PGDH^{RNAi}$ was cultured in HMI-9 with 25 mM glucose and split at day 0. Two cultures continued growth on glucose, while two additional cultures grown on fructose (25 mM). Tetracycline (1 $\mu g \cdot ml^{-1}$) was added at day 0, cells were counted daily and diluted down to $1 \cdot 10^5$ cells $\cdot$ mL^{-1} when required. At day 3, no life cells were observed in the cultures with tetracycline.

6.3. Discussion

In this chapter I showed preliminary data suggesting that the inhibition of 6PGDH in *T. brucei* is not lethal due to inhibition of PGI. Although preliminary, it does demonstrate how the model generated in Chapter 3 can utilised to investigate trypanosomal metabolism.

In silico analysis showed that either extreme accumulation of 6-phosphogluconate in the cytosol, or the diminished flux through the PPP are the reasons why the loss of 6-phosphogluconate is lethal for *T. brucei.* The two classes of models generated in chapter 3 diverge only at the very low 6PGDH activity range, which are unlikely to be reached *in vivo*, as the extreme accumulation of 6-PG would already be lethal to the parasites. Mathematical models of the use of fructose in trypanosomal glycolysis and PPP demonstrated that the lower affinity and activity of the hexose transporter for fructose would be able to rescue the parasite from loss of 6PGDH, however, the reduced ATP production flux would likely have severe effects on trypanosome growth. Nonetheless, the reduced 6PGDH activity still impairs the parasites ability to deal with oxidative stress.

The generation of a $6PGDH^{RNAi}$ (Dr Vincent Alibu) confirmed that reduced levels of 6PGDH are lethal to the parasites, and cannot be rescued by the addition of fructose, in concordance with the *in silico* prediction.

However, these results are preliminary and require extensive scrutiny. Activity measurements of 6PGDH in the $6PGDH^{RNAi}$ line would be essential to quantitate the level of 6PGDH activity required for parasite survival. Additionally, the fructose transport activity should be measured in cultured *T. brucei* that has adapted to growth on fructose, such that this variable can be excluded from the results. The measurement of pyruvate production by fructose-grown parasites can then be used to validate the model when updated with new kinetics for fructose.

Chapter 7

General discussion and future work

Predictive models of cellular physiology are of growing significance in biology, including in the selection of drug targets and in predictive toxicology (Pujol *et al.*, 2010). For instance, stoichiometric genome-scale reconstructions of metabolism, are valuable tools to identify targets in complex biological networks (Duarte *et al.*, 2007; Ma *et al.*, 2007; Folger *et al.*, 2011). These constraint-based models are relatively easily extended by adding the stoichiometry of new reactions – the expanded models are mathematically guaranteed to still provide feasible solutions if the starting model worked, adding reactions can only increase the size of the cone of possible fluxes, with all previous solutions still being part of the original solution space. As demonstrated in this thesis, this is not the case for bottom-up dynamic models: adding new reactions can reveal unexpected fragilities of the original model, and a much more careful approach is required when extending such models. Nonetheless, the generated dynamic models can present insights into metabolic pathways that stoichiometric models can not provide.

7.1. Unravelling glycosomal metabolism

In several rounds of experimentation and *in silico* simulations (Chapter 3), we added the glycosomal and cytosolic branch of the pentose phosphate pathway (PPP) to a model of trypanosomal glycolysis. The resulting models demonstrate the activation of the PPP by induced oxidative stress, while it became apparent during the model building process that balancing the glycosomal bound-phosphate levels is crucial for this system. The extension of the glycolytic model with the glycosomal PPP introduced the risk of a glycosomal phosphate leak. Two classes of solutions were explored in

more detail, represented by a glycosomal RK that maintains the conserved moiety of bound-phosphate within the glycosome, and an ATP:ADP antiporter that breaks the moiety altogether. While both solutions are able to prevent the phosphate leak, the antiporter would require tight regulation and the glycosomal RK only works at low ribose concentrations. Deviations from standard conditions in the models suggest that a more complex mechanism is involved in balancing the glycosomal bound-phosphates.

The compartmentalisation of a limited set of linear pathways can make a system rigid and fragile, as there are strict stoichiometric rules that need to be adhered to, with a very limited number of degrees of freedom. The presence of additional reactions can provide more flexibility to a compartmentalised network. This was demonstrated in Chapter 3, where a turbo explosion was observed when a glycosomal ATP:ADP antiporter was added to the glycolytic model. The presence of the pentose phosphate pathway did not prevent the turbo explosion, but the observed accumulation of sugar-phosphates was less profound.

Nonetheless, the extended models that were constructed–representing almost a doubling of the number of reactions in comparison to the original glycolysis model–still suffer from the rigid structure that is forced on the system due to the compartmentalisation. The recently described channels in the glycosomal membrane (Gualdrón-López *et al.*, 2012a,c) could provide additional flexibility to the system, and future work should therefore be focused on the properties and consequences of these glycosomal channels, as they could have important implications for the behaviour of glycosomal metabolism.

In preliminary mathematical modelling of glycosomal channels by Dr Fiona Achcar (unpublished data; University of Glasgow), it appears that the effects of the presence of such channels depends on which metabolites are and which are not transported across the glycosomal membrane. The glycosomal channels likely possess selectivity based on, for instance, charge, size or presence of a particular chemical group in the metabolite. Simulations of different selectivity of the glycosomal channels indicate that larger metabolites, such as ATP/ADP, NADH/NAD^+ and NADPH/$NADP^+$, are likely prevented from freely mixing with the cytosolic pools (unpublished data; Dr Fiona Achcar, University of Glasgow). The presence of glycosomal channels provides more flexibility to the system, however it is not sufficient to prevent the symptoms of the phosphate leak I addressed in this thesis. Experiments can be envisaged that can test the hypotheses that derive from the modelling of glycosomal channels, *e.g.* whether the sole cytosolic localisation of *one* glycolytic enzyme allows the parasite to survive (in contrast with the rather harsh ablation of PEX-proteins by RNAi that was done previously and would affect all enzymes localised to the glycosome; Furuya *et al.*, 2002; Kessler and Parsons, 2005; Haanstra *et al.*, 2008).

The presence of transport across the glycosomal membrane is not the only way that glycosomal metabolism might be more flexible than observed in the mathematical models. The presence of additional reactions and pathways in the cytosol could play essential roles in the functioning of the glycosome. Especially in combination with the channels in the glycosomal membrane, as "lone" enzymes (whose substrates and products are not involved in other reactions within the glycosome, therefore not forming a pathway) could be connected to enzymes and pathways in the cytosol. Phosphotransferases potentially play an important role in *Trypanosoma* and *Leishmania* energy management, as these species have the largest number of phosphotransferase isoforms found in a single cell (Pereira *et al.*, 2011). For instance ArgK is localised in the glycosome in *T. brucei* (Colasante *et al.*, 2006; Vertommen *et al.*, 2008) while no other enzymes have been shown to be present in the glycosome that can use arginine or arginine-phosphate as a substrate (Colasante *et al.*, 2006; Vertommen *et al.*, 2008). Those enzymes might well be present, but not detected in the proteomic experiments to date. However, if arginine can freely cross the glycosomal membrane, then glycosomal ArgK could provide an essential role in balancing the conserved moiety of bound phosphates in the glycosome. Perhaps arginine-phosphate is too large for the glycosomal channels, and can therefore function as a localised energy storage. Arginine-phosphate has recently been shown to be involved in stress-responses in *T. brucei*, where levels of metabolomics experiments demonstrated that arginine-phosphate levels are decreased upon oxidative stress, although further investigation in this is still ongoing (unpublished data; Dr Dong-Hyun Kim, University of Glasgow).

Additionally, recent metabolomics experiments have shown that a succinate fermentation pathway might be functioning in the glycosomes of bloodstream form *T. brucei* (unpublished data; Dr Darren Creek, University of Glasgow). Although the glycolytic flux is far larger than any other glycosomal flux, it is well possible that these smaller fluxes play essential roles in retaining redox and bound phosphate balances within the glycosome. Succinate fermentation produces NADH, and as NADH is potentially too large to pass through the glycosomal channels, it is possible that succinate fermentation plays an important role to provide more flexibility in the redox balancing in the glycosome.

Overall, a further unravelling of the metabolic processes that take place in glycosomes will be essential to fully understand the functioning of this unique organelle. This is of particular interest due to the absence of glycosomes in the mammalian hosts. It is therefore pivotal to compare the trypanosomal metabolism with the host's cells metabolism. Such a comparison is not only informative for the identification of potential drug targets against human African trypanosomiasis, but can potentially also provide insights into human diseases of metabolism.

It would be interesting to extensively compare the extended model of trypanosomal metabolism with the model that describes glycolysis and the PPP in erythrocytes (Mulquiney and Kuchel, 1999b, and briefly discussed in 1.8.4.2). In the first stage of trypanosomiasis, the parasites reside in the mammalian bloodstream. Delivering drugs in this stage is easier than in the later stage, where the parasite has crossed the blood-brain barrier. Comparison of the models of erythrocyte and trypanosomal metabolism might aid to indicate potential drug targets.

Glycolysis is the (almost) exclusive energy source for both erythrocytes (Chapman *et al.*, 1962) and bloodstream form trypanosomes, indicating that changes to glycolysis can have major influences on both cell types. However, there are also a number of differences between the erythrocyte and trypanosomes. For one, erythrocyte don't have glycosomes and therefore don't suffer from the risks affiliated to the strict intraglycosomal bound-phosphate balance that is seen in trypanosomes (see Chapter 3). On the other hand, 2,3-bisphosphoglycerate (2,3-BPG) is an important metabolite in erythrocytes and is highly regulated, as 2,3-BPG is a major modulator of haemoglobin oxygen affinity (Benesch and Benesch, 1967; Gerber *et al.*, 1973). In trypanosoma, 2,3-BPG has not been expected to play an important role in metabolism (Chevalier *et al.*, 2000).

7.2. How essential is the glycosomal PPP?

The hypothesis that a glycosomal RK could prevent the phosphate leak introduced by the glycosomal localisation of the PPP was tested by using genetic mutants in RK (Chapter 4). A combination of knockdown and conditional knockout mutants indicated that only a small quantity of RK is essential for trypanosomal survival. What has not been addressed in this thesis, however, but could play an important role in the investigation in the glycosomal PPP is whether the glycosomal localisation of the PPP is essential.

Various genetic mutants have shown that indiscriminate ablation of glycosomal and cytosolic PPP activity is lethal for bloodstream form *T. brucei* (Hanau *et al.*, 1996; Barrett and Gilbert, 2002). In Chapter 6 was showed how ablation of 6PGDH is lethal to *T. brucei*. It was anticipated that the loss of 6PGDH results in a lethal inhibition of PGI, however, we demonstrated that this is rather due to an impaired flux through the PPP or the extreme accumulation of 6-PG. In other cell types, growth on alternative sugars rescues a cell from the lethal loss of 6PGDH (Sukhatme and Chan, 2012), as the use of these sugars bypass the PGI that is inhibited by accumulation of 6-PG. However, it is possible that the lethality of these and other mutants is only a result of the cytosolic ablation and not the glycosomal loss of the PPP. Potentially, the NADPH requirements

in the glycosome can be regulated, such that the loss of PPP activity in the glycosome will not have such a profound effect as the loss of all PPP activity. This could then also explain why the ablation of RK activity did not affect trypanosome survival, as the down-regulation of the glycosomal PPP would prevent the phosphate leak induced by the loss of RK. Important for this is also whether the glycosomal channels are capable of transporting NADPH, potentially providing the glycosome with cytosolic produced NADPH.

A way of testing this would be to supplement one of the lethal RNAi mutants lacking a PPP enzyme, such as G6PDH, with the expression of a PTS-less version of the same enzyme. The originally ablated activity would then still be present in the cytosol, but no glycosomal activity should be present. This will allow to study the importance of the glycosomal PPP, while keeping the cytosolic PPP intact. With the PPP playing such an important role in the parasites redox balance, it is imperative to understand why the PPP is partly localised to the glycosomes.

7.3. Enzymes, the forgotten workhorses?

The investigations into trypanosomal metabolism in this thesis have also demonstrated how little is known about enzymes. In the post-genomic era, it is becoming ever cheaper, faster and easier to generate large datasets. The problem with acquiring large amounts of data is to interpret the data. Whole genome sequencing, for instance, is already becoming a routine procedure; however we only have limited understanding of the meaning of all those millions of nucleotides in each genome.

In Chapter 5, it was discussed how sequence analysis can be employed to annotate the genes by sequence similarity, but for a variety of reasons this cannot capture all of the characteristics of the proteins they encode and experimental data is required to really characterise the enzymes. Nonetheless, gene annotations based on sequence similarity can still be used to construct genome-scale models of metabolism, and various methods have been developed to analyse these metabolic networks without paying attention to the underlying complexity of the enzymes. Although studies of genome-scale models can be instrumental in the prioritisation of drug-targets and in synthetic biology, by identify choke-points that can be targeted, it can be disconcerting to realise that the real workhorses of metabolic pathways, the enzymes, are perhaps not given the research attention they deserve.

The catalytic activities of three putatively annotated *T. brucei* genes were investigated in Chapter 5 with an untargeted approach using metabolomics. The first gene, putatively annotated as arginase, did not show arginase or related ureohydrolase activity, but rather suggested a function as indole-oxygenase. The second gene, putatively annotated as *N*-acetylornithine deacetylase, demonstrated activity and substrate promiscuity comparable to *E. coli N*-acetylornithine deacetylase. However, the annotation as *N*-acetylornithine deacetylase is misleading, as the enzyme demonstrates wide substrate promiscuity and likely has a higher activity with *N*-acetylmethionine. The third gene, putatively annotated as nicotinamidase, showed the expected nicotinamidase activity, although a slight substrate promiscuity might exist.

Enzymology seems to be an art-form that is dying out, while the detailed analysis of enzymes can be crucial for the behaviour observed in the whole system. If we are to build silicon cells (Westerhoff, 2001; Snoep, 2005; Bakker *et al.*, 2010), then quantitative and accurate knowledge about enzyme promiscuity, moonlighting functions (Copley, 2003) and their evolutionary advantage (D'Ari and Casadesus, 1998) are certainly essential to be able to succeed.

References

Abbott A (2010). Germans cook up liver project. *Nature*, 468(7326):879.

Achcar F, Kerkhoven EJ, SilicoTryp Consortium, Bakker BM, Barrett MP, and Breitling R (2012). Dynamic modelling under uncertainty: the case of *Trypanosoma brucei* energy metabolism. *PLoS Comput Biol*, 8(1):e1002352.

Albert MA, Haanstra JR, Hannaert V, Van Roy J, Opperdoes FR, Bakker BM, and Michels PAM (2005). Experimental and in silico analyses of glycolytic flux control in bloodstream form *Trypanosoma brucei*. *J Biol Chem*, 280(31):28306–28315.

Alibu VP, Storm L, Haile S, Clayton C, and Horn D (2005). A doubly inducible system for RNA interference and rapid RNAi plasmid construction in *Trypanosoma brucei*. *Mol Biochem Parasitol*, 139(1):75–82.

Alsford S and Horn D (2008). Single-locus targeting constructs for reliable regulated RNAi and transgene expression in *Trypanosoma brucei*. *Mol Biochem Parasitol*, 161(1):76–79.

Alsford S, Turner DJ, Obado SO, Sanchez-Flores A, Glover L, Berriman M, Hertz-Fowler C, and Horn D (2011). High-throughput phenotyping using parallel sequencing of RNA interference targets in the African trypanosome. *Genome Res*, 21(6):915–924.

Aman RA, Kenyon GL, and Wang CC (1985). Cross-linking of the enzymes in the glycosome of *Trypanosoma brucei*. *J Biol Chem*, 260(11):6966–6973.

Anderson A and Cooper RA (1969). The significance of ribokinase for ribose utilization by *Escherichia coli*. *Biochim Biophys Acta*, 177(1):163–165.

Armengaud P, Breitling R, and Amtmann A (2004). The potassium-dependent transcriptome of Arabidopsis reveals a prominent role of jasmonic acid in nutrient signaling. *Plant Physiology*, 136(1):2556–2576.

Aslett M, Aurrecoechea C, Berriman M, *et al.* (2009). TriTrypDB: a functional genomic resource for the Trypanosomatidae. *Nucleic Acids Res*, 38(Database):D457–D462.

Atkinson MR, Johnson E, and Morton RK (1961). Equilibrium constants of phosphoryl transfer from C-1 to C-6 of alpha-D-glucose 1-phosphate and from glucose 6-phosphate to water. *Biochem J*, 79:12–15.

Bacchi CJ, Garofalo J, Mockenhaupt D, *et al.* (1983). In vivo effects of alpha-DL-difluoromethylornithine on the metabolism and morphology of *Trypanosoma brucei brucei*. *Mol Biochem Parasitol*, 7(3):209–225.

Bakker BM (1998). *Control and regulation of glycolysis in Trypanosoma brucei*. Ph.D. thesis, VU University.

Bakker BM, Krauth-Siegel RL, Clayton C, Matthews K, Girolami M, Westerhoff HV, Michels PAM, Breitling R, and Barrett MP (2010). The silicon trypanosome. *Parasitology*, 137(Special Issue 09):1333–1341.

Bakker BM, Mensonides FI, Teusink B, van Hoek P, Michels PA, and Westerhoff HV (2000). Compartmentation protects trypanosomes from the dangerous design of glycolysis. *Proc Natl Acad Sci U S A*, 97(5):2087–2092.

Bakker BM, Michels PAM, Opperdoes FR, and Westerhoff HV (1997). Glycolysis in bloodstream form *Trypanosoma brucei* can be understood in terms of the kinetics of the glycolytic enzymes. *J Biol Chem*, 272(6):3207–3215.

Bakker BM, Michels PAM, Opperdoes FR, and Westerhoff HV (1999a). What controls glycolysis in bloodstream form *Trypanosoma brucei*? *J Biol Chem*, 274(21):14551–14559.

Bakker BM, Walsh MC, ter Kuile BH, Mensonides FIC, Michels PAM, Opperdoes FR, and Westerhoff HV (1999b). Contribution of glucose transport to the control of the glycolytic flux in *Trypanosoma brucei*. *Proc Natl Acad Sci U S A*, 96(18):10098–10103.

Banks BE and Vernon CA (1970). Reassessment of the role of ATP in vivo. *J Theor Biol*, 29(2):301–326.

Baran R, Reindl W, and Northen TR (2009). Mass spectrometry based metabolomics and enzymatic assays for functional genomics. *Curr Opin Microbiol*, 12(5):547–552.

Barnard JP and Pedersen PL (1988). Purification in a single step and kinetic characterization of the pyruvate kinase of *Trypanosoma brucei*. *Mol Biochem Parasitol*, 31(2):141–147.

Barrett M and Gilbert I (2002). Perspectives for new drugs against trypanosomiasis and leishmaniasis. *Current Topics in Medicinal Chemistry*, 2(5):471–482.

Barrett MP (1997). The pentose phosphate pathway and parasitic protozoa. *Parasitol Today*, 13(1):11–16.

Barrett MP, Boykin DW, Brun R, and Tidwell RR (2007). Human African trypanosomiasis: pharmacological re-engagement with a neglected disease. *Br J Pharmacol*, 152(8):1155–1171.

Barrett MP, Burchmore RJ, Stich A, Lazzari JO, Frasch AC, Cazzulo JJ, and Krishna S (2003). The trypanosomiases. *Lancet*, 362(9394):1469–1480.

Barrett MP, Coombs GH, and Mottram JC (1999). Recent advances in identifying and validating drug targets in trypanosomes and leishmanias. *Trends Microbiol*, 7(2):82–88.

Barrett MP and Le Page RW (1993). A 6-phosphogluconate dehydrogenase gene from *Trypanosoma brucei*. *Mol Biochem Parasitol*, 57(1):89–99.

Barrett MP, Vincent IM, Burchmore RJ, Kazibwe AJ, and Matovu E (2011). Drug resistance in human African trypanosomiasis. *Future Microbiol*, 6(9):1037–1047.

Barrett MP, Zhang ZQ, Denise H, Giroud C, and Baltz T (1995). A diamidine-resistant *Trypanosoma equiperdum* clone contains a p2 purine transporter with reduced substrate affinity. *Mol Biochem Parasitol*, 73(1-2):223 – 229.

Benesch R and Benesch RE (1967). The effect of organic phosphates from the human erythrocyte on the allosteric properties of hemoglobin. *Biochem Biophys Res Commun*, 26(2):162–167.

Berrang-Ford L, Lundine J, and Breau S (2011). Conflict and human African trypanosomiasis. *Soc Sci Med*, 72(3):398–407.

Berriman M, Ghedin E, Hertz-Fowler C, *et al.* (2005). The genome of the African trypanosome *Trypanosoma brucei*. *Science*, 309(5733):416–422.

Bertelli M, El-Bastawissy E, Knaggs MH, Barrett MP, Hanau S, and Gilbert IH (2001). Selective inhibition of 6-phosphogluconate dehydrogenase from *Trypanosoma brucei*. *J Comput Aided Mol Des*, 15(5):465–475.

Besteiro S, Biran M, Biteau N, Coustou V, Baltz T, Canioni P, and Bringaud F (2002). Succinate secreted by *Trypanosoma brucei* is produced by a novel and unique glycosomal enzyme, NADH-dependent fumarate reductase. *J Biol Chem*, 277(41):38001–38012.

Bewley GC and Lucchesi JC (1975). Lethal effects of low and "null" activity alleles of 6-phosphogluconate dehydrogenase in *Drosophila Melanogaster*. *Genetics*, 79(3):451–457.

Biebinger S, Elizabeth Wirtz L, Lorenz P, and Clayton C (1997). Vectors for inducible expression of toxic gene products in bloodstream and procyclic *Trypanosoma brucei*. *Mol Biochem Parasitol*, 85(1):99–112.

Blangy D, Buc H, and Monod J (1968). Kinetics of the allosteric interactions of phosphofructokinase from *Escherichia coli*. *J Mol Biol*, 31(1):13–35.

Blattner J, Dörsam H, and Clayton CE (1995). Function of N-terminal import signals in trypanosome microbodies. *FEBS Lett*, 360(3):310–314.

Blum JA, Zellweger MJ, Burri C, and Hatz C (2008). Cardiac involvement in African and American trypanosomiasis. *Lancet Infect Dis*, 8(10):631–641.

Boiteux A, Goldbeter A, and Hess B (1975). Control of oscillating glycolysis of yeast by stochastic, periodic, and steady source of substrate: a model and experimental study. *Proc Natl Acad Sci U S A*, 72(10):3829–3833.

Booth IR (2007). SysMO: back to the future. *Nat Rev Microbiol*, 5(8):566–566.

Borger S, Liebermeister W, and Klipp E (2006). Prediction of enzyme kinetic parameters based on statistical learning. *Genome Inform*, 17(1):80–87.

Bradford MM (1976). A rapid and sensitive method for the quantitation of microgram quantities of protein utilizing the principle of protein-dye binding. *Anal Biochem*, 72:248–254.

Breitling R, Armengaud P, Amtmann A, and Herzyk P (2004). Rank products: a simple, yet powerful, new method to detect differentially regulated genes in replicated microarray experiments. *FEBS Lett*, 573(1-3):83–92.

Bridges DJ, Gould MK, Nerima B, Mäser P, Burchmore RJS, and Koning HPd (2007). Loss of the high-affinity pentamidine transporter is responsible for high levels of cross-resistance between arsenical and diamidine drugs in African trypanosomes. *Mol Pharmacol*, 71(4):1098–1108.

Bringaud F, Rivière L, and Coustou V (2006). Energy metabolism of trypanosomatids: Adaptation to available carbon sources. *Mol Biochem Parasitol*, 149(1):1–9.

Bruggeman FJ and Westerhoff HV (2007). The nature of systems biology. *Trends Microbiol*, 15(1):45–50.

Brun R, Blum J, Chappuis F, and Burri C (2010). Human African trypanosomiasis. *Lancet*, 375(9709):148–159.

Burkard G, Fragoso CM, and Roditi I (2007). Highly efficient stable transformation of bloodstream forms of *Trypanosoma brucei*. *Mol Biochem Parasitol*, 153(2):220–223.

Bursell E (1981). *The role of proline in energy metabolism.* Plenum Press, New York & London.

Callens M, Kuntz DA, and Opperdoes FR (1991). Characterization of pyruvate kinase of *Trypanosoma brucei* and its role in the regulation of carbohydrate metabolism. *Mol Biochem Parasitol*, 47(1):19–29.

Cappellini M and Fiorelli G (2008). Glucose-6-phosphate dehydrogenase deficiency. *Lancet*, 371(9606):64–74.

Casazza JP and Veech RL (1986). The interdependence of glycolytic and pentose cycle intermediates in ad libitum fed rats. *J Biol Chem*, 261(2):690–698.

Cecchi G, Mattioli RC, Slingenbergh J, and De La Rocque S (2008). Land cover and tsetse fly distributions in sub-Saharan Africa. *Med Vet Entomol*, 22(4):364–373.

Chambers JW, Kearns MT, Morris MT, and Morris JC (2008). Assembly of heterohexameric trypanosome hexokinases reveals that hexokinase 2 is a regulable enzyme. *J Biol Chem*, 283(22):14963–14970.

Chandrasekaran S and Price ND (2010). Probabilistic integrative modeling of genome-scale metabolic and regulatory networks in *Escherichia coli* and *Mycobacterium tuberculosis*. *Proc Natl Acad Sci U S A*, 107(41):17845–17850.

Chapman RG, Hennessey MA, Waltersdorph AM, Huennekens FM, and Gabrio BW (1962). Erythrocyte metabolism. v. levels of glycolytic enzymes and regulation of glycolysis. *J Clin Invest*, 41(6):1249–1256.

Chen L and Vitkup D (2007). Distribution of orphan metabolic activities. *Trends Biotechnol*, 25(8):343–348.

Chevalier N, Rigden DJ, Van Roy J, Opperdoes FR, and Michels PAM (2000). *Trypanosoma brucei* contains a 2,3-bisphosphoglycerate independent phosphoglycerate mutase. *Eur J Biochem*, 267(5):1464–1472.

Choi J and El-Sayed NM (2012). Functional genomics of trypanosomatids. *Parasite Immunol*, 34(2-3):72–79.

Chudzik DM, Michels PA, de Walque S, and Hol WG (2000). Structures of type 2 peroxisomal targeting signals in two trypanosomatid aldolases. *J Mol Biol*, 300(4):697–707.

Clarkson AB, Bienen EJ, Pollakis G, and Grady RW (1989). Respiration of bloodstream forms of the parasite *Trypanosoma brucei brucei* is dependent on a plant-like alternative oxidase. *J Biol Chem*, 264(30):17770–17776.

Clayton C (1999). Genetic manipulation of kinetoplastida. *Parasitol Today*, 15(9):372–378.

Clayton CE and Michels P (1996). Metabolic compartmentation in African trypanosomes. *Parasitol Today*, 12(12):465–471.

Colasante C, Ellis M, Ruppert T, and Voncken F (2006). Comparative proteomics of glycosomes from bloodstream form and procyclic culture form *Trypanosoma brucei brucei*. *Proteomics*, 6(11):3275–3293.

Constantinides KJ, Pryke JA, and Eisenthal R (1990). Role of the pentose phosphate pathway in the provision of precursors for nucleic acid biosynthesis in bloodstream *Trypanosoma brucei*. *Biochem Soc Trans*, 18(5):870–871.

Copley SD (2003). Enzymes with extra talents: moonlighting functions and catalytic promiscuity. *Curr Opin Chem Biol*, 7(2):265–272.

Cordeiro AT, Thiemann OH, and Michels PA (2009). Inhibition of *Trypanosoma brucei* glucose-6-phosphate dehydrogenase by human steroids and their effects on the viability of cultured parasites. *Bioorgan Med Chem*, 17(6):2483–2489.

Cortassa S and Aon MA (1994). Metabolic control analysis of glycolysis and branching to ethanol production in chemostat cultures of *Saccharomyces cerevisiae* under carbon, nitrogen, or phosphate limitations. *Enzyme Microb Technol*, 16(9):761–770.

Coustou V, Biran M, Besteiro S, Rivière L, Baltz T, Franconi JM, and Bringaud F (2006). Fumarate is an essential intermediary metabolite produced by the procyclic *Trypanosoma brucei*. *J Biol Chem*, 281(37):26832–26846.

Coustou V, Biran M, Breton M, Guegan F, Rivière L, Plazolles N, Nolan D, Barrett MP, Franconi JM, and Bringaud F (2008). Glucose-induced remodeling of intermediary and energy metabolism in procyclic *Trypanosoma brucei*. *J Biol Chem*, 283(24):16342–16354.

Creek DJ, Anderson J, McConville MJ, and Barrett MP (2012a). Metabolomic analysis of trypanosomatid protozoa. *Mol Biochem Parasitol*, 181(2):73–84.

Creek DJ, Chokkathukalam A, Jankevics A, Burgess KE, Breitling R, and Barrett MP (2012b). Stable isotope-assisted metabolomics for network-wide metabolic pathway elucidation. *Anal Chem*, page In press.

Creek DJ, Jankevics A, Breitling R, Watson DG, Barrett MP, and Burgess KEV (2011). Toward global metabolomics analysis with hydrophilic interaction liquid chromatography-mass spectrometry: Improved metabolite identification by retention time prediction. *Anal Chem*, 83(22):8703–8710.

Cronin CN, Nolan DP, and Paul Voorheis H (1989). The enzymes of the classical pentose phosphate pathway display differential activities in procyclic and bloodstream forms of *Trypanosoma brucei*. *FEBS Lett*, 244(1):26–30.

Cronin CN and Tipton KF (1987). Kinetic studies on the reaction catalysed by phosphofructokinase from *Trypanosoma brucei*. *Biochemical J*, 245(1):13–18.

Cross GaM (1975). Identification, purification and properties of clone-specific glycoprotein antigens constituting the surface coat of *Trypanosoma brucei*. *Parasitology*, 71(03):393–417.

Cross M, Kieft R, Sabatini R, Dirks-Mulder A, Chaves I, and Borst P (2002). J-binding protein increases the level and retention of the unusual base J in trypanosome DNA. *Mol Microbiol*, 46(1):37–47.

da Silva ER, Castilho TM, Pioker FC, Tomich de Paula Silva CH, and Floeter-Winter LM (2002). Genomic organisation and transcription characterisation of the gene encoding *Leishmania (Leishmania) amazonensis* arginase and its protein structure prediction. *Int J Parasitol*, 32(6):727–737.

da Silva ER, da Silva MFL, Fischer H, Mortara RA, Mayer MG, Framesqui K, Silber AM, and Floeter-Winter LM (2008). Biochemical and biophysical properties of a highly active recombinant arginase from *Leishmania (Leishmania) amazonensis* and subcellular localization of native enzyme. *Mol Biochem Parasitol*, 159(2):104–111.

da Silva MFL, Zampieri RA, Muxel SM, Beverley SM, and Floeter-Winter LM (2012). *Leishmania amazonensis* arginase compartmentalization in the glycosome is important for parasite infectivity. *PLoS ONE*, 7(3):e34022.

Dardonville C and Gilbert IH (2003). Synthesis of (R)-2-methyl-4-deoxy and (R)-2-methyl-4,5-dideoxy analogues of 6-phosphogluconate as potential inhibitors of 6-phosphogluconate dehydrogenase. *Org Biomol Chem*, 1(3):552–559.

Dardonville C, Rinaldi E, Barrett MP, Brun R, Gilbert IH, and Hanau S (2004). Selective inhibition of *Trypanosoma brucei* 6-phosphogluconate dehydrogenase by

high-energy intermediate and transition-state analogues. *J Med Chem*, 47(13):3427–3437.

Dardonville C, Rinaldi E, Hanau S, Barrett MP, Brun R, and Gilbert IH (2003). Synthesis and biological evaluation of substrate-based inhibitors of 6-phosphogluconate dehydrogenase as potential drugs against African trypanosomiasis. *Bioorgan Med Chem*, 11(14):3205–3214.

D'Ari R and Casadesus J (1998). Underground metabolism. *BioEssays*, 20(2):181–186.

de Walque S, Kiel JA, Veenhuis M, Opperdoes FR, and Michels PA (1999). Cloning and analysis of the PTS-1 receptor in *Trypanosoma brucei*. *Mol Biochem Parasitol*, 104(1):106–119.

Dixon H (1966). Blood platelets as a source of enzyme activity in washed trypanosome suspensions. *Nature*, 210(5034):428–428.

Duarte NC, Becker SA, Jamshidi N, Thiele I, Mo ML, Vo TD, Srivas R, and Palsson BÃ (2007). Global reconstruction of the human metabolic network based on genomic and bibliomic data. *Proc Natl Acad Sci U S A*, 104(6):1777–1782.

Duffieux F, Van Roy J, Michels PA, and Opperdoes FR (2000). Molecular characterization of the first two enzymes of the pentose-phosphate pathway of *Trypanosoma brucei*. glucose-6-phosphate dehydrogenase and 6-phosphogluconolactonase. *J Biol Chem*, 275(36):27559–27565.

Durieux PO, Schütz P, Brun R, and Köhler P (1991). Alterations in krebs cycle enzyme activities and carbohydrate catabolism in two strains of *Trypanosoma brucei* during in vitro differentiation of their bloodstream to procyclic stages. *Mol Biochem Parasitol*, 45(1):19–27.

Ebikeme C, Hubert J, Biran M, *et al.* (2010). Ablation of succinate production from glucose metabolism in the procyclic trypanosomes induces metabolic switches to the glycerol 3-phosphate/dihydroxyacetone phosphate shuttle and to proline metabolism. *J Biol Chem*, 285(42):32312–32324.

Fairlamb A and Bowman I (1977). *Trypanosoma brucei*: Suramin and other trypanocidal compounds' effects on sn-glycerol-3-phosphate oxidase. *Exp Parasitol*, 43(2):353–361.

Fairlamb AH, Blackburn P, Ulrich P, Chait BT, and Cerami A (1985). Trypanothione: a novel bis(glutathionyl)spermidine cofactor for glutathione reductase in trypanosomatids. *Science*, 227(4693):1485–1487.

Fairlamb AH and Cerami A (1992). Metabolism and functions of trypanothione in the Kinetoplastida. *Annu Rev Microbiol*, 46:695–729.

Fairlamb AH, Henderson GB, Bacchi CJ, and Cerami A (1987). In vivo effects of difluoromethylornithine on trypanothione and polyamine levels in bloodstream forms of *Trypanosoma brucei*. *Mol Biochem Parasitol*, 24(2):185–191.

Fairlamb AH, Opperdoes FR, and Borst P (1977). New approach to screening drugs for activity against African trypanosomes. *Nature*, 265(5591):270–271.

Feng X, Feistel T, Buffalo C, *et al.* (2011). Remodeling of protein and mRNA expression in *Leishmania mexicana* induced by deletion of glucose transporter genes. *Mol Biochem Parasitol*, 175(1):39–48.

Fenn K and Matthews KR (2007). The cell biology of *Trypanosoma brucei* differentiation. *Curr Opin Microbiol*, 10(6):539–546.

Folger O, Jerby L, Frezza C, Gottlieb E, Ruppin E, and Shlomi T (2011). Predicting selective drug targets in cancer through metabolic networks. *Mol Syst Biol*, 7:501.

Fromm HJ, Silverstein E, and Boyer PD (1964). Equilibrium and net reaction rates in relation to the mechanism of yeast hexokinase. *J Biol Chem*, 239:3645–3652.

Fry AJ, Towner P, Holman GD, and Eisenthal R (1993). Transport of D-fructose and its analogues by *Trypanosoma brucei*. *Mol Biochem Parasitol*, 60(1):9–18.

Furnham N, Garavelli JS, Apweiler R, and Thornton JM (2009). Missing in action: enzyme functional annotations in biological databases. *Nat Chem Biol*, 5(8):521–525.

Furuya T, Kessler P, Jardim A, Schnaufer A, Crudder C, and Parsons M (2002). Glucose is toxic to glycosome-deficient trypanosomes. *Proc Natl Acad Sci U S A*, 99(22):14177–14182.

Fyfe PK, Rao VA, Zemla A, Cameron S, and Hunter WN (2009). Specificity and mechanism of *Acinetobacter baumanii* nicotinamidase: Implications for activation of the front-line tuberculosis drug pyrazinamide. *Angew Chem*, 48(48):9176–9179.

Galland N, Demeure F, Hannaert V, Verplaetse E, Vertommen D, Van der Smissen P, Courtoy PJ, and Michels PAM (2007). Characterization of the role of the receptors PEX5 and PEX7 in the import of proteins into glycosomes of *Trypanosoma brucei*. *Biochim Biophys Acta*, 1773(4):521–535.

Garfinkel D, Garfinkel L, Pring M, Green SB, and Chance B (1970). Computer applications to biochemical kinetics. *Annu Rev Biochem*, 39(1):473–498.

Gerber G, Berger H, Jänig GR, and Rapoport SM (1973). Interaction of haemoglobin with ions. *Eur J Biochem*, 38(3):563–571.

Gerlt JA, Allen KN, Almo SC, *et al.* (2011). The enzyme function initiative. *Biochemistry (Mosc)*, 50(46):9950–9962.

Goldberg RN and Tewari YB (1995). Thermodynamics of enzyme-catalyzed reactions: Part 5. Isomerases and ligases. *J Phys Chem Ref Data*, 24(6):1765–1801.

Goldberg RN, Tewari YB, Bell D, Fazio K, and Anderson E (1993). Thermodynamics of enzyme-catalyzed reactions: Part 1. Oxidoreductases. *J Phys Chem Ref Data*, 22(2):515–582.

Goldberg RN, Tewari YB, and Bhat TN (2004). Thermodynamics of enzyme-catalyzed reactions-a database for quantitative biochemistry. *Bioinformatics*, 20(16):2874–2877.

Gould SJ, Keller GA, and Subramani S (1988). Identification of peroxisomal targeting signals located at the carboxy terminus of four peroxisomal proteins. *J Cell Biol*, 107(3):897–905.

Grant PT and Fulton JD (1957). The catabolism of glucose by strains of *Trypanosoma rhodesiense*. *Biochemical J*, 66(2):242–250.

Grunau S, Mindthoff S, Rottensteiner H, Sormunen RT, Hiltunen JK, Erdmann R, and Antonenkov VD (2009). Channel-forming activities of peroxisomal membrane proteins from the yeast *Saccharomyces cerevisiae*. *FEBS J*, 276(6):1698–1708.

Gualdrón-López M, Brennand A, Avilán L, and Michels PaM (2012a). Translocation of solutes and proteins across the glycosomal membrane of trypanosomes; possibilities and limitations for targeting with trypanocidal drugs. *Parasitology*, FirstView:1–20.

Gualdrón-López M, Brennand A, Hannaert V, Quiñones W, Cáceres AJ, Bringaud F, Concepción JL, and Michels PA (2012b). When, how and why glycolysis became compartmentalised in the Kinetoplastea. a new look at an ancient organelle. *Int J Parasitol*, 42(1):1–20.

Gualdrón-López M, Vapola MH, Miinalainen IJ, Hiltunen JK, Michels PAM, and Antonenkov VD (2012c). Channel-forming activities in the glycosomal fraction from the bloodstream form of *Trypanosoma brucei*. *PLoS ONE*, 7(4):e34530.

Guerra-Giraldez C, Quijada L, and Clayton CE (2002). Compartmentation of enzymes in a microbody, the glycosome, is essential in *Trypanosoma brucei*. *J Cell Sci*, 115(Pt 13):2651–2658.

Haanstra JR (2009). *The power of network-based drug design and the interplay between metabolism and gene expression in Trypanosoma brucei*. Ph.D. thesis, VU Unversity, Amsterdam.

Haanstra JR, Kerkhoven EJ, van Tuijl A, *et al.* (2011). A domino effect in drug action: from metabolic assault towards parasite differentiation. *Mol Microbiol*, 79(1):94–108.

Haanstra JR, Tuijl Av, Kessler P, Reijnders W, Michels PAM, Westerhoff HV, Parsons M, and Bakker BM (2008). Compartmentation prevents a lethal turbo-explosion of glycolysis in trypanosomes. *Proc Natl Acad Sci U S A*, 105(46):17718–17723.

Haanstra JR, van Tuijl A, van Dam J, van Winden W, Tielens AG, van Hellemond JJ, and Bakker BM (2012). Proliferating bloodstream-form *Trypanosoma brucei* use a negligible part of consumed glucose for anabolic processes. *Int J Parasitol*, 42(7):667–673.

Hammond DJ and Bowman IB (1980a). Studies on glycerol kinase and its role in ATP synthesis in *Trypanosoma brucei*. *Mol Biochem Parasitol*, 2(2):77–91.

Hammond DJ and Bowman IB (1980b). *Trypanosoma brucei*: the effect of glycerol on the anaerobic metabolism of glucose. *Mol Biochem Parasitol*, 2(2):63–75.

Hanau S, Rippa M, Bertelli M, Dallocchio F, and Barrett MP (1996). 6-phosphogluconate dehydrogenase from *Trypanosoma brucei*. *Eur J Biochem*, 240(3):592–599.

Hannaert V, Albert MA, Rigden DJ, Theresa da Silva Giotto M, Thiemann O, Garratt RC, Van Roy J, Opperdoes FR, and Michels PAM (2003a). Kinetic characterization, structure modelling studies and crystallization of *Trypanosoma brucei* enolase. *Eur J Biochem*, 270(15):3205–3213.

Hannaert V, Bringaud F, Opperdoes FR, and Michels PA (2003b). Evolution of energy metabolism and its compartmentation in Kinetoplastida. *Kinetoplastid Biol Dis*, 2:11.

Hara T, Kanbara H, Nakao M, and Fukuma T (1997). Rapid uptake and phosphorylation of D-mannose, and limited D-mannose. 6-phosphate isomerization in the glycolytic pathway of bloodstream forms of *Trypanosoma brucei gambiense*. *Kurume Med J*, 44(2):105–113.

Hart DT, Misset O, Edwards SW, and Opperdoes FR (1984). A comparison of the glycosomes (microbodies) isolated from *Trypanosoma brucei* bloodstream form and cultured procyclic trypomastigotes. *Mol Biochem Parasitol*, 12(1):25–35.

Heinrich R and Rapoport TA (1974). A linear steady-state treatment of enzymatic chains. *Eur J Biochem*, 42(1):89–95.

Heise N and Opperdoes FR (1999). Purification, localisation and characterisation of glucose-6-phosphate dehydrogenase of *Trypanosoma brucei*. *Mol Biochem Parasitol*, 99(1):21–32.

Helfert S, Estévez AM, Bakker B, Michels P, and Clayton C (2001). Roles of triosephosphate isomerase and aerobic metabolism in *Trypanosoma brucei*. *Biochemical J*, 357(Pt 1):117–125.

Heringa J (1999). Two strategies for sequence comparison: profile-preprocessed and secondary structure-induced multiple alignment. *Comput Chem*, 23(3-4):341–364.

Herman M, Pérez-Morga D, Schtickzelle N, and Michels PAM (2008). Turnover of glycosomes during life-cycle differentiation of *Trypanosoma brucei*. *Autophagy*, 4(3):294–308.

Hirumi H and Hirumi K (1989). Continuous cultivation of *Trypanosoma brucei* blood stream forms in a medium containing a low concentration of serum protein without feeder cell layers. *J Parasitol*, 75(6):985–989.

Hoops S, Sahle S, Gauges R, Lee C, Pahle J, Simus N, Singhal M, Xu L, Mendes P, and Kummer U (2006). COPASI–a COmplex PAthway SImulator. *Bioinformatics*, 22(24):3067–3074.

Hu G, Taylor AB, McAlister-Henn L, and Hart PJ (2007). Crystal structure of the yeast nicotinamidase Pnc1p. *Arch Biochem Biophys*, 461(1):66–75.

Hughes MB and Lucchesi JC (1977). Genetic rescue of a lethal "null" activity allele of 6-phosphogluconate dehydrogenase in *Drosophila Melanogaster*. *Science*, 196(4294):1114–1115.

Hunt M and Köhler P (1995). Purification and characterization of phospho enol pyruvate carboxykinase from *Trypanosoma brucei*. *Biochim Biophys Acta*, 1249(1):15–22.

Hutcheson SW and Kosuge T (1985). Regulation of 3-indoleacetic acid production in *Pseudomonas syringae pv. savastanoi*. purification and properties of tryptophan 2-monooxygenase. *J Biol Chem*, 260(10):6281–6287.

Igoillo-Esteve M and Cazzulo JJ (2006). The glucose-6-phosphate dehydrogenase from *Trypanosoma cruzi*: Its role in the defense of the parasite against oxidative stress. *Mol Biochem Parasitol*, 149(2):170–181.

Igoillo-Esteve M, Maugeri D, Stern AL, Beluardi P, and Cazzulo JJ (2007). The pentose phosphate pathway in *Trypanosoma cruzi*: a potential target for the chemotherapy of Chagas disease. *An Acad Bras Cienc*, 79(4):649–663.

Janson CA and Cleland WW (1974). The kinetic mechanism of glycerokinase. *J Biol Chem*, 249(8):2562–2566.

Javid-Majd F and Blanchard JS (2000). Mechanistic analysis of the argE-encoded N-acetylornithine deacetylase. *Biochemistry (Mosc)*, 39(6):1285–1293.

Joice AC, Lyda TL, Sayce AC, Verplaetse E, Morris MT, Michels PA, Robinson DR, and Morris JC (2012). Extra-glycosomal localisation of *Trypanosoma brucei* hexokinase 2. *Int J Parasitol*, 42(4):401–409.

Jones DC, Ariza A, Chow WHA, Oza SL, and Fairlamb AH (2010). Comparative structural, kinetic and inhibitor studies of *Trypanosoma brucei* trypanothione reductase with *T. cruzi*. *Mol Biochem Parasitol*, 169(1):12–19.

Joshi A and Palsson BO (1989). Metabolic dynamics in the human red cell: Part I-A comprehensive kinetic model. *J Theor Biol*, 141(4):515–528.

Joshi-Tope G (2004). Reactome: a knowledgebase of biological pathways. *Nucleic Acids Res*, 33(Database):D428–D432.

Kacser H and Burns JA (1973). The control of flux. *Symp Soc Exp Biol*, 27:65–104.

Kell DB (2004). Metabolomics and systems biology: making sense of the soup. *Curr Opin Microbiol*, 7(3):296–307.

Keller GA, Gould S, Deluca M, and Subramani S (1987). Firefly luciferase is targeted to peroxisomes in mammalian cells. *Proc Natl Acad Sci U S A*, 84(10):3264–3268.

Keseler IM, Bonavides-Martinez C, Collado-Vides J, *et al.* (2009). EcoCyc: a comprehensive view of *Escherichia coli* biology. *Nucleic Acids Res*, 37(Database):D464–D470.

Kessler PS and Parsons M (2005). Probing the role of compartmentation of glycolysis in procyclic form *Trypanosoma brucei*. RNA interference studies of PEX14, hexokinase and phosphofructokinase. *J Biol Chem*, 280(10):9030–9036.

Kessner D, Chambers M, Burke R, Agus D, and Mallick P (2008). ProteoWizard: open source software for rapid proteomics tools development. *Bioinformatics*, 24(21):2534–2536.

Kiaira J and Njogu R (1989). Evidence for glycerol 3-phosphate: glucose transphosphorylase activity in bloodstream *Trypanosoma brucei brucei*. *Int J Biochem*, 21(8):839–845.

Klein ATJ, Berg Mvd, Bottger G, Tabak HF, and Distel B (2002). *Saccharomyces cerevisiae* acyl-CoA oxidase follows a novel, non-PTS1, import pathway into peroxisomes that is dependent on Pex5p. *J Biol Chem*, 277(28):25011–25019.

Krakow JL and Wang CC (1990). Purification and characterization of glycerol kinase from *Trypanosoma brucei*. *Mol Biochem Parasitol*, 43(1):17–25.

Králová I, Rigden DJ, Opperdoes FR, and Michels PAM (2000). Glycerol kinase of *Trypanosoma brucei*. *Eur J Biochem*, 267(8):2323–2333.

Krauth-Siegel RL and Comini MA (2008). Redox control in trypanosomatids, parasitic protozoa with trypanothione-based thiol metabolism. *Biochim Biophys Acta*, 1780(11):1236–1248.

Krazy H and Michels PA (2006). Identification and characterization of three peroxins-PEX6, PEX10 and PEX12-involved in glycosome biogenesis in *Trypanosoma brucei*. *BBA-Mol Cell Res*, 1763(1):6–17.

Krieger S, Schwarz W, Ariyanayagam MR, Fairlamb AH, Krauth-Siegel RL, and Clayton C (2000). Trypanosomes lacking trypanothione reductase are avirulent and show increased sensitivity to oxidative stress. *Mol Microbiol*, 35(3):542–552.

Kuettel S, Wadum MCT, Güther MLS, Mariño K, Riemer C, and Ferguson MAJ (2012). The de novo and salvage pathways of GDP-mannose biosynthesis are both sufficient for the growth of bloodstream-form *Trypanosoma brucei*. *Mol Microbiol*, 84(2):340–351.

Kupor SR and Fraenkel DG (1972). Glucose metabolism in 6-phosphogluconolactonase mutants of *Escherichia coli*. *J Biol Chem*, 247(6):1904–1910.

Laemmli UK (1970). Cleavage of structural proteins during the assembly of the head of bacteriophage T4. *Nature*, 227(5259):680–685.

Lambeir Am, Loiseau AM, Kuntz DA, Vellieux FM, Michels PAM, and Opperdoes FR (1991). The cytosolic and glycosomal glyceraldehyde-3-phosphate dehydrogenase from *Trypanosoma brucei*. *Eur J Biochem*, 198(2):429–435.

Lambeir Am, Opperdoes FR, and Wierenga RK (1987). Kinetic properties of triose-phosphate isomerase from *Trypanosoma brucei brucei*. *Eur J Biochem*, 168(1):69–74.

Langer T, Lu C, Echols H, Flanagan J, Hayer MK, and Hartl FU (1992). Successive action of DnaK, DnaJ and GroEL along the pathway of chaperone-mediated protein folding. *Nature*, 356(6371):683–689.

Lee DS, Burd H, Liu J, Almaas E, Wiest O, Barabási AL, Oltvai ZN, and Kapatral V (2009). Comparative genome-scale metabolic reconstruction and flux balance analysis of multiple *Staphylococcus aureus* genomes identify novel antimicrobial drug targets. *J Bacteriol*, 191(12):4015–4024.

LePage RW and Barrett MP (1990). Cloning of the 6-phosphogluconate dehydrogenase gene from *Trypanosoma brucei* by complementation in *Escherichia coli*. *Biochem Soc Trans*, 18(5):724–727.

Lobo Z and Maitra PK (1982). Pentose phosphate pathway mutants of yeast. *Mol Gen Genet*, 185(2):367–368.

Loomis WF and Thomas SR (1976). Kinetic analysis of biochemical differentiation in *Dictyostelium discoideum*. *J Biol Chem*, 251(20):6252–6258.

Lorenzatto KR, Monteiro KM, Paredes R, Paludo GP, da Fonsêca MM, Galanti N, Zaha A, and Ferreira HB (2012). Fructose-bisphosphate aldolase and enolase from *Echinococcus granulosus*: Genes, expression patterns and protein interactions of two potential moonlighting proteins. *Gene*, 506(1):76–84.

Ma H, Sorokin A, Mazein A, Selkov A, Selkov E, Demin O, and Goryanin I (2007). The Edinburgh human metabolic network reconstruction and its functional analysis. *Mol Syst Biol*, 3:135.

Mackenzie NE, Hall JE, Flynn IW, and Scott AI (1983). 13C nuclear magnetic resonance studies of anaerobic glycolysis in *Trypanosoma brucei* spp. *Biosci Rep*, 3(2):141–151.

Mackenzie NE, Hall JE, Seed JR, and Scott AI (1982). Carbon-13 nuclear-magnetic-resonance studies of glucose catabolism by *Trypanosoma brucei* gambiense. *Eur J Biochem*, 121(3):657–661.

Maj MC and Gupta RS (2001). The effect of inorganic phosphate on the activity of bacterial ribokinase. *J Protein Chem*, 20(2):139–144.

Marchand M, Kooystra U, Wierenga RK, Lambeir AM, Van Beeumen J, Opperdoes FR, and Michels PA (1989). Glucosephosphate isomerase from *Trypanosoma brucei*. Cloning and characterization of the gene and analysis of the enzyme. *Eur J Biochem*, 184(2):455–464.

Marché S, Michels PA, and Opperdoes FR (2000). Comparative study of *Leishmania mexicana* and *Trypanosoma brucei* NAD-dependent glycerol-3-phosphate dehydrogenase. *Mol Biochem Parasitol*, 106(1):83–91.

Maugeri DA and Cazzulo JJ (2004). The pentose phosphate pathway in *Trypanosoma cruzi*. *FEMS Microbiol Lett*, 234(1):117–123.

Maugeri DA, Cazzulo JJ, Burchmore RJS, Barrett MP, and Ogbunude POJ (2003). Pentose phosphate metabolism in *Leishmania mexicana*. *Mol Biochem Parasitol*, 130(2):117–125.

McLaughlin J (1986). The association of distinct acid phosphatases with the flagella pocket and surface membrane fractions obtained from bloodstream forms of *Trypanosoma rhodesiense*. *Mol Cell Biochem*, 70(2):177–184.

McLuckey SA and Wells JM (2001). Mass analysis at the advent of the 21st century. *Chem Rev*, 101(2):571–606.

Meinnel T, Schmitt E, Mechulam Y, and Blanquet S (1992). Structural and biochemical characterization of the *Escherichia coli* argE gene product. *J Bacteriol*, 174(7):2323–2331.

Michels PA, Bringaud F, Herman M, and Hannaert V (2006). Metabolic functions of glycosomes in trypanosomatids. *BBA-Mol Cell Res*, 1763(12):1463–1477.

Michels PA, Hannaert V, and Bringaud F (2000). Metabolic aspects of glycosomes in trypanosomatidae - new data and views. *Parasitol Today*, 16(11):482–489.

Miclet E, Stoven V, Michels PA, Opperdoes FR, Lallemand JY, and Duffieux F (2001). NMR spectroscopic analysis of the first two steps of the pentose-phosphate pathway elucidates the role of 6-phosphogluconolactonase. *J Biol Chem*, 276(37):34840–34846.

Mielniczki-Pereira A, Chiavegatto C, López J, Colli W, Alves M, and Gadelha F (2007). *Trypanosoma cruzi* strains, Tulahuen 2 and Y, besides the difference in resistance to oxidative stress, display differential glucose-6-phosphate and 6-phosphogluconate dehydrogenases activities. *Acta Trop*, 101(1):54–60.

Misset O, Bos OJM, and Opperdoes FR (1986). Glycolytic enzymes of *Trypanosoma brucei*. *Eur J Biochem*, 157(2):441–453.

Misset O and Opperdoes FR (1987). The phosphoglycerate kinases from *Trypanosoma brucei*. *Eur J Biochem*, 162(3):493–500.

Mišković L and Hatzimanikatis V (2011). Modeling of uncertainties in biochemical reactions. *Biotechnol Bioeng*, 108(2):413–423.

Morris MT, DeBruin C, Yang Z, Chambers JW, Smith KS, and Morris JC (2006). Activity of a second *Trypanosoma brucei* hexokinase is controlled by an 18-amino-acid c-terminal tail. *Eukaryot Cell*, 5(12):2014–2023.

Moyersoen J, Choe J, Kumar A, Voncken FGJ, Hol WGJ, and Michels PAM (2003). Characterization of *Trypanosoma brucei* PEX14 and its role in the import of glycosomal matrix proteins. *Eur J Biochem*, 270(9):2059–2067.

Müller S (2004). Redox and antioxidant systems of the malaria parasite *Plasmodium falciparum*. *Mol Microbiol*, 53(5):1291–1305.

Mulquiney PJ and Kuchel PW (1999a). Model of 2,3-bisphosphoglycerate metabolism in the human erythrocyte based on detailed enzyme kinetic equations: computer simulation and metabolic control analysis. *Biochem J*, 342(Pt 3):597–604.

Mulquiney PJ and Kuchel PW (1999b). Model of 2,3-bisphosphoglycerate metabolism in the human erythrocyte based on detailed enzyme kinetic equations: equations and parameter refinement. *Biochem J*, 342(Pt 3):581–596.

Murabito E, Smallbone K, Swinton J, Westerhoff HV, and Steuer R (2011). A probabilistic approach to identify putative drug targets in biochemical networks. *J R Soc Interface*, 8(59):880–895.

Northen TR, Lee JC, Hoang L, Raymond J, Hwang DR, Yannone SM, Wong CH, and Siuzdak G (2008). A nanostructure-initiator mass spectrometry-based enzyme activity assay. *Proc Natl Acad Sci U S A*, 105(10):3678–3683.

Nwagwu M and Opperdoes FR (1982). Regulation of glycolysis in *Trypanosoma brucei*: hexokinase and phosphofructokinase activity. *Acta Trop*, 39(1):61–72.

Odiit M, Coleman PG, Liu WC, McDermott JJ, Fèvre EM, Welburn SC, and Woolhouse MEJ (2005). Quantifying the level of under-detection of *Trypanosoma brucei rhodesiense* sleeping sickness cases. *Trop Med Int Health*, 10(9):840–849.

Ogbunude POJ, Lamour N, and Barrett MP (2007). Molecular cloning, expression and characterization of ribokinase of *Leishmania major*. *Acta Biochim Biophys Sin*, 39(6):462–466.

Olin-Sandoval V, González-Chávez Z, Berzunza-Cruz M, Martínez I, Jasso-Chávez R, Becker I, Espinoza B, Moreno-Sánchez R, and Saavedra E (2012). Drug target validation of the trypanothione pathway enzymes through metabolic modelling. *FEBS J*, 279:1811–1833.

Olin-Sandoval V, Moreno-Sánchez R, and Saavedra E (2010). Targeting trypanothione metabolism in trypanosomatid human parasites. *Curr Drug Targets*, 11(12):1614–1630.

Olivier BG, Rohwer JM, and Hofmeyr JHS (2005). Modelling cellular systems with PySCeS. *Bioinformatics*, 21(4):560–561.

Opperdoes FR (1984). Localization of the initial steps in alkoxyphospholipid biosynthesis in glycosomes (microbodies) of *Trypanosoma brucei*. *FEBS Lett*, 169(1):35–39.

Opperdoes FR (1987). Compartmentation of carbohydrate metabolism in trypanosomes. *Annu Rev Microbiol*, 41(1):127–151.

Opperdoes FR (1988). Glycosomes may provide clues to the import of peroxisomal proteins. *Trends Biochem Sci*, 13(7):255–260.

Opperdoes FR, Baudhuin P, Coppens I, Roe CD, Edwards SW, Weijers PJ, and Misset O (1984). Purification, morphometric analysis, and characterization of the glycosomes (microbodies) of the protozoan hemoflagellate *Trypanosoma brucei*. *J Cell Biol*, 98(4):1178–1184.

Opperdoes FR and Borst P (1977). Localization of nine glycolytic enzymes in a microbody-like organelle in *Trypanosoma brucei*: the glycosome. *FEBS Lett*, 80(2):360–364.

Opperdoes FR and Szikora JP (2006). In silico prediction of the glycosomal enzymes of *Leishmania major* and trypanosomes. *Mol Biochem Parasitol*, 147(2):193–206.

Ormerod W, Parr C, Venkatesan S, and Welch S (1970). Lactate dehydrogenase and trypanosomes. *Trans R Soc Trop Med Hyg*, 64(1):176–177.

Pabón M, Cáceres A, Gualdrón M, Quiñones W, Avilán L, and Concepción J (2007). Purification and characterization of hexokinase from *Leishmania mexicana*. *Parasitol Res*, 100(4):803–810.

Pan Z and Raftery D (2007). Comparing and combining NMR spectroscopy and mass spectrometry in metabolomics. *Anal Bioanal Chem*, 387(2):525–527.

Park J, van Koeverden P, Singh B, and Gupta RS (2007). Identification and characterization of human ribokinase and comparison of its properties with *E. coli* ribokinase and human adenosine kinase. *FEBS Lett*, 581(17):3211–3216.

Parsons M (2004). Glycosomes: parasites and the divergence of peroxisomal purpose. *Mol Microbiol*, 53(3):717–724.

Pasti C, Rinaldi E, Cervellati C, Dallocchio F, Hardré R, Salmon L, and Hanau S (2003). Sugar derivatives as new 6-phosphogluconate dehydrogenase inhibitors selective for the parasite *Trypanosoma brucei*. *Bioorgan Med Chem*, 11(7):1207–1214.

Penketh PG and Klein RA (1986). Hydrogen peroxide metabolism in *Trypanosoma brucei*. *Mol Biochem Parasitol*, 20(2):111–121.

Pereira CA, Alonso GD, Torres HN, and Flawiá MM (2002). Arginine kinase: A common feature for management of energy reserves in African and American flagellated trypanosomatids. *J Eukaryot Microbiol*, 49(1):82–85.

Pereira CA, Bouvier LA, Cámara MdlM, and Miranda MR (2011). Singular features of Trypanosomatids' phosphotransferases involved in cell energy management. *Enzyme Research*, 2011:576483.

Peringer P, Blachere H, Corrieu G, and Lane AG (1974). A generalized mathematical model for the growth kinetics of *Saccharomyces cerevisiae* with experimental determination of parameters. *Biotechnol Bioeng*, 16(4):431–454.

Petterson G and Ryde-Petterson U (1988). A mathematical model of the Calvin photosynthesis cycle. *Eur J Biochem*, 175(3):661–672.

Phillips MA and Wang CC (1987). A *Trypanosoma brucei* mutant resistant to α-difluoromethylornithine. *Mol Biochem Parasitol*, 22(1):9–17.

Poulin R, Lu L, Ackermann B, Bey P, and Pegg AE (1992). Mechanism of the irreversible inactivation of mouse ornithine decarboxylase by alpha-difluoromethylornithine. characterization of sequences at the inhibitor and coenzyme binding sites. *J Biol Chem*, 267(1):150–158.

Pujol A, Mosca R, Farrés J, and Aloy P (2010). Unveiling the role of network and systems biology in drug discovery. *Trends Pharmacol Sci*, 31(3):115–123.

Rakitzis ET and Papandreou P (1998). Reactivity of 6-phosphogluconolactone with hydroxylamine: The possible involvement of glucose-6-phosphate dehydrogenase in endogenous glycation reactions. *Chem Biol Interact*, 113(3):205–216.

Räz B, Iten M, Grether-Bühler Y, Kaminsky R, and Brun R (1997). The Alamar Blue ® assay to determine drug sensitivity of African trypanosomes (*T.b. rhodesiense* and *T.b. gambiense*) in vitro. *Acta Trop*, 68(2):139–147.

Redmond S, Vadivelu J, and Field MC (2003). RNAit: an automated web-based tool for the selection of RNAi targets in *Trypanosoma brucei*. *Mol Biochem Parasitol*, 128(1):115–118.

Reynolds C (1975). The NAD-linked α-glycerophosphate dehydrogenase of trypanosomes. *Biochem Biophys Res Commun*, 67(2):538–543.

Richter O, Betz A, and Giersch C (1975). The response of oscillating glycolysis to perturbations in the NADH/NAD system: A comparison between experiments and a computer model. *BioSystems*, 7(1):137–146.

Riley E, Roberts SC, and Ullman B (2011). Inhibition profile of *Leishmania mexicana* arginase reveals differences with human arginase I. *Int J Parasitol*, 41(5):545–552.

Risby EL and Seed JR (1969). Purification and properties of purified hexokinase from the African trypanosomes and *Trypanosoma equiperdum*. *J Eukaryot Microbiol*, 16(1):193–197.

Risby EL, Seed TM, and Seed JR (1969). *Trypanosoma gambiense*, *T. rhodesiense*, *T. brucei*, *T. equiperdum*, and *T. lewisi*: Purification and properties of phosphohexose isomerase. *Exp Parasitol*, 25:101–106.

Rodriguez-Contreras D, Feng X, Keeney KM, Bouwer HA, and Landfear SM (2007). Phenotypic characterization of a glucose transporter null mutant in *Leishmania mexicana*. *Mol Biochem Parasitol*, 153(1):9–18.

Rokka A, Antonenkov VD, Soininen R, Immonen HL, Pirilä PL, Bergmann U, Sormunen RT, Weckström M, Benz R, and Hiltunen JK (2009). Pxmp2 is a channel-forming protein in mammalian peroxisomal membrane. *PLoS ONE*, 4(4):e5090.

Ruiz-Postigo JA, Franco JR, Lado M, and Simarro PP (2012). Human African trypanosomiasis in South Sudan: How can we prevent a new epidemic? *PLoS Negl Trop Dis*, 6(5):e1541.

Ryley J (1956). Studies on the metabolism of the protozoa. 7. Comparative carbohydrate metabolism of eleven species of trypanosome. *Biochem J*, 62:215–222.

Ryley J (1962). Studies on the metabolism of the protozoa. 9. Comparative metabolism of blood-stream and culture forms of *Trypanosoma rhodesiense*. *Biochem J*, 85:211–223.

Saghatelian A, Trauger SA, Want EJ, Hawkins EG, Siuzdak G, and Cravatt BF (2004). Assignment of endogenous substrates to enzymes by global metabolite profiling. *Biochemistry (Mosc)*, 43(45):14332–14339.

Saito N, Ohashi Y, Soga T, and Tomita M (2010). Unveiling cellular biochemical reactions via metabolomics-driven approaches. *Curr Opin Microbiol*, 13(3):358–362.

Saito N, Robert M, Kitamura S, Baran R, Soga T, Mori H, Nishioka T, and Tomita M (2006). Metabolomics approach for enzyme discovery. *J Proteome Res*, 5(8):1979–1987.

Saito N, Robert M, Kochi H, Matsuo G, Kakazu Y, Soga T, and Tomita M (2009). Metabolite profiling reveals YihU as a novel hydroxybutyrate dehydrogenase for alternative succinic semialdehyde metabolism in *Escherichia coli*. *J Biol Chem*, 284(24):16442–16451.

Sakanyan V, Desmarez L, Legrain C, Charlier D, Mett I, Kochikyan A, Savchenko A, Boyen A, Falmagne P, and Pierard A (1993). Gene cloning, sequence analysis, purification, and characterization of a thermostable aminoacylase from *Bacillus stearothermophilus. Appl Environ Microbiol*, 59(11):3878–3888.

Saunders EC, De Souza DP, Naderer T, *et al.* (2010). Central carbon metabolism of Leishmania parasites. *Parasitology*, 137(Special Issue 09):1303–1313.

Schellenberger W and Hervagault JF (1991). Irreversible transitions in the 6-phosphofructokinase/fructose 1,6-bisphosphatase cycle. *Eur J Biochem*, 195(1):109–113.

Scheltema RA, Jankevics A, Jansen RC, Swertz MA, and Breitling R (2011). PeakML/mzMatch: a file format, Java library, R library, and tool-chain for mass spectrometry data analysis. *Anal Chem*, 83(7):2786–2793.

Schliebs W (2006). Sleeping sickness: PEX and drugs. *BBA-Mol Cell Res*, 1763(1):4–5.

Schmitz JPJ, Riel NAWv, Nicolay K, Hilbers PAJ, and Jeneson JAL (2010). Silencing of glycolysis in muscle: experimental observation and numerical analysis. *Exp Physiol*, 95(2):380–397.

Schnoes AM, Brown SD, Dodevski I, and Babbitt PC (2009). Annotation error in public databases: Misannotation of molecular function in enzyme superfamilies. *PLoS Comput Biol*, 5(12):e1000605.

Schofield PJ and Sols A (1976). Rat liver 6-phosphogluconolactonase: a low km enzyme. *Biochem Biophys Res Commun*, 71(4):1313–1318.

Schumann Burkard G, Jutzi P, and Roditi I (2011). Genome-wide RNAi screens in bloodstream form trypanosomes identify drug transporters. *Mol Biochem Parasitol*, 175(1):91–94.

Schuster R and Holzhütter HG (1995). Use of mathematical models for predicting the metabolic effect of large-scale enzyme activity alterations. *Eur J Biochem*, 229(2):403–418.

Schuster R, Holzhütter HG, and Jacobasch G (1988). Interrelations between glycolysis and the hexose monophosphate shunt in erythrocytes as studied on the basis of a mathematical model. *BioSystems*, 22(1):19–36.

Schuster R, Jacobasch G, and Holzhütter HG (1989). Mathematical modelling of metabolic pathways affected by an enzyme deficiency. *Eur J Biochem*, 182(3):605–612.

Schuster S, Dandekar T, and Fell D (1999). Detection of elementary flux modes in biochemical networks: a promising tool for pathway analysis and metabolic engineering. *Trends Biotechnol*, 17(2):53–60.

Scott AG, Tait A, Michael C, and Turner R (1996). Characterisation of clones lines of *Trypanosoma brucei* expressing stable resistance to MelCy and suramin. *Acta Trop*, 60(4):251–262.

Seed JR, Byram J, and Gam AA (1967). Characterization and localization of acid phosphatase activity of *Trypanosoma gambiense*. *J Eukaryot Microbiol*, 14(1):117–125.

Seffernick JL, De Souza ML, Sadowsky MJ, and Wackett LP (2001). Melamine deaminase and atrazine chlorohydrolase: 98 percent identical but functionally different. *J Bacteriol*, 183(8):2405–2410.

Siegel TN, Hekstra DR, Wang X, Dewell S, and Cross GAM (2010). Genome-wide analysis of mRNA abundance in two life-cycle stages of *Trypanosoma brucei* and identification of splicing and polyadenylation sites. *Nucleic Acids Res*, 38(15):4946–4957.

Simarro PP, Franco J, Diarra A, Postigo JaR, and Jannin J (2012). Update on field use of the available drugs for the chemotherapy of human African trypanosomiasis. *Parasitology*, 139(07):842–846.

Simarro PP, Jannin J, and Cattand P (2008). Eliminating human African trypanosomiasis: Where do we stand and what comes next? *PLoS Med*, 5(2):e55.

Smith CA, Want EJ, O'Maille G, Abagyan R, and Siuzdak G (2006). XCMS: Processing mass spectrometry data for metabolite profiling using nonlinear peak alignment, matching, and identification. *Anal Chem*, 78(3):779–787.

Snoep JL (2005). The silicon cell initiative: working towards a detailed kinetic description at the cellular level. *Curr Opin Biotechnol*, 16(3):336–343.

Snoep JL, Bruggeman F, Olivier BG, and Westerhoff HV (2006). Towards building the silicon cell: A modular approach. *BioSystems*, 83(2-3):207–216.

Sommer JM, Cheng QL, Keller GA, and Wang CC (1992). In vivo import of firefly luciferase into the glycosomes of *Trypanosoma brucei* and mutational analysis of the c-terminal targeting signal. *Mol Biol Cell*, 3(7):749–759.

Sommer JM and Wang CC (1994). Targeting proteins to the glycosomes of African trypanosomes. *Annu Rev Microbiol*, 48(1):105–138.

Spitznagel D, Ebikeme C, Biran M, Nic a' Bháird N, Bringaud F, Henehan GTM, and Nolan DP (2009). Alanine aminotransferase of *Trypanosoma brucei*- a key role in proline metabolism in procyclic life forms. *FEBS J*, 276(23):7187–7199.

Steverding D (2008). The history of African trypanosomiasis. *Parasit Vectors*, 1(1):3.

Stoffel SA, Alibu VP, Hubert J, Ebikeme C, Portais JC, Bringaud F, Schweingruber ME, and Barrett MP (2011). Transketolase in *Trypanosoma brucei*. *Mol Biochem Parasitol*, 179(1):1–7.

Stuart K, Brun R, Croft S, Fairlamb A, Gürtler RE, McKerrow J, Reed S, and Tarleton R (2008). Kinetoplastids: related protozoan pathogens, different diseases. *J Clin Invest*, 118(4):1301–1310.

Sukhatme VP and Chan B (2012). Glycolytic cancer cells lacking 6-phosphogluconate dehydrogenase metabolize glucose to induce senescence. *FEBS Lett*, 586(16):2389–2395.

Sumner LW, Mendes P, and Dixon RA (2003). Plant metabolomics: large-scale phytochemistry in the functional genomics era. *Phytochemistry*, 62(6):817–836.

Sun H, Chattopadhaya S, Wang J, and Yao SQ (2006). Recent developments in microarray-based enzyme assays: from functional annotation to substrate/inhibitor fingerprinting. *Anal Bioanal Chem*, 386(3):416–426.

Swinkels BW, Gould SJ, Bodnar AG, Rachubinski RA, and Subramani S (1991). A novel, cleavable peroxisomal targeting signal at the amino-terminus of the rat 3-ketoacyl-CoA thiolase. *EMBO J*, 10(11):3255–3262.

Teusink B, Passarge J, Reijenga CA, *et al.* (2000). Can yeast glycolysis be understood in terms of in vitro kinetics of the constituent enzymes? Testing biochemistry. *Eur J Biochem*, 267(17):5313–5329.

Teusink B, Walsh MC, van Dam K, and Westerhoff HV (1998). The danger of metabolic pathways with turbo design. *Trends Biochem Sci*, 23(5):162–169.

Tewari YB, Steckler DK, Goldberg RN, and Gitomer WL (1988). Thermodynamics of hydrolysis of sugar phosphates. *J Biol Chem*, 263(8):3670–3675.

Thorburn DR and Kuchel PW (1985). Regulation of the human-erythrocyte hexose-monophosphate shunt under conditions of oxidative stress. a study using NMR spectroscopy, a kinetic isotope effect, a reconstituted system and computer simulation. *Eur J Biochem*, 150(2):371–386.

Tong J, Valverde O, Mahoudeau C, Yun O, and Chappuis F (2011). Challenges of controlling sleeping sickness in areas of violent conflict: experience in the Democratic Republic of Congo. *Conflict and Health*, 5(1):7.

Tran LM, Rizk ML, and Liao JC (2008). Ensemble modeling of metabolic networks. *Biophys J*, 95(12):5606–5617.

Tweeddale H, Notley-McRobb L, and Ferenci T (1998). Effect of slow growth on metabolism of *Escherichia coli*, as revealed by global metabolite pool ("Metabolome") analysis. *J Bacteriol*, 180(19):5109–5116.

Urbina JA and Crespo A (1984). Regulation of energy metabolism in *Trypanosoma (schizotrypanum) cruzi* epimastigotes, I. hexokinase and phosphofructokinase. *Mol Biochem Parasitol*, 11:225–239.

van Eunen K, Dool P, Canelas A, Kiewiet J, Bouwman J, van Gulik W, Westerhoff H, and Bakker B (2010). Time-dependent regulation of yeast glycolysis upon nitrogen starvation depends on cell history. *IET Syst Biol*, 4(2):157.

van Eunen K, Kiewiet JAL, Westerhoff HV, and Bakker BM (2012). Testing biochemistry revisited: How in vivo metabolism can be understood from in vitro enzyme kinetics. *PLoS Comput Biol*, 8(4):e1002483.

van Roermund CW, Drissen R, van Den Berg M, Ijlst L, Hettema EH, Tabak HF, Waterham HR, and Wanders RJ (2001). Identification of a peroxisomal ATP carrier required for medium-chain fatty acid beta-oxidation and normal peroxisome proliferation in *Saccharomyces cerevisiae*. *Mol Cell Biol*, 21(13):4321–4329.

Vanderheyden N, Wong J, and Docampo R (2000). A pyruvate-proton symport and an H+-ATPase regulate the intracellular pH of *Trypanosoma brucei* at different stages of its life cycle. *Biochemical J*, 346 Pt 1:53–62.

Vassella E, Acosta-Serrano A, Studer E, Lee SH, Englund PT, and Roditi I (2001). Multiple procyclin isoforms are expressed differentially during the development of insect forms of *Trypanosoma brucei*. *J Mol Biol*, 312(4):597–607.

Veitch N, Maugeri D, Cazzulo J, Lindqvist Y, and Barrett M (2004). Transketolase from *Leishmania mexicana* has a dual subcellular localization. *Biochem J*, 382(2):759.

Verlinde CL, Hannaert V, Blonski C, Willson M, Périé JJ, Fothergill-Gilmore LA, Opperdoes FR, Gelb MH, Hol WG, and Michels PA (2001). Glycolysis as a target for the design of new anti-trypanosome drugs. *Drug Resist Updat*, 4(1):50–65.

Verplaetse E, Rigden DJ, and Michels PAM (2009). Identification, characterization and essentiality of the unusual peroxin 13 from *Trypanosoma brucei*. *Biochim Biophys Acta*, 1793(3):516–527.

Vertommen D, Van Roy J, Szikora JP, Rider MH, Michels PAM, and Opperdoes FR (2008). Differential expression of glycosomal and mitochondrial proteins in the two major life-cycle stages of *Trypanosoma brucei*. *Mol Biochem Parasitol*, 158(2):189–201.

Vestal ML (2001). Methods of ion generation. *Chem Rev*, 101(2):361–376.

Villas-Bôas SG, Mas S, Akesson M, Smedsgaard J, and Nielsen J (2005). Mass spectrometry in metabolome analysis. *Mass Spectrom Rev*, 24(5):613–646.

Villet RH and Dalziel K (1969). The nature of the carbon dioxide substrate and equilibrium constant of the 6-phosphogluconate dehydrogenase reaction. *Biochem J*, 115(4):633–638.

Vincent IM (2011). *Using metabolomic analyses to study mode of action of and resistance to Eflornithine in Trypanosoma brucei*. Ph.D. thesis, University of Glasgow, Glasgow.

Vincent IM, Creek D, Watson DG, Kamleh MA, Woods DJ, Wong PE, Burchmore RJS, and Barrett MP (2010). A molecular mechanism for eflornithine resistance in African trypanosomes. *PLoS Pathog*, 6(11):e1001204.

Vincent IM, Creek DJ, Burgess K, Woods DJ, Burchmore RJS, and Barrett MP (2012). Untargeted metabolomics reveals a lack of synergy between nifurtimox and eflornithine against *Trypanosoma brucei*. *PLoS Negl Trop Dis*, 6(5):e1618.

Visser N and Opperdoes FR (1980). Glycolysis in *Trypanosoma brucei*. *Eur J Biochem*, 103(3):623–632.

Voet D, Voet JG, and Pratt CW (1999). *Fundamentals of biochemistry*. Wiley.

Walton PA, Hill PE, and Subramani S (1995). Import of stably folded proteins into peroxisomes. *Mol Biol Cell*, 6(6):675–683.

Wang L, Birol I, and Hatzimanikatis V (2004). Metabolic control analysis under uncertainty: Framework development and case studies. *Biophys J*, 87(6):3750–3763.

Weil-Malherbe H and Bone AD (1951). Activators and inhibitors of hexokinase in human blood. *Brit J Psychiat*, 97(409):635–662.

Westerhoff HV (2001). The silicon cell, not dead but live! *Metab Eng*, 3(3):207–210.

Westerhoff HV and Palsson BO (2004). The evolution of molecular biology into systems biology. *Nat Biotechnol*, 22(10):1249–1252.

WHO (2012). Human African trypanosomiasis (sleeping sickness).

Wiemer EA, Kuile BHT, Michels PA, and Opperdoes FR (1992). Pyruvate transport across the plasma membrane of the bloodstream form of *Trypanosoma brucei* is mediated by a facilitated diffusion carrier. *Biochem Biophys Res Commun*, 184(2):1028–1034.

Wurster B and Hess B (1970). Kinetic analysis of the glucosephosphate isomerase-glucose-6-phosphate dehydrogenase system from yeast in vitro. *H-S Z Physiol Chem*, 351(12):1537–1544.

Wurster B and Hess B (1973). Anomeric specificity and anomerase activity of glucosephosphate isomerase (EC 5.3.1.9) from baker's yeast. *H-S Z Physiol Chem*, 354(4):407–420.

Yamada T, Letunic I, Okuda S, Kanehisa M, and Bork P (2011). iPath2.0: interactive pathway explorer. *Nucleic Acids Res*, 39(Web Server):W412–W415.

Zhang H, Deng JY, Bi LJ, Zhou YF, Zhang ZP, Zhang CG, Zhang Y, and Zhang XE (2008). Characterization of *Mycobacterium tuberculosis* nicotinamidase/pyrazinamidase. *FEBS J*, 275(4):753–762.

Zhao B and Waterman MR (2011). Moonlighting cytochrome p450 monooxygenases. *IUBMB life*, 63(7):473–477.

Appendix A

Creek's minimal medium (CMM)

Note: unpublished

Compound	Concentration (µM)
Bathocuproine disulfonic acid	52
Phenolsulfonphtalein	42
HEPES	10,000
NaCl	77,590
$CaCl_2$	1,490
KCl	4,400
$MgSO_4$	814
$NaHCO_3$	35,950
D-Glucose	10,000
L-Glutamine	1,000
L-Cysteine	1,000
Mercaptoethanol	192
FBS Gold (PAA)	10 % [a]
Arginine	100 [a]
Tyrosine	100 [a]
Methionine	100 [a]
Leucine	100 [a]
Phenylalanine	100 [a]
Tryptophan	100 [a]

a: Arginine, tyrosine, methionine, leucine, phenylalanine and tryptophan are only added if a different brand of FBS is not able to support growth. Certified tetracycline-free FBS from Biosera requires the additional amino acids.

Table A.1.: Creek's minimal medium (CMM).

Appendix B

Elementary mode analysis of glycosomal proteome

A model of glycosomal metabolism was constructed, the metabolic reactions included in the model were taken from comprehensible glycosomal proteomics data (Colasante *et al.*, 2006; Vertommen *et al.*, 2008). Only those reactions expressed in the bloodstream form were included. All reactions were set as reversible, except for GPO, PFK, FBPase, PGL. Protons, Pi, PPi, H_2O, CO_2 and O_2 were not included in the reactions. Glucose, 3-PGA, ribose and glycerol were set as external metabolites.

Abbreviation	EC	Enzyme name	Mode	Ref.
OGDH	1.2.4.2	2-oxoglutarate dehydrogenase		a
SRD5A	1.3.99.5	3-oxo-5-alpha-steroid 4-dehydrogenase		a
6PGDH	1.1.1.43	6-phosphogluconate dehydrogenase	×	b
APRT	2.4.2.7	Adenine phosphoribosyltransferase	×	b
AdK	2.7.1.20	Adenosine kinase	×	b
ANase	3.2.2.7	Adenosine nucleosidase	×	b
AK	2.7.4.3	Adenylate kinase	×	a
AdSS	6.3.4.4	Adenylosuccinate synthetase		b
ALD	4.1.2.13	Aldolase	×	a, b
AGPS	2.5.1.26	Alkyl-dihydroxyacetone phosphate synthase		a
ArgK	2.7.3.3	Arginine kinase		a, b
FBPase	3.1.3.11	Fructose bisphosphatase	×	a
FRD	1.3.1.6	Fumarate reductase		b
G6PDH	1.1.1.49	Glucose-6-phosphate dehydrogenase	×	b
GAPDH	1.2.1.12	Glyceraldehyde-3-phosphate dehydrogenase	×	a, b
GK	2.7.1.30	Glycerol kinase	×	a, b
G3PDH	1.1.1.8	Glycerol-3-phosphate dehydrogenase	×	a, b
GPO	1.1.3.21	Glycerol-3-phosphate oxidase	×	a, b
GDA	3.5.4.15	Guanine deaminase		b
HGPRT	2.4.2.8	Guanine phosphoribosyltransferase		b
GNase	3.2.2.1	Guanosine nucleosidase		b
HXK	2.7.1.1	Hexokinase	×	a, b
HPRT	2.4.2.8	Hypoxanthine phosphoribosyltransferase		a
IRH	3.2.2.2	Inosine nucleosidase		b
IMPDH	1.1.1.205	Inosine-5'-monophosphate dehydrogenase		a, b
SOD	1.15.1.1	Iron superoxide dismutase		b
IDH	1.1.1.41	Isocitrate dehydrogenase		a, b
TDH	1.1.1.103	L-Threonine 3-dehydrogenase		a
LysoPLA	3.1.1.5	Lysophospholipase		a
MVK	2.7.1.36	Mevalonate kinase		b
NADPHu		NADPH utilization	×	
OMPRT	2.4.2.10	Orotate phosphoribosyltransferase		a, b
OMPDC	4.1.1.23	Orotidine-5-phosphate decarboxylase		a, b
PPI	5.3.1.6	Pentosephosphate isomerase	×	b
PEPCK	4.1.1.32	Phosphoenolpyruvate carboxykinase		b
PFK	2.7.1.11	Phosphofructokinase	×	a, b
PGL	3.1.1.31	Phosphogluconolactonase	×	
PGI	5.3.1.9	Phosphoglucose isomerase	×	a, b
PGK	2.7.2.3	Phosphoglycerate kinase	×	a, b
PMI	5.3.1.8	Phosphomannose isomerase		b
PRPPsyn	2.7.6.1	Phosphoribosyl pyrophosphate synthetase	×	b
PYK	2.7.1.40	Pyruvate kinase		a
RK	2.7.1.15	RK	×	a, b
TPI	5.3.1.1	Triosephosphate isomerase	×	a, b
GALE	5.1.3.2	UDP-galactose 4-epimerase		b
XNase	3.2.2.1	Xanthosine nucleosidase		b

Table B.1.: Additional glycosomal enzymes. All reactions present in the bloodstream form *T. brucei* glycosome, according to comprehensible glycosomal proteomics (ref. a: Colasante *et al.*, 2006; ref. b: Vertommen *et al.*, 2008). Only reactions present in the bloodstream form of the parasite are included. Abbreviations and EC numbers are given for each reaction. Indicated are what reactions are part of an elementary model (Table B.2).

Mode	Overall reaction	Individual reactions
1	Glc → 2 3-PGA	HXK, PGI, PFK, ALD, TPI, 2 GAPDH, 2 PGK, 2 G3PDH, 2 GPO
2	Glc → 3-PGA + Gly	HXK, PGI, PFK, ALD, GAPDH, PGK, G3PDH, GK
3	Gly → 3-PGA	–GK, 2 GPO, GDH, TPI, GAPDH, PGK
4	Glc → Rib	HXK, G6PDH, PGL, 6PGDH, PPI, 2 NADPHu, RK
5	Futile cycle	2 PFK, 2FBPase, RK, AK, APRT, ANase, –PRPPsyn, ADK
6	4 Gly → 2 Glc	4 –GK, 4 GPO, 2 TPI, 2 –ALD, 2 FBPase, 2 –PGI, 2 –HK, RK, AK, APRT, ANase, –PRPPsyn, ADK
7	4 Gly → 2 Rib	4 –GK, 4 GPO, 2 TPI, 2 –ALD, 2 FBPase, 2 –PGI, 2 G6PDH, 2 PGL, 2 6PGDH, 2 PPI, 3 RK, AK, APRT, ANase, –PRPPsyn, ADK, 4 NADPHu
8	2 3-PGA + 2 Gly → 2 Glc	2 –PGK, 2 –GAPDH, 2 –GK, 2 –GDH, 2 –ALD, 2 FBPase, 2 –PGI, 2 –HK, RK, AK, APRT, ANase, –PRPPsyn, ADK)
9	2 3-PGA + 2 Gly → 2 Rib	2 –PGK, 2 –GAPDH, 2 –GK, 2 –GDH, 2 –ALD, 2 FBPase, 2 –PGI, 2 G6PDH, 2 PGL, 2 6PGDH, 2 PPI, 3 RK, AK, APRT, ANase, –PRPPsyn, ADK, 4 NADPHu

Table B.2.: Elementary modes of glycosomal proteome. The resulting model has 9 elementary modes, of which modes 1–4 are comparable to modes 1–4 in Table 1.2. Elementary mode 5 is a futile cycle without external metabolites involved. Elementary modes 6–9 are unlikely to occur in dividing bloodstream trypanosomes, as a high glucose to pyruvate and glycerol flux is maintained. Additionally, the activity of FBPase could not be measured (Cronin *et al.*, 1989).

Appendix C

Parameter distributions

Courtesy of Dr Fiona Achcar, University of Glasgow.

C.1. Methods: sampling the parameters

The sampling methodology used is the same as described in (Achcar *et al.*, 2012). We sampled parameters simultaneously from the entire parameter space while respecting thermodynamic constraints, usually from a log-normal distribution using experimentally observed standard deviations. Thus, the distributions used to sample the parameters reflect our uncertainty about the value of each parameter. In comparison to Achcar *et al.*, the time limit allowed for a given model to reach steady-state (from the initial values based on the steady state of the fixed-parameter model) is increased to 1000 minutes (instead of 300) to account for the larger size of the models. Except for time series simulations, the results presented in the main manuscript are the steady state values of only those models that were able to reach steady state within 1000 minutes. For the glycolysis part of the models, the parameters and their uncertainties are the same as in (Achcar *et al.*, 2012) with the exception of the following parameters:

- The $V_{\max}$ of the phosphoglycerate mutase is still unknown. The accumulation of 3-phosphoglycerate described in (Achcar *et al.*, 2012) when this $V_{\max}$ is sampled in the lower range of its values is still occurring after addition of the pentose phosphate pathway. This issue is not modified by the addition of the pentose phosphate pathway in any of the topologies described in Figure 3.3. However, in order to limit the percentage of models that fail to reach steady state before 1000

minutes, we limited the sampling of the V_{max} of the phosphoglycerate mutase so that 95 % of the models have values in the range [202.5; 250] with a median of 225 nmol $\cdot$ min^{-1} $\cdot$ mg protein^{-1} (distribution is log normal (Achcar *et al.*, 2012))

- The V_{max} of the pyruvate transporter is set using the median value and standard deviation calculated from (Vanderheyden *et al.*, 2000) as described in (Achcar *et al.*, 2012). Similarly, as for the phosphoglycerate mutase, the accumulation of pyruvate observed when the V_{max} of the pyruvate transporter is in the lower range of its values is not modified by the addition of the pentose phosphate pathway.

New parameters: The parameters of the newly added reactions are sampled using the same rules as used for the glycolysis parameters. The median values are set as the fixed-parameter values described in the main article unless specified otherwise below. The standard deviations are set as described in the sources of the fixed-parameter values, when these mention a standard deviation or standard error of mean or using the mean standard error of the other measured parameters as described in (Achcar *et al.*, 2012).

Exceptions: The following parameter values remains fixed unless mentioned otherwise:

- The parameters of the black-box reactions of NADPH utilisation in the cytosol and the glycosome.

- The parameters of the ATP:ADP antiporter.

- The parameter k_{TOX} of trypanothione oxidation.

V_{max} of enzymes present in both the cytosol and the glycosome: The total activity is sampled as described above. The cytosolic fraction is then computed from this total activity and the fixed percentage of activity as described in the main article, the rest of the activity is the glycosomal activity. This percentage of cytosolic activity is fixed except for the cytosolic hexokinase activity, which is sampled from a uniform distribution between 1 and 10 percent, as its value has an important impact on some of the results as described in the main article.

Glucose 6-phosphate phosphatase V_{max}: This value is unknown. It is sampled from a uniform distribution between 1 and 40 nmol $\cdot$ min^{-1} $\cdot$ mg protein^{-1} (this latter value is in the range of the measured total phosphatase activity reported in (McLaughlin, 1986)).

Ribokinase V_{max}: This value is unknown. As the equilibrium constant of ribokinase favours the reverse direction more easily, we sampled the reverse V_{max} with a median of

1000 nmol $\cdot$ min^{-1} $\cdot$ mg protein^{-1} and 97.5 % of the value sampled lower than 4000 nmol $\cdot$ min^{-1} $\cdot$ mg protein^{-1} (log normal distribution).

Equilibrium constants: In addition to the equilibrium constants of the pentose phosphate pathway reactions, equilibrium constants were introduced for pyruvate kinase, hexokinase and phosphofructokinase as described in the methods subsection of the main manuscript. All the new equilibrium constants are sampled using the fixed-parameter value as a median and the relative standard error of the other equilibrium constants, except for glucose-6-phosphate dehydrogenase for which the value used is the median of the values published in (Wurster and Hess, 1970, 1973) corrected for pH (median equilibrium constant = 7.0), and the corresponding standard error.

C.2. Distributions

Distribution of parameters and steady state fluxes and concentrations in the sampled model based on model 6 (see Figure 3.2). Most parameters are sampled from a log normal distributions of mean and standard deviations based on experimental sources (see the SilicoTryp Wiki[1] for detailed data and calculations), some parameters are calculated from other sampled parameters for thermodynamical consistency. Detailed descriptions can be found in the section above and in (Achcar *et al.*, 2012). The vertical black lines indicate the value in the fixed- parameter model. The units of the x-axis are as follows: K_m, K_i and K_s: mM; V_{max}: nmol $\cdot$ min^{-1} $\cdot$ mg protein^{-1} ; others: unitless.

Distributions are shown from next page.

[1] http://silicotryp.ibls.gla.ac.uk/wiki

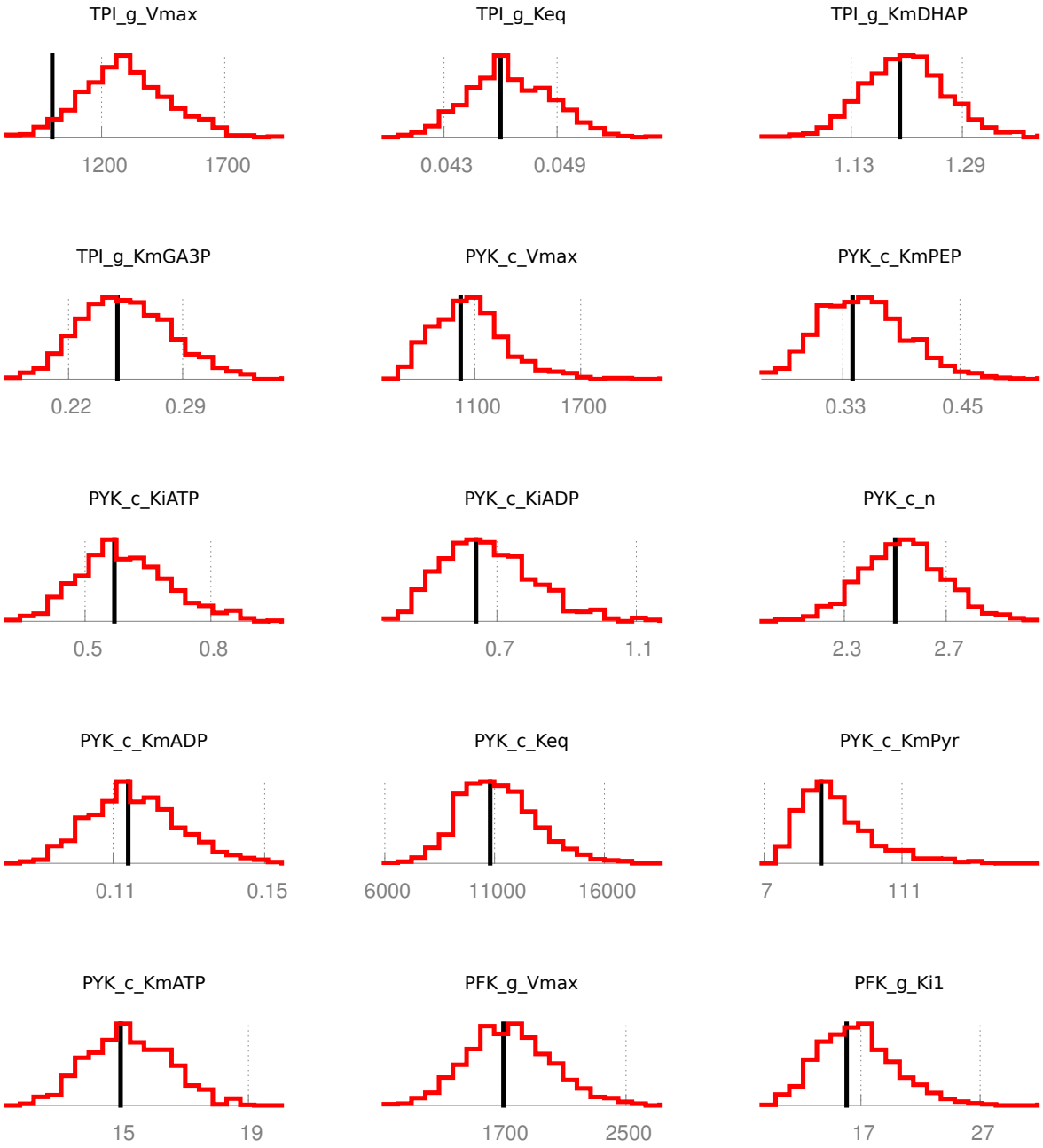
TPI_g_Vmax
1200
1700
TPI_g_Keq
0.043
0.049
TPI_g_KmDHAP
1.13
1.29
TPI_g_KmGA3P
0.22
0.29
PYK_c_Vmax
1100
1700
PYK_c_KmPEP
0.33
0.45
PYK_c_KiATP
0.5
0.8
PYK_c_KiADP
0.7
1.1
PYK_c_n
2.3
2.7
PYK_c_KmADP
0.11
0.15
PYK_c_Keq
6000
11000
16000
PYK_c_KmPyr
7
111
PYK_c_KmATP
15
19
PFK_g_Vmax
1700
2500
PFK_g_Ki1
17
27

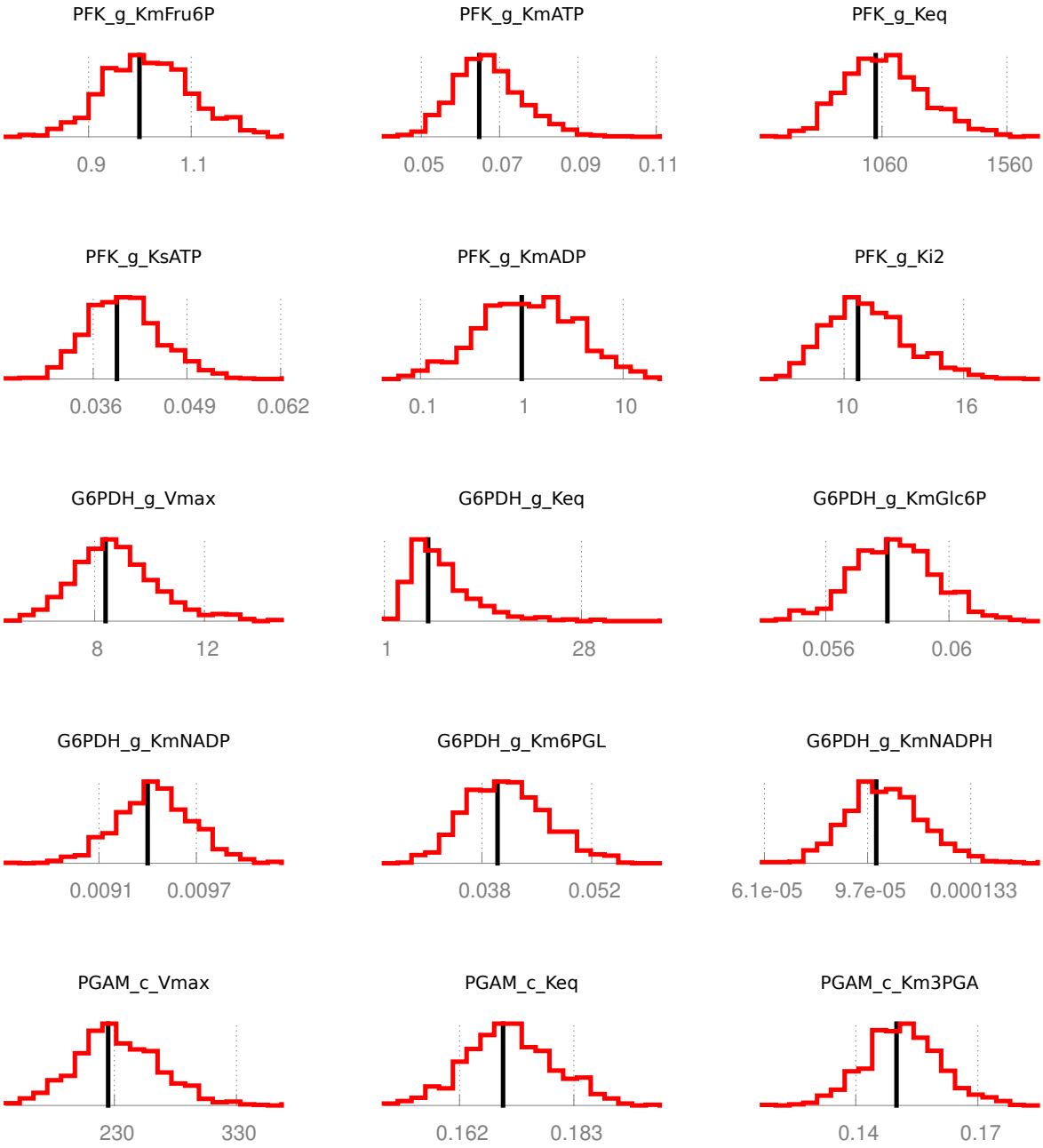
PFK_g_KmFru6P
0.9
1.1
PFK_g_KmATP
0.05
0.07
0.09
0.11
PFK_g_Keq
1060
1560
PFK_g_KsATP
0.036
0.049
0.062
PFK_g_KmADP
0.1
1
10
PFK_g_Ki2
10
16
G6PDH_g_Vmax
8
12
G6PDH_g_Keq
1
28
G6PDH_g_KmGlc6P
0.056
0.06
G6PDH_g_KmNADP
0.0091
0.0097
G6PDH_g_Km6PGL
0.038
0.052
G6PDH_g_KmNADPH
6.1e-05
9.7e-05
0.000133
PGAM_c_Vmax
230
330
PGAM_c_Keq
0.162
0.183
PGAM_c_Km3PGA
0.14
0.17

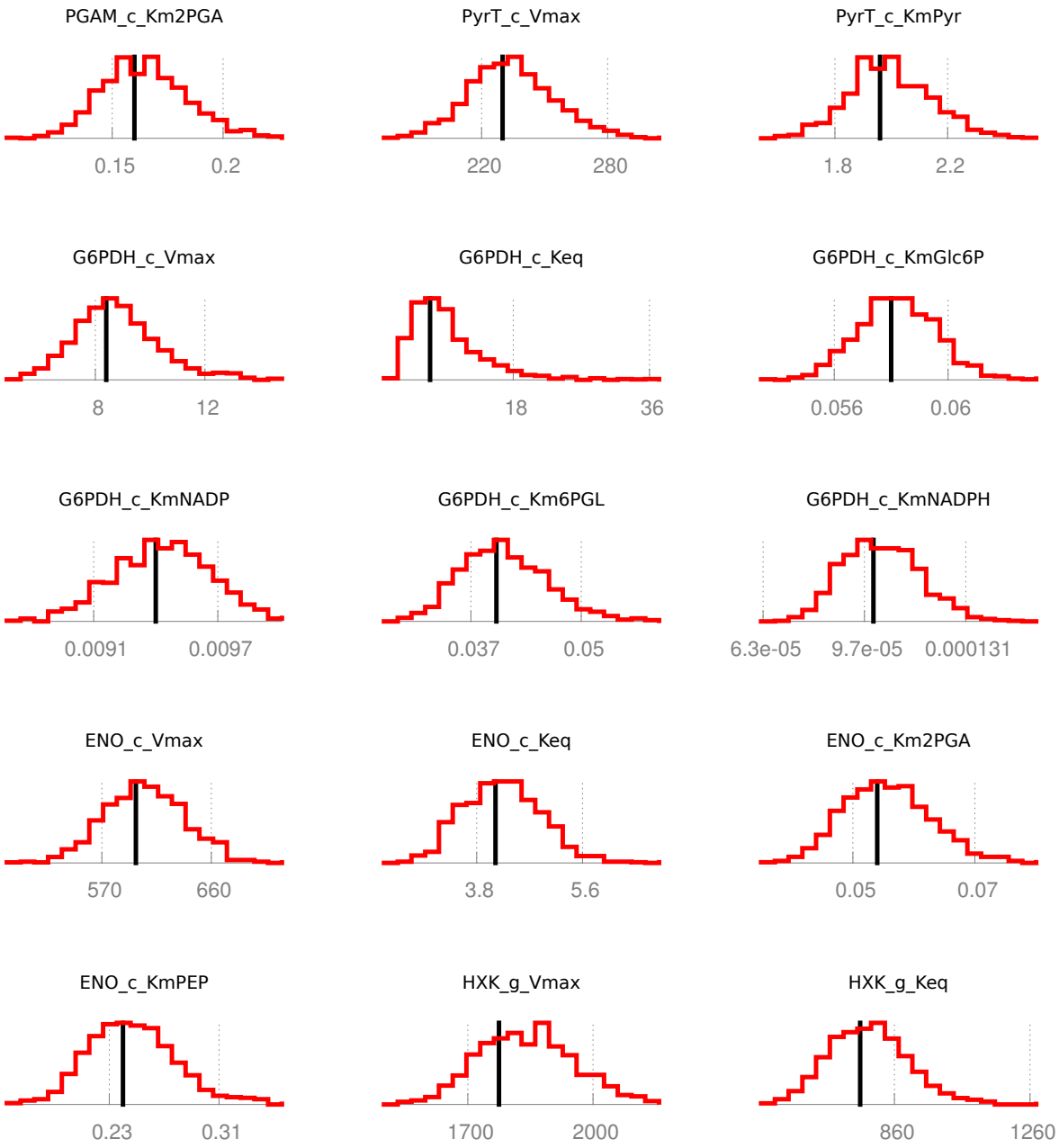
PGAM_c_Km2PGA
0.15
0.2
PyrT_c_Vmax
220
280
PyrT_c_KmPyr
1.8
2.2
G6PDH_c_Vmax
8
12
G6PDH_c_Keq
18
36
G6PDH_c_KmGlc6P
0.056
0.06
G6PDH_c_KmNADP
0.0091
0.0097
G6PDH_c_Km6PGL
0.037
0.05
G6PDH_c_KmNADPH
6.3e-05
9.7e-05
0.000131
ENO_c_Vmax
570
660
ENO_c_Keq
3.8
5.6
ENO_c_Km2PGA
0.05
0.07
ENO_c_KmPEP
0.23
0.31
HXK_g_Vmax
1700
2000
HXK_g_Keq
860
1260

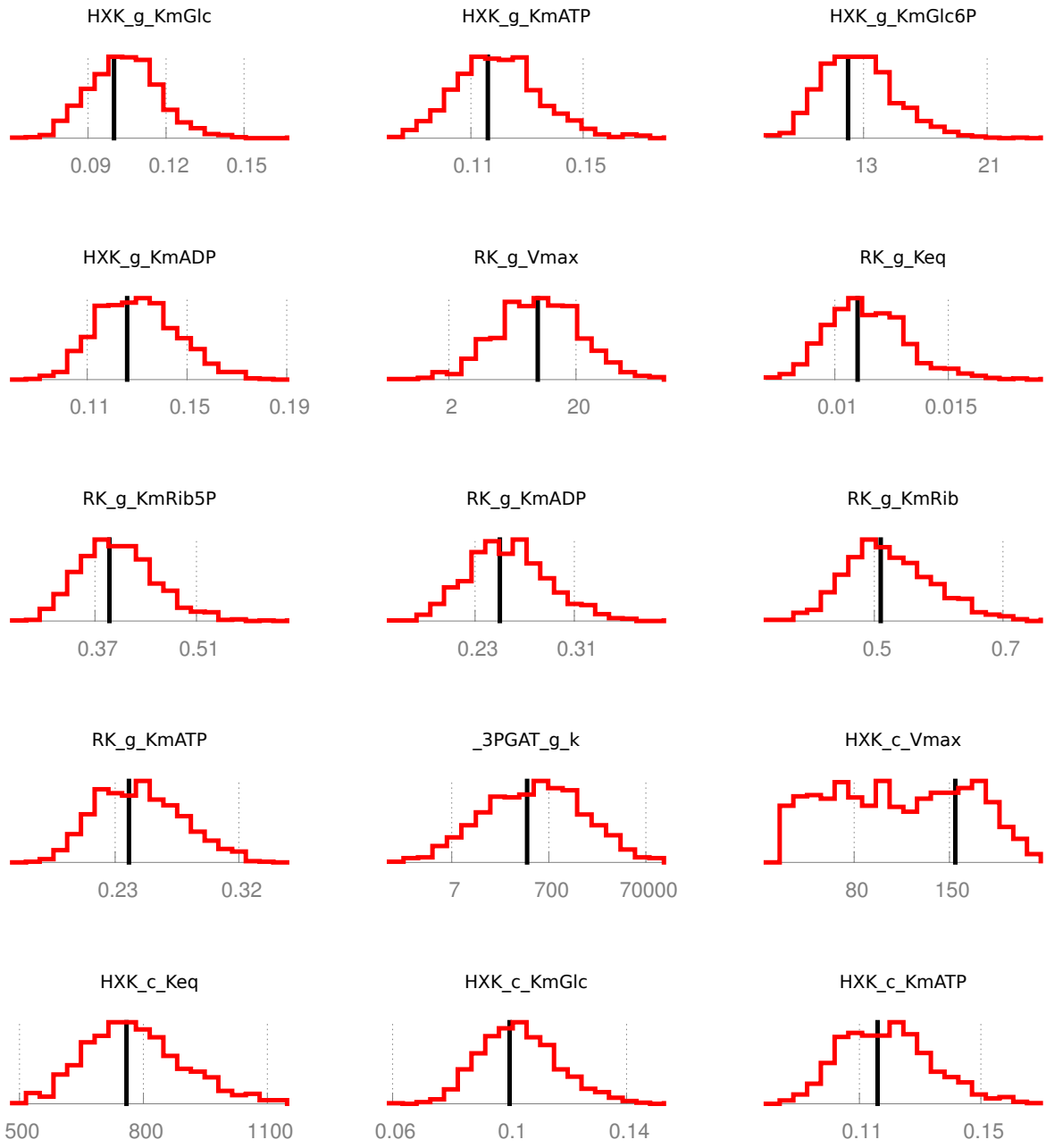
HXK_g_KmGlc
0.09
0.12
0.15
HXK_g_KmATP
0.11
0.15
HXK_g_KmGlc6P
13
21
HXK_g_KmADP
0.11
0.15
0.19
RK_g_Vmax
2
20
RK_g_Keq
0.01
0.015
RK_g_KmRib5P
0.37
0.51
RK_g_KmADP
0.23
0.31
RK_g_KmRib
0.5
0.7
RK_g_KmATP
0.23
0.32
_3PGAT_g_k
7
700
70000
HXK_c_Vmax
80
150
HXK_c_Keq
500
800
1100
HXK_c_KmGlc
0.06
0.1
0.14
HXK_c_KmATP
0.11
0.15

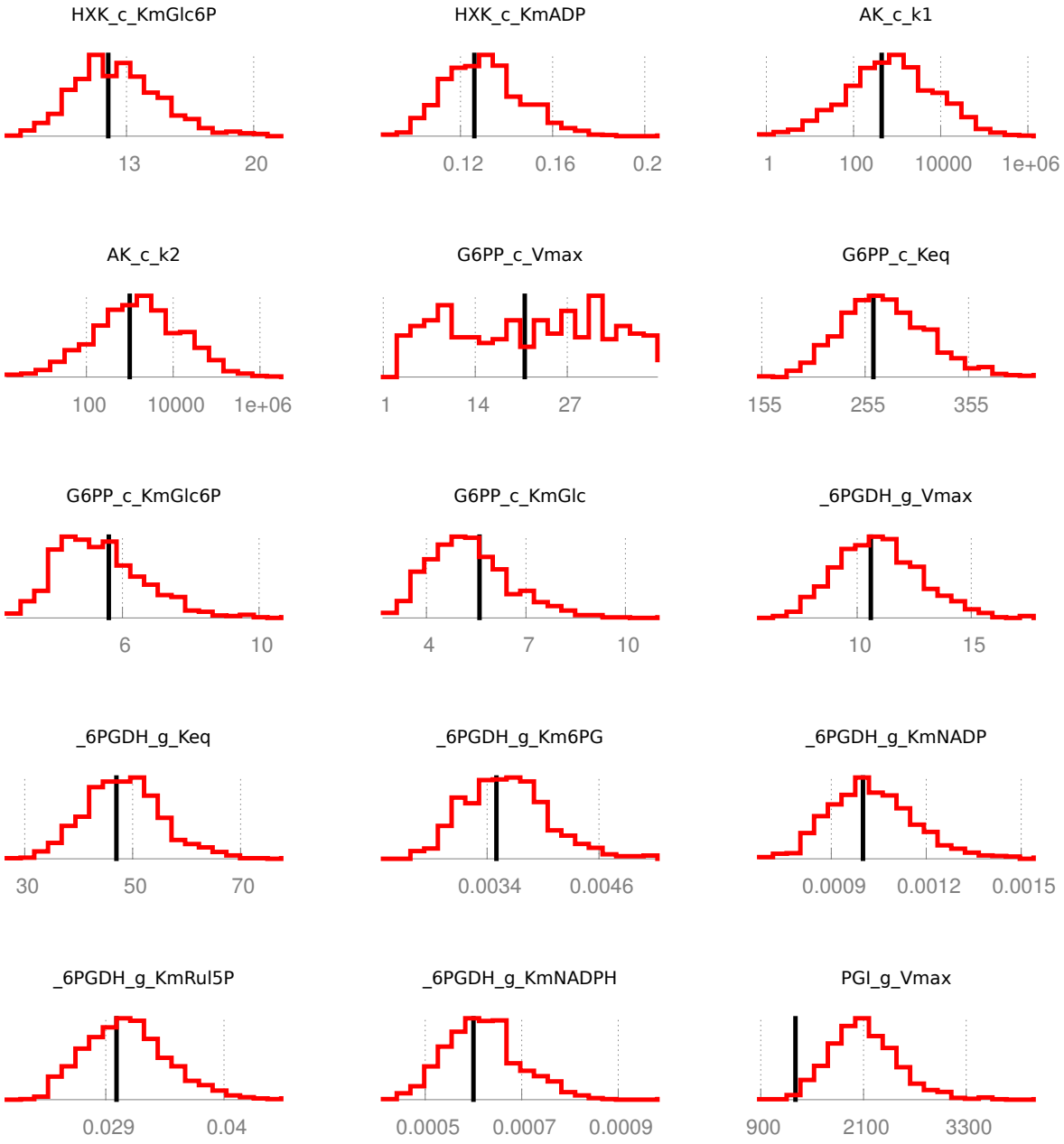
HXK_c_KmGlc6P
13
20
HXK_c_KmADP
0.12
0.16
0.2
AK_c_k1
1
100
10000
1e+06
AK_c_k2
100
10000
1e+06
G6PP_c_Vmax
1
14
27
G6PP_c_Keq
155
255
355
G6PP_c_KmGlc6P
6
10
G6PP_c_KmGlc
4
7
10
_6PGDH_g_Vmax
10
15
_6PGDH_g_Keq
30
50
70
_6PGDH_g_Km6PG
0.0034
0.0046
_6PGDH_g_KmNADP
0.0009
0.0012
0.0015
_6PGDH_g_KmRul5P
0.029
0.04
_6PGDH_g_KmNADPH
0.0005
0.0007
0.0009
PGI_g_Vmax
900
2100
3300

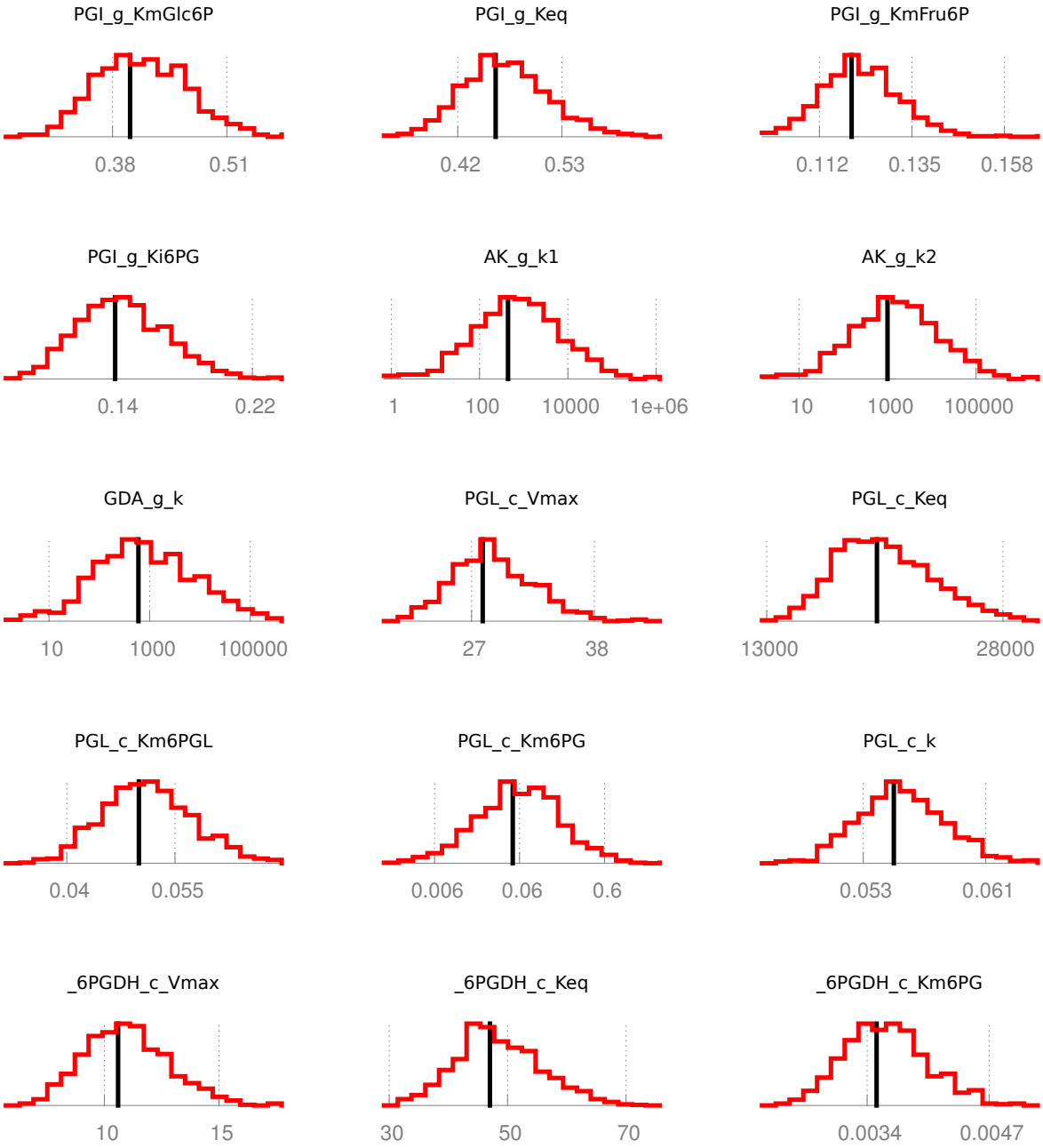
PGI_g_KmGlc6P
0.38
0.51
PGI_g_Keq
0.42
0.53
PGI_g_KmFru6P
0.112
0.135
0.158
PGI_g_Ki6PG
0.14
0.22
AK_g_k1
1
100
10000
1e+06
AK_g_k2
10
1000
100000
GDA_g_k
10
1000
100000
PGL_c_Vmax
27
38
PGL_c_Keq
13000
28000
PGL_c_Km6PGL
0.04
0.055
PGL_c_Km6PG
0.006
0.06
0.6
PGL_c_k
0.053
0.061
_6PGDH_c_Vmax
10
15
_6PGDH_c_Keq
30
50
70
_6PGDH_c_Km6PG
0.0034
0.0047

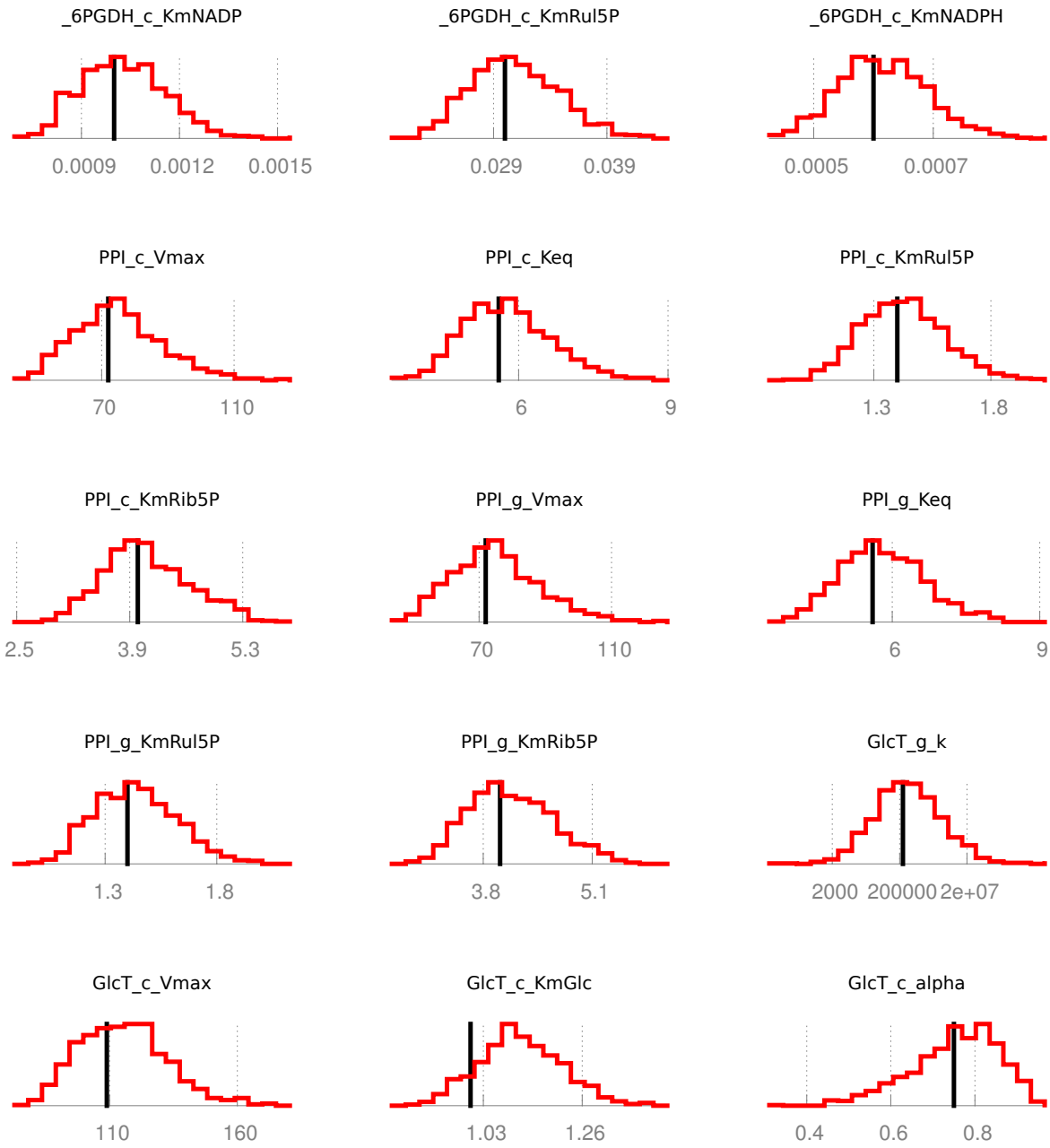
_6PGDH_c_KmNADP
0.0009
0.0012
0.0015
_6PGDH_c_KmRul5P
0.029
0.039
_6PGDH_c_KmNADPH
0.0005
0.0007
PPI_c_Vmax
70
110
PPI_c_Keq
6
9
PPI_c_KmRul5P
1.3
1.8
PPI_c_KmRib5P
2.5
3.9
5.3
PPI_g_Vmax
70
110
PPI_g_Keq
6
9
PPI_g_KmRul5P
1.3
1.8
PPI_g_KmRib5P
3.8
5.1
GlcT_g_k
2000
200000
2e+07
GlcT_c_Vmax
110
160
GlcT_c_KmGlc
1.03
1.26
GlcT_c_alpha
0.4
0.6
0.8

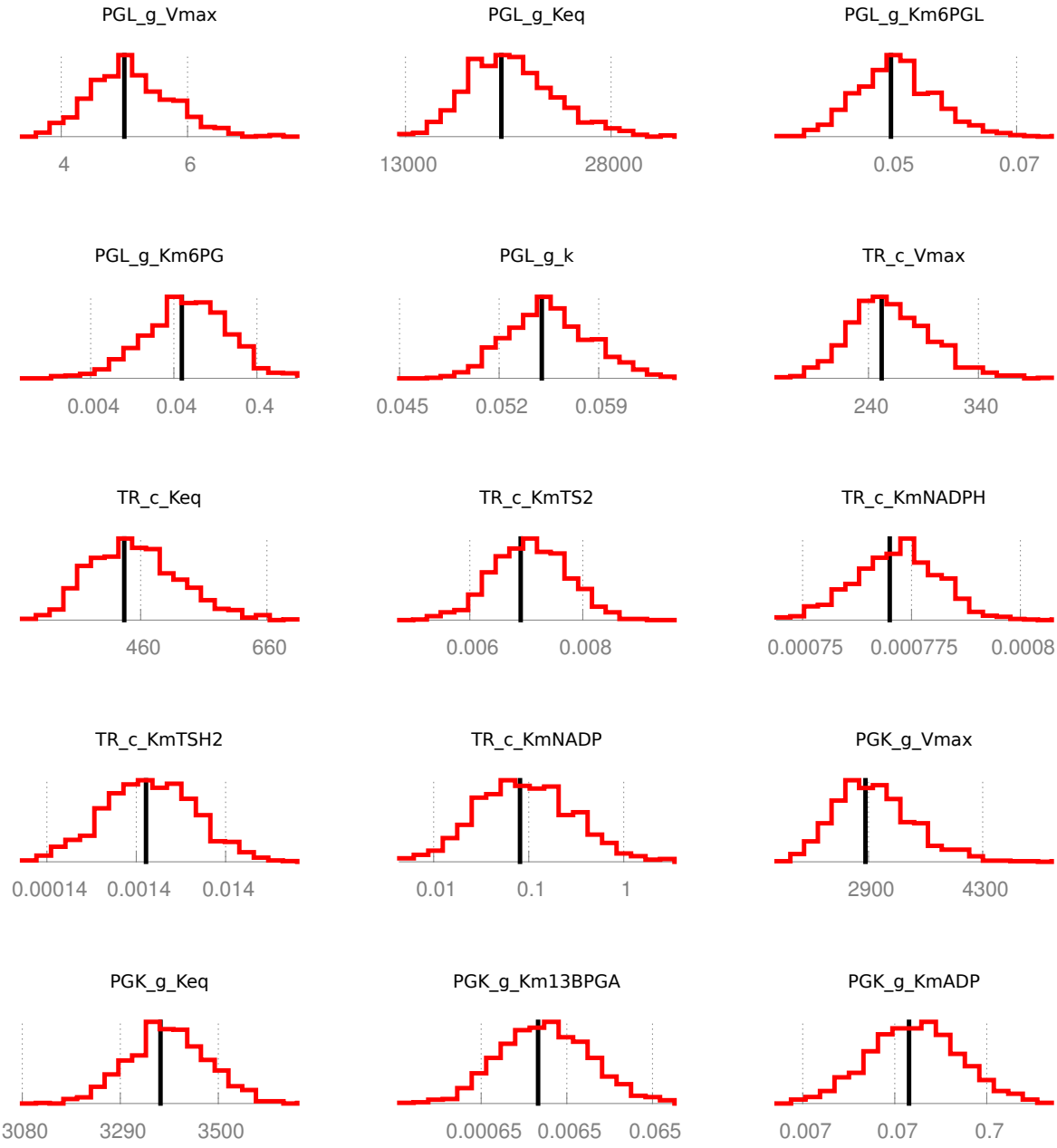
PGL_g_Vmax
4
6
PGL_g_Keq
13000
28000
PGL_g_Km6PGL
0.05
0.07
PGL_g_Km6PG
0.004
0.04
0.4
PGL_g_k
0.045
0.052
0.059
TR_c_Vmax
240
340
TR_c_Keq
460
660
TR_c_KmTS2
0.006
0.008
TR_c_KmNADPH
0.00075
0.000775
0.0008
TR_c_KmTSH2
0.00014
0.0014
0.014
TR_c_KmNADP
0.01
0.1
1
PGK_g_Vmax
2900
4300
PGK_g_Keq
3080
3290
3500
PGK_g_Km13BPGA
0.00065
0.0065
0.065
PGK_g_KmADP
0.007
0.07
0.7

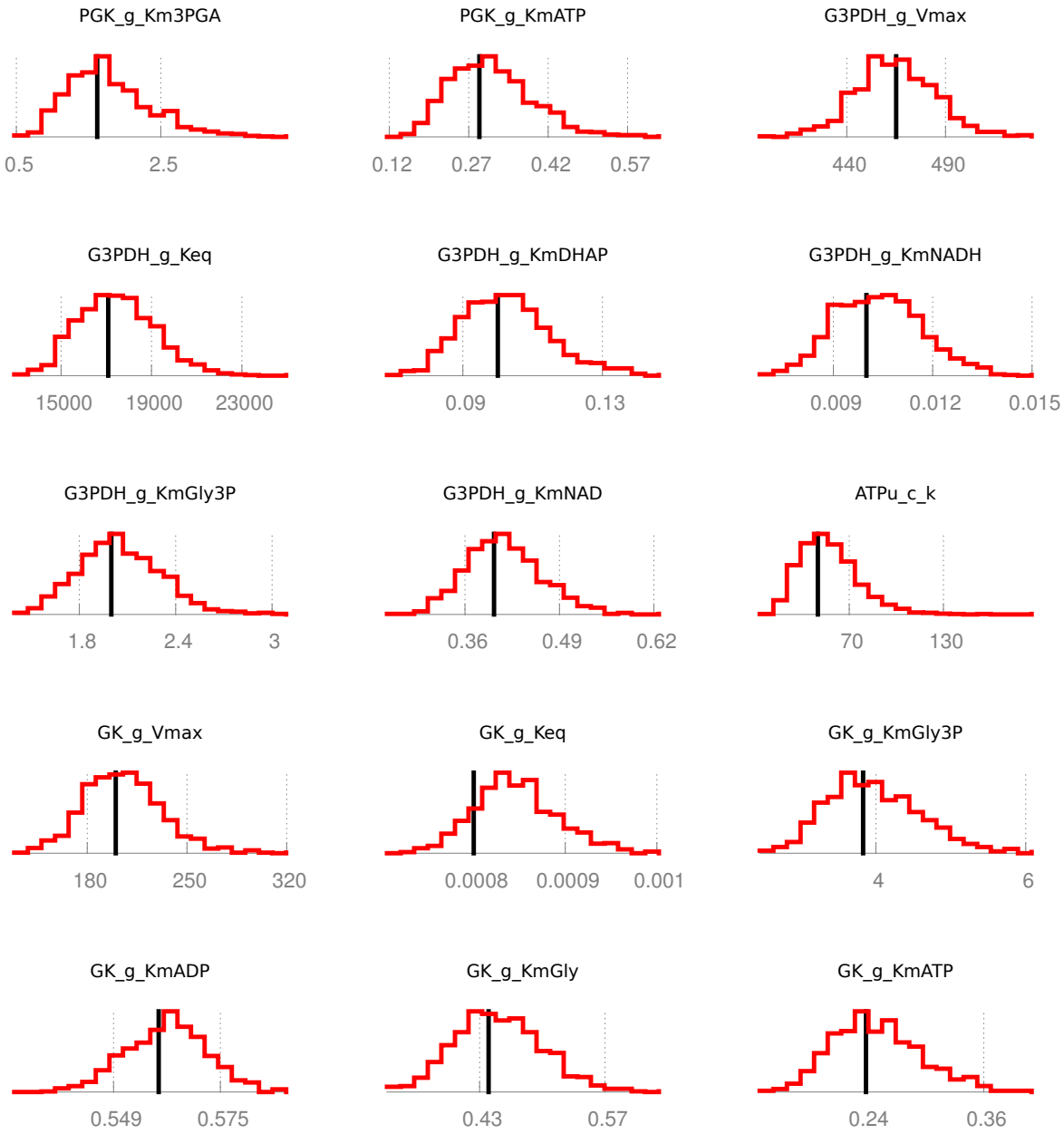
PGK_g_Km3PGA
0.5
2.5
PGK_g_KmATP
0.12
0.27
0.42
0.57
G3PDH_g_Vmax
440
490
G3PDH_g_Keq
15000
19000
23000
G3PDH_g_KmDHAP
0.09
0.13
G3PDH_g_KmNADH
0.009
0.012
0.015
G3PDH_g_KmGly3P
1.8
2.4
3
G3PDH_g_KmNAD
0.36
0.49
0.62
ATPu_c_k
70
130
GK_g_Vmax
180
250
320
GK_g_Keq
0.0008
0.0009
0.001
GK_g_KmGly3P
4
6
GK_g_KmADP
0.549
0.575
GK_g_KmGly
0.43
0.57
GK_g_KmATP
0.24
0.36

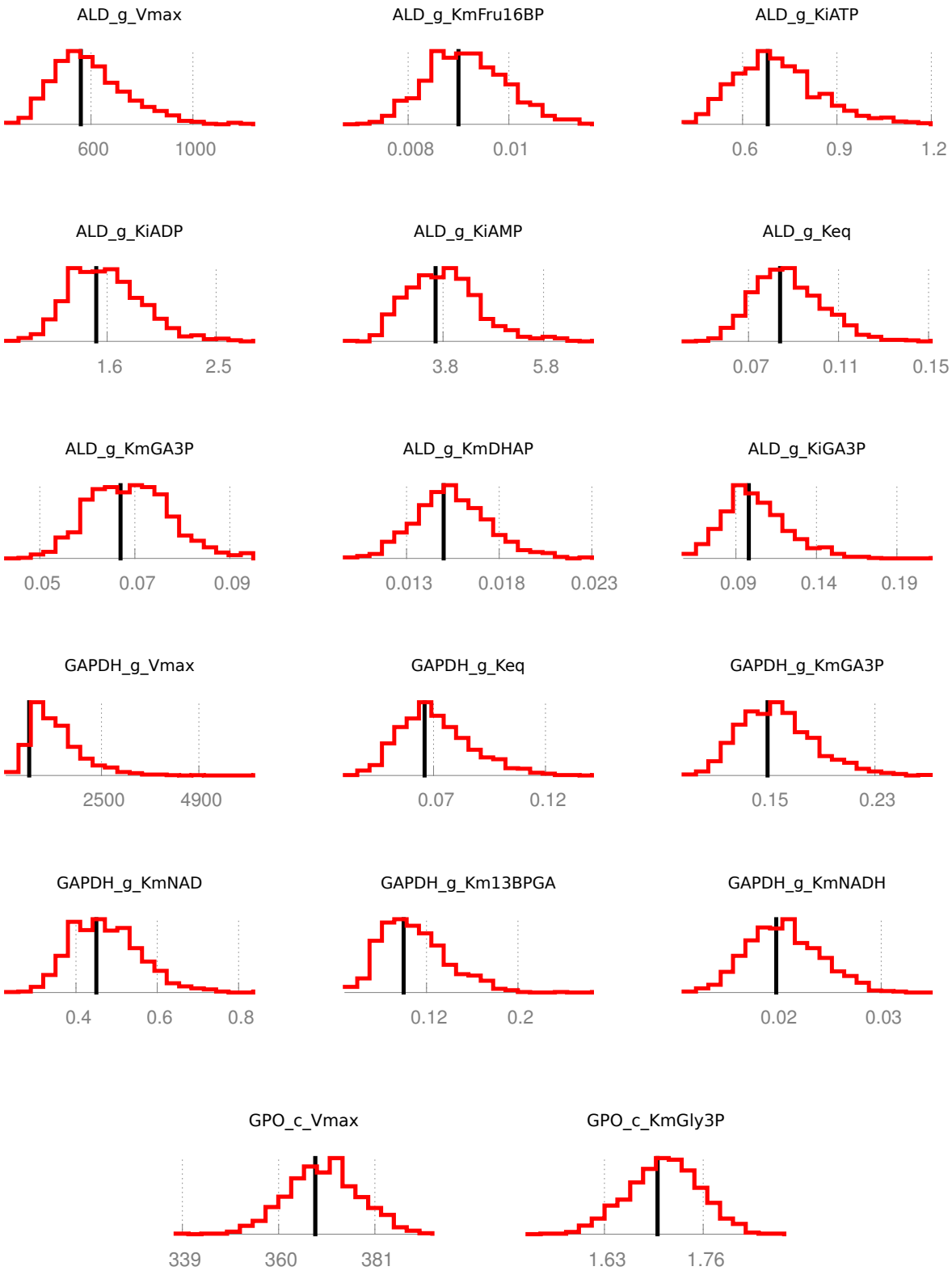
ALD_g_Vmax
600
1000
ALD_g_KmFru16BP
0.008
0.01
ALD_g_KiATP
0.6
0.9
1.2
ALD_g_KiADP
1.6
2.5
ALD_g_KiAMP
3.8
5.8
ALD_g_Keq
0.07
0.11
0.15
ALD_g_KmGA3P
0.05
0.07
0.09
ALD_g_KmDHAP
0.013
0.018
0.023
ALD_g_KiGA3P
0.09
0.14
0.19
GAPDH_g_Vmax
2500
4900
GAPDH_g_Keq
0.07
0.12
GAPDH_g_KmGA3P
0.15
0.23
GAPDH_g_KmNAD
0.4
0.6
0.8
GAPDH_g_Km13BPGA
0.12
0.2
GAPDH_g_KmNADH
0.02
0.03
GPO_c_Vmax
339
360
381
GPO_c_KmGly3P
1.63
1.76

Appendix D

Metabolomics

D.1. Standards

List of three standards mixtures that are run with every metabolomics experiments. RTs are typical retention times in minutes. ND is not detected.

Mix	Compound Name	Detected m/z	RT pHILIC	RT HILIC
1	(R)-3-Hydroxybutanoate	103.04002	ND	6.59
	2,3-Bisphospho-D-glycerate	264.95203	19.65	ND
	2-Methylcitrate	205.03525	18.40	ND
	2-Phenylglycine	152.07050	7.83	13.41
	3-Hydroxyphenylacetate	151.03989	8.78	ND
	3',5'-Cyclic AMP	328.04535	ND	15.38
	4-Aminobenzoate	138.05484	12.61	5.87
	4-Coumarate	163.03999	7.82	5.60
	6-Phospho-D-gluconate	275.01755	19.12	ND
	Adenine	136.06146	9.70	14.83
	ADP	426.02213	16.54	ND
	beta-Alanine	90.05499	16.68	18.26
	cis-Aconitate	173.00894	19.05	7.81
	CMP	322.04449	16.69	19.57
	Creatinine	114.06593	9.98	16.95
	Cytidine	244.09239	12.67	19.20
	D-Erythrose	119.03491	10.15	ND
	D-Fructose 1,6-bisphosphate	338.98883	19.58	ND
	D-Galactarate	209.02988	18.30	ND

Mix	Compound Name	Detected m/z	RT pHILIC	RT HILIC
1	D-Galacturonate	193.03517	17.64	16.04
	D-Glucosamine	180.08661	16.05	22.75
	D-Glucose	179.05595	12.99	11.76
	D-Glucose 6-phosphate	259.02228	18.36	18.92
	D-Ribose 5-phosphate	229.01178	17.26	17.18
	Deoxyuridine	227.06731	8.02	7.86
	dGMP	348.07071	16.96	17.02
	Ethanolamine phosphate	142.02647	17.62	19.33
	Gallate	169.01414	19.85	8.87
	Glycerol	93.05451	9.58	9.46
	Glycine	76.03936	16.96	18.39
	Guanine	152.05659	13.13	14.31
	IDP	427.00638	18.19	ND
	Imidazole-4-acetate	127.05024	11.71	16.00
	IMP	347.03989	16.21	15.03
	Inosine	269.08823	11.48	10.27
	L-Arginine	175.11890	27.49	26.19
	L-Asparagine	133.06085	16.46	18.47
	L-Aspartate	134.04475	16.40	17.46
	L-Citrulline	176.10289	17.24	18.88
	L-Cysteate	167.99702	16.95	16.99
	L-Cystine	241.03111	17.46	22.41
	L-Glutamate	146.04587	15.60	16.79
	L-Glutamine	147.07654	16.25	18.03
	L-Histidine	156.07668	16.02	25.16
	L-Leucine	132.10205	11.42	12.88
	L-Lysine	147.11285	25.92	26.53
	L-Methionine	150.05843	12.13	13.79
	L-Phenylalanine	166.08626	10.55	12.28
	L-Proline	116.07045	13.79	15.65
	L-Rhamnose	163.06119	ND	11.13
	L-Serine	106.04986	17.00	18.47
	L-Threonine	120.06551	ND	17.39
	L-Tryptophan	205.09727	12.25	13.03
	L-Valine	118.08630	13.31	14.68
	Malonate	103.00357	ND	7.24
	Maltose	341.10886	13.47	ND
	Melatonin	233.12839	4.45	5.64
	meso-2,6-Diaminoheptanedioate	191.10249	19.60	23.60

Mix	Compound Name	Detected m/z	RT pHILIC	RT HILIC
1	Methylmalonate	117.01925	ND	6.54
	MOPS	208.06473	7.29	13.88
	N^2-Acetyl-L-lysine	189.12329	16.40	17.46
	Nicotinate	124.03941	ND	7.56
	Orotate	155.00943	10.18	9.86
	Phenolsulfonphthalein	353.04907	ND	5.07
	Phenylhydrazine	109.07601	5.60	5.82
	Phosphoenolpyruvate	166.97491	18.60	ND
	Pyridoxine	170.08087	7.83	14.80
	Pyruvate	87.00870	7.29	ND
	Riboflavin	377.14578	8.51	7.82
	S-Adenosyl-L-methionine	399.14517	17.59	29.18
	Selenomethionine	192.00873	12.01	13.48
	sn-Glycero-3-Phosphocholine	258.11014	15.84	19.82
	Taurine	126.02199	15.90	16.33
	Thiamin	265.11218	22.65	29.06
	Thiamin diphosphate	423.03021	16.36	ND
	Thymidine	241.08310	7.29	7.24
	trans-4-Hydroxy-L-proline	132.06561	15.67	16.48
	UMP	323.02866	15.48	14.05
	Uridine	243.06180	10.10	9.06
	Xanthine	151.02574	11.94	8.79
2	(S)-Malate	133.01405	17.45	ND
	1-Aminocyclopropane-1-carboxylate	102.05508	13.31	14.45
	2-Oxoglutarate	145.01402	16.86	ND
	3-(4-Hydroxyphenyl)pyruvate	179.03455	7.26	ND
	4-(beta-Acetylaminoethyl)imidazole	154.09727	7.37	ND
	5-Oxoproline	130.04997	11.27	7.42
	5'-Methylthioadenosine	298.09683	7.25	ND
	6-Methylaminopurine	150.07736	7.81	ND
	Adenosine	268.10419	9.07	12.51
	agmatine	131.12848	19.63	ND
	Ala-Gly	147.07651	12.85	ND
	AMP	348.07016	15.11	17.87
	Betaine	118.08636	11.97	ND
	Biotin	245.09538	8.72	6.40
	Choline	104.10686	22.10	ND
	Citrate	191.01959	19.48	ND
	D-Erythrose 4-phosphate	199.00096	17.45	ND

Mix	Compound Name	Detected m/z	RT pHILIC	RT HILIC
2	D-Glucosamine 6-phosphate	260.05270	15.20	ND
	dAMP	332.07550	14.09	ND
	dCMP	308.06396	16.28	ND
	Deoxyadenosine	252.10902	8.08	ND
	dIMP	331.04501	15.82	ND
	dUMP	307.03372	15.16	ND
	Eflornithine	183.09323	14.17	ND
	FMN	455.09720	12.55	ND
	Folate	440.13263	18.18	ND
	Glycylglycine	133.06061	15.23	ND
	GMP	362.05078	17.18	ND
	HEPES	239.10591	10.87	22.65
	L-2,3-Diaminopropanoate	105.06606	17.20	ND
	L-2-Aminoadipate	162.07585	16.36	16.92
	L-Alanine	90.05489	15.99	ND
	L-Cystathionine	223.07468	18.25	ND
	L-Gulono-1,4-lactone	177.04036	14.53	ND
	L-Homoserine	120.06542	16.23	ND
	L-Isoleucine	132.10182	12.82	ND
	L-Kynurenine	209.09181	11.34	ND
	L-Tyrosine	182.08109	13.86	ND
	Lipoate	205.03580	4.36	ND
	Mesaconate	129.01926	16.78	ND
	Methylcysteine	136.04283	12.42	15.04
	Methylguanidine	74.07149	39.73	ND
	N-Acetylglutamine	187.07213	11.26	ND
	N-Acetylneuraminate	308.09875	14.43	ND
	N-Acetylornithine	175.10751	16.87	15.64
	NAD+	664.11432	15.54	19.97
	Nicotinamide	123.05527	7.25	8.70
	Orotidine	287.05203	13.13	12.94
	Oxalate	88.98808	19.10	ND
	Pantothenate	220.11780	8.48	ND
	Phenylacetylglycine	192.06660	4.49	6.01
	Phenylpyruvate	163.04007	4.41	6.08
	Picolinic acid	124.03931	8.43	ND
	Pyridoxal	168.06509	7.73	ND
	S-Adenosyl-L-homocysteine	385.12885	14.72	ND
	sn-Glycerol 3-phosphate	171.00630	16.40	ND

Mix	Compound Name	Detected m/z	RT pHILIC	RT HILIC
2	Succinate	117.01922	16.53	8.15
	Taurocholate	514.28467	4.25	ND
	Thiopurine S-methylether	167.03842	7.23	ND
	Thymine	127.04991	7.39	ND
	Trypanothione disulfide	722.29443	21.11	ND
3	2-Aminobutan-4-olide	102.05504	ND	18.53
	2-phospho-D-glycerate	184.98546	18.13	17.15
	5-Aminolevulinate	132.06548	14.31	17.95
	Acetoacetate	101.02438	14.50	ND
	Acetylcholine	146.11745	16.68	14.80
	acetylcysteine	162.02293	7.34	ND
	Benzoate	121.02946	7.31	5.51
	Biopterin	238.09389	8.82	ND
	Bis-γ-glutamylcystine	499.11731	19.30	ND
	D-Arabinose	149.04530	14.05	ND
	D-Fructose	179.05614	14.50	13.42
	D-Fructose 6-phosphate	259.02246	17.49	17.61
	D-Glucono-1,4-lactone	177.04031	8.37	8.27
	γ-L-Glutamyl-L-cysteine	251.06958	15.51	ND
	Glutathione	308.09140	15.74	ND
	Glutathione disulfide	613.15875	18.98	ND
	Homocystine	269.06201	17.44	ND
	Isonicotinic acid	124.03936	7.35	8.70
	Itaconate	129.01929	15.91	6.27
	L-Dehydroascorbate	173.00874	11.85	ND
	L-Homocysteine	136.04268	13.76	ND
	lipoamide	206.06689	5.17	ND
	Maleic acid	115.00362	12.70	6.66
	N-acetyl-L-glutamate	188.05626	15.45	7.14
	NADH	664.11823	14.65	ND
	O-Acetylcarnitine	204.12263	11.78	ND
	Orthophosphate	96.96973	13.40	16.54

D.2. Metabolomics data

Significantly changed metabolites (rank product, FDR<0.05) from different metabolomics experiments. The mass is given as measured by the machine at 2 ppm accuracy, predicted formula is the most likely chemical formula, putative metabolite is based on both the accurate mass and the retention time. Fold changes are versus control samples, and the FDR is derived from the rank product analysis.

Metabolomics data for RK^{RNAi} and NAM^{RNAi} are not shown here, as the tables in the main text already listed all significantly changed metabolites.

D.3. ARG metabolomics assay

Table D.2.: ARG metabolomics enzyme assay, cofactor mixture 1. Putatively identified metabolites with significant fold changes (rank product FDR<0.05).

Measured mass	Retention time (min)	Predicted formula	Isomers	Putative metabolite	Fold change
290.09005	9.26	$C_{14}H_{14}N_2O_5$	2	N2-Malonyl-D-tryptophan	24.4
205.03770	5.63	$C_{10}H_7NO_4$	2	6-Hydroxykynurenate	21.8
238.05890	9.41	$C_{10}H_{10}N_2O_5$	1	(3-nitrobenzoyl)alanine (fragment of peptide)	15.3
153.99346	15.24	$C_3H_6O_5S$	1	3-sulfopropanoate	14.5
163.06339	5.62	$C_9H_9NO_2$	4	3-Methyldioxyindole (fragment of 6-hydroxykynurenate)	12.1
211.04837	7.11	$C_9H_9NO_5$	5	5-(2'-Formylethyl)-4,6-dihydroxypicolinate (related to 5-methyl-barbiturate)	9.25
480.11531	14.99	$C_{18}H_{21}N_6O_8P$	1	7,8-H2pterin-6-yl-methyl-4-(β-D-ribofuranosyl)aminobenzene 5'-phosphate	9.03
246.10058	9.28	$C_{13}H_{14}N_2O_3$	4	N-Acetyl-D-tryptophan	8.76
253.02548	9.73	$C_{10}H_8N_3O_3Cl$	1	5-Amino-4-chloro-2-(2,3-dihydroxyphenyl)-3(2H)-pyridazinone	8.34
266.09023	7.08	$C_{12}H_{14}N_2O_5$	1	p-aminobenzoyl glutamate	7.8
175.06329	11.04	$C_{10}H_9NO_2$	12	3-Indoleglycolaldehyde (fragment of indole 3-acetamide)	7.5
135.06842	5.47	C_8H_9NO	4	2-Phenylacetamide	6.14
142.03769	7.07	$C_5H_6N_2O_3$	3	5-methyl-barbiturate (related to 5-(2'-Formylethyl)-4,6-dihydroxypicolinate)	6.06

Measured mass	Retention time (min)	Predicted formula	Isomers	Putative metabolite	Fold change
189.04258	5.82	$C_{10}H_7NO_3$	6	Kynurenate	5.8
147.03192	5.62	$C_8H_5NO_2$	2	Isatin (fragment of 6-hydroxykynurenate)	5.79
335.14806	9.41	$C_{16}H_{21}N_3O_5$	1	Gly-Pro-Tyr	4.65
358.12768	5.98	$C_{17}H_{18}N_4O_5$	1	202-791	4.62
165.04246	5.56	$C_8H_7NO_3$	8	Formylanthranilate (fragment of 3-methyldioxyindole)	4.44
264.08997	5.51	$C_{16}H_{12}N_2O_2$	1	Perlolyrine (fragment of 3-methyldioxyindole)	4.32
196.06370	5.4	$C_{12}H_8N_2O$	2	Pyocyanine-reduced (fragment of 2-phenylacetamide)	4.24
146.04802	6	$C_8H_6N_2O$	1	1(2H)-Phthalazinone	4.1
173.04773	5.99	$C_{10}H_7NO_2$	4	2-Quinolinecarboxylic acid	3.95
236.07972	10.45	$C_{11}H_{12}N_2O_4$	2	L-Formylkynurenine	3.87
145.05281	5.53	$C_9H_9NO_2$	4	3-Methyldioxyindole	3.53
174.07932	10.97	$C_{10}H_{10}N_2O$	4	Indole-3-acetamide	3.48
214.02403	14.42	$C_5H_{11}O_7P$	6	2-Deoxy-D-ribose 5-phosphate	3.24
250.06237	9.43	$C_8H_{14}N_2O_5S$	2	Glu-Cys	3.09
242.08052	5.66	$C_{12}H_{10}N_4O_2$	1	Lumichrome	3.03
137.99876	12.77	$C_3H_6O_4S$	2	2-oxopropane sulfonate	3.03
195.05317	8.46	$C_9H_9NO_4$	9	Dopaquinone	2.85
181.03737	7.09	$C_8H_7NO_4$	3	DIBOA	2.8
87.06843	13.23	C_4H_9NO	10	4-Aminobutanal	2.73
349.11248	13.8	$C_{12}H_{19}N_3O_9$	2	Thr-Asp-Asp	2.7
197.06888	13.12	$C_9H_{11}NO_4$	2	3,4-Dihydroxy-L-phenylalanine	2.46
168.06873	8.61	$C_{11}H_8N_2$	1	beta-Carboline	2.3
147.03553	14.74	$C_5H_9NO_2S$	1	Thiomorpholine 3-carboxylate	2.29
274.09113	19.39	$C_9H_{14}N_4O_6$	1	5-Amino-1-ribofuranosylimidazole-4-carboxyamide	2.28
123.98302	13.5	$C_2H_4O_4S$	1	Sulfoacetaldehyde	2.15
154.98877	8.9	$C_8H_{13}Cl_3O_6$	1	trichloroethanol glucoside	2.09
298.11699	14.73	$C_{13}H_{18}N_2O_6$	1	N-(4-nitrophenyl)validamine (fragment of peptide)	2.09
182.08442	8.27	$C_{12}H_{10}N_2$	1	Harman	2.04
172.06372	5.76	$C_{10}H_8N_2O$	1	indole-3-acetonitrile oxide	2
250.09533	5.93	$C_{12}H_{14}N_2O_4$	1	3-Oxohexobarbital	1.89
179.05815	5.83	$C_9H_9NO_3$	6	Hippurate	1.62
181.04072	13.79	$C_5H_{11}NO_4S$	1	DL-Methionine sulfone	1.59
165.04602	15.68	$C_5H_{11}NO_3S$	4	L-Methionine S-oxide	1.43
270.21916	5.16	$C_{16}H_{30}O_3$	19	[FA oxo(16:0)] 3-oxo-hexadecanoic acid	1.37
193.07367	5.68	$C_{10}H_{11}NO_3$	10	Phenylacetylglycine	1.37
312.22959	5.18	$C_{18}H_{32}O_4$	39	[FA (18:2)] 9S-hydroperoxy-10E,12Z-octadecadienoic acid	1.36
209.06887	6.07	$C_{10}H_{11}NO_4$	3	4-Hydroxyphenylacetylglycine	1.27
445.21743	12.26	$C_{18}H_{31}N_5O_8$	10	Ala-Leu-Asp-Gln	-1.5
361.18429	12.29	$C_{15}H_{27}N_3O_7$	2	Glu-Ile-Thr	-1.63

Measured mass	Retention time (min)	Predicted formula	Isomers	Putative metabolite	Fold change
289.16347	12.2	$C_{12}H_{23}N_3O_5$	5	Leu-Ala-Ser	-1.87
288.1796	23.84	$C_{12}H_{24}N_4O_4$	1	Lys-Ala-Ala	-2.01
248.05615	20.95	$C_8H_{13}N_2O_5P$	1	Pyridoxamine phosphate	-2.04
261.13238	23.35	$C_{10}H_{19}N_3O_5$	5	Lys-Asp	-2.06
372.21221	23.41	$C_{15}H_{28}N_6O_5$	1	Thr-Pro-Arg	-2.06
287.11226	20.15	$C_{11}H_{17}N_3O_6$	2	Asp-Gly-Pro	-2.13
266.10151	14.89	$C_{11}H_{14}N_4O_4$	1	8-Oxodeoxycoformycin	-2.32
274.16357	25.43	$C_{11}H_{22}N_4O_4$	2	Lys-Ala-Gly	-2.39
247.05152	5.84	$C_{12}H_{10}ClN_3O$	1	CPPU	-2.55
317.12233	20.87	$C_{12}H_{19}N_3O_7$	1	Asp-Pro-Ser	-2.56
300.06374	5.32	$C_{16}H_{12}O_6$	26	Peonidin	-2.58
261.14368	24.87	$C_9H_{19}N_5O_4$	1	Ser-Arg	-2.62
213.04404	19.21	$C_{13}H_{22}N_4O_8S_2$	2	S-glutathionyl-L-cysteine	-2.64
307.08380	19.21	$C_{10}H_{17}N_3O_6S$	3	Glutathione (fragment of S-glutathionyl-L-cysteine)	-2.78
133.06889	30.53	$C_{12}H_{18}N_4O_3$	1	L-lysine-p-nitroanilide	-2.9
299.10050	8.62	$C_{13}H_{17}NO_7$	1	p-aminobenzoate-β-D-glucopyranosyl ester	-2.91
301.14271	9.37	$C_{16}H_{19}N_3O_3$	3	Trp-Pro	-3.03
270.09608	23.42	$C_{10}H_{14}N_4O_5$	2	Asp-His	-3.06
199.05921	9.57	$C_7H_9N_3O_4$	5	5-Nitro-2-furancarboxaldehyde (2-hydroxyethyl)hydrazone (fragment of N-succinyl-L-citrulline)	-3.06
174.06423	8.82	$C_6H_{10}N_2O_4$	4	N-Formimino-L-glutamate	-3.23
305.13748	11.39	$C_{15}H_{19}N_3O_4$	1	Thr-Trp	-3.31
346.22224	22.22	$C_{15}H_{30}N_4O_5$	3	Leu-Lys-Ser	-3.82
334.13845	8.64	$C_{14}H_{26}N_2O_3S_2$	1	Lipoyllysine	-4.35
204.08995	10.55	$C_{11}H_{12}N_2O_2$	6	L-Tryptophan	-4.5

Table D.3.: ARG metabolomics enzyme assay, cofactor mixture 2. Putatively identified metabolites with significant fold changes (rank product FDR<0.05).

Measured mass	Retention time (min)	Predicted formula	Isomers	Putative metabolite	Fold change
163.06339	5.62	$C_9H_9NO_2$	4	3-Methyldioxyindole (fragment of 6-hydroxykynurenate)	5
175.06329	11.04	$C_{10}H_9NO_2$	12	3-Indoleglycolaldehyde (fragment of indole 3-acetamide)	4.48
211.04837	7.11	$C_9H_9NO_5$	5	5-(2'-Formylethyl)-4,6-dihydroxypicolinate (related to 5-methyl-barbiturate)	4.17
238.05890	9.41	$C_{10}H_{10}N_2O_5$	1	(3-nitrobenzoyl)alanine	3.78
253.02548	9.73	$C_{10}H_8N_3O_3Cl$	1	5-Amino-4-chloro-2-(2,3-dihydroxyphenyl)-3(2H)-pyridazinone	3.41
205.03770	5.63	$C_{10}H_7NO_4$	2	6-Hydroxykynurenate	3.35
264.08997	5.51	$C_{16}H_{12}N_2O_2$	1	Perlolyrine (fragment of 3-methyldioxyindole)	3.26
236.07972	10.45	$C_{11}H_{12}N_2O_4$	2	L-Formylkynurenine	1.82
189.04258	5.82	$C_{10}H_7NO_3$	6	Kynurenate	1.74
335.14806	9.41	$C_{16}H_{21}N_3O_5$	1	Gly-Pro-Tyr	1.71
196.06370	5.4	$C_{12}H_8N_2O$	2	Pyocyanine-reduced (fragment of 2-phenylacetamide)	1.62
191.07936	11	$C_7H_{13}NO_5$	1	2-amino-3,7-dideoxy-D-threo-hept-6-ulosonate	1.58
116.01104	6.33	$C_4H_4O_4$	3	Fumarate	1.54
173.04773	5.99	$C_{10}H_7NO_2$	4	2-Quinolinecarboxylic acid	1.49
261.09630	15.88	$C_9H_{15}N_3O_6$	4	Ala-Asp-Gly	-1.3
188.15253	22.97	$C_9H_{20}N_2O_2$	2	7,8-Diaminononanoate	-1.3
106.05809	18.91	$C_{10}H_{16}N_2O_3$	2	Pro-Pro	-1.32
151.09777	21.63	$C_{13}H_{26}N_4O_4$	1	Lys-Val-Gly	-1.37
301.12767	14.11	$C_{12}H_{19}N_3O_6$	2	Ala-Asp-Pro	-1.37
246.133	21.36	$C_9H_{18}N_4O_4$	2	N2-(D-1-Carboxyethyl)-L-arginine (fragment of peptide)	-1.39
226.10647	23.15	$C_9H_{14}N_4O_3$	3	Carnosine (fragment of peptide)	-1.39
220.06966	17.56	$C_7H_{12}N_2O_6$	2	Asp-Ser	-1.41
355.18527	26.62	$C_{15}H_{25}N_5O_5$	3	Leu-Ser-His	-1.43
314.1588	15.53	$C_{13}H_{22}N_4O_5$	2	Ala-Gln-Pro	-1.45
471.28061	20.97	$C_{20}H_{37}N_7O_6$	3	Arg-Leu-Pro-Ser	-1.49
217.10629	15.94	$C_8H_{15}N_3O_4$	3	Ala-Ala-Gly	-1.52
183.06609	20.53	$C_5H_{14}NO_4P$	1	Choline phosphate	-1.69
215.05801	5.51	$C_{12}H_9NO_3$	1	Robustine	-1.75
366.16521	9.32	$C_{15}H_{22}N_6O_5$	3	Orizabin (fragment of peptide)	-2.17
219.08569	18.28	$C_7H_{13}N_3O_5$	3	1D-1-Guanidino-1-deoxy-3-dehydro-scyllo-inositol (fragment of peptide)	-33.3

D.4. ARG null mutant metabolic profiling

Table D.4.: Δ*arg* metabolic profiling, pHILIC. Putatively identified metabolites with significant fold changes (rank product FDR<0.05).

Measured mass	Retention time (min)	Predicted formula	Isomers	Putative metabolite	Fold change
136.03854	10.75	$C_5H_4N_4O$	3	Hypoxanthine	1.54
276.02469	19.3	$C_6H_{13}O_{10}P$	2	6-Phospho-D-gluconate	8.72
543.33241	4.33	$C_{28}H_{50}NO_7P$	3	LysoPC(20:4(5Z,8Z,11Z,14Z))	4.41
372.54538	18.68	$C_{21}H_{30}N_7O_{17}P_3$	1	NADPH	2.92
545.34822	4.31	$C_{28}H_{52}NO_7P$	2	LysoPC(20:3(5Z,8Z,11Z))	2.8
495.33252	4.42	$C_{24}H_{50}NO_7P$	5	[PC (16:0)] 1-hexadecanoyl-sn-glycero-3-phosphocholine	2.78
523.36387	4.34	$C_{26}H_{54}NO_7P$	9	[PC (18:0)] 1-octadecanoyl-sn-glycero-3-phosphocholine	2.39
230.01906	17.25	$C_5H_{11}O_8P$	16	D-Ribose 5-phosphate	2.3
251.10206	7.57	$C_{10}H_{13}N_5O_3$	4	Deoxyadenosine	2.26
673.46819	3.94	$C_{36}H_{68}NO_8P$	5	[PC (14:1/14:1)] 1,2-di-(9Z-tetradecenoyl)-sn-glycero-3-phosphocholine	2.22
509.34872	4.38	$C_{25}H_{52}NO_7P$	8	LysoPC(17:0)	2.16
481.31676	4.47	$C_{23}H_{48}NO_7P$	8	[PC (15:0)] 1-pentadecanoyl-sn-glycero-3-phosphocholine	2.13
521.34856	4.35	$C_{26}H_{52}NO_7P$	11	1-Oleoylglycerophosphocholine	2.02
135.05453	9.92	$C_5H_5N_5$	1	Adenine	1.96
165.07902	10.8	$C_9H_{11}NO_2$	7	L-Phenylalanine	1.94
493.31666	4.45	$C_{24}H_{48}NO_7P$	3	[PC (16:1)] 1-(9Z-hexadecenoyl)-sn-glycero-3-phosphocholine	1.91
195.11062	22.26	$C_7H_{17}NO_5$	1	N-methyl glucamine	1.91
203.11587	12.06	$C_9H_{17}NO_4$	1	O-Acetylcarnitine	1.9
151.04935	13.38	$C_5H_5N_5O$	3	Guanine	1.84
791.56723	3.45	$C_{42}H_{82}NO_{10}P$	2	[PS (16:0/20:0)] 1-hexadecanoyl-2-eicosanoyl-sn-glycero-3-phosphoserine	1.8
567.33224	4.28	$C_{30}H_{50}NO_7P$	2	[PC (22:6)] 1-(4Z,7Z,10Z,13Z,16Z,19Z-docosahexaenoyl)-sn-glycero-3-phosphocholine	1.77
571.36376	4.24	$C_{30}H_{54}NO_7P$	1	LysoPC(22:4(7Z,10Z,13Z,16Z))	1.69
446.06067	18.06	$C_{11}H_{20}N_4O_{11}P_2$	1	CDP-ethanolamine	1.66

Measured mass	Retention time (min)	Predicted formula	Isomers	Putative metabolite	Fold change
136.03854	10.75	$C_5H_4N_4O$	3	Hypoxanthine	1.54
787.53577	3.51	$C_{42}H_{78}NO_{10}P$	8	[PS (18:1/18:1)] 1,2-di-(9E-octadecenoyl)-sn-glycero-3-phosphoserine	1.62
246.05037	14.03	$C_6H_{15}O_8P$	3	Glycerophosphoglycerol	1.62
183.06613	16.86	$C_5H_{14}NO_4P$	1	Choline phosphate	1.61
148.03713	16.37	$C_5H_8O_5$	18	(R)-2-Hydroxyglutarate	1.61
363.05812	18.38	$C_{10}H_{14}N_5O_8P$	5	GMP	1.56
147.05305	15.82	$C_5H_9NO_4$	14	L-Glutamate	1.52
350.06140	18.5	$C_9H_{19}O_{12}P$	1	nonulose 9-phosphate	1.52
259.04570	17.08	$C_6H_{14}NO_8P$	8	D-Glucosamine 6-phosphate	1.49
154.00305	12.32	$C_3H_7O_5P$	3	Propanoyl phosphate	1.47
304.24012	3.57	$C_{20}H_{32}O_2$	38	[FA (20:4)] 5Z,8Z,11Z,14Z-eicosatetraenoic acid	1.46
566.05561	18.04	$C_{15}H_{24}N_2O_{17}P_2$	3	UDP-glucose	1.43
297.08976	7.36	$C_{11}H_{15}N_5O_3S$	2	5'-Methylthioadenosine	1.42
488.10742	17.06	$C_{14}H_{26}N_4O_{11}P_2$	1	CDP-choline	1.4
302.22439	3.58	$C_{20}H_{30}O_2$	43	[FA (20:5)] 5Z,8Z,11Z,14Z,17Z-eicosapentaenoic acid	1.39
103.09965	22.23	$C_5H_{13}NO$	1	Choline	1.35
493.35298	4.33	$C_{25}H_{52}NO_6P$	1	[PC (17:1)] 1-(1Z-heptadecenyl)-sn-glycero-3-phosphocholine	-1.58
244.20375	3.66	$C_{14}H_{28}O_3$	12	2S-Hydroxytetradecanoic acid	-1.58
216.17251	3.75	$C_{12}H_{24}O_3$	11	12-Hydroxydodecanoic acid	-1.59
248.06453	19.19	$C_8H_{12}N_2O_7$	2	Asp-Asp	-1.61
188.14123	3.89	$C_{10}H_{20}O_3$	13	[FA hydroxy(10:0)] 9-hydroxy-decanoic acid	-1.64
104.01095	17.33	$C_3H_4O_4$	3	Malonate	-1.66
276.09568	14.09	$C_{10}H_{16}N_2O_7$	2	Glu-Glu	-1.86
232.06947	15.71	$C_{16}H_{24}N_4O_{12}$	2	Asp-Thr-Asp-Asp	-2.04
176.03203	16.7	$C_6H_8O_6$	15	2-Hydroxy-3-oxoadipate	-2.14
296.10068	15.78	$C_{13}H_{16}N_2O_6$	2	Asp-Tyr	-2.33
479.33749	4.37	$C_{24}H_{50}NO_6P$	5	[PC (16:1)] 1-(1Z-hexadecenyl)-sn-glycero-3-phosphocholine	-2.34
244.15357	14.66	$C_{20}H_{40}N_8O_6$	1	Arg-Lys-Val-Ser	-2.36
465.32187	4.4	$C_{23}H_{48}NO_6P$	3	[PC (15:1)] 1-(1Z-pentadecenyl)-sn-glycero-3-phosphocholine	-2.72
451.30624	4.46	$C_{22}H_{46}NO_6P$	2	[PC (14:1)] 1-(1E-tetradecenyl)-sn-glycero-3-phosphocholine	-2.76

Table D.5.: Δ*arg* metabolic profiling, HILIC. Putatively identified metabolites with significant fold changes (rank product FDR<0.05).

Measure mass	Retention time (min)	Predicted formula	Isomers	Putative metabolite	Fold change
258.01399	17.32	$C_6H_{11}O_9P$	6	D-Glucono-1,5-lactone 6-phosphate	19
495.33252	9.69	$C_{24}H_{50}NO_7P$	5	[PC (16:0)] 1-hexadecanoyl-sn-glycero-3-phosphocholine	4.03
230.01913	15.07	$C_5H_{11}O_8P$	16	D-Ribose 5-phosphate	3.71
509.34825	9.56	$C_{25}H_{52}NO_7P$	8	LysoPC(17:0)	3.13
545.34773	9.45	$C_{28}H_{52}NO_7P$	2	LysoPC(20:3(5Z,8Z,11Z))	3.07
264.10460	33.88	$C_{12}H_{16}N_4OS$	1	Thiamin	2.88
523.36404	9.45	$C_{26}H_{54}NO_7P$	9	[PC (18:0)] 1-octadecanoyl-sn-glycero-3-phosphocholine	2.84
290.04033	16.62	$C_7H_{15}O_{10}P$	6	D-Sedoheptulose 7-phosphate	2.71
151.04939	15.51	$C_5H_5N_5O$	3	Guanine	2.67
212.00852	15.83	$C_5H_9O_7P$	3	P-DPD	2.51
673.46780	7.59	$C_{36}H_{68}NO_8P$	5	[PC (14:1/14:1)] 1,2-di-(9Z-tetradecenoyl)-sn-glycero-3-phosphocholine	2.39
805.56200	7.44	$C_{46}H_{80}NO_8P$	28	[PC (16:0/22:6)] 1-hexadecanoyl-2-(4Z,7Z,10Z,13Z,16Z,19Z-docosahexaenoyl)-sn-glycero-3-phosphocholine	2.28
705.53133	7.57	$C_{38}H_{76}NO_8P$	22	[PC (15:0/15:0)] 1,2-dipentadecanoyl-sn-glycero-3-phosphocholine	2.18
521.34874	9.53	$C_{26}H_{52}NO_7P$	11	1-Oleoylglycerophosphocholine	2.18
677.49895	7.6	$C_{36}H_{72}NO_8P$	20	[PC (14:0/14:0)] 1,2-ditetradecanoyl-sn-glycero-3-phosphocholine	2.16
199.06857	33	$C_{15}H_{22}N_6O_5S$	1	S-Adenosyl-L-methionine	2.14
649.46769	7.65	$C_{34}H_{68}NO_8P$	21	[PE (14:0/15:0)] 1-tetradecanoyl-2-pentadecanoyl-sn-glycero-3-phosphoethanolamine	2.07
147.05318	17.92	$C_5H_9NO_4$	14	L-Glutamate	2.05
481.35346	9.99	$C_{24}H_{52}NO_6P$	4	[PC (16:2)] 1-hexadecyl-sn-glycero-3-phosphocholine	2.04
195.08953	13.96	$C_{10}H_{13}NO_3$	6	L-Tyrosine methyl ester	1.77
259.04582	16.94	$C_6H_{14}NO_8P$	8	D-Glucosamine 6-phosphate	1.64
144.04225	14.2	$C_6H_8O_4$	13	Methylitaconate	1.56
173.10519	5.75	$C_8H_{15}NO_3$	5	N-Acetyl-L-leucine	-1.42
148.07348	5.45	$C_6H_{12}O_4$	14	[FA methyl,hydroxy(5:0)] 3R-methyl-3,5-dihydroxy-pentanoic acid	-1.44
234.03515	9.21	$C_{12}H_{10}O_3S$	1	2-(2-Hydroxyphenyl)benzenesulfinate	-1.53
164.04735	5.48	$C_9H_8O_3$	13	4-Coumarate	-1.55
136.05241	5.47	$C_8H_8O_2$	16	Phenylacetic acid	-1.56
145.05276	5.6	C_9H_7NO	7	Quinolin-4-ol	-1.58

Measure mass	Retention time (min)	Predicted formula	Isomers	Putative metabolite	Fold change
132.04235	6.16	$C_5H_8O_4$	16	2-Acetolactate	-1.61
354.19029	19.41	$C_{16}H_{26}N_4O_5$	1	Ala-Ala-Pro-Pro	-1.65
216.17249	5.31	$C_{12}H_{24}O_3$	11	12-Hydroxydodecanoic acid	-1.72
219.05327	7.73	$C_{11}H_9NO_4$	2	8-Methoxykynurenate	-1.83
507.36909	9.38	$C_{26}H_{54}NO_6P$	6	[PC (18:1)] 1-(11Z-octadecenyl)-sn-glycero-3-phosphocholine	-1.89
298.07763	9.21	$C_{16}H_{14}N_2O_2S$	1	Mefenacet	-2.07
493.35331	9.52	$C_{25}H_{52}NO_6P$	1	[PC (17:1)] 1-(1Z-heptadecenyl)-sn-glycero-3-phosphocholine	-2.3
178.04768	9.01	$C_6H_{10}O_6$	26	D-Glucono-1,5-lactone	-2.36
216.11112	13.85	$C_9H_{16}N_2O_4$	3	gamma-Glutamyl-gamma-aminobutyraldehyde	-3.33
479.33769	9.64	$C_{24}H_{50}NO_6P$	5	[PC (16:1)] 1-(1Z-hexadecenyl)-sn-glycero-3-phosphocholine	-3.55
451.30618	9.93	$C_{22}H_{46}NO_6P$	2	[PC (14:1)] 1-(1E-tetradecenyl)-sn-glycero-3-phosphocholine	-3.74
465.32204	9.78	$C_{23}H_{48}NO_6P$	3	[PE (18:1)] 1-(9Z-octadecenyl)-sn-glycero-3-phosphoethanolamine	-4.43

D.5. NAO metabolomics enzyme assay

Table D.6.: NAO metabolomics enzyme assay, cofactor mixture 1. Putatively identified metabolites with significant fold changes (rank product FDR<0.05).

Measured mass	Retention time (min)	Predicted formula	Isomers	Putative metabolite	Fold change
91.06332	16.25	$C_3H_9NO_2$	2	3-Aminopropane-1,2-diol	4.55
116.01107	6.26	$C_4H_4O_4$	3	Fumarate	4.18
116.13130	26.82	$C_6H_{16}N_2$	1	1,6-diaminohexane	2.69
307.08411	13.56	$C_{10}H_{17}N_3O_6S$	3	Glutathione	2.18
247.11681	16.19	$C_9H_{17}N_3O_5$	3	Thr-Ala-Gly	2.06
192.08039	9.48	$C_{19}H_{28}O_6S$	1	3b-16a-Dihydroxyandrostenonesulfate	1.8
206.09052	16.2	$C_7H_{14}N_2O_5$	5	Thr-Ser	1.66
444.23244	11.12	$C_{18}H_{32}N_6O_7$	7	Ala-Leu-Asn-Gln	1.54
395.01239	17.6	$C_{10}H_{14}N_5O_6PS_2$	1	Molybdopterin	1.5
289.16349	12.33	$C_{12}H_{23}N_3O_5$	5	Leu-Ala-Ser	1.48
217.10631	16.02	$C_8H_{15}N_3O_4$	3	Ala-Ala-Gly	1.33
189.07500	16.15	$C_6H_{11}N_3O_4$	3	Asn-Gly	1.27
248.11955	9.7	$C_{10}H_{20}N_2O_3S$	1	Met-Val	1.24
181.07403	12.33	$C_9H_{11}NO_3$	11	L-Tyrosine	1.23
541.06101	18.44	$C_{15}H_{21}N_5O_{13}P_2$	1	Cyclic ADP-ribose (fragment of NAD)	1.2
208.05839	9.35	$C_7H_{12}O_7$	1	1-O-methyl-β-D-glucuronate	1.2
483.31712	16.15	$C_{22}H_{41}N_7O_5$	2	Arg-Leu-Val-Pro	1.18
271.25112	6.07	$C_{16}H_{33}NO_2$	4	[FA amino(16:0)] 2R-aminohexadecanoic acid	1.17
337.13079	13.64	$C_{12}H_{23}N_3O_6S$	1	Met-Thr-Ser	1.16
317.17402	8.82	$C_{17}H_{23}N_3O_3$	2	Leu-Trp	1.15
233.10131	16.03	$C_8H_{15}N_3O_5$	4	Ala-Gly-Ser	1.14
406.22167	12.51	$C_{20}H_{30}N_4O_5$	7	Leu-Phe-Gln	1.14
260.11206	17.79	$C_9H_{16}N_4O_5$	4	Ala-Asn-Gly	1.14
129.07901	13	$C_6H_{11}NO_2$	9	L-Pipecolate (fragment of peptide)	-1.54
187.12072	5.38	$C_9H_{17}NO_3$	3	N-Heptanoylglycine	-1.54
258.08519	7.78	$C_{10}H_{14}N_2O_6$	3	Ribothymidine	-1.54
264.07438	5.95	$C_{12}H_{12}N_2O_5$	1	diformylkynurenine	-1.56
288.05909	13.67	$C_{10}H_{12}N_2O_8$	1	Orotidine	-1.56
175.06326	11.2	$C_{10}H_9NO_2$	12	3-Indoleglycolaldehyde (fragment of indole 3-acetamide)	-1.59
173.10506	5.73	$C_8H_{15}NO_3$	5	N-Acetyl-L-leucine	-1.61
237.06341	6.98	$C_{16}H_{23}N_6O_9P$	1	glutamyl-beta-ketophosphonate-adenosine	-1.61
214.02401	14.56	$C_5H_{11}O_7P$	6	2-Deoxy-D-ribose 5-phosphate	-1.61

Measured mass	Retention time (min)	Predicted formula	Isomers	Putative metabolite	Fold change
203.07905	6.33	$C_8H_{13}NO_5$	2	N2-Acetyl-L-aminoadipate	-1.61
209.06889	6.03	$C_{10}H_{11}NO_4$	3	N-Benzyloxycarbonylglycine (fragment of 4-hydroxyphenylacetylglutamic acid)	-1.61
139.97787	15.56	$C_2H_4O_5S$	1	Sulfoacetate	-1.61
231.11083	5.75	$C_{10}H_{17}NO_5$	3	Suberylglycine (fragment of N-acetyl-L-leucine)	-1.61
161.06878	19.02	$C_6H_{11}NO_4$	10	N-Methyl-L-glutamate	-1.64
174.07931	11.07	$C_{10}H_{10}N_2O$	4	Indole-3-acetamide	-1.64
351.14660	13.03	$C_{13}H_{25}N_3O_6S$	1	Met-Thr-Thr	-1.67
252.07445	12.14	$C_{11}H_{12}N_2O_5$	1	5-Hydroxy-N-formylkynurenine	-1.69
238.09537	13.11	$C_{11}H_{14}N_2O_4$	2	Gly-Tyr	-1.69
165.04236	5.61	$C_8H_7NO_3$	8	Formylanthranilate (fragment of 3-methyldioxyindole)	-1.69
193.07366	5.7	$C_{10}H_{11}NO_3$	10	Phenylacetylglycine (fragment of N-acetyl-L-phenylalanine)	-1.75
165.04603	15.8	$C_5H_{11}NO_3S$	4	L-Methionine S-oxide	-1.75
223.08441	5.92	$C_{11}H_{13}NO_4$	2	Bendiocarb (fragment of N-acetylvanilalanine)	-1.82
147.03192	5.65	$C_8H_5NO_2$	2	Isatin (fragment of 6-hydroxykynurenate)	-1.92
248.07929	6.17	$C_{12}H_{12}N_2O_4$	1	5-Hydroxyindoleacetylglycine	-1.92
335.14806	9.49	$C_{16}H_{21}N_3O_5$	1	Gly-Pro-Tyr	-1.92
142.03766	7.06	$C_5H_6N_2O_3$	3	5-Hydroxymethyluracil	-1.96
182.08442	8.34	$C_{12}H_{10}N_2$	1	Harman	-2.04
168.06871	8.65	$C_{11}H_8N_2$	1	beta-Carboline	-2.04
243.10090	8.49	$C_{13}H_{13}N_3O_2$	1	methoxy-PU	-2.04
145.05282	5.54	C_9H_7NO	7	3-Methyleneoxindole	-2.13
207.08962	5.68	$C_{11}H_{13}NO_3$	6	N-Acetyl-L-phenylalanine	-2.17
146.04802	6.02	$C_8H_6N_2O$	1	1(2H)-Phthalazinone	-2.22
285.14768	7.75	$C_{16}H_{19}N_3O_2$	1	Cynometrine	-2.27
240.02364	20.29	$C_6H_{12}N_2O_4S_2$	2	L-Cystine	-2.38
189.04255	5.82	$C_{10}H_7NO_3$	6	Kynurenate	-2.44
284.10091	15.71	$C_{24}H_{32}N_4O_{12}$	1	Tyr-Glu-Glu-Glu	-2.5
190.07415	7.07	$C_{10}H_{10}N_2O_2$	2	L-5-benzyl-hydantoin	-2.63
197.06890	13.19	$C_9H_{11}NO_4$	2	3,4-Dihydroxy-L-phenylalanine	-3.13
288.14724	7.39	$C_{16}H_{20}N_2O_3$	4	Methyl 2-(4-isopropyl-4-methyl-5-oxo-2-imidazolin-2-yl)-p-toluate	-3.57
264.08982	5.53	$C_{16}H_{12}N_2O_2$	1	Perlolyrine (fragment of 3-methyldioxyindole)	-3.85
191.06129	5.89	$C_7H_{13}NO_3S$	1	N-Acetylmethionine	-3.85
177.04598	5.94	$C_6H_{11}NO_3S$	3	N-Formyl-L-methionine	-4.17
205.03768	5.66	$C_{10}H_7NO_4$	2	6-Hydroxykynurenate	-5.26

Table D.7.: NAO metabolomics enzyme assay, cofactor mixture 2. Putatively identified metabolites with significant fold changes (rank product FDR<0.05).

Measured mass	Retention time (min)	Predicted formula	Isomers	Putative metabolite	Fold change
116.01107	6.26	$C_4H_4O_4$	3	Fumarate	5.2
192.08039	9.48	$C_{19}H_{28}O_6S$	1	3b-16a-Dihydroxyandrostenonesulfate	2.29
389.17940	12.39	$C_{16}H_{27}N_3O_8$	2	Glu-Glu-Ile	1.78
429.29547	16.11	$C_{20}H_{39}N_5O_5$	5	Ala-Leu-Lys-Val	1.5
472.26365	24.38	$C_{20}H_{36}N_6O_7$	7	Gln-Lys-Thr-Pro	1.32
407.16585	18.41	$C_{14}H_{25}N_5O_9$	2	Asn-Thr-Ser-Ser	1.31
428.23813	24.37	$C_{18}H_{32}N_6O_6$	2	Ala-Lys-Asn-Pro	1.31
416.23841	20.35	$C_{17}H_{32}N_6O_6$	4	Ala-Lys-Ala-Gln	1.13
306.07606	18.75	$C_{20}H_{32}N_6O_{12}S_2$	1	Glutathione disulfide	1.13
348.20143	24.61	$C_{14}H_{28}N_4O_6$	1	Lys-Thr-Thr	1.12
253.02538	7.07	$C_{10}H_8N_3O_3Cl$	1	5-Amino-4-chloro-2-(2,3-dihydroxyphenyl)-3(2H)-pyridazinone	-1.33
252.07445	12.14	$C_{11}H_{12}N_2O_5$	1	5-Hydroxy-N-formylkynurenine	-1.36
117.04268	7.21	$C_4H_7NO_3$	5	succinamate	-1.46
358.12775	6	$C_{17}H_{18}N_4O_5$	1	202-791	-1.49
189.04255	5.82	$C_{10}H_7NO_3$	6	Kynurenate	-1.5
264.07438	5.95	$C_{12}H_{12}N_2O_5$	1	diformylkynurenine	-1.58
284.10091	15.71	$C_{24}H_{32}N_4O_{12}$	1	Tyr-Glu-Glu-Glu	-1.59
193.07366	5.7	$C_{10}H_{11}NO_3$	10	Phenylacetylglycine (fragment of N-acetyl-L-phenylalanine)	-1.63
173.10506	5.73	$C_8H_{15}NO_3$	5	N-Acetyl-L-leucine	-1.67
205.03768	5.66	$C_{10}H_7NO_4$	2	6-Hydroxykynurenate	-2.03
207.08962	5.68	$C_{11}H_{13}NO_3$	6	N-Acetyl-L-phenylalanine	-2.18
223.08441	5.92	$C_{11}H_{13}NO_4$	2	Bendiocarb (fragment of N-acetylvanilalanine)	-2.2
177.04598	5.94	$C_6H_{11}NO_3S$	3	N-Formyl-L-methionine	-3.62
191.06129	5.89	$C_7H_{13}NO_3S$	1	N-Acetylmethionine	-4.89

D.6. NAO null mutant metabolic profiling

Table D.8.: Δ*nao* metabolic profiling, pHILIC. Putatively identified metabolites with significant fold changes (rank product FDR<0.05).

Measured mass	Retention time (min)	Predicted formula	Isomers	Putative metabolite	Fold change
296.10068	15.78	$C_{13}H_{16}N_2O_6$	2	Asp-Tyr	1.89
246.13286	18.76	$C_9H_{18}N_4O_4$	2	N2-(D-1-Carboxyethyl)-L-arginine (fragment of peptide)	1.53
543.33241	4.33	$C_{28}H_{50}NO_7P$	3	LysoPC(20:4(5Z,8Z,11Z,14Z))	-1.34
465.32187	4.4	$C_{23}H_{48}NO_6P$	3	[PC (15:1)] 1-(1Z-pentadecenyl)-sn-glycero-3-phosphocholine	-1.39
509.34872	4.38	$C_{25}H_{52}NO_7P$	8	LysoPC(17:0)	-1.43
451.30624	4.46	$C_{22}H_{46}NO_6P$	2	[PC (14:1)] 1-(1E-tetradecenyl)-sn-glycero-3-phosphocholine	-1.43
154.00305	12.32	$C_3H_7O_5P$	3	Propanoyl phosphate	-1.46
523.36387	4.34	$C_{26}H_{54}NO_7P$	9	[PC (18:0)] 1-octadecanoyl-sn-glycero-3-phosphocholine	-1.48
495.33252	4.42	$C_{24}H_{50}NO_7P$	5	[PC (16:0)] 1-hexadecanoyl-sn-glycero-3-phosphocholine	-1.5
509.38550	4.41	$C_{26}H_{56}NO_6P$	8	LysoPC(O-18:0)	-1.54
481.31676	4.47	$C_{23}H_{48}NO_7P$	8	[PC (15:0)] 1-pentadecanoyl-sn-glycero-3-phosphocholine	-1.55
310.28727	3.55	$C_{20}H_{38}O_2$	16	[FA (20:0)] 11Z-eicosenoic acid	-1.55
753.53031	3.91	$C_{42}H_{76}NO_8P$	25	[PC (14:0/20:4)] 1-tetradecanoyl-2-(5Z,8Z,11Z,14Z-eicosatetraenoyl)-sn-glycero-3-phosphocholine	-1.55
135.05453	9.92	$C_5H_5N_5$	1	Adenine	-1.63
112.02734	8.59	$C_4H_4N_2O_2$	2	Uracil	-1.73
338.31849	3.53	$C_{22}H_{42}O_2$	9	[FA (22:0)] 13Z-docosenoic acid	-1.73
133.07388	7.39	$C_5H_{11}NO_3$	4	3-nitro-2-pentanol (fragment of 5-methylthioadenosine)	-1.74
297.08976	7.36	$C_{11}H_{15}N_5O_3S$	2	5'-Methylthioadenosine	-1.78
247.06925	17.94	$C_9H_{13}NO_7$	1	N-Succinyl-L-glutamate	-2.12
339.99585	19.67	$C_6H_{14}O_{12}P_2$	14	D-Fructose 1,6-bisphosphate	-2.8

Table D.9.: Δ*nao* metabolic profiling, HILIC. Putatively identified metabolites with significant fold changes (rank product FDR<0.05).

Measured mass	Retention time (min)	Predicted formula	Isomers	Putative metabolite	Fold change
191.06171	5.94	$C_7H_{13}NO_3S$	1	N-Acetylmethionine	2.97
649.46769	7.65	$C_{34}H_{68}NO_8P$	21	[PE (14:0/15:0)] 1-tetradecanoyl-2-pentadecanoyl-sn-glycero-3-phosphoethanolamine	1.84
368.34439	5.24	$C_{27}H_{44}$	1	[ST] (5Z,7E)-9,10-seco-5,7,10(19)-cholestatriene	1.7
517.31638	9.72	$C_{26}H_{48}NO_7P$	4	[PC (18:3)] 1-(9Z,12Z,15Z-octadecatrienoyl)-sn-glycero-3-phosphocholine	-1.32
567.33238	9.34	$C_{30}H_{50}NO_7P$	2	[PC (22:6)] 1-(4Z,7Z,10Z,13Z,16Z,19Z-docosahexaenoyl)-sn-glycero-3-phosphocholine	-1.39
569.34826	9.33	$C_{30}H_{52}NO_7P$	2	LysoPC(22:5(4Z,7Z,10Z,13Z,16Z))	-1.45
571.36385	9.25	$C_{30}H_{54}NO_7P$	1	LysoPC(22:4(7Z,10Z,13Z,16Z))	-1.47
495.33252	9.69	$C_{24}H_{50}NO_7P$	5	[PC (16:0)] 1-hexadecanoyl-sn-glycero-3-phosphocholine	-1.47
297.08978	11.33	$C_{11}H_{15}N_5O_3S$	2	5'-Methylthioadenosine	-1.49
353.23310	7.92	$C_{20}H_{33}O_5$	2	13,14-Dihydro- lipoxin A4	-1.56
220.10589	20.55	$C_8H_{16}N_2O_5$	3	Thr-Thr	-1.82
358.18509	20.52	$C_{15}H_{26}N_4O_6$	3	Ala-Thr-Ala-Pro	-1.85
208.58234	20.6	$C_{19}H_{23}N_5O_6$	1	Phe-Asp-His	-1.92
422.08255	17.26	$C_{12}H_{23}O_{14}P$	5	alpha,alpha'-Trehalose 6-phosphate	-2.13
236.08295	20.46	$C_8H_{16}N_2O_4S$	1	Met-Ser	-2.27
252.08579	20.6	$C_{10}H_{12}N_4O_4$	2	N-D-Ribosylpurine (fragment of peptide)	-2.33

D.7. NAM metabolomics enzyme assay

Table D.10.: NAM metabolomics enzyme assay, cofactor mixture 1. Putatively identified metabolites with significant fold changes (rank product FDR<0.05).

Measured mass	Retention time (min)	Predicted formula	Isomers	Putative metabolite	Fold change
123.03210	7.46	$C_6H_5NO_2$	4	Nicotinate	2.81
309.10597	17.27	$C_{11}H_{19}NO_9$	5	N-Acetylneuraminate	2.45
248.10080	18.71	$C_9H_{16}N_2O_6$	1	Glu-Thr	2.4
132.04224	6.13	$C_5H_8O_4$	16	2-Acetolactate	1.94
222.06736	22.74	$C_7H_{14}N_2O_4S$	4	L-Cystathionine	1.92
147.05319	16.64	$C_5H_9NO_4$	14	L-Glutamate	1.83
189.06379	7.16	$C_7H_{11}NO_5$	4	N-Acetyl-L-glutamate	1.79
351.19078	15.7	$C_{16}H_{25}N_5O_4$	1	Val-Pro-His	1.76
277.10981	15.03	$C_{10}H_{19}N_3O_4S$	3	Met-Ala-Gly	1.69
118.02663	6.43	$C_4H_6O_4$	7	Succinate	1.64
133.03753	17.59	$C_4H_7NO_4$	4	L-Aspartate	1.57
257.10294	20.07	$C_8H_{20}NO_6P$	1	sn-glycero-3-Phosphocholine	1.51
145.07386	27.04	$C_6H_{11}NO_3$	9	5-hydroxy-pipecolate (fragment of peptide)	1.48
308.15822	27.02	$C_{12}H_{24}N_2O_7$	2	Fructoselysine	1.38
123.57660	29.57	$C_{10}H_{21}N_3O_4$	1	Lys-Thr	1.3
345.04732	15.69	$C_{10}H_{12}N_5O_7P$	3	3',5'-Cyclic GMP	1.27
379.21084	12.44	$C_{19}H_{29}N_3O_5$	3	Leu-Phe-Thr	-1.37
155.03487	19.62	$C_3H_{10}NO_4P$	3	N-Methylethanolamine phosphate	-1.4
131.05820	6.58	$C_5H_9NO_3$	14	N-Acetyl-beta-alanine	-1.41
117.04262	6.74	$C_4H_7NO_3$	5	succinamate	-1.43
392.20200	7.03	$C_{22}H_{32}O_4S$	1	[ST hydroxy(2:0/2:0)] (7E)-(3S,6RS)-3-hydroxy-6,19-epithio-23,24-dinor-9,10-seco-5(10),7-choladien-22-al S,S-dioxide	-1.47
138.57299	27.92	$C_{11}H_{23}N_3O_3S$	1	Lys-Met	-1.48
321.18005	26.4	$C_{15}H_{23}N_5O_3$	1	Phe-Arg	-1.48
172.12126	26.03	$C_{16}H_{32}N_4O_4$	1	Lys-Val-Val	-1.49
424.26875	12.96	$C_{21}H_{36}N_4O_5$	2	Ile-Val-Pro-Pro	-1.54
384.24826	25.49	$C_{17}H_{32}N_6O_4$	2	Leu-Pro-Arg	-1.56
470.18344	14.69	$C_{20}H_{30}N_4O_7S$	5	Ala-Met-Ser-Tyr	-1.57
384.23755	13.06	$C_{18}H_{32}N_4O_5$	3	Ala-Val-Val-Pro	-1.62
502.26292	6.16	$C_{22}H_{46}O_8S_2$	1	[FA (22:0/2:0/2:0)] Docosanediol-1,14-disulfate	-1.65
271.25093	7.84	$C_{16}H_{33}NO_2$	4	[FA amino(16:0)] 2R-aminohexadecanoic acid	-1.76

Measured mass	Retention time (min)	Predicted formula	Isomers	Putative metabolite	Fold change
129.15178	11.08	$C_8H_{19}N$	2	Octylamine	-1.89
145.15790	43.66	$C_7H_{19}N_3$	1	Spermidine	-2.11
352.13067	7.31	$C_{21}H_{20}O_5$	10	[Fv] Pongachalcone II	-2.95
122.04802	8.63	$C_6H_6N_2O$	4	Nicotinamide	-17.7

Table D.11.: NAM metabolomics enzyme assay, cofactor mixture 2. Putatively identified metabolites with significant fold changes (rank product FDR<0.05).

Measured mass	Retention time (min)	Predicted formula	Isomers	Putative metabolite	Fold change
260.13719	13.59	$C_{11}H_{20}N_2O_5$	4	Glu-Leu	2.86
246.10381	13.51	$C_{10}H_{18}N_2O_3S$	2	Met-Pro	2.75
123.03210	7.46	$C_6H_5NO_2$	4	Nicotinate	2.64
435.22368	16.07	$C_{19}H_{29}N_7O_5$	2	Phe-Asn-Arg	2.55
116.01094	6.12	$C_4H_4O_4$	3	Fumarate	1.91
277.10981	15.03	$C_{10}H_{19}N_3O_4S$	3	Met-Ala-Gly	1.84
351.19078	15.7	$C_{16}H_{25}N_5O_4$	1	Val-Pro-His	1.84
301.14272	13.07	$C_{16}H_{19}N_3O_3$	3	Trp-Pro	1.44
257.10294	20.07	$C_8H_{20}NO_6P$	1	sn-glycero-3-Phosphocholine	1.41
443.18407	16	$C_{18}H_{29}N_5O_6S$	1	Cys-Gln-Pro-Pro	1.4
464.24182	15.01	$C_{18}H_{36}N_6O_6S$	1	Cys-Lys-Lys-Ser	1.38
309.10597	17.27	$C_{11}H_{19}NO_9$	5	N-Acetylneuraminate	1.32
189.07485	21.22	$C_6H_{11}N_3O_4$	3	Asn-Gly	1.31
135.05462	14.54	$C_5H_5N_5$	1	Adenine	1.25
135.06836	5.67	C_8H_9NO	4	2-Phenylacetamide	1.19
344.20588	13.57	$C_{15}H_{28}N_4O_5$	9	Leu-Val-Asn	1.01
186.13685	23.93	$C_{18}H_{36}N_4O_4$	3	Leu-Leu-Lys	-1.38
309.16870	14.79	$C_{15}H_{23}N_3O_4$	2	Lys-Tyr	-1.42
186.12421	25.74	$C_{16}H_{32}N_6O_4$	1	Val-Val-Arg	-1.43
384.23755	13.06	$C_{18}H_{32}N_4O_5$	3	Ala-Val-Val-Pro	-1.44

Measured mass	Retention time (min)	Predicted formula	Isomers	Putative metabolite	Fold change
189.10014	6.23	$C_8H_{15}NO_4$	5	2 -(Butylamido)-4-hydroxybutanoic acid	-1.44
206.07245	14.82	$C_7H_{14}N_2O_3S$	1	Met-Gly	-1.46
345.18996	13.51	$C_{15}H_{27}N_3O_6$	3	Leu-Val-Asp	-1.5
280.10601	13.5	$C_{13}H_{16}N_2O_5$	2	Phe-Asp	-1.51
263.09396	15.08	$C_9H_{17}N_3O_4S$	3	Ala-Ala-Cys	-1.52
379.21084	12.44	$C_{19}H_{29}N_3O_5$	3	Leu-Phe-Thr	-1.53
328.17468	14.83	$C_{14}H_{24}N_4O_5$	3	Val-Asn-Pro	-1.61
502.26292	6.16	$C_{22}H_{46}O_8S_2$	1	[FA (22:0/2:0/2:0)] Docosanediol-1,14-disulfate	-1.62
72.05753	5.69	C_4H_8O	4	Butanal	-1.65
129.15178	11.08	$C_8H_{19}N$	2	Octylamine	-1.65
147.05316	7.7	$C_5H_9NO_4$	14	N-hydroxy-N-isopropyloxamate	-1.74
262.10263	10.28	$C_{22}H_{32}N_6O_7S$	2	Asn-Met-Phe-Asn	-1.85
455.27449	12.79	$C_{21}H_{37}N_5O_6$	5	Asn-Leu-Leu-Pro	-1.98
122.04802	8.63	$C_6H_6N_2O$	4	Nicotinamide	-9.72

Appendix E

Publications

The following published paper contains work presented in this thesis, and is reproduced under the Creative Commons Attribution License:

Achcar F, Kerkhoven EJ, The SilicoTryp Consortium, Bakker BM, Barrett MP, Breitling R, **(2012)** Dynamic modelling under uncertainty: the case of *Trypanosoma brucei* energy metabolism. *PLoS Comput Biol* 8:e1002352. doi:10.1371/journal.pcbi.1002352

The following published paper contains work that is not presented in this thesis, and permission to reproduce has been granted by John Wiley and Sons:

Haanstra JR, Kerkhoven EJ, van Tuijl A, Blits M, Wurst M, van Nuland R, Albert M-A, Michels PAM, Bouwman J, Clayton C, Westerhoff HV, Bakker BM **(2011)**. A domino effect in drug action: from metabolic assault towards parasite differentiation. *Molecular Microbiology* 79:94–108. doi:10.1111/j.1365-2958.2010.07435.x

OPEN ACCESS Freely available online

PLoS COMPUTATIONAL BIOLOGY

Dynamic Modelling under Uncertainty: The Case of *Trypanosoma brucei* Energy Metabolism

Fiona Achcar[1,2], Eduard J. Kerkhoven[3], The SilicoTryp Consortium[¶], Barbara M. Bakker[4], Michael P. Barrett[3], Rainer Breitling[1,2]*

1 Institute of Molecular, Cell and Systems Biology, College of Medical, Veterinary and Life Sciences, University of Glasgow, Glasgow, United Kingdom, **2** Groningen Bioinformatics Centre, Groningen Biomolecular Sciences and Biotechnology Institute, University of Groningen, Groningen, The Netherlands, **3** Wellcome Trust Centre for Molecular Parasitology, Institute of Infection, Immunity and Inflammation, College of Medical, Veterinary and Life Sciences, University of Glasgow, Glasgow, United Kingdom, **4** Department of Liver, Digestive and Metabolic Diseases, University Medical Centre Groningen, University of Groningen, The Netherlands

Abstract

Kinetic models of metabolism require detailed knowledge of kinetic parameters. However, due to measurement errors or lack of data this knowledge is often uncertain. The model of glycolysis in the parasitic protozoan *Trypanosoma brucei* is a particularly well analysed example of a quantitative metabolic model, but so far it has been studied with a fixed set of parameters only. Here we evaluate the effect of parameter uncertainty. In order to define probability distributions for each parameter, information about the experimental sources and confidence intervals for all parameters were collected. We created a wiki-based website dedicated to the detailed documentation of this information: the SilicoTryp wiki (http://silicotryp.ibls.gla.ac.uk/wiki/Glycolysis). Using information collected in the wiki, we then assigned probability distributions to all parameters of the model. This allowed us to sample sets of alternative models, accurately representing our degree of uncertainty. Some properties of the model, such as the repartition of the glycolytic flux between the glycerol and pyruvate producing branches, are robust to these uncertainties. However, our analysis also allowed us to identify fragilities of the model leading to the accumulation of 3-phosphoglycerate and/or pyruvate. The analysis of the control coefficients revealed the importance of taking into account the uncertainties about the parameters, as the ranking of the reactions can be greatly affected. This work will now form the basis for a comprehensive Bayesian analysis and extension of the model considering alternative topologies.

Citation: Achcar F, Kerkhoven EJ, The SilicoTryp Consortium, Bakker BM, Barrett MP, et al. (2012) Dynamic Modelling under Uncertainty: The Case of *Trypanosoma brucei* Energy Metabolism. PLoS Comput Biol 8(1): e1002352. doi:10.1371/journal.pcbi.1002352

Editor: Jason A. Papin, University of Virginia, United States of America

Received September 14, 2011; **Accepted** November 30, 2011; **Published** January 19, 2012

Funding: This work was supported by SysMO (http://www.sysmo.net/), NWO-Vidi (http://www.nwo.nl/nwohome.nsf/pages/NWOP_5VTGQW_Eng) and SULSA (http://www.sulsa.ac.uk/). Barbara Bakker is the recipient of a Rosalind Franklin Fellowship (http://www.rug.nl/fwn/onderzoek/rff/index). The funders had no role in study design, data collection and analysis, decision to publish, or preparation of the manuscript.

Competing Interests: The authors have declared that no competing interests exist.

* E-mail: Rainer.Breitling@glasgow.ac.uk

¶ Membership of The SilicoTryp Consortium is provided in the Acknowledgments.

Introduction

Kinetic models of metabolism require quantitative knowledge of detailed kinetic parameters (e.g. maximum reaction rates, enzyme affinities for substrates and regulators). However, our knowledge about these parameters is often uncertain. When the parameters are measured, various sources of error can affect the results: experimental noise at the technical and biological levels, systematic bias introduced by parameters being measured *in vitro* instead of *in vivo* or by the choice of specific experimental conditions (pH, temperature, ionic strength, etc.). Moreover, a substantial number of important parameters have never been measured and the estimates included in models are based either on values measured in closely related species or on the general distribution of similar parameters [1]. Few general methods for dealing with this uncertainty have been suggested [2–6].

Here we present an analysis of the effect of parameter uncertainties on a particularly well defined example of a quantitative metabolic model: the model of glycolysis in blood-stream form *Trypanosoma brucei* [7] (see Fig. 1). This ordinary differential equation (ODE) model is mainly using parameters measured on purified enzymes rather than fitted, and, since its first publication in 1997, it has been updated [8] and extended [9–11] several times, making it one of the most highly refined dynamic models of a metabolic pathway published to date. The model has been successfully used to predict the "turbo explosion" that would happen in the absence of the glycosome, the subcellular compartment in which the first seven enzymes of glycolysis are localized in *T. brucei* [8]. This important property was confirmed experimentally more than 10 years after the model was initially proposed [11]. In this paper we used the last updated version of the model published [11] with slight modifications to take into account the equilibrium constants of all reactions (see methods).

Explicitly considering the uncertainties of parameters in the analysis of the model allowed us to gain interesting new insights into its behaviour. Most importantly, our analysis allowed us to quantify the degree of confidence concerning diverse properties of the system, including the hierarchy of control which is relevant for prioritizing potential drug targets. The resulting quantitative profile of model uncertainties, including the identification of

Author Summary

An increasing number of mathematical models are being built and analysed in order to obtain a better understanding of specific biological systems. These quantitative models contain parameters that need to be measured or estimated. Because of experimental errors or lack of data, our knowledge about these parameters is uncertain. Our work explores the effect of including these uncertainties in model analysis. Therefore, we studied a particularly well curated model of the energy metabolism of the parasite *Trypanosoma brucei*, responsible for African sleeping sickness. We first collected all the information we could find about how the model parameters were defined on a website, the SilicoTryp wiki (http:///silicotryp.ibls.gla.ac.uk/wiki/). From this information, we were able to quantify our uncertainty about each parameter, thus allowing us to analyse the model while explicitly taking these uncertainties into account. We found that, even though the model was well-defined and most of its parameters were experimentally measured, taking into account the remaining uncertainty allows us to gain more insight into model behavior. We were able to identify previously unrecognised fragilities of the model, leading to new hypotheses amenable to experimental testing.

major fragilities and areas in need of further examination, provides a solid basis for future model extensions. These will in turn introduce new uncertainties and should be dealt with using the same general framework established here.

Results

Collecting information

In order to specify the uncertainty associated with each parameter, we gathered all available information relating to the sources of the values used in the model. Information included data on how kinetics were measured, the number of replicates and the standard error of mean values when available, additional calculations used to estimate the parameter from the observed values, and any "corrections" for additional factors such as temperature or pH. For this purpose, we created the "SilicoTryp" wiki, a MediaWiki-based (http://www.wikimedia.org) website dedicated to the detailed documentation of the sources of parameters used in the latest version of the model of glycolysis in *T. brucei* (http://silicotryp.ibls.gla.ac.uk/wiki/Glycolysis) [10]. Each reaction is described on its own page, which contains the rate equation and the detailed references and calculations for each parameter (see Fig. 2 for an example).

From the information collected, probability distributions could be inferred for each parameter as described in Methods. supplementary text S1 shows the estimated distributions for all parameters.

The effects of uncertainty

To model the effect of uncertainty, we sampled values for each parameter according to its probability distribution, generating a ensemble of alternative models. Together these alternative models accurately represent our degree of uncertainty about the correct parameters, assuming that our knowledge of each parameter value is independent of the other parameters (see Methods for one example, the equilibrium constant, where this assumption is violated and needs to be accounted for). This collection of models can then be used to analyse model behavior and the associated uncertainties. The same properties that were studied with the fixed parameter version of the model can be studied with each alternative model. The distribution of the results shows the robustness and the degree of certainty we have about the inferred model properties (e.g. the steady-state concentrations of the metabolites and the control coefficients) considering our current knowledge about the parameters and the topology of the model.

Reaching steady-state. The first property of the models that we analyzed is whether or not a steady-state is reached in a reasonable time. Our simulation uses the steady-state of the model with the fixed set of parameters to set the initial concentrations of the metabolites. From this initial state, each model is simulated until steady-state is reached. Considering the generous threshold we set for these simulations, steady-state should be reached rapidly. Yet, only 33% of the 10,000 models reached steady-state within 50 simulated minutes or less, and only 36% within 300 simulated minutes. As shown in Fig. 3, models that could not reach steady-state within 300 minutes had all produced a very high concentration of either 3-phosphoglycerate (3-PGA) or pyruvate. The accumulation of these metabolites to unreasonable concentrations indicates that the models contain fragilities. These cases are studied in more detail below (section Effects on steady-state concentrations).

Effects on steady-state flux. In bloodstream form *T. brucei*, glucose is mainly converted to pyruvate in aerobic conditions, while it is divided equally between pyruvate production and glycerol production under anaerobic conditions [12,13]. These flux distributions were also observed in cultured cell [14] and reproduced by the model [7] (anaerobic conditions are modelled by setting the V_{max} of glycerol 3-phosphate oxidase (GPO, reaction used to model the mitochondrial glycerol 3-phosphate dehydrogenase coupled with the trypanosome alternative oxidase) to zero, the only model reaction requiring oxygen; the experimental measurements correspond to its inhibition as *T. brucei* does not survive total anaerobic conditions [9]).

This property is well-conserved in all our models using the full range of plausible parameter values (see Fig. 4). As expected, the effect of uncertainty is more important in aerobic conditions: for most of the models that do reach steady-state within 300 minutes, the proportion of glucose that ends in glycerol varies between 0 and 20% (mean $\pm$ standard deviation of the models that reaches steady-state within 300 minutes: $9.1 \pm 5.9\%$). In contrast, under anaerobic conditions, the glycolytic flux is always shared 50/50% between the production of glycerol and pyruvate ($50.0 \pm 4 * 10^{-4}\%$; the small error is most probably due to numerical rounding effects).

Indeed, anaerobically, the flux distribution is entirely determined by the topology and stoichiometry of the model: the 6-carbon product derived from glucose (fructose 1,6-bisphosphate) is split into two 3-carbon products by aldolase. Anaerobically, the NADH formed in the pyruvate branch can only be reoxidized to NAD^+ in the glycerol branch [7]. Hence the 50/50% split is independent of the parameters of the model as expected from the topology of the model. Under aerobic conditions, glycerol 3-phosphate is mostly reoxidized using the mitochondrial glycerol 3-phosphate dehydrogenase (GPO) and then re-routed through the pyruvate branch via triose-phosphate isomerase [7]. However, a small proportion of the flux ends with the production of glycerol. This small proportion depends on the parameters used in the model. No single parameter can easily predict the proportion of the flux that ends in the production of glycerol.

The fixed-parameter version of the model (i.e. the model with the set of parameter defined to be as close as possible to the model described in [10]) predicted only a very small portion of the

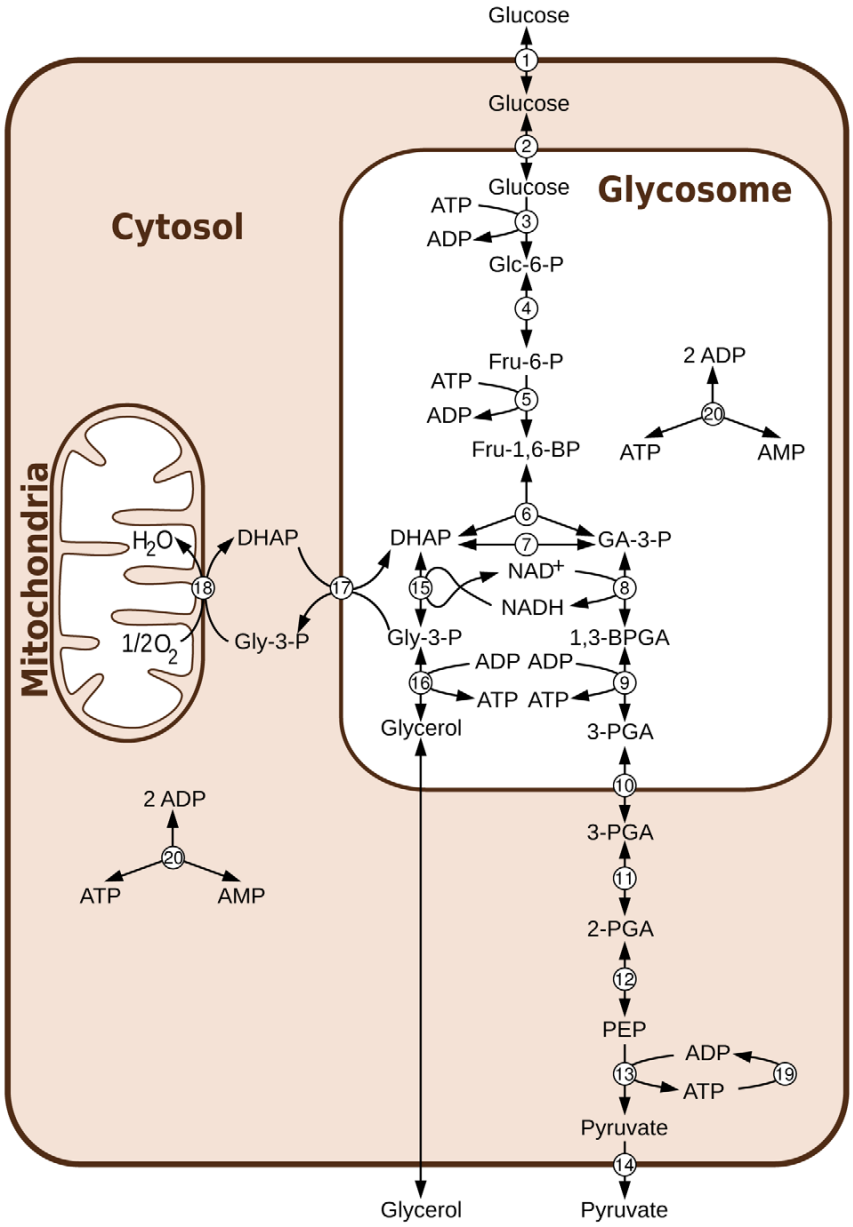

Figure 1. Aerobic glycolysis in bloodstream form *T. brucei*. Abbreviations: Metabolites: Glc-6-P = Glucose 6-phosphate, Fru-6-P = Fructose 6-phosphate, Fru-1,6-BP = Fructose 1,6-bisphosphate, DHAP = dihydroxyacetone phosphate, GA-3-P = glyceraldehyde 3-phosphate, Gly-3-P = glycerol 3-phosphate, 1,3-BPGA = 1,3-bisphosphoglycerate, 3-PGA = 3-phosphoglycerate, 2-PGA = 2-phosphoglycerate, PEP = phosphoenolpyruvate. Reactions: 1 = transport of glucose across the cytosolic membrane, 2 = transport of glucose across the glycosomal membrane, 3 = hexokinase, 4 = phosphoglucose isomerase, 5 = phosphofructokinase, 6 = aldolase, 7 = triosephosphate isomerase, 8 = glyceraldehyde 3-phosphate dehydrogenase, 9 = phosphoglycerate kinase, 10 = transport of 3-PGA across the glycosomal membrane, 11 = phosphoglycerate mutase, 12 = enolase, 13 = pyruvate kinase, 14 = transport of pyruvate across the cytosolic membrane, 15 = glycerol 3-phosphate dehydrogenase, 16 = glycerol kinase, 17 = DHAP-Gly-3-P antiporter, 18 = glycerol-3-phosphate oxidation, 19 = ATP utilisation, 20 = adenylate kinase.
doi:10.1371/journal.pcbi.1002352.g001

glycolytic flux through the glycerol branch, while a wider range of plausible values are permitted when parameter uncertainty is considered. Indeed, a wide range of aerobic flux distributions has been measured experimentally: from a few percent glycerol measured by [14] to about 9% glycerol measured by [15]. This range of observed biological variety can be explained using the variety of kinetic parameters included in our collection of models, or by partial anaerobiosis leading to a mixture of oxygenation states in individual cells within the population measured.

Effects on steady-state concentrations. Using our collection of models, we are able to see the effect of parameter uncertainties on the steady-state concentration estimates.

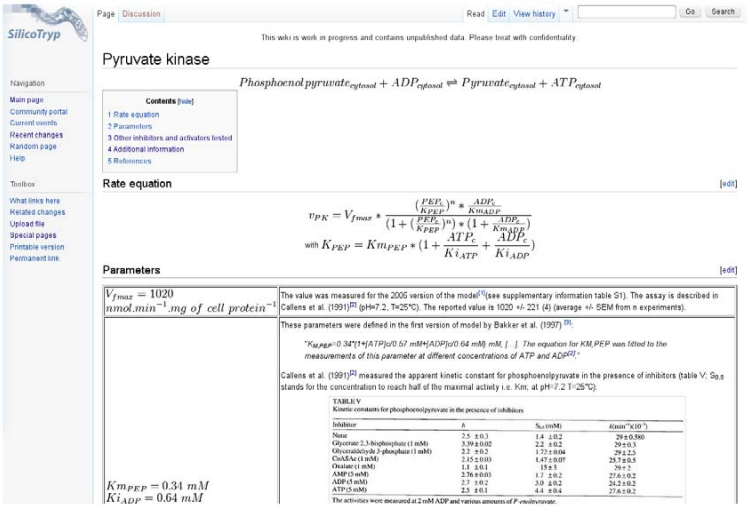

Figure 2. Example of a page of the SilicoTryp wiki. Each reaction of the model has its own page. On this page, the rate equation is specified and a table includes all parameters with their detailed source and calculations when necessary.
doi:10.1371/journal.pcbi.1002352.g002

Considering only the models that reach steady-state within 300 simulated minutes, several cases can be distinguished (see Fig. 5 and supplementary text S2):

- For many metabolites, steady-state concentrations are well-conserved in all plausible models and their distribution is approximately log-normal: glucose 6-phosphate, fructose 6-phosphate, glycosomal glyceraldehyde 3-phosphate, cytosolic and glycosomal dihydroxyacetone phosphate and glycerol 3-phosphate, $mathrmNAD^+$, NADH, 2-phosphoglycerate and phosphoenolpyruvate. These distributions may be expected, given that most of the parameters are sampled from log-

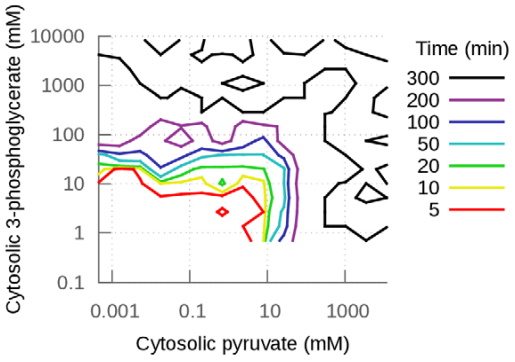

Figure 3. Steady-state concentration of pyruvate as a function of the concentration of 3-phosphoglycerate at steady-state or t = 300 minutes if steady-state is not reached before. The contour lines indicate when steady-state was reached (in minutes of simulated time). If steady-state was not reached before, simulations were stopped at 300 minutes (see Methods). When a model did not reach steady-state before 300 minutes, the concentrations of pyruvate and/or 3-phosphoglycerate reached unreasonably high concentrations (black contour lines). Note that the models that do not reach steady-state within 300 minutes because of 3-PGA accumulation will eventually reach steady-state at very high 3-PGA concentrations if the simulations are run much longer. This is not the case for the models that show pyruvate accumulation. Since pyruvate kinase is not product-sensitive in the model, nothing stops the accumulation of pyruvate and steady state is never reached (see supplementary Fig. S1 for example of simulations).
doi:10.1371/journal.pcbi.1002352.g003

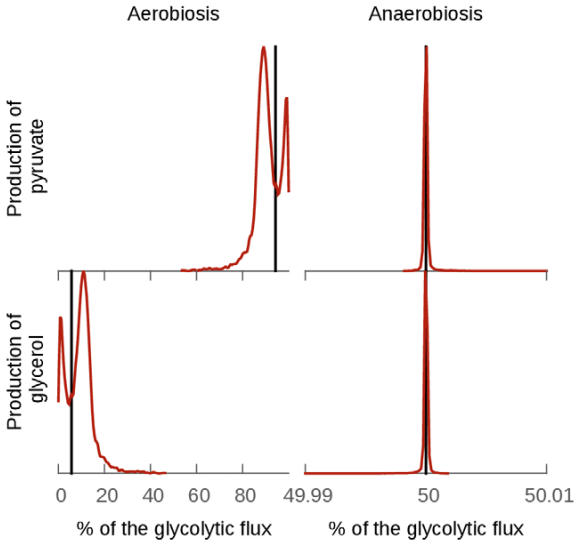

Figure 4. Effect of the uncertainties on the distribution of the glycolytic flux between the production of pyruvate and glycerol. The glycolytic flux is defined as the sum of the fluxes producing glycerol and pyruvate. The black lines represents the percentage of the glycolytic flux in the pyruvate branch (top) and the glycerol branch (bottom) in the fixed parameter model. The red line is the distribution of the percentage of the glycolytic flux in the collection of models generated from the parameter probability distributions. The division of the flux between the pyruvate branch and the glycerol branch is well conserved. The effect of the uncertainties of the parameters is almost non-existent in anaerobic conditions (simulated by setting the glycerol 3-phosphate oxidase V_{max} parameter to 0). In aerobic conditions the effect is more important, indicating that this division is not entirely due to the topology of the model in this case.
doi:10.1371/journal.pcbi.1002352.g004

normal distributions and thus approximately log-normal distributions for the steady-state concentrations are expected too.

- For several metabolites, steady-state concentrations do not follow approximate log-normal distributions, although their steady-state concentrations are distributed within a range of values consistent with physiological metabolite concentrations. These include glycosomal and cytosolic ATP, ADP, AMP, glycosomal and cytosolic glucose, fructose 1,6-bisphosphate and glycosomal 1,3-bisphosphoglycerate. For example, the concentration of glycosomal ATP and AMP is predicted to be between 0 and 6 mM (see Fig. 5 B. for ATP), compared to the fixed-parameter values of 4.2 mM and 0.25 mM respectively. The concentration is bounded by the fact that the total adenine nucleotide concentration in the glycosome is set to 6 mM in the model. Given the uncertainty regarding the exact parameters, any ratio between ATP and AMP seems possible and consistent with our parameter knowledge.
- For two metabolites, 3-phosphoglycerate and pyruvate, the steady-state concentration distribution has a long, heavy tail, indicating that some combinations of plausible parameter values can lead to extreme predicted concentrations (several hundreds to thousands of mmol/l, see Fig. 3). These cases were studied in more detail as they point to interesting fragilities in the existing model, which indicate a need to refine our knowledge of some parameters and/or model topology.

The accumulation of 3-phosphoglycerate (3-PGA) and/or pyruvate to unreasonable concentrations causes some models to reach steady-state at extremely high concentrations or to fail reaching steady-state within 300 minutes. This occurs when the maximum reaction rates (V_{max}) of phosphoglycerate mutase (PGAM) for the 3-PGA accumulation or pyruvate transport (PyrT) for the pyruvate accumulation are smaller than their mean values. Fig. 6 shows the percentage of models that break as a function of PGAM V_{max} (Fig. 6 A) and PyrT V_{max} (Fig. 6 B). The data show that these models break even when these parameters have values very close to the original value used in the fixed-parameter version of the model. Yet, these two reactions can both be inhibited experimentally *in vivo*. When PGAM was inhibited using tetracycline-inducible RNAi, diminishing V_{max} to 51% of its original value [10], no adverse effects on the viability of the organism were observed. The pyruvate transporter can also be inhibited substantially before the cells start dying [16]. The reason for the newly revealed model fragilities thus could be twofold: either the relevant parameter values are significantly higher than the currently used values (which are fitted, not measured; [10]), or some unknown regulatory interaction or missing reaction stabilizes the biological system. The pyruvate accumulation is due to a known fragility of the model: the pyruvate kinase is insensitive to its products, which can lead to the accumulation of pyruvate when the V_{max} of its transporter is not high enough.

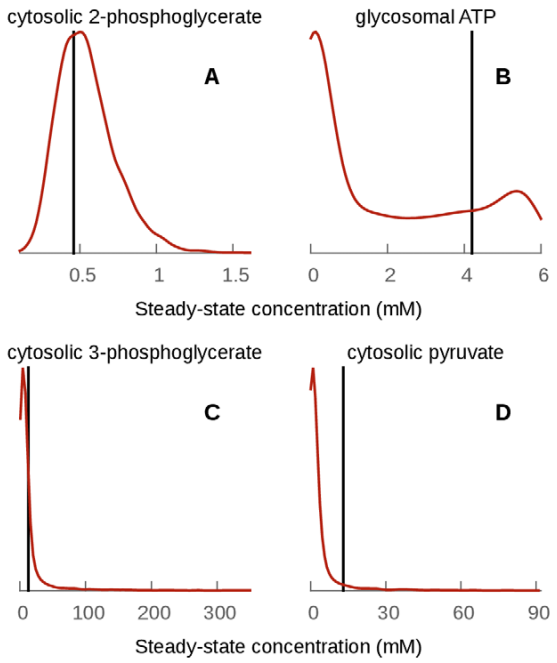

Figure 5. Distribution of the steady-state concentrations of four metabolites. The cytosolic 2-phosphoglycerate and glycosomal ATP steady-state concentrations are consistent with physiological metabolite concentration, whereas 3-phosphoglycerate and pyruvate sometimes reach hundreds of millimoles per liter. The value for the fixed parameter model is indicated by a vertical black line.
doi:10.1371/journal.pcbi.1002352.g005

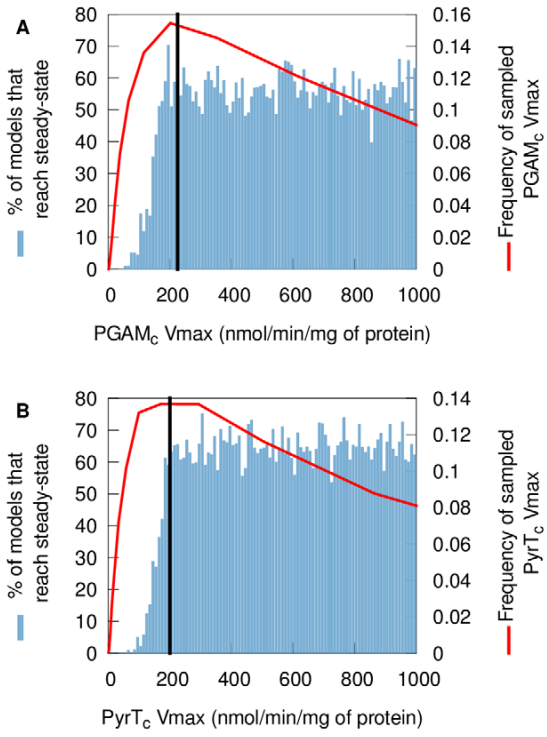

Figure 6. Percentage of sampled models that reach steady-state within 300 minutes as a function of the V_{max} of pyruvate transport and phosphoglycerate mutase. (A) Percentage of models that reach steady-state within 300 minutes as a function of phosphoglycerate mutase V_{max} (B) Percentage of models that reach steady-state within 300 minutes as a function of pyruvate transport V_{max}. The red line is the distribution of the parameter as it is usually sampled. The black line is the fixed-parameter value. A model which has a value for one of these two parameters smaller than the mean will easily fail to reach steady-state, whatever the other parameter values and despite these V_{max} values still being close to their mean. This reveals fragilities in the model.
doi:10.1371/journal.pcbi.1002352.g006

Vanderheyden et al. have measured the pyruvate efflux V_{max} at 37°C in bloodstream form *T. brucei* [17] as 499 ± 34 nmol/min/mg of protein (mean $\pm$ SD). Assuming an activation energy of 50 kJ/mol, the V_{max} at 25°C would be about 230 nmol/min/mg of protein, very close to the 200 nmol/min/mg of protein currently used in the model. Using Vanderheyden et al.'s value to compute the probability distribution of the V_{max} of pyruvate transport (using the corrected mean and calculating the standard deviation as for any value with a measured mean and unknown standard deviation; see methods), only 0.58% of models cannot rapidly reach a steady-state because of pyruvate accumulation (pyruvate concentration at 300 minutes higher than 100 mM), compared to 35.4% when the V_{max} is set as described in Methods). But this still imply that even a small inhibition of the pyruvate transporter should kill the cells, which is inconsistent with the experimental observations [16]. Therefore, there is probably an additional mechanism that prevents the accumulation of pyruvate in the cytosol. Among the possible hypotheses, it is interesting to note that alanine aminotransferase activity has been measured in bloodstream forms by Spitznagel et al. [18] (419 ± 10 nmol/min/mg of protein in whole cell extracts at 37°C). This enzyme, which catalyses the reversible reaction $pyruvate + glutamate \leftrightarrow alanine + 2-oxoglutarate$, was shown to be essential in bloodstream form trypanosomes and might have a significant role in the regulation of the intracellular pyruvate concentration.

Adding alanine aminotransferase into the model would require adding several other reactions as well: the production and recycling of 2-oxoglutarate and glutamate need to be incorporated, as well as the export of alanine [19,20] and probably 2-oxoglutarate [21].

Effects on control coefficients. Control coefficients are one of the most important high-level properties of kinetic models of metabolism: they allow the quantification of how much influence each reaction has on the flux of the pathway. In the glycolytic model of *T. brucei*, individual control coefficients have been used to predict the most promising trypanocidal drug targets. The *T. brucei* glycolysis model published by Alberts et al. [10] indicated that the glucose consumption flux is controlled mainly by the glucose transporter at 5 mM of extracellular glucose (control coefficient $C_{GlcT_c} = 0.98$ [10]). As the sum of the control coefficients over the pathway is one [22], the other enzymes have no or very little control over the glucose consumption flux in this fixed-parameter model.

Using our collection of models, we calculated the control coefficients for every reaction and every model (see Methods). These control coefficients were then ranked from the highest to the lowest. Our analysis (Fig. 7) shows that, given our uncertainty on the parameters, we cannot be certain about the identity of the reaction that has most control over the glucose consumption flux. Moreover, we show that the fixed-parameter model scenario, where almost all the control is held by one reaction - the glucose transporter - is not the only scenario possible, but that even at 5 mM of glucose the control might be shared by several reactions.

Fig. 7A (red) shows the reaction that has the highest control coefficient over the glucose consumption flux as a percentage of the sampled model. The glucose transporter has the highest control over the glucose consumption flux in only 40.3% of the models. A substantial proportion of models yield either the phosphoglycerate mutase (PGAM, 31.1%) or GAPDH (28.5%) as having the highest control coefficient.

In 1999, Bakker et al. [23] estimated the control coefficient over the oxygen consumption flux of the glucose transporter experimentally (at 5 mM of extracellular glucose) as being between 0.3 and 0.5. In the fixed-parameter model, the V_{max} of the glucose transporter was fitted to this control coefficient (0.4) by Alberts et al. [10]. In 17.3% of our models, the glucose transporter has the highest control coefficient over the oxygen consumption flux (Fig. 7A (blue)). Among these models, the control coefficient of the glucose transporter varies between 0.2 and 1.0; when another reaction has the largest control coefficient, the control coefficient of the glucose transporter is always lower than 0.4. A similar distribution of the control coefficient is observed over the glucose consumption flux. No single parameter alone can explain the wide range of values of C_{GlcT}. It has been shown, however, that the extreme sensitivity of C_{GlcT} to various parameters can be attributed to the large difference between the K_m values of the glucose transporter and the next enzyme, hexokinase, towards intracellular glucose [24].

Fig. 7B represents the number of reactions that exert some control over the glucose consumption flux (defined as the reactions with control coefficients above 0.001) as a percentage

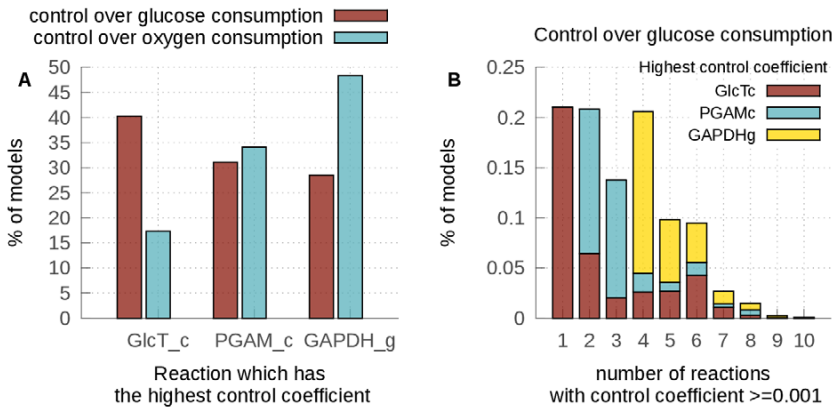

Figure 7. Control coefficients in the collection of models. (A) Percentage of models which have either the glucose transporter (GlcTc), phosphoglycerate mutase (PGAM) or glyceraldehyde 3-phosphate dehydrogenase (GAPDH) as the reaction with the highest control coefficient either over the glucose consumption flux (red) or the oxygen consumption flux (blue). (B) Percentage of models vs. the number of reactions that have a control coefficient higher than 0.001. The color inside the bars represents the proportion that has either the glucose transporter, PGAM or GAPDH as the reaction with the highest control coefficient over the glucose consumption flux within these subgroups.
doi:10.1371/journal.pcbi.1002352.g007

of the sampled models. For 21% of the sampled models, only one reaction controls the glucose consumption flux and this reaction is most of the time the glucose transporter, as is the case in the fixed-parameter model. When PGAM exerts most control over the flux, it shares the control with at least one other reaction. When GAPDH exerts most control over the flux, it shares the control with at least four other reactions. Interestingly, the activity of GAPDH has been reported to be inhibited by an unknown compound [25]. If this inhibition is physiological and also occurs *in vivo*, it might have an important role in the control of glycolytic flux. Indeed, partial inhibition of GAPDH has already been shown to decrease the glycolytic flux and kill the cell [26]. The fact that PGAM exerts the most control in some models might reflect our lack of knowledge about the parameters describing the rate of this reaction. Further analysis of the kinetics of this reaction is necessary to know whether it really exerts some control over the glycolytic flux and thus represents interesting potential drug target.

In the fixed-parameter model, shared control was only seen at glucose concentrations higher than 5 mM [8]. Taking our uncertainty about the parameters values into account shows that this might be the case already at 5 mM of glucose, as has already been suggested by the preliminary analysis of the sensitivity of control coefficients to variations in V_{max} values in this model [8]. Improving our knowledge about GAPDH and PGAM parameters will allow us to know with a higher degree of confidence if only one of these scenarios is relevant *in vivo* or if a similar diversity can be found in a parasite population. This knowledge will be essential to predict if a single glycolytic drug target is sufficient or if multiple reactions need to be inhibited to control parasite infections.

Discussion

Dynamic models of metabolism are powerful tools to infer interesting and often unexpected properties of cellular physiology. However, the data used to build models from diverse sources can lack accuracy and precision. Here we demonstrate how model output can vary when the uncertainties associated with incomplete and variable datasets are explicitly considered in studying a model. We took as an example the well characterised model of the compartmentalised glycolysis in the parasitic protozoan *T. brucei*. It should be noted that our assessment of the effect of parameter uncertainty on the conclusions that are possible is very conservative. Whenever possible, we have restricted our uncertainty estimates to the level of experimental uncertainty seen within a single assay. This ignores the systematic effects of differences in, e.g., temperature, pH or ion compositions, or biases introduced in sample preparation, all of which would increase uncertainty as can also be seen when parameter values from different laboratories are compared. However, even with these relatively limited uncertainties, we were able to assess the robustness and variability of various properties of the model.

The first property that we studied is the ability of the model to reach steady-state rapidly. Surprisingly, a significant proportion (60%) of the models we generated by sampling the parameters did not allow the model to reach steady-state within 300 minutes, due to the accumulation of either 3-phosphoglycerate or pyruvate in the cytosol. This phenomenon could be attributed to two individual parameters, the maximal reaction rates of phosphoglycerate mutase and pyruvate transport which, when operating below their mean value (but still very close to it), caused the accumulation of two metabolites (3-phosphoglycerate and pyruvate respectively). For the pyruvate transporter, the analysis suggested a mechanism that could avoid this problem: alanine aminotransferase has been shown, unexpectedly, to be essential in bloodstream form *T. brucei* [18], and its activity comparable with the rate of pyruvate efflux. This would be sufficient to exert a substantial influence on the intracellular pyruvate concentration. The maximal reaction rate of phosphoglycerate mutase is difficult to measure directly [27], therefore further experimental and theoretical studies are required to refine our knowledge about this reaction. Indeed, the model predicts that current values for PGAM are probably lower than those operative in *T. brucei*, and some effort should be made to determine whether the values are indeed higher.

We then analysed the distribution of the steady-state fluxes between the pyruvate and glycerol producing branches of glycolysis both in aerobic and anaerobic conditions. In totally anaerobic conditions, the distribution was very well conserved. Indeed, this property is entirely constrained by the topology of the model and thus this result was expected. Our analysis shows that the distribution of the fluxes is more variable in aerobic conditions, consistent with previously unexplained variation in experimental observations (although changes in oxygen tension within different cells in measured populations would create the same effect).

Further analysis of the steady-state concentrations allowed us to distinguish the metabolites that are only moderately affected by the parameter uncertainties and follow an approximate log-normal distribution, such as NAD^+ and NADH, from the metabolites that follow a more complex distribution such as glycosomal ATP. ATP is constrained by a conserved sum, therefore its steady-state concentration always stays within reasonable limits. Technical limitations mean that the concentration of glycosomal ATP is not directly accessible for experimentation (glycosomes cannot be purified efficiently enough). Therefore, only by acquiring additional data about the parameters of the model can assumptions about these concentrations at steady-state be refined.

Finally, we analysed the control coefficients of each enzyme using our collection of models. These properties are especially important in the case of glycolysis in *T. brucei*, as they allow us to identify potential drug targets. Our analysis reveals that, although the reaction that has the most control over the glucose consumption flux is the glucose transporter in 40.3% of the models, two other reactions maximally control the flux in a significant proportion of the models: PGAM (31.1%) and GAPDH (28.5%). Moreover, the activity of GAPDH has been reported to be inhibited by an unknown metabolite [25]; if this inhibition occurs *in vivo*, it might have an important role in the control of glycolytic flux. Interestingly, partial inhibition of GAPDH has been shown to affect parasite growth and glycolytic flux [26], and selective inhibitors of the *T. brucei* enzyme have been shown to be trypanocidal [28]. The rest of the control coefficient hierarchy is more variable. Either this variability is a true reflexion of biological noise or the result of our lack of knowledge about some parameters of the model.

The data derived from the work performed here point to several further studies, including analysis of the role of alanine amino transferase in the regulation of pyruvate concentration and more exact quantification of pyruvate transport and phosphoglycerate mutase kinetics. The detailed description of parameter uncertainty will now form the basis for a comprehensive Bayesian analysis and extension of the model using alternative topologies [29]. These analyses will allow us to quantify our posterior belief about the parameters of the model when it is confronted with new experimental data such as measured metabolite concentrations in different conditions.

Methods

The model

The model used in this paper is the last updated version [10,11] of the glycolysis model of *T. brucei* first published by Bakker et al. in 1997 [7] (see Fig. 1).

To allow a straight-forward sampling of parameters, the rate equations were rewritten to contain the equilibrium constant instead of the ratio of V_{max} values (reverse over forward), using the Haldane equation [30]. This does not change the rates, but simplifies the sampling of the parameters, as we do not need to check for consistency with the thermodynamic equilibrium constant. For example, the phosphoglucose isomerase (PGI) rate equation was:

$$v_{PGI} = Vmax * \frac{\frac{Glc6P_g}{Km_{Glc6P}} - r * \frac{Fru6P_g}{Km_{Fru6P}}}{1 + \frac{Glc6P_g}{Km_{Glc6P}} + \frac{Fru6P_g}{Km_{Fru6P}}} \quad (1)$$

where $r = \frac{Vmax_{reverse}}{Vmax_{forward}}$. The Haldane equation gives:

$$Keq_{PGI} = \frac{Vmax_{forward} * Km_{Fru6P}}{Vmax_{reverse} * Km_{Glc6P}} \quad (2)$$

Therefore, the rate equation of PGI can be rewritten as:

$$v_{PGI} = Vmax * \frac{\frac{Glc6P_g}{Km_{Glc6P}} * (1 - \frac{Fru6P_g}{Glc6P_g * Keq})}{1 + \frac{Glc6P_g}{Km_{Glc6P}} + \frac{Fru6P_g}{Km_{Fru6P}}} \quad (3)$$

The list of sources used to compute the values of the equilibrium constants is available in supplementary text S3 and on the SilicoTryp wiki (http://silicotryp.ibls.gla.ac.uk/wiki/Glycolysis). The model in [11] considered the transport reactions between the cytosol and the glycosome and adenylate kinase (see special cases) to be very fast compared the other reactions of the model. Therefore, they were not explicitly modelled. To enable consideration of the effect of parameter uncertainty on the rate of these transport reactions, we modelled them explicitly using mass action kinetics. As we considered that these reactions have an equilibrium constant of unity (no preferential accumulation or exclusion in one of the compartments), we used a single rate parameter for each transport reaction. For example, the transport of glucose between the cytosol and the glycosome is modelled as:

$$v_{GlcTg} = k * Glc_c - k * Glc_g \quad (4)$$

The model is available as supplementary dataset S1 (SBML file [31]). The parameter values are as in [11]. The equilibrium constant are calculated from the K_m values and the ration of $V_{max}reverse$ over $V_{max}forward$ when necessary.

Probability distributions of the parameters

In order to sample the model parameters, we needed to define a probability distribution for each parameter. These distributions can be defined empirically using arbitrary shapes, but for the sake of convenience it is usually appropriate to use standard shapes (e.g. normal or log-normal distributions) and then to estimate the parameters of these distributions (usually the mean and standard deviation).

Km/Ki. These parameters represent concentrations, therefore they cannot be negative and our uncertainty about their values is best represented by a log-normal distribution.

For each K_m or K_i value of the model, the mean and standard deviation of the corresponding log-normal distribution must be estimated from available experimental data (indicated as *lmean* and *lsd*). Five situations occur:

- The parameter has been measured experimentally: a mean (m) and standard deviation (SD) or standard error ($SEM = SD * \sqrt{n}$, where n is the number of observations) are available. $lmean = log_{10}(m)$ and $lsd = log_{10}(\frac{SEM}{m} + 1)$. If a standard deviation is available and the number of observations is not specified, n is supposed to be 3.
- The parameter has been measured experimentally, but only a mean value is reported. *lmean* is computed as above, *lsd* is computed using the average relative standard error (RSE) of all K_m values of the model for which SD or SEM is available. The value of RSE calculated from the published data is usually between 10 and 20%, indicating that the RSE can be expected to be similar for those K_m values where it has not been specified.
- The parameter has not been measured, and no estimate of its value is available. When no other information is available, the parameter is calculated from the list of K_m values of all *T. brucei* enzymes retrieved from BRENDA [32] ($lmean = -1.1$, $lsd = 1.35$, Fig. 8).
- The parameter has not been measured, but some indication of its mean is available, e.g. a value measured for a phylogenetically closely related species (*Trypanosoma cruzi* or a *Leishmania* species). This heterologous mean is used to compute the *lmean* as above. As this value is considered to be more uncertain than a value measured in *T. brucei*, the *lsd* is calculated so that the upper or lower limit of the 95% confidence interval equals the upper or lower limit of the 95% confidence interval of all *T. brucei* enzyme retrieved from BRENDA (if the heterologous mean is higher than the mean calculated from all *T. brucei*

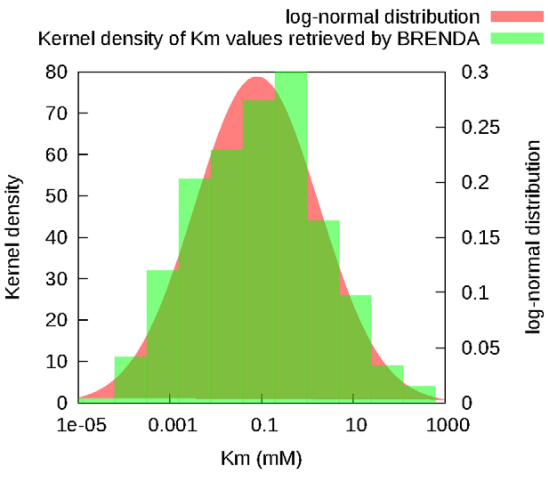

Figure 8. Distribution of the K_m values retrieved from the BRENDA database. K_m values retrieved from the database (green) and a log-normal distribution with the same mean and standard-deviation (red) are shown.
doi:10.1371/journal.pcbi.1002352.g008

enzyme retrieved from BRENDA, then the upper limit is used, otherwise, the lower limit is used). However, if the 95% confidence interval calculated is bigger than $[0.1 * mean; 10 * mean]$ then $[0.1 * mean; 10 * mean]$ is used to calculate *lsd*.

The K_m values of PGAM used in the published version of the model were measured in the presence of cobalt, as this was believed to be the cofactor used by the enzyme. However, the nature of the metallic cofactor used by this enzyme has recently been questioned: Fuad et al. (2011) [33] have shown that the concentration of cobalt is too small to be relevant *in vivo*. For this reason, the K_m values of PGAM were set according to the earlier measurements done by Chevalier et al. (2000) [27]: $K_m(3-\mathrm{PGA}) = 0.15 \pm 0.02$ mM and $K_m(2\mathrm{PGA}) = 0.16 \pm 0.03$ mM.

Keq. The equilibrium constants, K_{eq}, can be calculated from the Gibbs free energy of a reaction, ΔG_r, using equation 5:

$$K_{eq} = exp(\frac{-\Delta G_r^{o'}}{RT}) \quad (5)$$

$\Delta G_r^{o'}$ is expressed in J/mol and can be positive, negative or null. Therefore, we assumed that our uncertainty about the exact value of $\Delta G_r^{o'}$ can be described by a normal distribution. As a consequence, according to equation 5, the plausible values of the equilibrium constant will be log-normally distributed.

As the equilibrium constant does not depend on the organism (assuming constant temperature, pH and ionic strength), the mean and standard-deviation of the distribution can be calculated from the various values reported in the literature (see supplementary text S3). When only one published value could be found, the standard deviation was calculated using the mean relative standard deviation of the other equilibrium constants in the model as described above.

Vmax. The maximum rate of the reactions (V_{max}) can only have positive values. The V_{max} values are linked to the equilibrium constant and K_m values by the Haldane equation. Therefore, we assume again that our uncertainty about them can best be described by a log-normal distribution.

For each V_{max}, the mean and standard deviation of the log-normal distribution must be defined (respectively *lmean* and *lsd*). When the V_{max} had been measured, the *lmean* and *lsd* were calculated the same way as for the K_m values. When no information was available, the *lmean* was set using the value fitted by Alberts et al. [10] for the fixed-parameter model. In these cases, the *lsd* was then set so that the upper limit of the confidence interval (95%) is 4000 nmol/min/mg protein (the largest V_{max} in the model is 2862 nmol/min/mg protein for phosphoglycerate kinase [10]).

If the V_{max} was measured in the reverse direction (V^r_{max}), V^r_{max} is sampled. V_{max} is then calculated from the sampled V^r_{max}, K_{eq} and K_m values using the Haldane equation. The value used for phosphoglycerate kinase is calculated from the measured V^r_{max}. However, as two of the K_m values were not measured and therefore have large standard deviations, sampling this V_{max} from the V^r_{max}, K_m and K_{eq} would result in sampling values much larger than 4000 nmol/min/mg of proteins. Therefore, the phosphoglycerate kinase V_{max} was sampled using the calculated value as a mean, and the standard deviation was calculated so that the upper limit of the confidence interval (95%) is 4000 nmol/min/mg protein.

The V_{max} of GAPDH reported in the literature [10] was measured in crude extracts where a non-identified metabolite seems to inhibit it [25]. The inhibition factor (F) was estimated by Misset et al. [25] as about three-fold and was sampled separately in our study. As F needs to be higher than 1, it was sampled using a log-normal distribution (with $mean = 2$ and sd calculated so that the upper limit of the confidence interval (95%) is 3.5) to which 1 is added. The V_{max} of GAPDH in the model is then multiplied by this sampled inhibition factor.

The glucose transporter V_{max} was set according to the measurements of Seyfang et al. [34]. Using the V_{max} at 37°C and the activation energy they measured, we estimated the V_{max} of glucose transporter at 25°C to 111.7 ± 19.1 nmol/min/mg of protein. Note that this value is close to the fitted value used in [10] (108.9 nmol/min/mg of protein).

Transport reactions. The model includes several transport reactions. Among them, only the transport rates across the cytosolic membrane have been measured. The transport rates across the glycosomal membrane have not been characterised and are currently modelled using mass action kinetics (i.e., as non-saturable, non-enzymatic reactions) to maintain maximal compatibility with the published model [10,11]. The corresponding parameters have not been measured. The equilibrium constant of these transport reactions is assumed to be 1, so that only one kinetic parameter is required per transport reaction.

No information is available about the uncertainty of these parameters. As these parameters are strictly positive, they are sampled using a log-normal distribution as are K_m and V_{max} values. The means are set to the minimum value so that the reaction will be within 5% of equilibrium (using the mean values for all the other parameters). The standard deviation is calculated so that the upper limit of the confidence interval (95%) is equal to 100 times the mean to allow a large exploration of the parameter space.

Specific cases. Bakker et al. [7] and the following versions of the model included adenylate kinase implicitly, considering this reaction to be at equilibrium. We modelled adenylate kinase using mass action kinetics, with two rate constants k_1 and k_2. As only the equilibrium constant of this reaction is known, k_2 is sampled using the same methods as for the parameters of the transport reactions. k_1 is then calculated from k_2 and the sampled equilibrium constant: $k_1 = K_{eq} * k_2$.

ATP utilization is modelled using mass action kinetics with a single rate constant. As this reaction represents all of the cytosolic reactions that consume ATP and are not explicitly included in the model, the rate constant of this reaction is unknown. As for glycosomal transport reactions, this parameter was sampled according to a log-normal distribution. The mean used is the value fitted by Bakker et al. [7]. The standard deviation is calculated so that the upper limit of the 95% confidence interval equals 2 times the mean.

The glucose transport across the cytosolic membrane is assumed to be symmetric [7] based on experimental evidence [35]. Moreover, it exhibits a trans-acceleration phenomenon [36] which is quantify by a parameter, α in the underlying model of the transporter kinetics. As this parameter varies between 0 and 1, it was sampled using a logit-normal distribution. The estimated value from Bakker et al. [7] was used as a mean. The standard deviation was arbitrarily set so that the upper limit of the 95% confidence interval is the mean +20%.

Parameter sampling

All parameters were sampled using the MT19937 random number generator of Makoto Matsumoto and Takuji Nishimura [37] implemented in the GNU Scientific Library (GSL) [38]. The random numbers where then transformed to follow their assumed

probability distribution using the random number distribution function implemented in the GSL library.

Steady-state calculations

The steady states were calculated using the SOSlib library [39]. Steady-state is considered if the mean+standard deviation of the rates of change of all metabolite concentrations is lower than a user-defined parameter *ssThreshold* of SOSlib. The initial conditions were set using the steady-state concentrations calculated using the mean values of all parameters. For any sampled model, it is assumed that steady state should be reached within 300 minutes of simulated time (steady state detection threshold $ssThreshold = 0.01$, parameter $PrintStep = 1$ per simulated minute). We checked that the steady-state calculations give similar results in COPASI [40] and PySCeS [41] using their default parameters. We also verified that the parameter sets that do not allow the model to reach steady state in these conditions show accumulation of individual metabolites beyond reasonable concentrations (hundreds or thousands of millimol per liter, see Results and Fig. 3).

Control coefficients

The control coefficients were computed using the methodology described by Bakker et al. [8]. The computation of control coefficients requires more precise steady-states calculations. Therefore, the parameters of SOSlib were set to: maximal time $Time = 100000$ minutes and the threshold $ssThreshold = 10^{-6}$.

Supporting Information

Dataset S1 Fixed-parameter model (sbml file).
(XML)

Figure S1 Examples of simulations of models unable to reach steady-state (within 1000 simulated minutes). (A) Simulation of pyruvate concentration in a model unable to reach steady-state because of pyruvate accumulation. Models of this type will never reach steady-state. (B) Simulation of glycosomal 3-PGA concentration in a model unable to reach steady-state because of 3-PGA accumulation. Models of this type will eventually reach steady-state, but at extremely high concentrations of 3-PGA.
(TIFF)

Text S1 Distributions of the sampled parameters.
(PDF)

Text S2 Distributions of the steady-state concentrations of the metabolites in mmol/l.
(PDF)

Text S3 Sources used for the calculation of the equilibrium constants mean and standard deviations.
(PDF)

Acknowledgments

The authors would like to thank Rainer Machné for his help with SOSLib.

The members of the SysMO2-funded SilicoTryp Consortium are: Rainer Breitling, Michael P. Barrett, Barbara M. Bakker, Keith Matthews, Christine Clayton, Luise Krauth-Siegel, Mark Girolami, Fiona Achcar, Eduard J. Kerkhoven, Dong-Hyun Kim, Jurgen R. Haanstra, Federico Rojas, Abeer Fadda, and Alejandro Leroux.

Author Contributions

Conceived and designed the experiments: FA RB. Performed the experiments: FA. Analyzed the data: FA EJK BMB MPB RB. Contributed reagents/materials/analysis tools: FA RB. Wrote the paper: FA EJK BMB MPB RB.

References

1. Borger S, Liebermeister W, Klipp E (2006) Prediction of enzyme kinetic parameters based on statistical learning. Genome Inform Ser 17: 80–87.
2. Wang L, Birol I, Hatzimanikatis V (2004) Metabolic control analysis under uncertainty: Framework development and case studies. Biophys J 87: 3750–3763.
3. Tran LM, Rizk ML, Liao JC (2008) Ensemble modeling of metabolic networks. Biophys J 95: 5606–5617.
4. Rizk ML, Liao JC (2009) Ensemble modeling and related mathematical modeling of metabolic networks. J Taiwan Inst Chem E 40: 595–601.
5. Mišković L, Hatzimanikatis V (2011) Modeling of uncertainties in biochemical reactions. Biotechnol Bioeng 108: 413–423.
6. Murabito E, Smallbone K, Swinton J, Westerhoff HV, Steuer R (2011) A probabilistic approach to identify putative drug targets in biochemical networks. J Roy Soc Interface 8: 880–895.
7. Bakker BM, Michels PA, Opperdoes FR, Westerhoff HV (1997) Glycolysis in bloodstream form *Trypanosoma brucei* can be understood in terms of the kinetics of the glycolytic enzymes. J Biol Chem 272: 3207–3215.
8. Bakker BM, Michels PAM, Opperdoes FR, Westerhoff HV (1999) What controls glycolysis in bloodstream form *Trypanosoma brucei*? J Biol Chem 274: 14551–14559.
9. Helfert S, Estévez AM, Bakker B, Michels P, Clayton C (2001) Roles of triosephosphate isomerase and aerobic metabolism in Trypanosoma brucei. Biochem J 357: 117–125.
10. Albert M, Haanstra JR, Hannaert V, Van Roy J, Opperdoes FR, et al. (2005) Experimental and in silico analyses of glycolytic ux control in bloodstream form Trypanosoma brucei. J Biol Chem 280: 28306–28315.
11. Haanstra JR, van Tuijl A, Kessler P, Reijnders W, Michels PAM, et al. (2008) Compartmentation prevents a lethal turbo-explosion of glycolysis in trypanosomes. Proc Natl Acad Sci USA 105: 17718–17723.
12. Ryley JF (1956) Studies on the metabolism of the protozoa. 7. comparative carbohydrate metabolism of eleven species of trypanosome. Biochem J 62: 215–222.
13. Hammond DJ, Bowman IB (1980) *Trypanosoma brucei*: the effect of glycerol on the anaerobic metabolism of glucose. Mol Biochem Parasit 2: 63–75.
14. Haanstra J (2009) The power of network-based drug design and the interplay between metabolism and gene expression in *Trypanosoma brucei*. Ph.D. thesis, Vrije Universiteit Amsterdam.
15. Eisenthal R, Panes A (1985) The aerobic/anaerobic transition of glucose metabolism in *Try-panosoma brucei*. FEBS Lett 181: 23–27.
16. Wiemer EA, Michels PA, Opperdoes FR (1995) The inhibition of pyruvate transport across the plasma membrane of the bloodstream form of *Trypanosoma brucei* and its metabolic implications. Biochem J 312(Pt 2): 479–484.
17. Vanderheyden N, Wong J, Docampo R (2000) A pyruvate-proton symport and an H+-ATPase regulate the intracellular pH of *Trypanosoma brucei* at different stages of its life cycle. Biochem J 346 Pt 1: 53–62.
18. Spitznagel D, Ebikeme C, Biran M, Nic a' Bháird N, Bringaud F, et al. (2009) Alanine aminotransferase of *Trypanosoma brucei*–a key role in proline metabolism in procyclic life forms. FEBS J 276: 7187–7199.
19. Newport GR, Page CR, III, Ashman PU, Stibbs HH, Seed JR (1977) Alteration of free serum amino acids in voles infected with trypanosoma brucei gambiense. J Parasitol 63: 15–24.
20. Mackenzie NE, Hall JE, Seed JR, Scott AI (1982) Carbon-13 Nuclear-Magnetic-Resonance studies of glucose catabolism by trypanosoma brucei gambiense. Eur J Biochem 121: 657–661.
21. Grant PT, Fulton JD (1957) The catabolism of glucose by strains of trypanosoma rhodesiense. Biochem J 66: 242–250.
22. Kacser H, Burns JA (1973) The control of ux. Sym Soc Exp Biol 27: 65–104.
23. Bakker BM, Walsh MC, ter Kuile BH, Mensonides FI, Michels PA, et al. (1999) Contribution of glucose transport to the control of the glycolytic ux in *Trypanosoma brucei*. Proc Natl Acad Sci USA 96: 10098–10103.
24. Bakker BM, Michels PAM, Westerhoff HV (1996) Control of the glycolytic flux in *Trypanosoma brucei*: why control can shift suddenly. In: Snoep JL, Westerhoff HV, Sluse FE, Wijker JE, Kholodenko BN, eds. Biothermokinetics of the living cell. Amsterdam: Biothermokinetics Press. pp 136–142. Available: http://dare.uva.nl/record/16345.
25. Misset O, Bos OJ, Opperdoes FR (1986) Glycolytic enzymes of *Trypanosoma brucei*. Eur J Biochem 157: 441–453.
26. Cáceres AJ, Michels PA, Hannaert V (2010) Genetic validation of aldolase and glyceraldehyde-3-phosphate dehydrogenase as drug targets in *Trypanosoma brucei*. Mol Biochem Parasit 169: 50–54.
27. Chevalier N, Rigden DJ, Van Roy J, Opperdoes FR, Michels PA (2000) *Trypanosoma brucei* contains a 2,3-bisphosphoglycerate independent phosphoglycerate mutase. Eur J Biochem 267: 1464–1472.
28. Aronov AM, Suresh S, Buckner FS, Van Voorhis WC, Verlinde CL, et al. (1999) Structure-based design of submicromolar, biologically active inhibitors of trypanosomatid glyceraldehyde-3-phosphate dehydrogenase. Proc Natl Acad Sci USA 96: 4273–4278.

29. Xu T, Vyshemirsky V, Gormand A, von Kriegsheim A, Girolami M, et al. (2010) Inferring signaling pathway topologies from multiple perturbation measurements of specific biochemical species. Sci Signal 3: ra20.
30. Haldane JBS (1930) Enzymes. Longmans, Green.
31. Cornish-Bowden A, Hunter PJ, Cuellar AA, Mjolsness ED, Juty NS, et al. (2003) The systems biology markup language (SBML): a medium for representation and exchange of biochemical network models. Bioinformatics 19: 524–531.
32. Scheer M, Grote A, Chang A, Schomburg I, Munaretto C, et al. (2011) BRENDA, the enzyme information system in 2011. Nucleic Acids Res 39: D670–676.
33. Fuad FAA, Fothergill-Gilmore LA, Nowicki MW, Eades LJ, Morgan HP, et al. (2011) Phosphoglycerate mutase from trypanosoma brucei is hyperactivated by cobalt in vitro, but not in vivo. Metallomics 3: 1310–1317.
34. Seyfang A, Duszenko M (1991) Specificity of glucose transport in *Trypanosoma brucei*. Eur J Biochem 202: 191–196.
35. Eisenthal R, Game S, Holman GD (1989) Specificity and kinetics of hexose transport in *Try-panosoma brucei*. Biochim Biophys Acta 985: 81–89.
36. Stein WD, Lieb WR (1986) Transport and diffusion across cell membranes Academic Press.
37. Matsumoto M, Nishimura T (1998) Mersenne Twister: A 623-dimensionally equidistributed uniform pseudorandom number generator. ACM T Model Comput S 8: 3–30.
38. Galassi M, Davies J, Theiler J, Gough B, Jungman G, et al. (2009) GNU scientific library reference manual: (v. 1.12). Bristol, UK: Network Theory Ltd.
39. Machné R, Finney A, Müller S, Lu J, Widder S, et al. (2006) The SBML ODE solver library: a native API for symbolic and fast numerical analysis of reaction networks. Bioinformatics 22: 1406–1407.
40. Hoops S, Sahle S, Gauges R, Lee C, Pahle J, et al. (2006) COPASI–a COmplex PAthway SImulator. Bioinformatics 22: 3067–3074.
41. Olivier BG, Rohwer JM, Hofmeyr JS (2005) Modelling cellular systems with PySCeS. Bioinformatics 21: 560–561.

Molecular Microbiology (2011) 79(1), 94–108 ■
doi:10.1111/j.1365-2958.2010.07435.x
First published online 5 November 2010

A domino effect in drug action: from metabolic assault towards parasite differentiation

Jurgen R. Haanstra,[1†‡] Eduard J. Kerkhoven,[2†] Arjen van Tuijl,[1] Marjolein Blits,[1] Martin Wurst,[3] Rick van Nuland,[1§] Marie-Astrid Albert,[4] Paul A. M. Michels,[4] Jildau Bouwman,[1] Christine Clayton,[3] Hans V. Westerhoff[1,5] and Barbara M. Bakker[1,6*]

[1]*Department of Molecular Cell Physiology, Faculty of Earth and Life Sciences, Vrije Universiteit Amsterdam, De Boelelaan 1085, NL-1081 HV Amsterdam, the Netherlands.*
[2]*Institute of Biomedical and Life Sciences, Division of Infection and Immunity, University of Glasgow, Glasgow, UK.*
[3]*Zentrum für Molekulare Biologie, Universität Heidelberg, Heidelberg, Germany.*
[4]*Research Unit for Tropical Diseases, de Duve Institute and Laboratory of Biochemistry, Université catholique de Louvain, Brussels, Belgium.*
[5]*AstraZeneca Chair for Systems Biology, Manchester Centre for Integrative Systems Biology, Manchester, UK.*
[6]*Department of Pediatrics, Centre for Liver, Digestive and Metabolic Diseases University Medical Centre Groningen, University Groningen Hanzeplein 1, NL-9713 GZ Groningen, the Netherlands.*

Summary

Awareness is growing that drug target validation should involve systems analysis of cellular networks. There is less appreciation, though, that the composition of networks may change in response to drugs. If the response is homeostatic (e.g. through upregulation of the target protein), this may neutralize the inhibitory effect. In this scenario the effect on cell growth and survival would be less than anticipated based on affinity of the drug for its target. Glycolysis is the sole free-energy source for the deadly parasite *Trypanosoma brucei* and is therefore a possible target pathway for anti-trypanosomal drugs. Plasma-membrane glucose transport exerts high control over trypanosome glycolysis and hence the transporter is a promising drug target. Here we show that at high inhibitor concentrations, inhibition of trypanosome glucose transport causes cell death. Most interestingly, sublethal concentrations initiate a domino effect in which network adaptations enhance inhibition. This happens via (i) metabolic control exerted by the target protein, (ii) decreases in mRNAs encoding the target protein and other proteins in the same pathway, and (iii) partial differentiation of the cells leading to (low) expression of immunogenic insect-stage coat proteins. We discuss how these 'anti-homeostatic' responses together may facilitate killing of parasites at an acceptable drug dosage.

Accepted 7 October, 2010. *For correspondence. E-mail: B.M. Bakker@med.umcg.nl; Tel. (+31) 503611542; Fax (+31) 503611746. †These authors contributed equally. ‡Present address: Department of Hematology, ErasmusMC, Rotterdam, the Netherlands. §Present address: Department of Physiological Chemistry, UMCU, Utrecht, the Netherlands.

Introduction

Living organisms combat external perturbations through homeostatic response mechanisms. For example, if a substrate becomes limiting, the transporter that takes it up might be upregulated, through either increased expression or post-translational mechanisms. Similarly, during treatment with a drug that inhibits an enzyme, the enzyme activity might be increased, neutralizing drug action.

Much current research is devoted to validation of new molecular targets for antimicrobial drugs. The major criteria for such targets include (i) that they should be essential for microbial growth or survival and (ii) that there should be a sufficient difference between the host and the pathogen to allow specific inhibition of the pathogen target. Since a large proportion of microbial proteins may fulfil both conditions, it is useful also to add additional criteria. For example, high concentrations of an enzyme substrate will out-compete substrate analogues; and if the target is present in huge excess, then very high levels of inhibition will be required to kill the pathogen. Either of these situations would hinder development of a specific inhibitor that can be given at acceptable doses. The ability of the microbial system to homeostatically adapt to inhibition adds an additional complication.

To deal with these issues, it is useful to apply a systems biology approach, including metabolic modelling, when choosing potential targets for antimicrobial drugs. Because adaptation may involve various aspects of regulation,

target validation ideally should integrate not only metabolic, but also signalling and gene-expression networks (Alberghina and Westerhoff, 2005). So far, however, of the few successful network-based drug design studies that exist (Noble, 2006), none addresses the potential adaptation of the network.

Trypanosoma brucei causes deadly African sleeping sickness in humans, and the related disease 'Nagana' in cattle. As currently available drugs are inadequate and toxic while drug resistance is increasing rapidly, new and more selective medication is needed (Barrett *et al*., 2003).

T. brucei is transmitted by tse-tse flies. After growing to a certain density in the mammalian bloodstream, the proliferating 'long-slender' bloodstream forms differentiate into non-dividing 'short-stumpy' trypanosomes. The short-stumpy trypanosomes differentiate further into the 'procyclic' (insect-form) cells in the midgut of the tse-tse fly after the latter has taken a blood meal (Matthews, 2005). The most prominent differences between the life-cycle stages inside the mammalian host and inside the insect vector are at the level of metabolism and surface-protein expression. The long-slender bloodstream-form trypanosome relies merely on the glycolytic pathway with pyruvate as the main end-product. Metabolism in procyclic trypanosomes is more complex: they can utilize more substrates and, in contrast to bloodstream form cells, they use extensive mitochondrial metabolism (Hellemond *et al*., 2005). The bloodstream-form cells are shielded from the mammalian immune system by a dense layer of variant surface glycoproteins (VSG) (Cross, 1975; Borst and Ulbert, 2001). Upon ingestion by the tse-tse fly, or transfer to procyclic culture conditions, the VSG coat is shed and replaced by a coat of EP and GPEET proteins of the procyclin family (Vassella *et al*., 2001; Urwyler *et al*., 2005; Gruszynski *et al*., 2006). The short-stumpy cells undergo some minor metabolic changes in the direction of procyclic forms. Both stumpy forms and non-dividing trypanosomes in the early stages of differentiation *in vitro* express lower levels of many mRNAs required for growth, and show upregulation of plasma-membrane tricarboxylic acid transporters that are involved in sensing the differentiation signal (Dean *et al*., 2009; Jensen *et al*., 2009; Kabani *et al*., 2009; Queiroz *et al*., 2009). Bloodstream-form trypanosomes that have been cultured continuously are called 'monomorphic' because they have lost the ability to develop into stumpy forms; in some cases they are no longer able to differentiate into growing procyclic forms (Fenn and Matthews, 2007).

The reliance of bloodstream-form *T. brucei* on glycolysis suggests that this pathway could be an excellent drug target, should selective inhibition be possible (Verlinde *et al*., 2001). Previously, we combined Metabolic Control Analysis (Kacser and Burns, 1973; Heinrich and Rapoport, 1974; Groen *et al*., 1982), a theoretical framework to analyse the relative importance of each protein for cellular fluxes, with computer modelling and experimentation (Bakker *et al*., 1999a,b; Albert *et al*., 2005; Caceres *et al*., 2010) to study which enzyme(s) control(s) glycolytic flux in trypanosomes. We demonstrated that glucose transport across the plasma membrane is the dominant factor controlling the free-energy metabolism (the ATP synthesis flux) of African trypanosomes. The amino acid sequence of the trypanosome glucose transporter (THT1) is only ~19% identical and 42% similar to that of the human erythrocyte glucose transporter GLUT1 (Bringaud and Baltz, 1992): thus it may be possible to find a highly specific inhibitor of THT1, and to capitalize on the unique dependence of the parasites upon its transport activity. This made the glucose transporter a promising candidate drug target. However, the possibility of homeostatic adaptation via gene expression had not been addressed.

Trypanosomes do not regulate transcription of individual genes by RNA polymerase II, since transcription is polycistronic. Yet they do regulate mRNA processing, mRNA degradation and translation (Clayton and Shapira, 2007; Haile and Papadopoulou, 2007). Gene-expression changes in trypanosomes have almost exclusively been studied in the context of differentiation. There have, however, been a few studies investigating the responses to glucose availability. In bloodstream-form trypanosomes, glucose deprivation induced the expression of procyclic surface-coat proteins (Milne *et al*., 1998). And in procyclic forms, which can obtain energy either from glucose or from proline, inhibition of the glucose transporter by *N*-acetyl D-glucosamine caused a shift towards proline-dependent metabolism (Ebikeme *et al*., 2008). In procyclic forms, also, RNAi targeting of either the glucose transporter or hexokinase caused a switch from one procyclic-specific surface protein to another (Morris *et al*., 2002).

In the present study we aim to quantitatively link the metabolic response of trypanosomes to glucose transport inhibition with adaptations in gene expression, growth and differentiation. We show that while high concentrations of glucose transport inhibitors kill trypanosomes, sublethal concentrations evoke a multilayered adaptation of the network. Unexpectedly, this adaptation is not homeostatic: instead, it potentiates the effect of the primary inhibition. This anti-homeostatic response enhances the status of the trypanosome glucose transporter as a potential drug target.

Results

Chemical inhibition of glucose transport leads to a decrease of glycolytic flux and growth rate of trypanosomes

To study the effects of glucose-transport inhibition beyond metabolism, we inhibited glucose transport with either

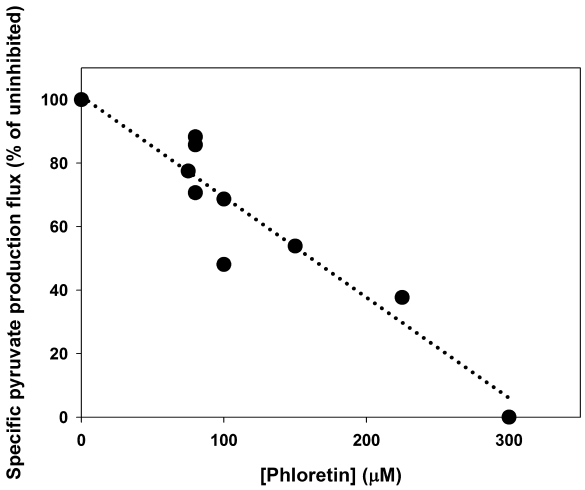

Fig. 1. Glycolytic flux upon inhibition by phloretin. Glycolytic flux (measured as the specific pyruvate production flux) in bloodstream-form trypanosomes after 24 h exposure to various phloretin concentrations. Each point in the graph is based on an independent culture and its control. The uninhibited pyruvate flux, i.e. in the absence of phloretin, was 373 ± 57.1 nmol min^{-1} (10^8 cells)$^{-1}$ (SEM, $n = 5$). At the beginning of each experiment we split cultures into one that remained untreated and was used as control, and another that was treated with the indicated concentration of phloretin. The measured flux in the untreated control culture was used as the 100% reference, to correct for variations between experiments. The dotted line is a linear fit to the data ($R^2 = 0.92$).

phloretin (Bakker *et al.*, 1999b) or 2-deoxy-D-glucose (2-DOG) (Tetaud *et al.*, 1997), two chemically unrelated inhibitors. Phloretin is a general inhibitor of facilitated diffusion transporters and has been shown to be a competitive inhibitor of the trypanosome glucose transporter (Bakker *et al.*, 1999b). 2-DOG is a glucose analogue that cannot be metabolized beyond phosphorylation by hexokinase. 2-DOG therefore acts as a competitive inhibitor of glucose transport, and – depending on its intracellular concentration – also of hexokinase (HXK). As far as side-effects are known, they are quite different for the two compounds. Phloretin remains outside cells, but may hit other transporters (Krupka and Deves, 1980) while intracellular 2-DOG affects HXK. Effects that are seen for both inhibitors are therefore likely to be due to the inhibition of glucose transport specifically. The inhibitors have the advantage that they act very rapidly on the transporter; in contrast to RNAi, their use allows assessment of changes of the transporter itself. All of our studies were conducted with a monomorphic trypanosome line 449 derived from strain Lister 427. These trypanosomes were chosen because their glycolytic metabolism has been exhaustively characterized; they are however unable to undergo complete differentiation to procyclic forms.

Phloretin reduced the glycolytic flux, measured as the pyruvate production flux (Fig. 1), and the specific growth rate (Fig. 2A) of bloodstream-form trypanosomes. 2-DOG gave similar results (Fig. 2B). At all inhibitor concentrations we found production of only small amounts of glycerol and neither succinate nor acetate. Above 100 μM phloretin the cells started dying within the first 24 h, although the glycolytic flux was only inhibited by 50% (Fig. 1). The latter result is not specific for inhibition of glucose transport, but was also previously found for various glycolytic enzymes. A compilation of results obtained with RNAi of various glycolytic targets and those of the phloretin and 2-DOG experiments shows that a partial (30–50%) inhibition of the glycolytic flux sufficed to block growth (Fig. 3). A further inhibition of the pathway

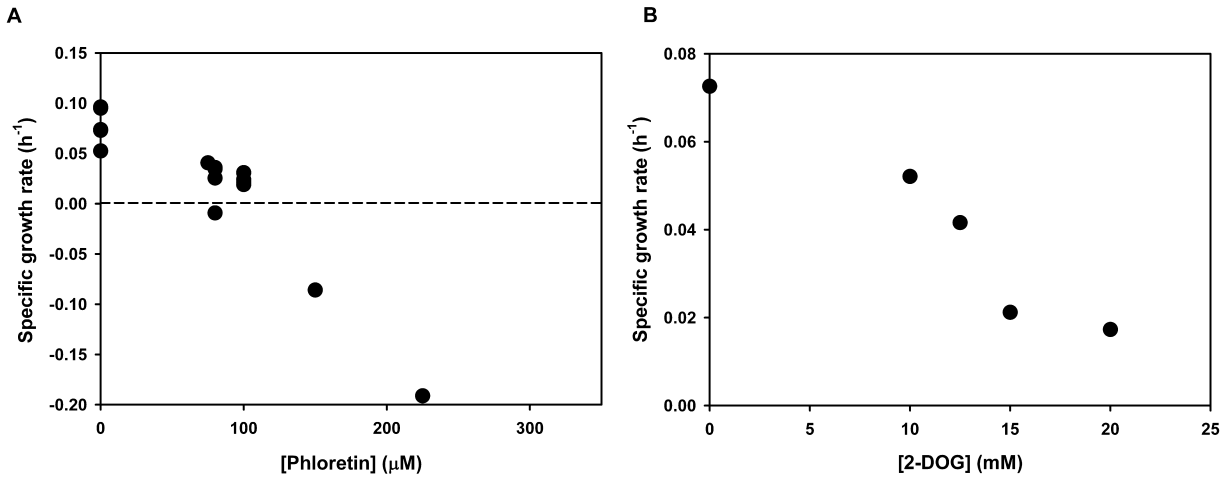

Fig. 2. Effect of inhibition of glucose transport on the specific growth rate of trypanosomes. Specific growth rate (μ, see *Experimental procedures*) as determined in the first 24 h after inhibition by various concentrations of phloretin (A) or 2-DOG (B). The negative growth rates should be interpreted as death rates. Further experiments were all performed at 100 μM phloretin or 12.5 mM 2-DOG, doses at which the cells remain alive but hardly grow. Each point in the graph is based on an independent culture.

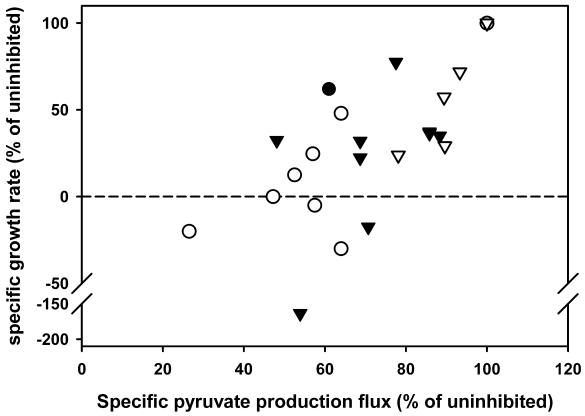

Fig. 3. Relation between growth rate and glycolytic flux in trypanosomes with impaired activities of glycolytic enzymes or glucose transport. Specific growth rates plotted against specific pyruvate production flux (= glycolytic flux) after 24 h inhibition with various concentrations of phloretin (▼) or 2-DOG (▽) (this article), RNAi against several glycolytic enzymes (○) (Albert *et al.*, 2005; Caceres *et al.*, 2010) and a knockout of the alternative oxidase (●) (Helfert *et al.*, 2001). Percentages were calculated relative to control cultures in the same experiment. For phloretin, data of Figs 1 and 2A were combined. Each point in the graph shows an independent experiment.

caused cell death. Unlike phloretin, 2-DOG was only tested at sublethal concentrations. Over the tested concentration range the relation between specific growth rate and pyruvate production flux was similar for the two inhibitors (open and closed triangles in Fig. 3). Growth inhibition by phloretin was reversible during the first 24 h (Fig. S1).

Inhibition by phloretin or 2-DOG evokes a gene-expression response in bloodstream-form T. brucei

We next studied mRNA levels in cells treated with sublethal concentrations of phloretin and 2-DOG, concentrating on the glycolytic enzymes. Strikingly, the *THT1* mRNA, encoding the major glucose transporter in the bloodstream form, was *down*- rather than *up*regulated after inhibition of glucose transport (Fig. 4A). Hence, the parasites adapted, not homeostatically, but in a way that aggravated their situation.

Further analysis of glycolytic gene expression revealed a general downregulation of mRNAs encoding glycolytic enzymes that are normally expressed in bloodstream-form trypanosomes [see, e.g. pyruvate kinase (*PYK*) in Fig. 4A and the complete data set in Fig. 4B]. Procyclic cells have been demonstrated to express the majority of these enzymes at a lower protein level than bloodstream-form cells (Hart *et al.*, 1984; Aman and Wang, 1986). Furthermore, typical procyclic isoforms of the glucose transporter (*THT2*) and of phosphoglycerate kinase (*PGKB*) were upregulated to the detriment of their bloodstream-form counterparts *THT1* and *PGKC* respectively. The expression of *PGKB* was surprising, since this isoform has a subcellular localization different from that of *PGKC* and its expression is normally toxic in bloodstream-form trypanosomes (Blattner *et al.*, 1998). It is unlikely that the increased mRNA levels of *THT2* can compensate for the decreased expression of *THT1*: the absolute change is much larger for *THT1* since its initial level was 40 times higher than that of *THT2* (Bringaud and Baltz, 1993). Moreover, growth of procyclic trypanosomes was inhibited by phloretin (data not shown), suggesting that also the procyclic glucose transporter THT2 is sensitive to this inhibitor. However, this last finding may also be attributed to an unknown side-effect on other targets or to catabolite repression of proline metabolism [as was suggested previously (Lamour *et al.*, 2005)].

Finally we also observed increased mRNA levels for the genes encoding the Krebs' cycle enzyme citrate synthase (CS), as well as pyruvate orthophosphate dikinase (PPDK) and proline dehydrogenase (PRODH). These enzyme activities are absent in bloodstream-form trypanosomes (Jenkins *et al.*, 1988; Priest and Hajduk, 1994; Bringaud *et al.*, 1998). To test whether the mRNA changes were reflected by changes at the level of functional proteins, we measured CS activity. This was low in untreated bloodstream forms, but rose 3.5-fold after 48 h inhibition of glucose transport, to a level that was even higher than that of procyclic trypanosomes (Fig. 4C).

Phloretin treatment causes transcriptome changes indicative of partial differentiation

To characterize the effects of phloretin treatment on the entire transcriptome, we treated exponentially growing bloodstream-form trypanosomes for 24 h with 100 μM phloretin, then extracted RNA. RNA from untreated trypanosomes served as a control. Fluorescently labelled cDNAs were hybridized to *T. brucei* oligonucleotide microarrays (see *Experimental procedures*). We found that 54 RNAs were significantly increased at $P < 0.05$, 45 of these being altered by 1.5-fold or more. A total of 276 RNAs were significantly decreased after the treatment, 153 of them at least 1.5-fold (see Table S1). For mRNAs that were analysed with both techniques, the microarray results corresponded qualitatively with those of the qPCR analysis, although, as expected, the latter tended to yield somewhat larger changes in expression (Table S1).

We have previously shown that during differentiation of *in vitro* cultured pleomorphic trypanosomes, 1113 mRNAs showed significant changes in abundance, with detailed time-courses that could be classified according to 62 groups with different patterns of regulation. (Queiroz *et al.*, 2009). The 62 patterns fell into four broad categories: highest expression in bloodstream forms; highest

A

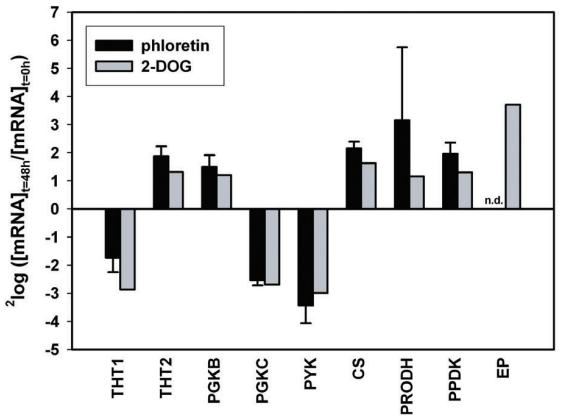

B

	Phloretin						2-DOG	
	24			48			24	48
	average	SEM	sig	average	SEM	sig		
THT1	0.25	0.10	*	0.34	0.11	*	0.84	0.14
THT2	1.22	0.42		3.89	0.90		2.27	2.48
HXK	0.35	0.12	*	0.38	0.10	*	0.91	0.27
PGI	0.32	0.07	*	0.37	0.06	*	0.50	0.23
PFK	0.29	0.11	*	0.19	0.07	*	0.81	0.22
ALD	0.35	0.14	*	0.25	0.11	*	0.28	0.28
TIM	0.34	0.15	*	0.40	0.12	*	0.64	0.64
G3PDH	0.24	0.08	*	0.26	0.07	*	0.75	0.26
GK	0.32	0.11	*	0.41	0.11	*	1.14	0.43
AOX	0.56	0.20		0.73	0.30		1.32	0.85
GAPDH	0.26	0.12	*	0.17	0.06	*	0.46	0.13
PGKB	1.34	0.47		3.05	0.77		2.26	2.30
PGKC	0.27	0.11	*	0.17	0.02	*	0.57	0.16
PGAM	0.77	0.26		1.26	0.31		1.92	1.57
ENO	0.31	0.11	*	0.35	0.11	*	0.44	0.40
PYK	0.17	0.07	*	0.11	0.04	*	0.30	0.13
CS	2.82	1.17		4.59	0.70		4.08	3.08
PRODH	13.11	10.46		17.11	20.68		2.91	2.23
PPDK	2.48	1.08		4.18	1.05		2.97	2.46
EP1	n.d.			n.d.			1.56	13.06

C

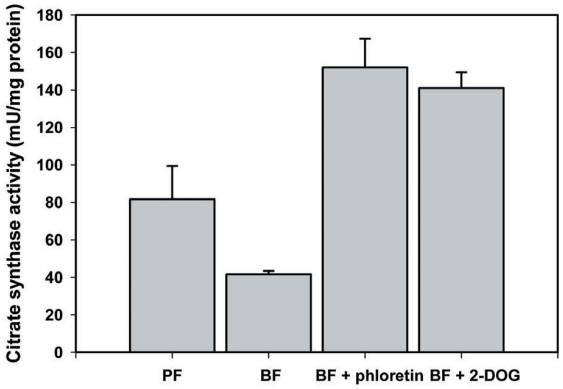

Fig. 4. Effect of phloretin and 2-DOG on gene expression

A. mRNA levels in bloodstream-form trypanosomes after 48 h inhibition by 100 μM phloretin or 12.5 mM 2-DOG as compared with expression before inhibition. For phloretin the error bars indicate the SEM of three independent experiments. For PRODH, the error was not SEM, but a standard deviation of two experiments. *EP* was only measured in the 2-DOG-treated cultures.

B. mRNA fold changes for cultures treated with 100 μM phloretin or 12.5 mM 2-DOG compared with uninhibited cultures after 24 or 48 h. Colour coding: green = twofold or more upregulated; red = twofold or more downregulated; yellow = less than twofold change. n.d., not determined. An asterisks in the column 'sig' (for significance) indicates a $P < 0.05$ in a one-sided Student's *t*-test comparing the measurements to a value of 1 (for no change in expression).

2-DOG, 2-deoxy-D-glucose; ALD, aldolase; AOX, alternative oxidase; CS, citrate synthase; ENO, enolase; EP, EP procyclin; HXK, hexokinase; G3PDH, glycerol-3-phosphate dehydrogenase; GAPDH, glyceraldehyde-3-phosphate dehydrogenase; PGAM, phosphoglycerate mutase; PGK, phosphoglycerate kinase; PFK, phosphofructokinase; PGI, phosphoglucose isomerase; PYK, pyruvate kinase; PPDK, pyruvate orthophosphate dikinase; PRODH, proline dehydrogenase; THT, trypanosome hexose transporter; TIM, triosephosphate isomerase.

C. Citrate synthase activity was measured in procyclic cultures (PF; $n = 2$), in ethanol-treated (control) bloodstream-form cultures (BF; $n = 4$) and in bloodstream forms exposed for 48 h to a (sublethal) dose of either 100 μM phloretin ($n = 2$) or 12.5 mM 2-DOG ($n = 4$).

expression in procyclic forms; and either increased, or decreased, expression during differentiation. The gene-expression patterns between 1 and 12 h after initiation of differentiation were indicative of growth arrest and partial induction of a stumpy-like phenotype, with surface-coat switching initiating at around 12 h (Queiroz *et al.*, 2009). We compared our microarray data after phloretin treatment with the previous differentiation data set (Fig. 5 and Tables S1 and S2). When we examined the 153 mRNAs that were at least 1.5-fold downregulated after phloretin treatment, we found that less than 10% were preferentially expressed in procyclic forms. In contrast, a quarter of them were preferentially expressed in bloodstream forms, and another quarter decreased in level during differentiation (Fig. 5A). The category preferentially expressed in bloodstream forms included, as expected, 20 proteins involved in glucose metabolism, including glycolytic and other glycosomal enzymes, and glycosome assembly proteins. The mRNAs that were decreased during differentiation, and also decreased after phloretin, included no fewer than 24 genes encoding components of the flagellum (Fig. 5B): flagellar biosynthesis halts in non-dividing cells.

The 45 mRNAs that increased at least 1.5 times after phloretin treatment fell into more groups, but RNAs that are preferentially expressed in procyclics, or are

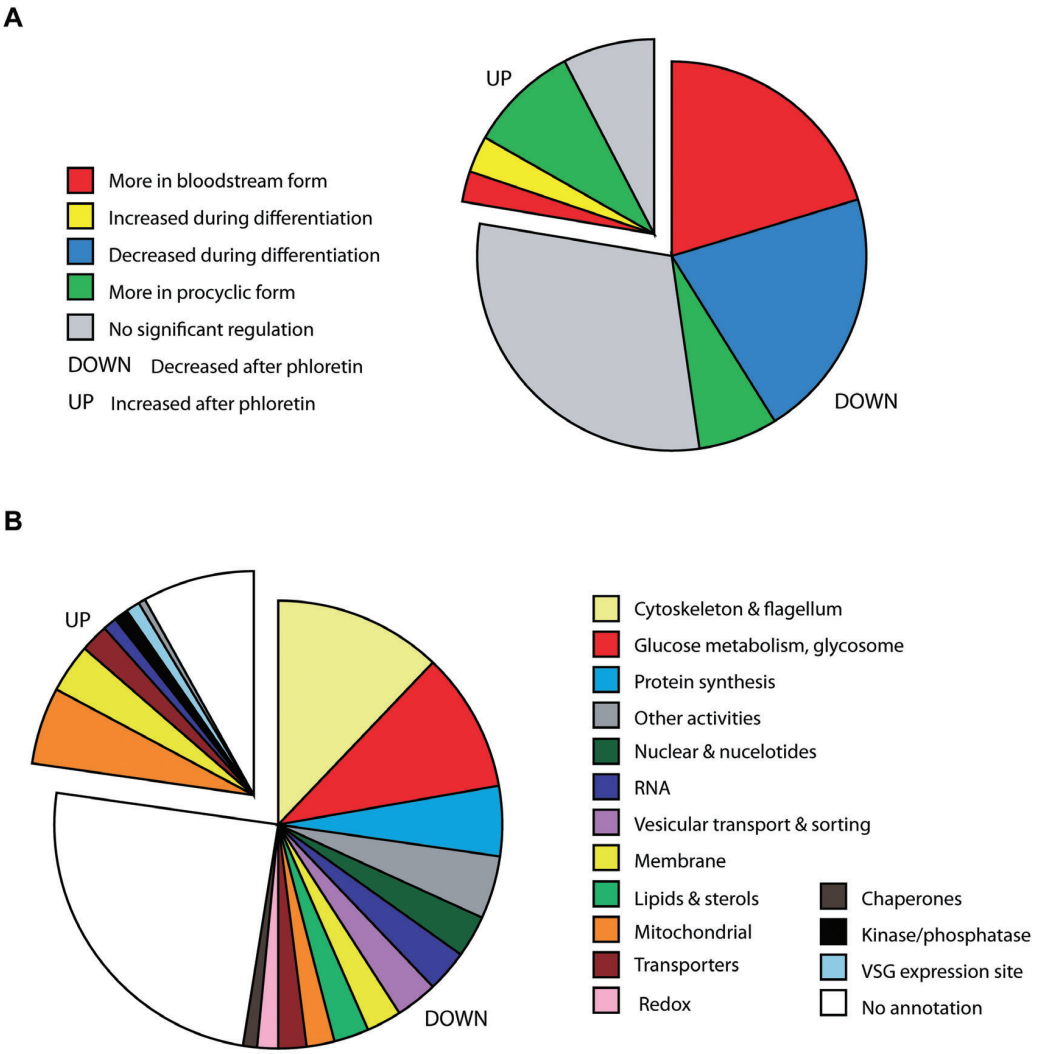

Fig. 5. Effects of phloretin treatment on the bloodstream-form transcriptome. Exponentially growing bloodstream-form trypanosomes (density 6×10^5 cells ml^{-1}) were treated with 100 μM phloretin for 24 h and subsequently their RNA was prepared for microarray analysis using untreated cells as a control, exactly as described in Queiroz *et al.* (2009). Results shown are for five slides including three biological replicates, with dye-swap, and include all spots showing significant $P < 0.05$ differences of at least 1.5-fold. The colour key is in the figure.
A. Regulated RNAs classified according to regulation during differentiation, as seen in Queiroz *et al.* (2009).
B. Regulated mRNAs classified according to the function of the encoded protein [automated and manual annotation, as in Queiroz *et al.* (2009)].

increased during differentiation, predominated (Fig. 5A). They included mitochondrial proteins and procyclic-specific membrane proteins (Fig. 5B). Notably, the upregulated mRNAs included those that encode two citrate/*cis*-aconitate transporters involved in differentiation, PAD1 and PAD2. PAD1 is a marker of growth-arrested stumpy forms (Dean *et al.*, 2009).

The overlap between the phloretin and differentiation data sets was only partial: just 124 RNAs were both affected by phloretin (at least 1.5-fold) and significantly regulated during differentiation. Using the phloretin data for just these 124 mRNAs, we calculated correlation coefficients with data from the different differentiation time points. The best correlation coefficients, i.e. 0.72 and 0.79, were for the 1 and 12 h time points respectively. These results indicated that our phloretin treatment had caused a subset of transcriptome changes similar to those seen during the early stages of differentiation to procyclic forms, when the parasites undergo growth arrest and initiate the switch from bloodstream-form to procyclic-form gene expression.

We also compared the phloretin microarray results with a data set generated using a tiling array (Fig. S2). The populations tested included stumpy trypanosomes

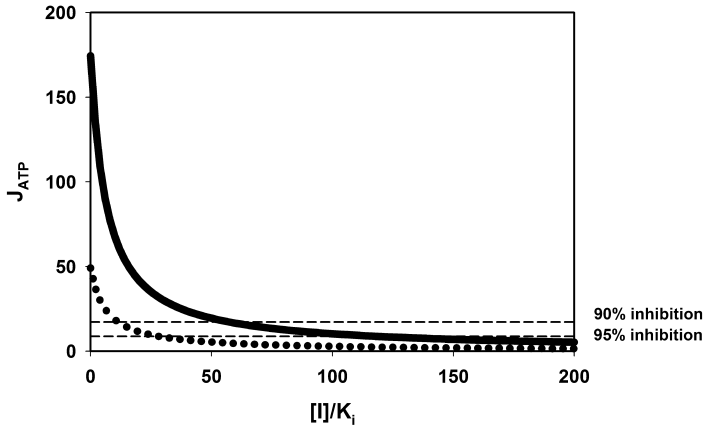

	gene-expression adaptation	
	No	Yes
[I]/K_i 90% inhibition	56	11
[I]/K_i 95% inhibition	118	28

Fig. 6. The impact of gene-expression adaptation on the reduction of the glycolytic flux. The steady-state ATP synthesis flux was calculated as a function of the concentration [I] of a competitive inhibitor of glucose transport across the plasma membrane. The concentration [I] was normalized with respect to the inhibition constant K_i, which equals the dissociation constant of the inhibitor from the transport protein. Calculations were performed for the original model as described in Albert *et al.* (2005) (solid line) and when the V_{max} values were altered with the same factor as the corresponding transcript levels as measured (dotted line). The glucose concentration was 5 mM, like the blood glucose concentration. Details of the modelling are given in *Experimental procedures*.

generated in mice, as well as comparisons of bloodstream and procyclic forms (Jensen *et al.*, 2009) (Fig. S2A). In addition, we looked at a comparison of bloodstream and procyclic-form transcriptomes generated by cDNA sequencing (Siegel *et al.*, 2010) (Fig. S2B). As before, the mRNAs that were increased by phloretin showed a rather heterogeneous regulation pattern, with a bias towards procyclic-specific mRNAs. The results confirmed that many of the mRNAs that decreased after phloretin-treatment were preferentially expressed in bloodstream forms. Moreover, an even larger group of the mRNAs decreased after phloretin treatment showed expression that was suppressed in the stumpy forms.

We concluded that phloretin induced gene-expression changes characteristic of growth arrest and early differentiation. The next step was to assess the implications of these changes for trypanosome metabolism.

Decreased expression of glycolytic enzymes renders trypanosome glycolysis more sensitive to glucose transport inhibition

We investigated the impact of the altered gene expression on the inhibition of the glycolytic flux, using the previously developed computer model of *T. brucei* glycolysis (Albert *et al.*, 2005). The model takes the enzyme expression (concentration or V_{max}) and the kinetic parameters of the enzymes as input. It predicts how the glycolytic flux and the metabolite concentrations respond to substrate availability, enzyme expression or specific inhibitors. We calculated how the (glycolytic) ATP production flux will respond to an increasing concentration of a competitive inhibitor of glucose transport, like phloretin (Fig. 6). In the calculations the inhibitor concentration [I] was normalized against its inhibition constant K_i, which equals the dissociation constant of the inhibitor from the transport protein. This was done to generalize the results to any competitive inhibitor of glucose transport.

If gene expression were not taken into account, a flux reduction of 90% would be achieved at an inhibitor concentration that was 56 times the inhibition constant for the transporter. A flux reduction of 95% would require 118 times the inhibition constant (Fig. 6, solid line). Next, the V_{max} values in the model were altered by the same factor as the observed change of the corresponding mRNA after 24 h of phloretin treatment (Fig. 4B). Now, the required inhibitor concentrations for flux reductions of 90% or 95% were only 11 times, or 28 times the inhibition constant respectively (Fig. 6, dotted line). Hence, according to the model the same flux reduction is achieved at a four to five times lower drug dosage when the gene-expression response is included, than when it is not.

Obviously, the assumption that the actual change in protein concentrations equals that in the mRNAs is an approximation. The rationale behind this assumption is that during trypanosome differentiation from the bloodstream to the procyclic form not only mRNAs of glycolytic proteins are downregulated (Jensen *et al.*, 2009; Queiroz *et al.*, 2009; Nilsson *et al.*, 2010), but also protein levels and V_{max} values (Hart *et al.*, 1984; Aman and Wang, 1986). The fact that the phloretin-treated cells are hardly dividing would diminish the changes in protein as com-

pared with those in mRNA, if the proteins were stable. During trypanosome differentiation, however, 'old' glycosomal enzymes are degraded through autophagy of glycosomes (Herman *et al*., 2008).

Given the uncertainties in the protein response, the above calculations should be considered as an illustration of how the gene-expression response will affect the required drug dosage, rather than as an exact prediction. Nevertheless, the calculations were in surprisingly good agreement with the measured inhibition of the glycolytic flux by phloretin (Fig. 1). The K_i of phloretin for the trypanosome glucose transporter THT1 is 21 μM (Bakker *et al*., 1999b). In the presence of 20 mM glucose – like in our experiments – the model predicts that 100 μM phloretin will inhibit the flux by 13% without a gene-expression response, and by 75% if the gene-expression adaptation is taken into account. In reality we measure 30% inhibition at 100 μM phloretin (linear fit to the curve in Fig. 1). We have to be aware, however, that the used K_i value for phloretin has been measured in a buffer that differs substantially from the medium used here.

Expression of EP procyclins on the surface and sensitivity to Concanavalin A

Results so far indicated that the phloretin- or 2-DOG-treated cells had entered into a differentiation programme towards the procyclic stage. We therefore next investigated whether the procyclic features expressed by the phloretin- or 2-DOG-treated cells also encompassed the surface coat, since the mRNA encoding EP procyclin came up after glucose-transport inhibition (Fig. 4A and B). In procyclic trypanosomes the glycosylated EP1 and EP3 proteins bind the lectin Concanavalin A (ConA), which then kills the cells via an unknown mechanism (Hwa and Khoo, 2000; Pearson *et al*., 2000; Morris *et al*., 2002). Bloodstream-form trypanosomes do not normally express procyclin proteins and are resistant to ConA killing (Fig. 7A). In contrast, 20–30% of the cells died from exposure to ConA after pre-treatment with phloretin (Fig. 7A), suggesting either that some cells had incorporated procyclins into their coats, or else that the surface VSG had undergone unusual carbohydrate modification. However, we were unable to detect EP procyclins by Western blot (Fig. 7B) or flow cytometry (Fig. S3), so if they are expressed, the level must be very low.

More evidence for a functional change to the procyclic life stage came from experiments with procyclic culture conditions. Phloretin-treated bloodstream-form cells survived incubation under procyclic culture conditions (i.e. in a procyclic culture medium at 28°C) for more than 4 days, while untreated bloodstream-form cells died (Fig. 7C and an independent experiment in Fig. S4A). As a control we subjected the untreated bloodstream-form cells to a temperature downshift from 37°C to 28°C. Under those conditions the cells survived, although they almost stopped growing (Fig. S4B). This result excluded the possibility that the death of untreated trypanosomes under procyclic culture conditions was merely a result of the change in temperature. After 72 h under procyclic culture conditions, the phloretin-treated cells were as sensitive to ConA (Fig. 7D and Fig. S4C) as are procyclic cultures (see Fig. 7A) and Western blot analysis revealed a strong signal for EP procyclin proteins (Fig. 7E). This result indicated that the phloretin treatment had potentiated the ability of the trypanosomes to undergo a differentiation programme.

Probing the metabolic signal for differentiation

We did some first experiments to determine the metabolic signal that triggers differentiation in response to glucose transport inhibition. A lowered [ATP]/[ADP] ratio could be excluded, since the [ATP]/[ADP] ratio did not change (Fig. 8A). Conditional knock-down of the next enzyme of the pathway, HXK, led to upregulation rather than downregulation of THT1 in the first 24 h (Fig. 8B). However, after 48 h, *THT1* mRNA levels had returned to initial levels. These results are compatible with intracellular glucose being the molecule that initiates the signal cascade, but more detailed dynamics are required. It is known that changes in the activities of mitochondrial enzymes influence expression of procyclins (Vassella *et al*., 2004). Phloretin as well as HXK depletion caused upregulation of mitochondrial enzymes in our experiments and therefore one may expect secondary effects on coat protein expression (Vassella *et al*., 2004).

Discussion

In a network-based approach to identify and validate a new drug target within trypanosome glycolysis, we have systematically investigated first the metabolic responses (Bakker *et al*., 1999a,b) and subsequently (this article) the gene-expression responses that follow inhibition of the glucose transporter. Instead of homeostatic adaptation, inhibition of glucose transport initiated a domino effect that rendered the parasite increasingly vulnerable: first a decrease in the glycolytic flux via metabolic control, then a downregulation of the mRNAs encoding the glucose transporter and most other glycolytic enzymes. Results of a transcriptome analysis indicated that the phloretin treatment had caused the trypanosomes to partially undergo the early stages of differentiation, with some changes typical of growth-arrested stumpy forms with early further differentiation. Consistent with this, the phloretin-treated bloodstream cells had an

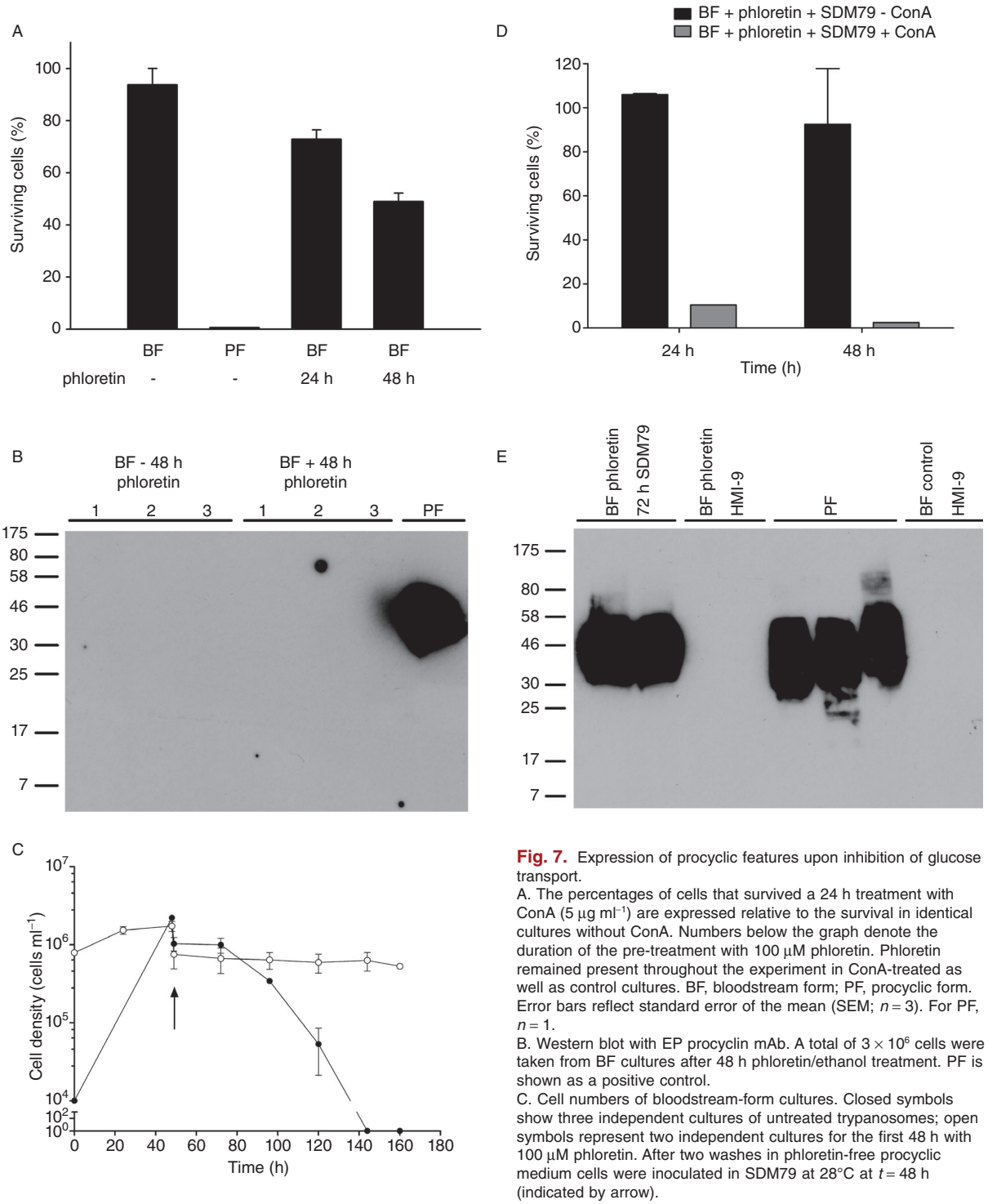

Fig. 7. Expression of procyclic features upon inhibition of glucose transport.

A. The percentages of cells that survived a 24 h treatment with ConA (5 μg ml^{-1}) are expressed relative to the survival in identical cultures without ConA. Numbers below the graph denote the duration of the pre-treatment with 100 μM phloretin. Phloretin remained present throughout the experiment in ConA-treated as well as control cultures. BF, bloodstream form; PF, procyclic form. Error bars reflect standard error of the mean (SEM; $n = 3$). For PF, $n = 1$.

B. Western blot with EP procyclin mAb. A total of 3×10^6 cells were taken from BF cultures after 48 h phloretin/ethanol treatment. PF is shown as a positive control.

C. Cell numbers of bloodstream-form cultures. Closed symbols show three independent cultures of untreated trypanosomes; open symbols represent two independent cultures for the first 48 h with 100 μM phloretin. After two washes in phloretin-free procyclic medium cells were inoculated in SDM79 at 28°C at $t = 48$ h (indicated by arrow).

D. After 72 h in procyclic culture medium part of the cell culture was subjected to ConA (5 μg ml^{-1}) treatment. The percentages of cells that survived a 24 and 48 h treatment with ConA (5 μg ml^{-1}) are expressed relative to the survival in identical cultures without ConA. Error bars indicate standard deviations among two independent experiments.

E. Western blot with EP procyclin mAb. A total of 3×10^6 cells were taken from cultures after 48 h with phloretin treatment (lanes 3 and 4, $t = 48$ h in C), after 72 h in procyclic medium (lanes 1 and 2, $t = 120$ in C), from untreated procyclic cultures (lanes 5, 6 and 7) and from untreated bloodstream-form cultures (lanes 8 and 9, $t = 48$ h in C). Replicate samples were taken from independent cultures.

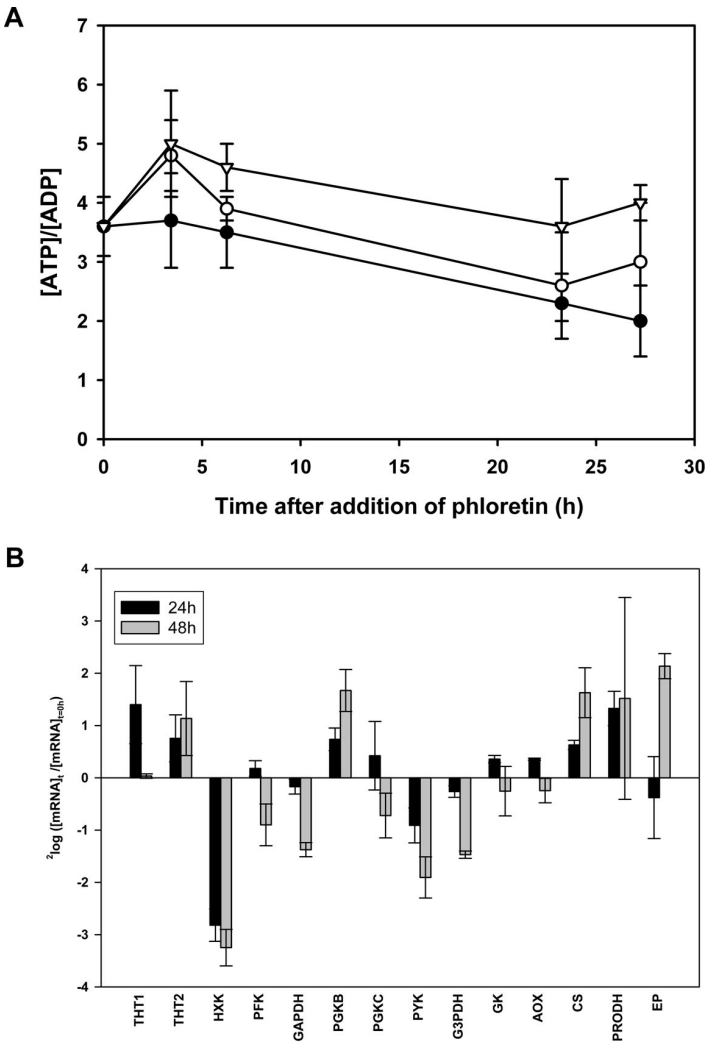

Fig. 8. Probing the metabolic signal for differentiation after phloretin treatment.
A. [ATP]/[ADP] ratio in untreated and phloretin-inhibited bloodstream-form trypanosomes. Symbols denote: (●) untreated; (○) 50 μM phloretin; (▽) 100 μM phloretin. Values represent averages ± standard deviations of results obtained from two independent cultures
B. Changes in mRNA levels after HXK RNAi. An inducible HXK RNAi mutant (Albert *et al.*, 2005) was induced by addition of 0.25 μg ml^{-1} tetracycline. mRNA levels at 24 and 48 h were measured by quantitative PCR and compared with levels before induction. Error bars show standard deviations of results from two independent experiments. THT, trypanosome hexose transporter; HXK, hexokinase; PFK, phosphofructokinase; GAPDH, glyceraldehyde-3-phosphate dehydrogenase; PGK, phosphoglycerate kinase; PYK, pyruvate kinase; G3PDH, glycerol-3-phosphate dehydrogenase; AOX, alternative oxidase; CS, citrate synthase; PRODH, proline dehydrogenase; EP, EP procyclin.

enhanced ability to undergo subsequent differentiation steps upon transfer to procyclic culture conditions. The fact that they did not fully differentiate, and were not able to divide under procyclic culture conditions (Fig. 7C), is likely to be due to the fact that we used a monomorphic strain which cannot complete a full life cycle. In addition, glucose transport inhibition might not be sufficient to induce the full spectrum of changes seen in stumpy forms. To address this issue, future studies should be performed with pleomorphic trypanosomes.

As noted in the introduction, alterations of coat-protein expression in glucose-deprived trypanosomes had been observed before, although the resulting transcriptome had not been analysed and the implications for drug treatment were not explored. Is the transcript response to glucose deprivation specific to this particular metabolic challenge, or is it simply a reaction to growth arrest? It has long been known that treatment with dihydrofluoromethyl ornithine, which causes cell-cycle arrest but has no obvious connection to signalling or energy metabolism, can enhance the ability of monomorphic trypanosomes to undergo initial steps of differentiation (Giffin *et al.*, 1986). Growth arrest is known to be important in the differentiation process, and various growth-inhibitory treatments have been shown to induce expression of EP procyclins or their mRNAs (Fenn and Matthews, 2007). We do not really know which of these treatments targeted physiological differentiation control mechanisms, or whether any sort of growth inhibition will do. We therefore examined transcriptome data for bloodstream trypanosomes following treatments that inhibited growth, but had no obvious link to differentiation. None of the treatments caused the differentiation-related gene-expression changes reported in this article. They were: RNAi targeting the small RNA-binding proteins UBP1 and UBP2, or overexpression of UBP2 (Hartmann *et al.*, 2007); RNAi targeting the 14-3-3

proteins (C. Benz and C. Clayton, unpubl. data); knockdown of clathrin expression or treatment with tunicamycin (Koumandou *et al*., 2008); and treatment with dithiothreitol (Koumandou *et al*., 2008; Goldshmidt *et al*., 2010). We cannot rule out the possibility that induction of EP procyclins was missed in all of these experiments because the timing was wrong, or because the parasites were too debilitated to initiate such a response. However, so far, it seems that the transcriptome response to glucose deprivation is not solely a response to growth arrest.

We suggest that trypanosome differentiation can be triggered by a variety of stimuli, but that the intracellular glucose concentration may be a critical intermediate signal. In the case of glucose transport inhibition, the cells seem to be misled by the low glucose influx and respond as if they are in the glucose-poor environment of the tse-tse fly, switching on their differentiation programme. A recently identified phosphatase that is critical for trypanosome differentiation, PIP39, is located inside the glycosome. It is tempting to speculate that this phosphatase is a key player in monitoring glycosomal glucose levels (Szoor *et al*., 2010).

An anti-trypanosomal drug needs to have a very low cost and to be easy to deliver. It therefore needs to be cheap to manufacture and must be active at low concentrations. It also needs to have as few side-effects as possible, so must be selective for the parasite target. What are the implications of the present study for the use of glucose-transport inhibition against trypanosome infections? To answer this question, we will distinguish two different aspects, namely (i) inhibition of parasite growth and (ii) side-effects on human metabolism.

(i) To cure trypanosomiasis, either all parasites must be killed by the drug, or growth of all of them must be inhibited for a sufficient time to enable elimination of all existing antigenic variants by adaptive immunity. Escape of a single trypanosome with a novel variant surface coat will be sufficient to reinitiate the infection. Ideally therefore we need to attain a drug concentration adequate to kill at least 99% of the parasites (LD99) in the blood and tissues without causing significant side-effects. The LD99 is also influenced by the response of the biochemical network. The high flux control coefficient of the glucose transporter in *T. brucei* will contribute to a low LD_{99}, especially since 50% inhibition of glycolytic flux is sufficient to kill the parasite (Fig. 3). On top of this, according to our model calculations, the observed downregulation of glycolytic gene expression upon transporter inhibition led to a four- to fivefold decrease of the inhibitor concentration required to reduce the glycolytic flux. Thus the results of our analyses are favourable to THT1 as a target. If, in line with the results presented here, the few surviving trypanosomes start expressing invariable procyclins this may be an extra, efficient target for the mammalian immune system. The ConA-sensitive mannose residues on the EP proteins (Hwa and Khoo, 2000; Pearson *et al*., 2000) may be recognized by the mannan-binding lectin of the innate immune system. Whether glucose transporter inhibition is able, by itself, to prompt sufficient surface EP procyclin expression to activate either innate or adaptive immunity is currently unclear: this should be assessed in pleomorphic parasites.

(ii) A low therapeutic drug concentration is of no use if those low levels also kill host cells. And even minor inhibition of glycolysis may be deleterious to some host cell types. Therefore, even if selectivity at the level of molecular recognition is attained, additional selectivity at the network level would be helpful. Simulations with a detailed model of erythrocyte glycolysis (Schuster and Holzhutter, 1995) showed that glucose transport hardly controls erythrocyte glycolysis at all (B. M. Bakker *et al*., in preparation). This implies that erythrocytes will be less vulnerable to glucose transport inhibition than bloodstream-form trypanosomes. However, a quantitative analysis of potential side-effects on other cell types – including potential homeostatic adaptations – is required.

In the present study, phloretin and 2-DOG were used to inhibit glucose transport in *in vitro* cultures of *T. brucei*. Phloretin has already been used in *in vivo* studies in rats for its anti-tumour activity (Nelson and Falk, 1993) and the LD50 of phloretin for rat hepatocytes in a 2 h incubation was reported as 400 μM (Sabzevari *et al*., 2004). The concentrations of phloretin and 2-DOG used against trypanosomes in this study (micromolar range) are too high to use in humans, and even too high to serve as a lead compound. Hexose analogues with anti-trypanosome activity have already been developed (Azema *et al*., 2004) but the mechanism of action was unclear since in many cases the LD50 for the parasite was lower than the K_i for the transporter. For either phloretin or the analogues, a direct comparison of LD50s between trypanosomes and mammalian cells under similar conditions has, to our knowledge, not been performed. It is clear that if inhibitors are to be found, substantial effort will need to be made in screening and in chemical modification, since viable leads are not yet available.

We conclude that although development of specific and potent inhibitors may be a considerable challenge, glucose transport is a more promising drug target in trypanosomes than was thought based on metabolic control alone (Bakker *et al*., 1999b). Furthermore, this study may open a new avenue to systems biology-based drug target discovery, aiming at tricking microorganisms into lethal

adaptation strategies. Importantly, our results exemplify the importance of monitoring the adaptations of cellular networks in drug target validation (Hornberg and Westerhoff, 2006). Besides identifying cases where a homeostatic response of the pathogen would incapacitate the drug (enabling an early defocusing from that target), it may also reveal more cases like the present one, in which the cellular response is anti-homeostatic. If such an anti-homeostatic response is absent from the human host, the prospects for enhanced specificity of drugs against such targets are substantial.

Experimental procedures

Strains and cultivation

Monomorphic bloodstream-form *T. brucei* of cell line 449 [a derivative of strain Lister 427 (Biebinger *et al.*, 1997)] were cultivated in HMI-9 (Hirumi and Hirumi, 1989), supplemented with 10% fetal calf serum (FCS, Invitrogen) and 0.2 μg ml^{-1} phleomycin (Cayla) in a water-vapour-saturated incubator at 5% CO_2 and 37°C.

Monomorphic procyclic *T. brucei* 449 cells and bloodstream-form cultures subjected to procyclic culture conditions were cultivated in SDM-79 or SOGG-medium [a non-glucose formulation of SDM-79 (Furuya *et al.*, 2002)], supplemented with 10 mM glucose (v/v), 10% FCS and 0.5 μg ml^{-1} phleomycin at 28°C.

Growth was monitored by counting cell numbers in culture samples with a Burker-Türk haemocytometer. The specific growth rate μ was determined from the increase of the cell numbers in time, by fitting equation $X(t) = X(0) \cdot e^{\mu t}$ to the data. Here $X(t)$ represents the cell density in the culture at time point t.

Inhibition

Phloretin, 2-DOG and ConA were purchased from Sigma.

Phloretin was dissolved in 70% ethanol; 2-DOG and ConA in demineralized water. Final concentrations of ethanol were always below 0.7% and the highest ethanol concentration was used in the control cultures.

Increasing cell densities decreased the sensitivity of the cells to phloretin. At constant cell density ($8{\cdot}10^5$ cells ml^{-1} in our experiments), phloretin treatment gave reproducible effects for a given concentration. We used similar cell densities in 2-DOG experiments.

RNA isolation and cDNA synthesis

Total RNA was isolated from $1–4 \times 10^7$ cells by adding 1 ml of Trizol (Invitrogen) to cell pellets according to the manufacturer's protocol. Isolated RNA was DNase-1 (Finnzymes) treated, purified by phenol/chloroform extraction and 1 μg was used in a cDNA synthesis reaction with random hexamer primers (Finnzymes).

Microarray

Fluorescently labelled cDNA was synthesized and hybridized to oligonucleotide microarrays (NIAID) as previously described (Queiroz *et al.*, 2009). Data analysis was performed using the ExpressConverter and MIDAS software which are freely available at http://www.tm4.org. Files obtained from the scan were transformed into .mev files using the ExpressConverter. Using MIDAS the signal intensities were normalized by locally weighted linear regression and duplicate spots on each slide were merged. Log_2 transformed data were exported to SAM as described (Tusher *et al.*, 2001). The complete microarray dataset has been uploaded to NCBI GEO with accession number GSE24275 and can be accessed online via: http://www.ncbi.nlm.nih.gov/geo/query/acc.cgi?acc=GSE24275.

Real-time quantitative PCR

Amplification, data collection and data analysis were performed in the ABI 7700 Prism Sequence Detector (once 2 min at 50°C; once 10 min at 95°C; and 40 cycles of 15 s at 95°C followed by 1 min at 59°C). The calculated cycle of threshold values (Ct) were exported to and further analysed in Microsoft Excel. Cycles of threshold for the different genes were normalized to the Ct of hypoxanthine-guanine phosphoribosyl transferase (HGPRT) transcript in the same sample (ΔCt). Transcripts of two other housekeeping genes (60S rRNA and β-tubulin) were assayed as an internal check. Subsequently the normalized Ct values of the different time points were, for each transcript, compared with the Ct of that transcript at time point zero to calculate the fold changes of the mRNA concentrations according to: $mRNA/mRNA_{t=0} = 2^{(\Delta Ct(0)-\Delta Ct(t))}$. Dissociation curves proved that only a single-sized product was formed in every qPCR reaction. Primers used in the qPCR are listed in Table S3 in *Supporting information* of this article and were tested for efficiency.

Metabolite assays

Glucose, pyruvate, glycerol, succinate and acetate were measured by HPLC (Rossell *et al.*, 2005). ATP and ADP levels were measured with a luciferase assay as described previously (Rohwer *et al.*, 1996).

CS activity assay

Approximately 3×10^8 cells were washed twice in ice-cold PBS (140 mM NaCl, 2.7 mM KCl, 10.1 mM Na_2HPO_4, 1.8 mM KH_2PO_4) and resuspended in 0.5 ml of PBS. Cells were lysed using 0.6 g ml^{-1} acid-washed glass beads (425–600 μm, Sigma) in a Thermo Savant FastPrep FP120 Homogenizer (four cycles of 5 s, speed 6.0, with cooling on ice between cycles for at least 1 min). Cell lysate was transferred to a new tube, centrifuged (maximum speed, at 4°C) and supernatant was used to measure CS activity. CS (E.C. 2.3.3.1) was measured in an automated spectrophotometer (Cobas FARA, Roche) at 412 nm, with an assay modified from Morgunov and Srere (1998). Final concentrations in the assay mixture were 100 mM Tris-HCl (pH 8.0), 0.1 mM oxaloacetic acid; 0.1 mM 5,5′-dithio-bis(2-nitrobenzoic acid (DTNB) and 40 mM KCl. The reaction was started by addition of 0.5 mM acetyl-CoA and the increase in A_{412} (due to conversion of DTNB to TNB) was followed in time. Activities

were determined from the linear part of the A_{412} curves, based on an extinction coefficient for DTNB at 412 nm of 13.6 mM^{-1} cm^{-1}. Enzyme activities were normalized to the protein contents of the cell extracts, based on a BCA protein assay (Pierce).

Modelling

The modelling was performed with the most recent version of the glycolysis model (Albert *et al.*, 2005) in the open-source software Jarnac (Sauro, 2000; Sauro *et al.*, 2003). To calculate the effect of phloretin, a competitive inhibitor [I] which only binds to the outside (Bakker *et al.*, 1999b) with an inhibition constant K_i was included in the rate equation for glucose transport across the plasma membrane. To this end, the K_m for extracellular glucose was multiplied with a factor $1 + [I]/K_i$. This yielded the following equation:

$$v_{THT} = \frac{V_{max}^{f}}{K_m^{Glc}\cdot\left(1+\frac{[I]}{K_i}\right)}\cdot \frac{[Glc]_{out}-[Glc]_{in}}{1+\frac{[Glc]_{out}}{K_m^{Glc}\cdot\left(1+\frac{[I]}{K_i}\right)}+\frac{[Glc]_{in}}{K_m^{Glc}}+\alpha\cdot\frac{[Glc]_{out}}{K_m^{Glc}\cdot\left(1+\frac{[I]}{K_i}\right)}\cdot\frac{[Glc]_{in}}{K_m^{Glc}}}$$

In the version in which gene expression was ignored (solid line in Fig. 6) the original V_{max} values were used (Albert *et al.*, 2005). When altered gene expression was taken into account the V_{max} values were multiplied with the fold change of the transcript levels as measured by qPCR after 24 h (dashed line Fig. 6). In the case of glucose transport, for which two transport proteins exist, we made use of earlier findings that THT1 represented 97.5% and THT2 2.5% of the total THT mRNA pool (Bringaud and Baltz, 1993). This gave rise to the following V_{max} values [in nmol min^{-1} (mg protein)$^{-1}$]:

THT: 108.9·(0.975·0.25 + 0.025·1.22); HXK: 1929·0.35; PGI: 1305·0.32; PFK: 1708·0.29; ALD: 560·0.35; TIM: 999.3·0.34; G3PDH: 465·0.24; GK: 200·0.32; AOX: 368·0.56; GAPDH 720.9·0.26; PGKC: 2862·0.27; PGAM: 225·0.77; ENO: 598·0.31; PYK: 1020·0.17.

Western blotting

For Western blot analysis, 3×10^6 parasites were harvested by centrifugation, washed in PBS, resuspended in 30 µl of Lämmli buffer and stored at −80°C before analysis. Samples were boiled for 10 min at 95°C and 20 µl was separated on SDS-PAGE (Novex 4–20% Tris-glycine, Invitrogen or 12.5% Tris-glycine) at 125 V and transferred to a nitrocellulose membrane (Hybond-ECL, Amersham) at 150 mA for 4 h. Membranes were blocked for 2 h at room temperature with 5% milk in PBS-T (PBS with 0.05% Tween-20), washed three times with PBS-T, and probed with primary antibody (anti-*Trypanosoma brucei* procyclin mAb, Cedarlane) diluted 1:2000 in 1% milk in PBS-T overnight at 4°C. After three washes with PBS-T, the membrane was incubated with secondary antibody (goat anti-mouse IgG peroxidase conjugate, Calbiochem) 1:2000 in 1% milk in PBS-T for 2 h at room temperature. After five washes with PBS-T, horseradish peroxidase activity was measured with SuperSignal HRP substrate (Novagen).

Acknowledgements

We thank Professor A.B. Smit and Dr S. Spijker for the use of the qPCR and Dr J. van Hellemond, Professor A. Tielens and Dr Th. Geijtenbeek for discussions. Support from Nederlandse Organisatie voor Wetenschappelijk Onderzoek-Vernieuwings-impuls and IOP Genomics (grants to B.M.B.) from the Scottish Universities Life Science Alliance (studentship to E.J.K.), from the Fonds de la Recherche Scientifique Médicale (FRSM) and the Interuniversity Attraction Poles – Belgian Federal Office for Scientific, Technical and Cultural Affairs (IAP) to P.A.M.M., and from the Nederlandse Organisatie voor Wetenschappelijk Onderzoek, European Union (FP7; BioSim, NucSys, EC-MOAN, YSBN), AstraZeneca and BBSRC to H.V.W. (BBC0082191, BBD0190791, BBF0035281) is acknowledged.

Martin Wurst is supported by the DFG (Sonderforschungsbereich 544). We thank Rafael Queiroz and other members of the Hoheisel lab for assistance with the microarrays, and NIAID for the free microarray slides.

References

Alberghina, L., and Westerhoff, H.V. (2005) *Systems Biology: Definitions and Perspectives*. Berlin: Springer Verlag.

Albert, M.-A., Haanstra, J., Hannaert, V., Van Roy, J., Opperdoes, F., Bakker, B., and Michels, P. (2005) Experimental and *in silico* analyses of glycolytic flux control in bloodstream form *Trypanosoma brucei*. *J Biol Chem* **280:** 28306–28315.

Aman, R.A., and Wang, C.C. (1986) An improved purification of glycosomes from the procyclic trypomastigotes of *Trypanosoma brucei*. *Mol Biochem Parasitol* **21:** 211–220.

Azema, L., Claustre, S., Alric, I., Blonski, C., Willson, M., Perie, J., *et al.* (2004) Interaction of substituted hexose analogues with the *Trypanosoma brucei* hexose transporter. *Biochem Pharmacol* **67:** 459–467.

Bakker, B.M., Michels, P.A., Opperdoes, F.R., and Westerhoff, H.V. (1999a) What controls glycolysis in bloodstream form *Trypanosoma brucei*? *J Biol Chem* **274:** 14551–14559.

Bakker, B.M., Walsh, M.C., ter Kuile, B.H., Mensonides, F.I., Michels, P.A., Opperdoes, F.R., and Westerhoff, H.V. (1999b) Contribution of glucose transport to the control of the glycolytic flux in *Trypanosoma brucei*. *Proc Natl Acad Sci USA* **96:** 10098–10103.

Barrett, M.P., Burchmore, R.J., Stich, A., Lazzari, J.O., Frasch, A.C., Cazzulo, J.J., and Krishna, S. (2003) The trypanosomiases. *Lancet* **362:** 1469–1480.

Biebinger, S., Wirtz, L.E., and Clayton, C.E. (1997) Vectors for inducible over-expression of potentially toxic gene products in bloodstream and procyclic *Trypanosoma brucei*. *Mol Biochem Parasitol* **85:** 99–112.

Blattner, J., Helfert, S., Michels, P., and Clayton, C.E. (1998) Compartmentation of phosphoglycerate kinase in *Trypanosoma brucei* plays a critical role in parasite energy metabolism. *Proc Natl Acad Sci USA* **95:** 11596–11600.

Borst, P., and Ulbert, S. (2001) Control of VSG gene expression sites. *Mol Biochem Parasitol* **114:** 17–27.

Bringaud, F., and Baltz, T. (1992) A potential hexose transporter gene expressed predominantly in the bloodstream form of *Trypanosoma brucei*. *Mol Biochem Parasitol* **52:** 111–121.

Bringaud, F., and Baltz, T. (1993) Differential regulation of two distinct families of glucose transporter genes in *Trypanosoma brucei*. *Mol Cell Biol* **13:** 1146–1154.

Bringaud, F., Baltz, D., and Baltz, T. (1998) Functional and molecular characterization of a glycosomal PPi-dependent enzyme in trypanosomatids: pyruvate phosphate dikinase. *J Biol Chem* **95:** 7963–7968.

Caceres, A.J., Michels, P.A., and Hannaert, V. (2010) Genetic validation of aldolase and glyceraldehyde-3-phosphate dehydrogenase as drug targets in *Trypanosoma brucei*. *Mol Biochem Parasitol* **169:** 50–54.

Clayton, C., and Shapira, M. (2007) Post-transcriptional regulation of gene expression in trypanosomes and leishmanias. *Mol Biochem Parasitol* **156:** 93–101.

Cross, G.A. (1975) Identification, purification and properties of clone-specific glycoprotein antigens constituting the surface coat of *Trypanosoma brucei*. *Parasitology* **71:** 393–417.

Dean, S., Marchetti, R., Kirk, K., and Matthews, K.R. (2009) A surface transporter family conveys the trypanosome differentiation signal. *Nature* **459:** 213–217.

Ebikeme, C.E., Peacock, L., Coustou, V., Riviere, L., Bringaud, F., Gibson, W.C., and Barrett, M.P. (2008) *N*-acetyl D-glucosamine stimulates growth in procyclic forms of *Trypanosoma brucei* by inducing a metabolic shift. *Parasitology* **135:** 585–594.

Fenn, K., and Matthews, K.R. (2007) The cell biology of *Trypanosoma brucei* differentiation. *Curr Opin Microbiol* **10:** 539–546.

Furuya, T., Kessler, P., Jardim, A., Schnaufer, A., Crudder, C., and Parsons, M. (2002) Glucose is toxic to glycosome-deficient trypanosomes. *Proc Natl Acad Sci USA* **99:** 14177–14182.

Giffin, B.F., McCann, P.P., Bitonti, A.J., and Bacchi, C.J. (1986) Polyamine depletion following exposure to DL-alpha-difluoromethylornithine both *in vivo* and *in vitro* initiates morphologival alterations and mitochondrial activation in a monomorphic strain of *Trypanosoma brucei brucei*. *J Protozool* **33:** 238–243.

Goldshmidt, H., Matas, D., Kabi, A., Carmi, S., Hope, R., and Michaeli, S. (2010) Persistent ER stress induces the spliced leader RNA silencing pathway (SLS), leading to programmed cell death in *Trypanosoma brucei*. *PLoS Pathog* **6:** e1000731.

Groen, A.K., Wanders, R.J., Westerhoff, H.V., van der Meer, R., and Tager, J.M. (1982) Quantification of the contribution of various steps to the control of mitochondrial respiration. *J Biol Chem* **257:** 2754–2757.

Gruszynski, A.E., van Deursen, F.J., Albareda, M.C., Best, A., Chaudhary, K., Cliffe, L.J., *et al.* (2006) Regulation of surface coat exchange by differentiating African trypanosomes. *Mol Biochem Parasitol* **147:** 211–223.

Haile, S., and Papadopoulou, B. (2007) Developmental regulation of gene expression in trypanosomatid parasitic protozoa. *Curr Opin Microbiol* **10:** 569–577.

Hart, D.T., Misset, O., Edwards, S.W., and Opperdoes, F.R. (1984) A comparison of the glycosomes (microbodies) isolated from *Trypanosoma brucei* bloodstream form and cultured procyclic trypomastigotes. *Mol Biochem Parasitol* **12:** 25–35.

Hartmann, C., Benz, C., Brems, S., Ellis, L., Luu, V.D., Stewart, M., *et al.* (2007) Small trypanosome RNA-binding proteins TbUBP1 and TbUBP2 influence expression of F-box protein mRNAs in bloodstream trypanosomes. *Eukaryot Cell* **6:** 1964–1978.

Heinrich, R., and Rapoport, T.A. (1974) A linear steady-state treatment of enzymatic chains. General properties, control and effector strength. *Eur J Biochem* **42:** 89–95.

Helfert, S., Estevez, A.M., Bakker, B., Michels, P., and Clayton, C. (2001) Roles of triosephosphate isomerase and aerobic metabolism in *Trypanosoma brucei*. *Biochem J* **357:** 117–125.

Hellemond, J.J., Bakker, B.M., and Tielens, A.G. (2005) Energy metabolism and its compartmentation in *Trypanosoma brucei*. *Adv Microb Physiol* **50:** 199–226.

Herman, M., Perez-Morga, D., Schtickzelle, N., and Michels, P.A. (2008) Turnover of glycosomes during life-cycle differentiation of *Trypanosoma brucei*. *Autophagy* **4:** 294–308.

Hirumi, H., and Hirumi, K. (1989) Continuous cultivation of *Trypanosoma brucei* blood stream forms in a medium containing a low concentration of serum protein without feeder cell layers. *J Parasitol* **75:** 985–989.

Hornberg, J.J., and Westerhoff, H.V. (2006) Oncogenes are to lose control on signaling following mutation: should we aim off target? *Mol Biotechnol* **34:** 109–116.

Hwa, K.Y., and Khoo, K.H. (2000) Structural analysis of the asparagine-linked glycans from the procyclic *Trypanosoma brucei* and its glycosylation mutants resistant to Concanavalin A killing. *Mol Biochem Parasitol* **111:** 173–184.

Jenkins, T.M., Eisenthal, R., and Weitzman, P.D. (1988) Two distinct succinate thiokinases in both bloodstream and procyclic forms of *Trypanosoma brucei*. *Biochem Biophys Res Commun* **151:** 257–261.

Jensen, B.C., Sivam, D., Kifer, C.T., Myler, P.J., and Parsons, M. (2009) Widespread variation in transcript abundance within and across developmental stages of *Trypanosoma brucei*. *BMC Genomics* **10:** 482.

Kabani, S., Fenn, K., Ross, A., Ivens, A., Smith, T.K., Ghazal, P., and Matthews, K. (2009) Genome-wide expression profiling of *in vivo*-derived bloodstream parasite stages and dynamic analysis of mRNA alterations during synchronous differentiation in *Trypanosoma brucei*. *BMC Genomics* **10:** 427.

Kacser, H., and Burns, J.A. (1973) The control of flux. *Symp Soc Exp Biol* **27:** 65–104.

Koumandou, V.L., Natesan, S.K., Sergeenko, T., and Field, M.C. (2008) The trypanosome transcriptome is remodelled during differentiation but displays limited responsiveness within life stages. *BMC Genomics* **9:** 298.

Krupka, R.M., and Deves, R. (1980) Evidence for allosteric inhibition sites in the glucose carrier of erythrocytes. *Biochim Biophys Acta* **598:** 127–133.

Lamour, N., Riviere, L., Coustou, V., Coombs, G.H., Barrett, M.P., and Bringaud, F. (2005) Proline metabolism in procyclic *Trypanosoma brucei* is down-regulated in the presence of glucose. *J Biol Chem* **280:** 11902–11910.

Matthews, K.R. (2005) The developmental cell biology of *Trypanosoma brucei*. *J Cell Sci* **118:** 283–290.
Milne, K.G., Prescott, A.R., and Ferguson, M.A. (1998) Transformation of monomorphic *Trypanosoma brucei* bloodstream form trypomastigotes into procyclic forms at 37 degrees C by removing glucose from the culture medium. *Mol Biochem Parasitol* **94:** 99–112.
Morgunov, I., and Srere, P.A. (1998) Interaction between citrate synthase and malate dehydrogenase. Substrate channeling of oxaloacetate. *J Biol Chem* **273:** 29540–29544.
Morris, J.C., Wang, Z., Drew, M.E., and Englund, P.T. (2002) Glycolysis modulates trypanosome glycoprotein expression as revealed by an RNAi library. *EMBO J* **21:** 4429–4438.
Nelson, J.A., and Falk, R.E. (1993) The efficacy of phloridzin and phloretin on tumor cell growth. *Anticancer Res* **13:** 2287–2292.
Nilsson, D., Gunasekera, K., Mani, J., Osteras, M., Farinelli, L., Baerlocher, L., *et al*. (2010) Spliced leader trapping reveals widespread alternative splicing patterns in the highly dynamic transcriptome of *Trypanosoma brucei*. *PLoS Pathog* **6:** pii: e1001037.
Noble, D. (2006) Systems biology and the heart. *Biosystems* **83:** 75–80.
Pearson, T.W., Beecroft, R.P., Welburn, S.C., Ruepp, S., Roditi, I., Hwa, K.Y., *et al*. (2000) The major cell surface glycoprotein procyclin is a receptor for induction of a novel form of cell death in African trypanosomes *in vitro*. *Mol Biochem Parasitol* **111:** 333–349.
Priest, J.W., and Hajduk, S.L. (1994) Developmental regulation of mitochondrial biogenesis in *Trypanosoma brucei*. *J Bioenerg Biomembr* **26:** 179–191.
Queiroz, R., Benz, C., Fellenberg, K., Hoheisel, J.D., and Clayton, C. (2009) Transcriptome analysis of differentiating trypanosomes reveals the existence of multiple post-transcriptional regulons. *BMC Genomics* **10:** 495.
Rohwer, J.M., Jensen, P.R., Shinohara, Y., Postma, P.W., and Westerhoff, H.V. (1996) Changes in the cellular energy state affect the activity of the bacterial phosphotransferase system. *Eur J Biochem* **235:** 225–230.
Rossell, S., van der Weijden, C., Kruckeberg, A., Bakker, B., and Westerhoff, H. (2005) Hierarchical and metabolic regulation of glucose influx in starved *Saccharomyces cerevisiae*. *FEMS Yeast Res* **5:** 611–619.
Sabzevari, O., Galati, G., Moridani, M.Y., Siraki, A., and O'Brien, P.J. (2004) Molecular cytotoxic mechanisms of anticancer hydroxychalcones. *Chem Biol Interact* **148:** 57–67.
Sauro, H.M. (2000) Jarnac: a system for interactive metabolic analysis. In *Animating the Cellular Map: Proceedings of the 9th International Meeting on BioThermoKinetics*. Hofmeyr, J.H.S., Rohwer, J.M., and Snoep, J.L. (eds). South Africa: Stellenbosch University Press, pp. 221–228.
Sauro, H.M., Hucka, M., Finney, A., Wellock, C., Bolouri, H., Doyle, J., and Kitano, H. (2003) Next generation simulation tools: the Systems Biology Workbench and BioSPICE integration. *Omics* **7:** 355–372.
Schuster, R., and Holzhutter, H.G. (1995) Use of mathematical models for predicting the metabolic effect of large-scale enzyme activity alterations. Application to enzyme deficiencies of red blood cells. *Eur J Biochem* **229:** 403–418.
Siegel, T.N., Hekstra, D.R., Wang, X., Dewell, S., and Cross, G.A. (2010) Genome-wide analysis of mRNA abundance in two life-cycle stages of *Trypanosoma brucei* and identification of splicing and polyadenylation sites. *Nucleic Acids Res* **38:** 4946–4957.
Szoor, B., Ruberto, I., Burchmore, R., and Matthews, K.R. (2010) A novel phosphatase cascade regulates differentiation in *Trypanosoma brucei* via a glycosomal signaling pathway. *Genes Dev* **24:** 1306–1316.
Tetaud, E., Barrett, M.P., Bringaud, F., and Baltz, T. (1997) Kinetoplastid glucose transporters. *Biochem J* **325 (**Part 3)**:** 569–580.
Tusher, V.G., Tibshirani, R., and Chu, G. (2001) Significance analysis of microarrays applied to the ionizing radiation response. *Proc Natl Acad Sci USA* **98:** 5116–5121.
Urwyler, S., Vassella, E., Van Den Abbeele, J., Renggli, C.K., Blundell, P., Barry, J.D., and Roditi, I. (2005) Expression of procyclin mRNAs during cyclical transmission of *Trypanosoma brucei*. *PLoS Pathog* **1:** e22.
Vassella, E., Acosta-Serrano, A., Studer, E., Lee, S.H., Englund, P.T., and Roditi, I. (2001) Multiple procyclin isoforms are expressed differentially during the development of insect forms of *Trypanosoma brucei*. *J Mol Biol* **312:** 597–607.
Vassella, E., Probst, M., Schneider, A., Studer, E., Renggli, C., and Roditi, I. (2004) Expression of a major surface protein of *Trypanosoma brucei* insect forms is controlled by the activity of mitochondrial enzymes. *Mol Biol Cell* **15:** 3986–3993.
Verlinde, C.L., Hannaert, V., Blonski, C., Willson, M., Perie, J.J., Fothergill-Gilmore, L.A., *et al*. (2001) Glycolysis as a target for the design of new anti-trypanosome drugs. *Drug Resist Updat* **4:** 50–65.

Supporting information

Additional supporting information may be found in the online version of this article.

Please note: Wiley-Blackwell are not responsible for the content or functionality of any supporting materials supplied by the authors. Any queries (other than missing material) should be directed to the corresponding author for the article.